1976

Aeolian tones from circular cylinders of non-uniform cross section

Cohen, Steven Robert

Monterey, California. Naval Postgraduate School

http://hdl.handle.net/10945/47502

NAVAL POSTGRADUATE SCHOOL
Monterey, California

THESIS

AEOLIAN TONES FROM CIRCULAR CYLINDERS
OF NON-UNIFORM CROSS SECTION

by

Steven Robert Cohen

June 1976

Thesis Advisor: J.V. Sanders

REPORT DOCUMENTATION PAGE

READ INSTRUCTIONS BEFORE COMPLETING FORM

1. REPORT NUMBER	2. GOVT ACCESSION NO.	3. RECIPIENT'S CATALOG NUMBER
4. TITLE (and Subtitle) Aeolian Tones from Circular Cylinders of Non-Uniform Cross Section		5. TYPE OF REPORT & PERIOD COVERED Ph.D. Thesis; June 1976 6. PERFORMING ORG. REPORT NUMBER
7. AUTHOR(s) Steven Robert Cohen		8. CONTRACT OR GRANT NUMBER(s)
9. PERFORMING ORGANIZATION NAME AND ADDRESS Naval Postgraduate School Monterey, California 93940		10. PROGRAM ELEMENT, PROJECT, TASK AREA & WORK UNIT NUMBERS
11. CONTROLLING OFFICE NAME AND ADDRESS Naval Postgraduate School Monterey, California 93940		12. REPORT DATE June 1976 13. NUMBER OF PAGES 280
14. MONITORING AGENCY NAME & ADDRESS(if different from Controlling Office)		15. SECURITY CLASS. (of this report) Unclassified 15a. DECLASSIFICATION/DOWNGRADING SCHEDULE

16. DISTRIBUTION STATEMENT (of this Report)

Approved for public release; distribution unlimited.

17. DISTRIBUTION STATEMENT (of the abstract entered in Block 20, if different from Report)

18. SUPPLEMENTARY NOTES

19. KEY WORDS (Continue on reverse side if necessary and identify by block number)

Aerolian Tones
Non-Uniform Cylinders
Circular Cylinders
Lighthill's theory of aerodynamic sound
Lift Force
Correlation Length

20. ABSTRACT (Continue on reverse side if necessary and identify by block number)

Lighthill's theory of aerodynamic sound is reviewed. Applications of this theory to different cylinder classes are synthesized and extended to cylinder types not addressed previously. An experiment wherein cylinders are placed in an open jet, permitting simultaneous measurement of total lift force, correlation parameters and radiated sound intensity, is conducted. Over the

(20. ABSTRACT Continued)

Reynolds number range 10^3 to 5×10^4, the theory of aerodynamic sound is validated for uniform, roughened, skewed, finned and notched cylinders and for cylinders with splitter plates. Reduction of lift force, by any means, is shown to reduce radiated sound intensity, and local lift force is found to vary monotonically with the two dimensionality of the vortex wake.

Aeolian Tones from Circular Cylinders
of Non-Uniform Cross Section

by

Steven Robert Cohen
Lieutenant Commander, United States Navy
B.A., University of Virginia, 1961
M.S., Naval Postgraduate School, 1968

Submitted in partial fulfillment of the
requirements for the degree of

DOCTOR OF PHILOSOPHY

from the

NAVAL POSTGRADUATE SCHOOL
June 1976

Author [redacted]

[redacted]pproved by:

[redacted]
J [redacted] Sanders
Assoc. Professor of Physics
Thesis Advisor

[redacted]
Professor of Physics

[redacted]
Assoc. Professor of
Electrical Engineering

[redacted]
K. E. Woehler
Professor of Physics

[redacted]
T. M. H[redacted]
Assoc. [redacted]

[redacted]
[redacted]ea Center

Approved by: [redacted]irman, Department [redacted]hysic[redacted] and Chemistry

[redacted]
Academic Dean

ABSTRACT

Lighthill's theory of aerodynamic sound is reviewed. Applications of this theory to different cylinder classes are synthesized and extended to cylinder types not addressed previously. An experiment wherein cylinders are placed in an open jet, permitting simultaneous measurement of total lift force, correlation parameters and radiated sound intensity, was conducted. Over the Reynolds number range 10^3 to 5×10^4, the theory of aerodynamic sound is validated for uniform, roughened, skewed, finned and notched cylinders and for cylinders with splitter plates. Reduction of lift force, by any means, is shown to reduce radiated sound intensity, and local lift force is found to vary monotonically with the two dimensionality of the vortex wake.

ACKNOWLEDGMENTS

In the interest of brevity, it is impossible to mention all who provided support during this research. However, I find it impossible not to thank Professor J. V. Sanders, my principal advisor, who permitted my pursuit of unproductive paths just long enough to maximize my learning experience, but who also, with subtle suggestion, succeeded in appropriately redirecting my efforts. Similarly, I am in debt to the other members of my doctoral committee who always furnished friendly ears and provided expert guidance and appreciated advice. I must also thank Dr. O. M. Griffen of the Naval Research Laboratory who suggested this avenue of research and supplied initial direction.

Construction of the wind tunnel would have been seriously delayed without the assistance of OM-1 Ken Richardson. Kudos also are due Bob Moeller who possesses the unique ability to convert rough sketches, words, and arm motions into perfectly fabricated mechanisms.

Finally, I owe special thanks to my wife, Carolyn, and to my two sons, Michael and Jeffrey who always understood why I spent evenings and weekends in the laboratory.

TABLE OF CONTENTS

LIST OF TABLES

LIST OF FIGURES

LIST OF PLATES

INTRODUCTION

Although aeolian tones were known in antiquity, their scientific study did not begin until Strouhal's experiment in 1878.[1,2] Strouhal discovered that the frequency ($\omega/2\pi$) of the aeolian tone increased with wind velocity ($\overline{U}$) and decreased with diameter (d). This dependence is now expressed in the dimensionless Strouhal number, $S = \omega d/2\pi\overline{U}$.

Strouhal's effort became known to Lord Rayleigh who, over the next twenty years, established that aeolian tones were both directional in nature[2,3] and associated with vortex sheet instability in the cylinder's wake.[4] Other experiments continued, and by the second decade of this century, the first pictures of the alternating vortex wake behind a cylinder had been obtained:[5,6] the vortex frequency was found to be identical to that of the aeolian tone;[7,8] van Karman's vortex stability theory was published;[9] and the transverse force on the cylinder was associated with alternating circulatory flow about the cylinder.[10] Lord Rayleigh observed that aeolian tones occurred in the absence of cylinder vibration[11] and further noted that the Strouhal number was solely a function of Reynolds number ($Re = \overline{U}d/\nu$).[11]

Subsequent efforts, continuing into the 1950's, experimentally quantified this Strouhal-Reynolds number relationship and confirmed that the Strouhal frequency applied to both the wake and the aeolian tone over the range of Reynolds

numbers from 100 to 10^6.[2,12-17] Several of these contributors concluded that the aeolian tone originated in the total lift force exerted by the flow on the cylinder, and furthermore, they confirmed that the directionality of the produced sound was that of a dipole with axis perpendicular to the axis of the cylinder and to the direction of flow.

In spite of these extensive experimental efforts, however, it was not until publication of Lighthill's now classic paper on the theory of aerodynamic sound that a mathematical prediction of the generated sound field could be attempted.[18] Curle extended Lighthill's general theory to account for the presence of solid boundaries,[19] and shortly thereafter, Phillips derived an expression for the intensity of sound produced by flow over a fixed, rigid, uniform cylinder.[2] Phillips related sound intensity (I) to local lift force (f_L), $\overline{U}$, d and a quantity he termed correlation distance (ℓ_c). This last quantity, now usually called correlation length, was introduced to account for phase variation of f_L along the length of the cylinder. It was interpreted to be the effective length over which f_L is of relatively constant phase.

Within the next ten years, several not entirely successful experiments were conducted to validate equations identical or essentially equivalent to that derived by Phillips.[2,15,20,21] These experiments measured I and compared this intensity to that predicted from measured or reported values of f_L

and ℓ_c. In no case were all three quantities measured simultaneously, a task which Lighthill understood to be extremely difficult.[22] As late as 1961, Lighthill noted that "the equation (for predicted sound intensity) must be considered unproved while no simultaneous measurement of all its terms exists."[22]

More recently, because of increased interest in this area, more refined equations for I as a function of f_L, ℓ_c and other parameters have been derived.[6,21,23,25] In addition, limited verification of their validity, satisfying Lighthill's above quoted simultaneity criterion, has occurred.[6,25] However, before discussing these theoretical and experimental advances, it is appropriate to address the rationale for this increased concern with the generation of aeolian tones.

In both air and water, flow over blunt bodies is a common occurrence. For cylinders, flow frequently occurs in the range of Reynolds number between 300 and 3×10^5. Throughout this range, the flow is characterized by a laminar boundary layer which separates at about 80 degrees from the stagnation point[26] and by a wake composed of alternating vortices, laminar near the cylinder, but growing turbulent several diameters downstream. The shedding of these vortices results in an alternating lift force on the cylinder and in an accompanying aeolian tone.

If the natural frequency of the body's motion is near that of the lift force, and if damping is small, the vortex shedding frequency becomes locked-in to or synchronized with

the body's frequency.[8,27-30] Large amplitude oscillatory motion in the lift direction occurs, and the lift force is amplified. This phenomenon of synchronization, wherein the vortex shedding mechanism interacts with resonant vibrations of a rigid body in the manner of a non-linear feedback oscillator, has recently received considerable engineering attention in that it is the cause of costly structural failures. Moreover, with synchronization, laboratory studies of cylinders are facilitated as lock-in removes three dimensional effects from the flow and thereby potentially simplifies experiments on aeolian tones.

Even without synchronization the lift force and resulting vibrations are of engineering interest. For example, this lift force may cause tow cable vibrations, usually termed cable strum, in water. These vibrations often are mechanically coupled to the towed body, and if the latter is a hydrophone, they may be coupled acoustically as well. As such, aeolian tone generation has application to oceanographic studies and to naval sonar technology.

These applications as well as general scientific interest have motivated revisions and extensions of Phillips' original formula for the sound generated by flow over a uniform smooth cylinder. Frenkiel more completely accounted for the concept of effective length.[24] Fitzpatrick and Strassberg reported an equation applicable to a particular class of non-rigid smooth cylinders,[23] and Koopmann derived an expression for a cylinder oscillating under conditions of synchronization.[6]

More recently, Leehey and Hanson experimentally verified a modification of Phillips' formula using a uniform cylinder at Reynolds numbers of 4100 and 6150.[25] Similarly, Koopmann's experiment validated his equation for a synchronized cylinder at a Reynolds number of 21,500.[6]

On the other hand, no synthesis of the various formulas applicable to uniform cylinders exists, and no theory for non-uniform cylinders has been developed. Experimentally, equations appropriate to uniform cylinders have been validated at only three particular Reynolds numbers, and no simultaneous measurement of f_L, ℓ_c and I have been made for non-uniform, roughened, or skewed cylinders, nor for cylinders with splitter plates. Moreover, the lack of experimental investigation into these areas is important in view of the above noted applications and of the wide scatter exhibited by f_L and ℓ_c data reported in the literature.[6,21,25,30-42] This scatter, in turn, is now understood in terms of variation in cylinder end conditions and in the turbulence level of the undisturbed flow.[21,43-45]

The purpose of the study herein reported, then, is to extend previous knowledge in these areas. Specifically, this research addresses the validation of the theory of aerodynamic sound for uniform cylinders over a broader Reynolds number range. In addition, it examines the relation between radiated sound and total lift force for a roughened cylinder, for two cylinders with splitter plates, and for finned, notched and skewed cylinders.

The present study also departs from previous research in that it compares directly measured total lift force (F_L) with radiated sound intensity (I). As such, it achieves the major advantage of an experiment using synchronization without the necessity of obtaining synchronization in the laboratory. Nevertheless, the synchronization phenomena is studied herein, although somewhat abortively. Finally, this experimental effort also measures ℓ_c so that parallel to the calculations of F_L from f_L and ℓ_c reported in earlier work, f_L is herein calculated from F_L and ℓ_c.

In Section I, the theory of aerodynamic sound is developed and applied to a variety of uniform cylinders, thereby providing, in one place and with a correction, a complete summary of previously reported theory. This development then is extended to a specified class of non-uniform cylinders. Sections II and III describe the instrumentation of the experiment, discuss the measurement techniques employed and report raw data. Section IV presents the processed results obtained and compares these results to those reported in previous investigations. This section also reports an effect wherein the local lift force is amplified or attenuated as the two-dimensionality of the vortex wake is increased or decreased. Conclusions appear in Section V, and some suggestions for future studies are included in Section VI.

I. THEORY

BASIC THEORY

In 1952, Lighthill introduced the theory of aerodynamic sound.[18] His paper remains so eminently readable that even a condensation of its essential elements is best presented in the format of the original, namely a qualitative discussion followed by a mathematical treatment.

Sound generation is the conversion of kinetic to acoustic energy. A source represents first order conversion, the fluctuation of mass in a fixed region of space. A dipole is second order conversion, the fluctuation of the rate of mass flux or momentum. Fluctuation of the rate of momentum flux ($\rho v_i v_j$) is third order conversion, is termed a quadrupole, and is the mechanism whereby aerodynamic sound is produced.

In a medium at rest, the local stress is the acoustic pressure ($a_o^2 \rho \delta_{ij}$), while in a flow the stress is more complex. Regardless of the form the latter stress takes, however, one may define the instantaneous applied stress (T_{ij}) as the difference between the true stress and the local pressure that would be present in the absence of flow. Equating this applied stress to a forcing function relative to the acoustic medium at rest then permits calculation of the radiated sound field.

This approach is exact in that T_{ij} includes the generation of sound, its convection with the flow, dissipation,

and all other flow or medium connected phenomena. Moreover, this approach is independent of the flow model used; for example, the flow is not required to be that of a Stokesian fluid. Nevertheless, the flow must be known, and when the flow is not describable in closed form, neither in general is the sound field, although simplifying assumptions may permit a closed form expression.

The basic description of linear acoustics encompasses an exact continuity equation

$$\frac{\partial \rho}{\partial t} + \frac{\partial (\rho v_i)}{\partial y_i} = 0 \tag{1}$$

and an approximate momentum equation

$$\frac{\partial}{\partial t}(\rho v_i) + a_o^2 \frac{\partial \rho}{\partial y_i} = 0 \; . \tag{2}$$

Differentiation of the first with respect to space and the second with time yields the homogeneous wave equation

$$\frac{\partial^2 \rho}{\partial t^2} - a_o^2 \nabla^2 \rho = 0 \; . \tag{3}$$

In flow, the exact momentum equation

$$\frac{\partial}{\partial t}(\rho v_i) + \frac{\partial}{\partial y_j}(\rho v_i v_j + p_{ij}) = 0 \tag{4}$$

must be used. The fluctuating Reynolds stress $(\rho v_i v_j)$

represents momentum convection, and p_{ij} is the compressive stress tensor.

T_{ij}, by definition, is

$$T_{ij} = \rho v_i v_j + p_{ij} - a_o^2 \rho \delta_{ij} \ . \tag{5}$$

Differentiating (5) with respect to y_j and combining with (4) gives

$$\frac{\partial}{\partial t}(\rho v_i) + a_o^2 \frac{\partial \rho}{\partial y_i} = - \frac{\partial T_{ij}}{\partial y_j} \ . \tag{6}$$

Finally, the inhomomogeneous wave equation

$$\frac{\partial^2 \rho}{\partial t^2} - a_o^2 \nabla^2 \rho = \frac{\partial^2 T_{ij}}{\partial y_i \partial y_j} \tag{7}$$

results from differentiating (1) and (6) just as (3) was obtained from (1) and (2). Equation (7), then, is the governing equation for aerodynamic sound.

The solution of (7) is the well known[46] Kirchhoff solution of the inhomogeneous wave equation:

$$\rho(x,t) - \rho_o = \frac{1}{4\pi a_o^2} \int_V \frac{1}{r}\left[\frac{\partial^2 T_{ij}}{\partial y_i \partial y_j}\right] dV(y)$$
$$+ \frac{1}{4\pi} \int_S \left[\frac{1}{r} \frac{\partial \rho}{\partial n} + \frac{1}{r^2} \frac{\partial r}{\partial n} \rho + \frac{1}{a_o r} \frac{\partial r}{\partial n} \frac{\partial \rho}{\partial t}\right] dS(y) \ . \tag{8}$$

The brackets indicate that the quantity contained within is to be evaluated at the retarded time, $t' = t - (\frac{r}{a_o})$. $r = |x_i - y_i|$, and the second term accounts for solid boundaries with normal $\vec{n}$.

In the absence of boundaries, the second term is zero, leaving only the quadrupole field. However, in most applications, including the present one, boundaries are of primary interest, and therefore, this development now must address Curle's extension[19] of Lighthill's theory.

First, it is desirable to convert (8) to a more appropriate form. To this end, one may write, for any function $f(y,t)$,

$$\frac{\partial(\frac{[f]}{r})}{\partial y} = \frac{\partial(f(y,t-\frac{r}{a_o})/r)}{\partial y} = -\frac{1}{r^2}\frac{\partial r}{\partial y}[f(y,t)] + \frac{1}{r}\frac{\partial[f(y,t)]}{\partial y} .$$

But,

$$(9) \quad \frac{\partial f(y,t-\frac{r}{a_o})}{\partial y} = [\frac{\partial f}{\partial y}] + \frac{\partial f(y,t-\frac{r}{a_o})}{\partial(t-\frac{r}{a_o})}\frac{\partial(t-\frac{r}{a_o})}{\partial y} = [\frac{\partial f}{\partial y}] - \frac{1}{a_o}\frac{\partial r}{\partial y}[\frac{\partial f}{\partial t}].$$

Therefore,

$$(10) \quad \frac{\partial(\frac{[f]}{r})}{\partial y} = \frac{1}{r}[\frac{\partial f}{\partial y}] - \frac{1}{a_o r}\frac{\partial r}{\partial y}[\frac{\partial f}{\partial t}] - \frac{1}{r^2}\frac{\partial r}{\partial y}[f].$$

Also,

$$(11)\quad \frac{\partial\left(\frac{[f]}{r}\right)}{\partial x} = -\frac{1}{a_o r}\frac{\partial r}{\partial x}\left[\frac{\partial f}{\partial t}\right] - \frac{1}{r_2}\frac{\partial r}{\partial x}[f]$$

$$= \frac{1}{a_o r}\frac{\partial r}{\partial y}\left[\frac{\partial f}{\partial t}\right] + \frac{1}{r^2}\frac{\partial r}{\partial y}[f].$$

Hence, from (10) and (11),

$$(12)\quad \frac{1}{r}\left[\frac{\partial f}{\partial y}\right] = \frac{\partial}{\partial y}\left(\frac{[f]}{r}\right) + \frac{\partial}{\partial x}\left(\frac{[f]}{r}\right).$$

Now applying (12) to the first term of (8) twice, letting the general function f first be $\frac{\partial T_{ij}}{\partial y_j}$ and then be T_{ij}, yields

$$(13)\quad \int_V \frac{1}{r}\left[\frac{\partial^2 T_{ij}}{\partial y_i \partial y_j}\right] dV(y) = \frac{\partial^2}{\partial x_j \partial x_i}\int_V \frac{[T_{ij}]}{r}\, dV(y)$$

$$+ \frac{\partial}{\partial x_i}\int_V \frac{\partial}{\partial y_j}\left(\frac{[T_{ij}]}{r}\right) dV(y)$$

$$+ \int_V \frac{\partial}{\partial y_i}\left(\frac{1}{r}\left[\frac{\partial T_{ij}}{\partial y_j}\right]\right) dV(y)$$

which, upon application of the divergence theorem, becomes

$$(14)\quad \int_V \frac{1}{r}\left[\frac{\partial^2 T_{ij}}{\partial y_i \partial y_j}\right] dV(y) = \frac{\partial^2}{\partial x_i \partial x_j}\int_V \frac{[T_{ij}]}{r}\, dV(y)$$

$$+ \frac{\partial}{\partial x_i}\int_S \ell_j \frac{[T_{ij}]}{r}\, dS(y)$$

$$+ \int_S \frac{\ell_i}{r}\left[\frac{\partial T_{ij}}{\partial y_j}\right] dS(y).$$

ℓ_j is the direction cosine of $\vec{n}$.

Holding (14) in abeyance and noting that for any function (f), $\frac{\partial f}{\partial n} = \frac{\partial f}{\partial y_i} \ell_i$, permits expression of the second term of (8) as

$$\frac{1}{4\pi} \int_S \left[\frac{1}{r} \frac{\partial \rho}{\partial n} + \frac{1}{r^2} \frac{\partial r}{\partial n} \rho + \frac{1}{a_o r} \frac{\partial r}{\partial n} \frac{\partial \rho}{\partial t}\right] dS(y)$$

$$= \frac{1}{4\pi} \int_S \frac{\ell_i}{r} \left[\frac{\partial \rho}{\partial y_i}\right] dS(y)$$

$$+ \frac{1}{4\pi} \int_S \ell_i \left(\frac{1}{r^2} \frac{\partial r}{\partial y_i}[\rho] + \frac{1}{a_o r} \frac{\partial r}{\partial y_i}\left[\frac{\partial \rho}{\partial t}\right]\right) dS(y).$$

Applying (11) to the second term of this expression yields

$$(15) \quad \frac{1}{4\pi} \int_S \left[\frac{1}{r} \frac{\partial \rho}{\partial n} + \frac{1}{r^2} \frac{\partial r}{\partial n} \rho + \frac{1}{a_o r} \frac{\partial r}{\partial n} \frac{\partial \rho}{\partial t}\right] dS(y)$$

$$= \frac{1}{4\pi} \int_S \frac{\ell_i}{r} \left[\frac{\partial (\rho \delta_{ij})}{\partial y_j}\right] dS(y)$$

$$+ \frac{1}{4\pi} \frac{\partial}{\partial x_i} \int_S \ell_i \frac{[\rho]}{r} dS(y).$$

Then, the appropriate form for interpreting (8) is obtained by combining (8), (14) and (15).

$$(16) \quad \rho(x,t) - \rho_o = \frac{1}{4\pi a_o^2} \frac{\partial^2}{\partial x_i \partial x_j} \int_V \frac{[T_{ij}]}{r} dV(y)$$

$$+ \frac{1}{4\pi a_o^2} \frac{\partial}{\partial x_i} \int_S \frac{\ell_j}{r}[a_o^2 \rho \delta_{ij} + T_{ij}] dS(y)$$

$$+ \frac{1}{4\pi a_o^2} \int_S \frac{\ell_i}{r} \left[\frac{\partial}{\partial y_j}(a_o^2 \rho \delta_{ij} + T_{ij})\right] dS(y).$$

In (16), the monopole and dipole terms from the homogeneous solution appear as does an original quadrupole contribution arising from the flow. Additionally, the second part of the second and third terms shows that the interaction of the flow with the boundary produces monopole and dipole sound contributions as well. Finally, using (4) and (5) in the latter two terms of (6) results in

$$(17) \quad \rho(x,t) - \rho_o = \frac{1}{4\pi a_o^2} \frac{\partial^2}{\partial x_i \partial x_j} \int_V \frac{[T_{ij}]}{r} dV(y) + \frac{1}{4\pi a_o^2} \frac{\partial}{\partial x_i} \int_S \frac{\ell_j}{r}[\rho\, v_i\, v_j + p_{ij}]\, dS(y) - \frac{1}{4\pi a_o^2} \int_S \frac{\ell_i}{r} [\frac{\partial(\rho v_i)}{\partial t}]\, dS(y),$$

the form most appropriate for the present application. An original quadrupole contribution of strength T_{ij} again appears in this equation. The second term is a summed distribution of dipoles, with axis in the i direction, of strength $(\rho\, v_i\, v_{normal} + p_{inormal})$ at the internal boundary, and the third term is a distribution of monopole sources of strength $\rho\, v_{normal}$ at this boundary.

APPLICATION TO UNIFORM CYLINDERS

Before applying (17) to the case of interest, namely cylinders, it is useful to examine the first term. Both Lighthill and Curle noted that this quadrupole field is of order $(M_a)^2$ below that of the dipole term, where M_a is the

ratio of flow speed to sound speed.[18,19] Since, in the experiment under consideration, M_a is less than 0.15, ignoring this term introduces an error of less than two percent in sound pressure and less than 0.4 percent in intensity. Equation (17) is thus simplified to

$$(18) \quad \rho(x,t) - \rho_o = -\frac{1}{4\pi a_o^2} \int_S \frac{\ell_i}{r} \left[\frac{\partial(\rho v_i)}{\partial t}\right] dS(y) + \frac{1}{4\pi a_o^2} \frac{\partial}{\partial x_i} \int_S \frac{\ell_j}{r} [\rho\, v_i\, v_j + p_{ij}]\, dS(y).$$

To further reduce complexity, ρ may be equated to ρ_o on the right side of (18), permitting it to be removed from the integral in the first term.

Continued reduction then requires specification of the characteristics of the uniform cylinder under consideration. Here, three cases are of interest; stationary cylinders, non-stationary but rigid so that all motion is that of a rigid body, and both non-rigid and non-stationary.

Stationary Cylinders.

Since v_i is identically zero, application of (11) to perform the differentiation in the second term immediately converts (18) to

$$(19) \quad \rho(x,t) - \rho_o = -\frac{1}{4\pi a_o^3} \int_S \frac{\ell_j}{r} \frac{\partial r}{\partial x_i} \left[\frac{\partial p_{ij}}{\partial t}\right] dS(y) - \frac{1}{4\pi a_o^2} \int_S \frac{\ell_j}{r^2} \frac{\partial r}{\partial x_i} [p_{ij}]\, dS(y).$$

To obtain a still more useful form, two further assumptions are appropriate. The first is that the field point is far from the cylinder relative to cylinder size ($x_i >> y_i$). Second, cylinder size is assumed small compared to the wave length of radiated sound so that retarded time is given by $t' = t - \frac{r(x)}{a_o}$, where r is a function of x alone. Then, defining P_i as the force per unit area exerted in the i direction by the fluid on the cylinder ($P_i = \ell_j \, p_{ij}$) permits rewriting (19) as

$$(20) \quad \rho(x,t) - \rho_o = - \frac{1}{4\pi a_o^3} \frac{x_i}{r^2} \int_S [\frac{dP_i}{dt}] \, dS(y)$$

$$- \frac{1}{4\pi a_o^2} \frac{x_i}{r^3} \int_S [P_i] \, dS(y) .$$

This equation is the general expression applicable to stationary cylinders; however, its experimental validation requires further specification. Such specification will be addressed later in this section, following examination of the other two cases.

Non-Stationary but Rigid Cylinders.

Following Phillips[2] and Koopmann[6], simplification begins with application of the divergence theorem to the first term of (18) after ρ_o has been removed from the integral, so that

$$(21)\quad -\frac{\rho_o}{4\pi a_o^2}\int_S \frac{\ell_i}{r}\left[\frac{\partial v_i}{\partial t}\right] dS(y) = -\frac{\rho_o}{4\pi a_o^2}\int_S \frac{\partial}{\partial y_i}\left(\frac{1}{r}\left[\frac{\partial v_i}{\partial t}\right]\right) dV(y)$$

$$= -\frac{\rho_o}{4\pi a_o^2}\int_V \frac{1}{r}\left[\frac{\partial^2 v_i}{\partial y_i \partial t}\right] dV(y)$$

$$-\frac{\rho_o}{4\pi a_o^2}\int_V \frac{x_i - y_i}{r}\left(\frac{1}{a_o r}\left[\frac{\partial^2 v_i}{\partial t^2}\right] + \frac{1}{r^2}\left[\frac{\partial v_i}{\partial t}\right]\right) dV(y)$$

where (10) has been used to differentiate with respect to y. Using (11) to perform the indicated differentiation in the second term of (16) yields

$$(22)\quad \frac{1}{4\pi a_o^2}\frac{\partial}{\partial x_i}\int_S \frac{\ell_j}{r}[\rho v_i v_j + p_{ij}]\, dS(y)$$

$$= -\frac{1}{4\pi a_o^2}\int_S \ell_j \frac{x_i - y_i}{r}\left(\frac{1}{a_o r}\left[\frac{\partial}{\partial t}(\rho v_i v_j + p_{ij})\right]\right.$$

$$\left. + \frac{1}{r^2}[\rho v_i v_j + p_{ij}]\right) dS(y),$$

and the sum of (21) and (22) is equivalent to the right side of (18).

Rigidity implies that the first integral on the right side of (21) is zero. Moreover, it also implies that v_i in the second term of (21) as well as in (22) may be replaced by $U_i + \varepsilon_{ijk}\,\omega_j y_k$ where U_i is the velocity of the cylinder's center of mass and ω_j is the angular velocity of the cylinder

about this center.* Then, again assuming that $x_i >> y_i$ and that $t' = t - \frac{r(x)}{a_o}$, and using the definition of P_i, this sum of (21) and (22) becomes

$$\text{(23)} \quad \rho(x,t) - \rho_o = -\frac{\rho_o x_i}{4\pi a_o{}^3 r^2}[\ddot{U}_i]V - \frac{\rho_o x_i}{4\pi a_o{}^3 r^2}\int_V [\frac{\partial^2}{\partial t^2}(\varepsilon_{ijk}\omega_j y_k)]dV(y)$$

$$- \frac{\rho_o x_i}{4\pi a_o{}^2 r^3}[\dot{U}_i]V - \frac{\rho_o x_i}{4\pi a_o{}^2 r^3}\int_V [\frac{\partial}{\partial t}(\varepsilon_{ijk}\omega_j y_k)]dV(y)$$

$$- \frac{\rho_o x_i}{4\pi a_o{}^3 r^2}\int_S \ell_j [\frac{\partial}{\partial t}((U_i + \varepsilon_{ik\ell}\omega_k y_\ell)(U_j + \varepsilon_{jpq}\omega_p y_q))]dS(y)$$

$$- \frac{\rho_o x_i}{4\pi a_o{}^2 r^3}\int_S \ell_j [(U_i + \varepsilon_{ik\ell}\omega_k y_\ell)(U_j + \varepsilon_{jpq}\omega_p y_q)]dS(y)$$

$$- \frac{x_i}{4\pi a_o{}^3 r^2}\int_S [\dot{P}_i]dS(y)$$

$$- \frac{x_i}{4\pi a_o{}^2 r^3}\int_S [P_i]dS(y).$$

To further simplify requires consideration of the fifth and sixth terms. Applying the divergence theorem to the integral of the sixth term, and noting that $\frac{\partial [f]}{\partial y} = [\frac{\partial f}{\partial y}]$ in

---

*Both Phillips and Koopmann omit this perhaps unusual sound field contribution resulting from rotation of a rigid cylinder in a flow. A letter noting this omission and reporting the correction developed in this paper has been sent to Professor Phillips in his capacity as an editor of the Journal of Fluid Mechanics.

(10) per the $r = r(x)$ assumption, gives

$$(24) \quad \int_S \ell_j[(U_i + \varepsilon_{ik\ell}\omega_k y_\ell)(U_j + \varepsilon_{jpq}\omega_p y_q)]dS(y)$$

$$= \int_V [\frac{\partial}{\partial y_j}((U_i + \varepsilon_{ik\ell}\omega_k y_\ell)(U_j + \varepsilon_{jpq}\omega_p y_q))]dV(y)$$

$$= \int_V [(\varepsilon_{ik\ell}\omega_k \delta_{\ell j})(U_j + \varepsilon_{jpq}\omega_p y_q)$$

$$+ (U_i + \varepsilon_{ik\ell}\omega_k y_\ell)(\varepsilon_{jpq}\omega_p \delta_{jq})]dV(y)$$

$$= \int_V [\varepsilon_{ikj}\omega_k U_j + \varepsilon_{jik}\varepsilon_{jpq}\omega_k \omega_p y_q]dV(y)$$

$$= \int_V [-\varepsilon_{ijk}U_j\omega_k + (\delta_{ip}\delta_{kq} - \delta_{kp}\delta_{iq})\omega_k\omega_p y_q]dV(y)$$

$$= \int_V [-\varepsilon_{ijk}U_j\omega_k + \omega_i\omega_j y_j - \omega_j\omega_j y_i]dV(y)$$

Similarly applying the divergence theorem to the fifth term of (23) and interchanging the order of differentiation results in an equation identical to (24) except that the retarded time derivative of the above integrand appears. In all, then, the general expression applicable to this case is

$$(25)\quad \rho(x,t) - \rho_o = -\frac{\rho_o x_i}{4\pi a_o^3 r^2}[\ddot{U}_i]V - \frac{\rho_o x_i}{4\pi a_o^3 r^2}\int_V [\frac{\partial^2}{\partial t^2}(\varepsilon_{ijk}\omega_j y_k)$$

$$-\frac{\partial}{\partial t}(\varepsilon_{ijk}U_j\omega_k - \omega_i\omega_j y_j + \omega_j\omega_j y_i)]dV(y)$$

$$-\frac{\rho_o x_i}{4\pi a_o^2 r^3}[\dot{U}_i]V - \frac{\rho_o x_i}{4\pi a_o^2 r^3}\int_V [\frac{\partial}{\partial t}(\varepsilon_{ijk}\omega_j y_k)$$

$$-(\varepsilon_{ijk}U_j\omega_k - \omega_i\omega_j y_j + \omega_j\omega_j y_i)]dV(y)$$

$$-\frac{x_i}{4\pi a_o^3 r^2}\int_S [\dot{P}_i]dS(y) - \frac{x_i}{4\pi a_o^2 r^3}\int_S [P_i]dS(y)\ .$$

Within this case, the behavior of a cylinder under synchronization is of primary interest. However, before applying (25) to this phenomenon, further definitions are in order. First, let the cylinder's axis be the Z axis and let ϕ be the polar angle at the center of the cylinder (see Figure C-1). Then the local lift force in the i direction (f_i) is given by $f_i = \int_\phi P_i \frac{d}{2}\, d\phi$, and the total force in the i direction (F_i) is $F_i = \int_Z f_i dz$, so that $F_i = \int_S P_i dS(y)$.

Now, with synchronization, as discussed on page 17, cylinder motion and the vortex shedding process interact, and the vortex wake becomes truly two dimensional. In turn, the lift and drag forces exerted by the fluid on the cylinder are in phase along Z, and $F_i = f_i L$ as no rotation is present.

Then (25) becomes

$$(26) \quad \rho(x,t) - \rho_o = - \frac{x_i}{4\pi a_o{}^3 r^2} [\rho_o \ddot{U}_i V + \dot{F}_i] - \frac{x_i}{4\pi a_o{}^2 r^3} [\rho_o \dot{U}_i V + F_i].$$

As the drag force fluctuates at twice the frequency of the lift force and with fluctuation amplitude small compared to that of the lift force[2], attention is restricted to the latter. Taking x_2 as the direction of cylinder motion, replacing the subscript "2" by "L" for lift, defining θ as the angle between x_2 and r (see Figure C-1), and converting to acoustic pressure p yields

$$(27) \quad p = - \frac{\cos\theta}{4\pi r} \left[\frac{\rho_o \ddot{U}_L V + \dot{F}_L}{a_o} + \frac{\rho_o \dot{U}_L V + F_L}{r}\right]$$

or equivalently,

$$(28) \quad p = \frac{\partial}{\partial x_L} \left[\frac{F_L + \rho_o V \dot{U}_L}{4\pi r}\right].$$

Koopmann[6] experimentally verified the second or near field term of (27).

Finally, it should be noted that (27) and (28) relate the phase of radiated sound to that of both lift force and cylinder motion.

Non-Rigid and Non-Stationary.

Equations (21) and (22), derived for the previous case before introduction of assumptions peculiar to that case, apply to this still more general consideration. As before, their sum represents the total sound field and also as before, the $x_i >> y_i$ as well as the $t' = t - \frac{r(x)}{a_o}$ assumptions are made. Then again defining P_i and adding (21) and (22) yields

$$(29) \quad \rho(x,t) - \rho_o = -\frac{\rho_o}{4\pi a_o^2 r} \int_V [\frac{\partial^2 v_i}{\partial y_i \partial t}] \, dV(y)$$

$$- \frac{\rho_o x_i}{4\pi a_o^3 r^2} \int_V [\frac{\partial^2 v_i}{\partial t^2}] dV(y) - \frac{\rho_o x_i}{4\pi a_o^2 r^3} \int_V [\frac{\partial v_i}{\partial t}] dV(y)$$

$$- \frac{x_i}{4\pi a_o^3 r^2} \int_S \ell_j [\frac{\partial}{\partial t}(\rho \, v_i \, v_j)] dS(y)$$

$$- \frac{x_i}{4\pi a_o^2 r^3} \int_S \ell_j [\rho \, v_i \, v_j] dS(y)$$

$$- \frac{x_i}{4\pi a_o^3 r^2} \int_S [\frac{\partial P_i}{\partial t}] dS(y) - \frac{x_i}{4\pi a_o^2 r^3} \int_S [P_i] dS(y)$$

In a manner still parallel to previous results, the last two terms are seen as far and near field contributions from the flow-caused lift force. The first term is unique to this complex case and is the source contribution resulting from cylinder deformation. The remaining terms, then, are

the far (second and fourth terms) and near (third and fifth terms) field dipole contributions attributable to cylinder motion.

To verify this explanation, however, it is desirable to make several assumptions which will produce tractable mathematics. Therefore, restricted cylinder deformation and motion are stipulated as follows: the only deformation is pure dilatation, and cylinder motion is such that each cross section moves as a rigid body so that the cylinder may be viewed as vibrating like a thick string.

With these assumptions in hand, the first term of (29) now will be simplified. In this term, the volume V(y) refers to the volume of the cylinder; within this volume, continuity (1) holds and thus

$$\frac{\partial \rho_c}{\partial t} + v_i \frac{\partial \rho_c}{\partial y_i} + \rho_c \frac{\partial v_i}{\partial y_i} = 0$$

where ρ_c is the density of the cylinder ($\rho_c = m/V$). Uniform dilatation implies that $\frac{\partial \rho_c}{\partial y_i} = 0$, and hence $\frac{\partial v_i}{\partial y_i} = -\frac{1}{\rho_c}\frac{\partial \rho_c}{\partial t}$ for this case. Therefore,

$$-\frac{\rho_o}{4\pi a_o^2 r}\int_V\left[\frac{\partial^2(v_i)}{\partial y_i \partial t}\right]dV(y) = \frac{\rho_o}{4\pi a_o^2 r}\int_V\left[\frac{\partial}{\partial t}\left(\frac{1}{\rho_c}\frac{\partial \rho_c}{\partial t}\right)\right]dV(y).$$

Taking the derivative of the integrand gives

$$\frac{\partial}{\partial t}\left(\frac{1}{\rho_c}\frac{\partial \rho_c}{\partial t}\right) = -\frac{1}{\rho_c^2}\left(\frac{\partial \rho_c}{\partial t}\right)^2 + \frac{1}{\rho_c}\frac{\partial^2 \rho_c}{\partial t^2}.$$

The dilatation now is assumed small so that the second order term may be ignored. Evaluating the second derivative,

$$\frac{\partial}{\partial t}\left(\frac{\partial \rho_c}{\partial t}\right) = \frac{\partial}{\partial t}\frac{\partial\left(\frac{m}{V}\right)}{\partial t} = \frac{\partial}{\partial t}\left(-\frac{m}{V^2}\frac{\partial V}{\partial t}\right) = -\frac{\rho_c}{V}\frac{\partial^2 V}{\partial t^2} \quad \text{to first order.}$$

Hence,

$$-\frac{\rho_o}{4\pi a_o{}^2 r}\int_V \left[\frac{\partial^2 v_i}{\partial t \partial y_i}\right] dV(y) = -\frac{\rho_o}{4\pi a_o{}^2 r}\int_V \left[\frac{1}{V}\frac{\partial^2 V}{\partial t^2}\right] dV(y)$$

Finally, uniform dilatation implies that the integrand is independent of y.

Thus,

$$-\frac{\rho_o}{4\pi a_o{}^2 r}\int_V \left[\frac{\partial^2 v_i}{\partial t \partial y_i}\right] dV(y) = -\frac{\rho_o}{4\pi a_o{}^2 r}\left[\frac{1}{V}\frac{d^2 V}{dt^2}\right] V$$

$$(30) \qquad = -\frac{\rho_o}{4\pi a_o{}^2 r}[\ddot{V}] \qquad \text{to first order.}$$

(30) is the source contribution previously reported by Fitzpatrick and Strassberg.[23]

Of the terms which in general describe cylinder motion the two surface integrals, the fourth and fifth terms of (29), are best approached first. In these terms, setting $\rho = \rho_o$ followed by subsequent application of the divergence theorem results in volume integrals, the integrands of which are of the form

$$[\frac{\partial}{\partial y_j} (v_i \ v_j)]$$

where the order of the time and space derivatives are interchanged as required.

The specific vibratory motion previously assumed now permits definition of the quantity $u_i(z,t')$, the velocity of a rigid segment, of length dz, of the cylinder (see Figure C-1). The assumption also requires that the direction of u be perpendicular to z for small amplitude motion.

Then, the integral over the volume, of this derivative, involves terms of the form

$$u_i \frac{\partial u_j}{\partial y_j} + u_j \frac{\partial u_i}{\partial y_j} ,$$

which by rigidity of the dz segment are zero unless j = z. However, if j = z, then $u_j = u_z = 0$, and therefore, the fourth and fifth terms are zero.

The remaining sound field contribution, then, results from the second and third terms of (29). Letting A be the cross sectional area of the cylinder and using the definition of u_i gives

$$(31) \quad - \frac{\rho_o x_i}{4\pi a_o{}^3 r^2} \int_V [\frac{\partial^2 v_i}{\partial t^2}] dV - \frac{\rho_o x_i}{4\pi a_o{}^2 r^3} \int_V [\frac{\partial v_i}{\partial t}] dV$$

$$= - \frac{\rho_o x_i A}{4\pi a_o{}^3 r^2} \int_z [\frac{\partial^2 u_i}{\partial t^2}] dz - \frac{\rho_o x_i A}{4\pi a_o{}^2 r^3} \int_z [\frac{\partial u_i}{\partial t}] dz.$$

The first of these is identical to that reported by Leehey and Hanson[25] as describing the far field contribution of cylinder vibration. The second is the corresponding near field contribution. It is also pertinent to note that if u_i is z independent, then $u_i = U_i$, and this expression reduces to the corresponding portion of that derived for a rigidly moving cylinder (27).

In all, therefore, the explanation of (29) has been shown valid for several specific cases, with results derived herein in agreement with results reported but not derived in the literature. Equation (29) is the most general expression, but reduction of it to useful form would be extremely difficult without appropriate assumptions; nevertheless, it contains the two previously addressed simpler cases.

Before addressing in detail the further application of the stationary cylinder result (20) to the present experiment, two notes should be added. First, the contribution to the sound field from either dilatation (30) or vibratory motion (31) have been shown by Leehey and Hanson[25], based on the approach of Laird and Cohen[47], to be at minimum some 25 db below that of the lift force. This emphasizes the fact that aeolian tones are not analogous to the sound produced by a plucked string; instead they are caused by the fluctuating lift force and occur with or without cylinder motion of any sort, although motion may result in their amplification.

Second, the preceding development did not account for boundary motion (i.e., for the time dependence of the coordinates of a surface element (dS)). A completely rigorous mathematical development would replace (8) with Morgans'[48] modification of the Kirchhoff solution to the wave equation, a modification which includes boundary motion. However, examination of Morgans' formula reveals that so long as the Mach number (now defined as the ratio of boundary velocity to sound speed) and the ratio of body size to sound wavelength are small, the original Kirchhoff expression is only insignificantly affected. Therefore, (8) is indeed a sound basis for the above development.

APPLICATION TO THE PRESENT EXPERIMENT

The present experiment is concerned primarily with far field sound intensity emanating from stationary cylinders. The governing equation is that derived for uniform smooth cylinders with the near-field term omitted.

$$(32)\quad \rho(x,t) - \rho_o = -\frac{x_i}{4\pi a_o{}^3 r^2} \int_S [\dot{P}_i]\, dS(y)$$

This single term still presents difficulty in that, in general, minute variation of cylinder diameter or slight instability in the incoming flow cause three dimensional effects in the vortex wake; in turn, the lift force then is not phase invariant along the length of the cylinder. Although the previous definition of f_i and F_i still apply

(see page 33), F_i no longer is equal to $f_i L$. Accordingly, evaluation of (32) first requires the introduction of additional concepts.

In the three term sum on the right side of (32), only the second or i = 2 term (see Figure C-1) is of significant magnitude. Retaining only this term, replacing the subscript 2 by L for lift, using the definition of f_i, and converting to acoustic pressure (p) permits (32) to be rewritten as

$$(33) \quad p = -\frac{1}{4\pi a_o} \frac{\cos\theta}{r} \int_0^L \dot{f}_L(z,t')\,dz.$$

Following Graham,[49] the local lift force, regardless of its phase variation with z, is assumed to be narrowband and sinusoidal. Then $\dot{f}_L = \omega f_L e^{i\pi/2}$, and

$$(34) \quad p = -\frac{\omega}{4\pi a_o} \frac{\cos\theta}{r} e^{i\pi/2} \int_0^L f_L(z,t')\,dz.$$

However, (34) cannot be verified because of f_L's varying phase. Therefore, attention is focused on the mean square pressure amplitude,

$$(35) \quad p^2 = \frac{\omega^2}{16\pi^2 a_o^2} \frac{\cos^2\theta}{r^2} \int_{z_1=0}^{L} \int_{z_2=0}^{L} \overline{f_{L_1}(z_1,t) f_{L_2}(z_2,t)}\,dz_1 dz_2,$$

where the bar indicates a time average and where the statistics of the local lift force are assumed invariant with z and t. That is, the local lift force is assumed stationary in the statistical sense (which is not to be confused with

the cylinder remaining stationary in the physical sense). Of course $\overline{F_L^2}$, the mean square lift force, is given by

(36) $$\overline{F_L^2} = \int_0^L \int_0^L \overline{f_{L_1}(z_1,t) f_{L_2}(z_2,t)}\, dz_1 dz_2 \ .$$

The problem then is to evaluate

(37) $$p^2 = \frac{\omega^2}{16\pi^2 a_o^2} \frac{\cos^2\theta}{r^2} \overline{F_L^2} \ .$$

To this end, as suggested by Frenkiel[24], define the correlation function $R(\gamma)$ by

(38) $$R(\gamma) = \frac{\overline{f_{L_1}(z_1,t) f_{L_2}(z_2,t)}}{\overline{f_L^2}}$$

where $R(\gamma)$ is a function of $\gamma = z_2 - z_1$ alone (see Figure C-2). Define the correlation length (ℓ_c) by

(39) $$\ell_c = \int_{-L}^{L} R(\gamma)\, d\gamma.$$

Then

(40) $$\ell_c = 2 \int_0^L R(\gamma) d\gamma$$

as $R(\gamma)$, by virtue of its definition, is an even function. Let $\overline{\gamma}$ be the centroid of the area under the right half of the correlation curve (the plot of $R(\gamma)$ vs γ).

$$(41) \qquad \bar{\gamma} = \frac{\int_0^L \gamma R(\gamma)\,d\gamma}{\int_0^L R(\gamma)\,d\gamma} = \frac{\int_0^L \gamma R(\gamma)\,d\gamma}{\ell_c/2}$$

Then, substituting $R(\gamma)$ into the integral of (36) yields

$$(42) \qquad \overline{F_L^{\,2}} = \int_0^L \int_0^L \overline{f_{L_1}(z_1,t) f_{L_2}(z_2,t)}\; dz_1 dz_2$$

$$= \int_0^L \int_0^L \overline{f_L^{\,2}}\, R(\gamma) dz_1 dz_2 \ .$$

As f_L is stationary, $\overline{f_L^{\,2}}$ may be removed from the integral, and the problem becomes the evaluation of $\int_0^L \int_0^L R(\gamma) dz_1 dz_2$. To accomplish this evaluation, substitute $\gamma + z_1$ for z_2.

$$\int_0^L \int_0^L R(\gamma) dz_1 dz_2 = \int_{z_1=0}^{L} \int_{\gamma=-z_1}^{L-z_1} R(\gamma)\, d\gamma dz_1$$

Now integrate by parts with respect to z_1;

$$\text{let } \tilde{u} = \int_{\gamma=-z_1}^{L-z_1} R(\gamma)\,d\gamma \qquad d\tilde{v} = dz_1,$$

so that

$$d\tilde{u} = \frac{d\tilde{u}}{dz_1}\, dz_1 \qquad \tilde{v} = z_1.$$

Using Liebnitz' rule to evaluate $\frac{d\tilde{u}}{dz_1}$, noting that $R(\gamma)$ is a function of γ alone, gives $\frac{d\tilde{u}}{dz_1} = R(-z_1) - R(L - z_1)$, and

so the integral is

$$\int_0^L \int_0^L R(\gamma)\,dz_1 dz_2 = \left[z_1 \int_{\gamma=-z_1}^{L-z_1} R(\gamma)\,d\gamma\right]_{z_1=0}^{L}$$

$$+ \int_0^L z_1 R(L-z_1)\,dz_1 - \int_0^L z_1 R(-z_1)\,dz_1$$

Substituting γ for $L - z_1$ and for $-z_1$ respectively in the latter two integrals gives

$$\int_0^L \int_0^L R(\gamma)\,dz_1 dz_2 = L \int_{-L}^{0} R(\gamma)\,d\gamma - \int_L^0 (L-\gamma) R(\gamma)\,d\gamma - \int_0^{-L} \gamma R(\gamma)\,d\gamma$$

$$= 2L \int_0^L R(\gamma)\,d\gamma - 2\overline{\gamma} \int_0^L R(\gamma)\,d\gamma$$

since $R(\gamma)$ is even and $\gamma R(\gamma)$ is odd. Finally, using the definitions of ℓ_c and $\overline{\gamma}$,

$$\int_0^L \int_0^L R(\gamma)\,dz_1 dz_2 = (L - \overline{\gamma})\ \ell_c \tag{43}$$

Hence, $\overline{F_L^{\,2}}$ has been shown to be given by

$$\overline{F_L^{\,2}} = \overline{f_L^{\,2}}\ (L - \overline{\gamma})\ \ell_c\ . \tag{44}$$

With synchronization, the flow is correlated (i.e., two dimensional).

$$R(\gamma) = 1, \quad 0 \leq \gamma \leq L. \quad \ell_c = 2L, \quad \overline{\gamma} = \frac{\ell_c}{4} = \frac{L}{2}$$

and

$$\overline{F_L^2} = \overline{f_L^2}\, L^2$$

as required.

In a highly uncorrelated flow, $R(\gamma)$ is approximately $\ell_c\, \delta(\gamma)$, $\overline{\gamma} = 0$, and $\overline{F_L^2} = \overline{f_L^2}\, L\, \ell_c$. Thus ℓ_c and $\overline{\gamma}$ are the factors accounting for the reduction in F_L caused by phase variation in f_L. The total lift force is that which would be produced by a shorter cylinder of length $\sqrt{(L-\overline{\gamma})\,\ell_c}$, having in-phase lift forces. Alternatively, ℓ_c may be considered an effective length, with $\overline{\gamma}$ a first order correction term. Physically, then, ℓ_c is about twice the length over which f_L is approximately phase invariant.

Substituting (44) into (37) yields

$$(45) \qquad p^2 = \frac{\omega^2}{16\,\pi^2 a_o^{\,2}} \; \frac{\cos^2\theta}{r^2} \; \overline{f_L^2}\,(L - \overline{\gamma})\; \ell_c,$$

and the acoustic intensity I is

$$(46) \qquad I = \frac{\omega^2}{16\pi^2 a_o^{\,3} \rho_o} \; \frac{\cos^2\theta}{r^2} \; \overline{f_L^2}\,(L - \overline{\gamma})\; \ell_c.$$

To express I in the form more often seen in the literature, define the root mean square local lift coefficient

$$(47) \qquad C_L = \frac{\sqrt{\overline{f_L^{\,2}}}}{\frac{1}{2}\rho_o \overline{U}^2 d}$$

Then, substituting $\frac{2\pi S\overline{U}}{d}$ for ω yields the desired form that was verified experimentally by Leehey and Hanson[25] at two discrete Reynolds numbers.

$$(48) \qquad I(\omega) = \frac{1}{16} \frac{\rho_o}{a_o^{\,3}} \frac{\cos^2\theta}{r^2} C_L^{\,2} \, \overline{U}^6 \, S^2 \, (L - \overline{\gamma}) \, \ell_c$$

As noted previously, in the current experiment, F_L is measured vice f_L. Therefore, for this experiment, the appropriate equation is

$$(49) \qquad I = \frac{\omega^2}{16\pi^2 \rho_o a_o^{\,3}} \; \frac{\cos^2\theta}{r^2} \overline{F_L^{\,2}}$$

which was obtained directly from (37). Of course, by the above development, (49) is equivalent to (48) for uniform smooth cylinders, but it has the additional advantage of applicability to any stationary rigid cylinder, regardless of the relationship between F_L and f_L for that cylinder.

NEW APPLICATIONS

The previous results apply only to uniform smooth cylinders. Although the present experiment involves cylinders of this type, it also studies other configurations. In particular, it is concerned with cylinders on which

uniform smooth sections are divided at regular intervals by fins or notches (see Figure C-3). Accordingly, this section extends the previously developed results to such cylinders. Following this extension it also briefly addresses the more complex case of a cylinder with a sinusoidal surface (see Figure C-4).

<u>Regularly Divided Cylinders</u>.

As (49) is valid for any rigid stationary cylinder, it of course is applicable for the subclass of periodically divided cylinders. Application of (49), then, only requires that F_L be related to both f_L and measurable correlation factors. However, the determination of this relation first requires further definition. This definition, in turn, will be followed by a development paralleling that used to obtain (44).

Let the cylinder of length L be divided by M partitions into M+1 segments each of length L'. (L' = L/(M+1)).

Between partitions, define $R_w(\gamma)$ by

$$R_w(\gamma) = \frac{\overline{f_{L_1}(z_1,t)\, f_{L_2}(z_2,t)}}{\overline{f_L^{\,2}}}, \tag{50}$$

z_1 and z_2 within the same partition. As f_L is stationary, $R_w(\gamma)$ is a function of $\gamma = z_2 - z_1$ alone. Similarly define ℓ_{c_w} and $\overline{\gamma}_w$:

$$(51) \qquad \ell_{c_W} = 2 \int_0^{L'} R_W(\gamma)\, d\gamma$$

$$(52) \qquad \bar{\gamma}_W = \frac{\int_0^{L'} \gamma R_W(\gamma)\, d\gamma}{\ell_{c_W}/2}$$

Across partitions, define γ by $\gamma = z_2 - z_1$ with the stipulation that γ in the interval $((n-1)L', (n+1)L')$ implies that z_1 and z_2 are in segments separated by n partitions, n a positive integer (see Figure C-3).

Subject to this stipulation, $R_A(\gamma)$, defined by

$$(53) \qquad R_A(\gamma) = \frac{\overline{f_{L_1}(z_1,t)\, f_{L_2}(z_2,t)}}{\overline{f_L^{\,2}}},$$

is a function of γ alone.

Define:

$$(54) \qquad \ell_{c_A} = 2 \int_0^{L} R_A(\gamma)\, d\gamma$$

$$(55) \qquad \bar{\gamma}_A = \frac{\int_0^{L} \gamma R_A(\gamma)\, d\gamma}{\ell_{c_A}/2}$$

$$(56) \qquad \ell_{c_A}' = 2 \int_0^{L'} R_A(\gamma)\, d\gamma$$

$$(57) \qquad \bar{\gamma}_A' = \frac{\int_0^{L'} \gamma R_A(\gamma)\, d\gamma}{\ell_{c_A}'/2}$$

By definition, as before

$$(36) \qquad \overline{F_L^2} = \int_0^L \int_0^L \overline{f_{L_1} f_{L_2}} \, dz_1 dz_2 \; .$$

Expanding each component integral of (36) into the sum of integrals over segments within partitions gives

$$(58) \quad \overline{F_L^2} = \sum_{i=0}^{M} \int_{z_1=iL'}^{(i+1)L'} \int_{z_2=iL'}^{(i+1)L'} \overline{f_{L_1} f_{L_2}} \, dz_1 dz_2$$

$$+ \sum_{i=0}^{M} \sum_{\substack{j=0 \\ i \neq j}}^{M} \int_{z_1=iL'}^{(i+1)L'} \int_{z_2=jL'}^{(j+1)L'} \overline{f_{L_1} f_{L_2}} \, dz_1 dz_2$$

As $R_w(\gamma)$ must be of identical form within each segment, the first sum of (37) is equivalent to the sum of (M+1) integrals over any segment, say, the first; thus,

$$\sum_{i=0}^{M} \int_{z_1=iL'}^{(i+1)L'} \int_{z_2=iL'}^{(i+1)L'} \overline{f_{L_1} f_{L_2}} \, dz_1 dz_2$$

$$= (M+1) \int_0^{L'} \int_0^{L'} \overline{f_{L_1} f_{L_2}} \, dz_1 dz_2$$

$$= (M+1) \int_0^{L'} \int_0^{L'} \overline{f_L^2} \, R_w(\gamma) \, dz_1 dz_2 ,$$

where (50) has been applied. Comparison of the last expression with (42) reveals an exact parallel, and therefore

$$(59)\quad \sum_{i=0}^{M} \int_{z_1=iL'}^{(i+1)L'} \int_{z_2=iL'}^{(i+1)L'} \overline{f_{L_1} f_{L_2}}\, dz_1 dz_2$$

$$= \overline{f_L^{\,2}}\,(M+1)(L'-\overline{\gamma}_w)\,\ell_{c_w}$$

is immediately obtained.

It remains, then, to evaluate the second term of (58). Applying (53) and removing $\overline{f_L^{\,2}}$ from the integral permits expression of this second term (Y) as

$$Y = \sum_{i=0}^{M} \sum_{\substack{j=0 \\ i\neq j}}^{M} \int_{z_1=iL'}^{(i+1)L'} \int_{z_2=jL'}^{(j+1)L'} \overline{f_{L_1} f_{L_2}}\, dz_1 dz_2$$

$$= \overline{f_L^{\,2}} \sum_{i=0}^{M} \sum_{\substack{j=0 \\ i\neq j}}^{M} \int_{z_1=iL'}^{(i+1)L'} \int_{z_2=jL'}^{(j+1)L'} R_A(\gamma)\, dz_1 dz_2$$

Substituting $\gamma+z_1$ for z_2,

$$\frac{Y}{\overline{f_L^{\,2}}} = \sum_{i=0}^{M} \sum_{\substack{j=0 \\ i\neq j}}^{M} \int_{z_1=iL'}^{(i+1)L'} \int_{\gamma=jL'-z_1}^{(j+1)L'-z_1} R_A(\gamma)\, d\gamma dz_1 .$$

Integrating by parts with respect to z_1, let

$$\tilde{u} = \int_{jL'-z_1}^{(j+1)L'-z_1} R_A(\gamma)\,d\gamma \qquad d\tilde{v} = dz_1 \ ,$$

so that

$$d\tilde{u} = \frac{d\tilde{u}}{dz_1}\,dz_1 \qquad \tilde{v} = z_1 \ .$$

Using Liebnitz' rule to evaluate $\frac{d\tilde{u}}{dz_1}$ gives

$$\frac{d\tilde{u}}{dz_1} = R_A(jL'-z_1) - R_A((j+1)L'-z_1) \ ,$$

whence

$$\frac{Y}{f_L^{\,2}} = \sum_{i=0}^{M} \sum_{\substack{j=0\\ i\neq j}}^{M} \{[z_1 \int_{jL'-z_1}^{(j+1)L'-z_1} R_A(\gamma)\,d\gamma]_{z_1=iL'}^{z_1=(i+1)L'}$$

$$- \int_{iL'}^{(i+1)L'} z_1\, R_A(jL'-z_1)\,dz_1$$

$$+ \int_{iL'}^{(i+1)L'} z_1\, R_A((j+1)L'-z_1)\,dz_1$$

Substituting γ for $(jL'-z_1)$ and $((j+1)L'-z_1)$ respectively in the last two integrals gives:

$$(60)\quad \frac{Y}{f_L^{\,2}} = \sum_{\substack{i=0\\ i\neq j}}^{M} \sum_{j=0}^{M} \{(i+1)L' \int_{(j-i-1)L'}^{(j-i)L'} R_A(\gamma)\,d\gamma$$

$$- iL' \int_{(j-i)L'}^{(j-i+1)L'} R_A(\gamma)\,d\gamma$$

$$+ jL' \int_{(j-i)L'}^{(j-i-1)L'} R_A(\gamma)\,d\gamma$$

$$- (j+1)L' \int_{(j-i+1)L'}^{(j-i)L'} R_A(\gamma)\,d\gamma$$

$$+ \int_{(j-i+1)L'}^{(j-i)L'} \gamma R_A(\gamma)\,d\gamma$$

$$- \int_{(j-i)L'}^{(j-i-1)L'} \gamma R_A(\gamma)\,d\gamma\}$$

Consider first the last two terms of (60). In the fifth let $k = j+1$; then

$$(61)\quad \sum_{\substack{i=0\\ i\neq j}}^{M} \sum_{j=0}^{M} \int_{(j-i+1)L'}^{(j-i)L'} \gamma R_A(\gamma)\,d\gamma$$

$$= \sum_{i=0}^{M} \sum_{\substack{k=1\\ k\neq(i+1)}}^{M+1} \int_{(k-i)L'}^{(k-i-1)L'} \gamma R_A(\gamma)\,d\gamma$$

Changing the dummy index on the right from k to j and subtracting the last term of (60) from the right side of (61) gives:

$$(62)\quad \sum_{i=0}^{M}\sum_{\substack{j=0\\ i\neq j}}^{M}\left[\int_{(j-i+1)L'}^{(j-i)L'}\gamma R_A(\gamma)\,d\gamma - \int_{(j-i)L'}^{(j-i-1)L'}\gamma R_A(\gamma)\,d\gamma\right.$$

$$= \sum_{i=0}^{M-1}\int_{[M-(i-1)]L'}^{(M-i)L'}\gamma R_A(\gamma)\,d\gamma + \sum_{i=1}^{M}\int_{0}^{-L'}\gamma R_A(\gamma)\,d\gamma$$

$$- \sum_{i=1}^{M}\int_{-iL'}^{-(i+1)L'}\gamma R_A(\gamma)\,d\gamma - \sum_{i=0}^{M-1}\int_{-L'}^{0}\gamma R_A(\gamma)\,d\gamma$$

$$= -\left(\int_0^{L}\gamma R_A(\gamma)\,d\gamma - \int_0^{L'}\gamma R_A(\gamma)\,d\gamma\right) + M\int_0^{L'}\gamma R_A(\gamma)\,d\gamma$$

$$-\left(\int_0^{L}\gamma R_A(\gamma)\,d\gamma - \int_0^{L'}\gamma R_A(\gamma)\,d\gamma\right) + M\int_0^{L'}\gamma R_A(\gamma)\,d\gamma$$

(since $\gamma R_A(\gamma)$ is an odd function)

$$= 2(M+1)\int_0^{L'}\gamma R_A(\gamma)\,d\gamma - 2\int_0^{L}\gamma R_A(\gamma)\,d\gamma$$

$$= (M+1)\,\overline{\gamma}_A{}'\,\ell_{c_A}{}' - \overline{\gamma}_A\,\ell_{c_A}$$

Similarly, for the first four terms of (60), now denoted by X, interchange i and j in the third and fourth terms. Then, noting that $R_A(\gamma)$ is an even function gives:

$$X = 2 \sum_{\substack{i=0 \\ i\neq j}}^{M} \sum_{j=0}^{M} \left[(i+1)L' \int_{[j-(i+1)]L'}^{(j-i)L'} R_A(\gamma)\,d\gamma - iL' \int_{(j-i)L'}^{[j-(i-1)]L'} R_A(\gamma)\,d\gamma \right].$$

Then, in the first term on the right, using the substitution $k = i+1$ to obtain new limits and then replacing the dummy index k by i gives

$$X = 2 \sum_{\substack{j=0 \\ j\neq i-1}}^{M} \sum_{i=1}^{M+1} i \int_{(j-i)L'}^{(j-(i-1))L'} R_A(\gamma)\,d\gamma$$

$$- 2 \sum_{\substack{j=0 \\ i\neq j}}^{M} \sum_{i=0}^{M} i \int_{(j-i)L'}^{[j-(i-1)]L'} R_A(\gamma)\,d\gamma.$$

Performing the indicated subtraction, again noting that $R_A(\gamma)$ is even and using the definitions of ℓ_{c_A} and ℓ_{c_A}', results in

$$(63) \qquad X = (M+1)L'(\ell_{c_A} - \ell_{c_A}') = L(\ell_{c_A} - \ell_{c_A}')$$

Combining (60), (62) and (63) reveals that

$$\frac{Y}{f_L^{\,2}} = (L - \overline{\gamma}_A)\ \ell_{c_A} - (M+1)(L' - \overline{\gamma}_A')\ \ell_{c_A}'$$

Therefore upon including the result of (59), (58) has been shown to be

$$\text{(64)} \quad \overline{F_L^{\,2}} = \overline{f_L^{\,2}}((M+1)(L'-\overline{\gamma}_W)\ell_{c_W} - (M+1)(L'-\overline{\gamma}_A{}')\ell_{c_A}{}' + (L-\overline{\gamma}_A)\ell_{c_A}).$$

It should be noted that (64) reduces correctly to the previous smooth cylinder result (44) because in the absence of periodic divisions, $R_A(\gamma) = R(\gamma)$, $\ell_{c_A} = \ell_c$, $\overline{\gamma}_A = \overline{\gamma}$, $\ell_{c_W} = \ell_{c_A}{}'$ and $\overline{\gamma}_W = \overline{\gamma}_A{}'$. Moreover, (64) is intuitively satisfying in that the correlation factor is the sum of correlation within divisions and correlation across divisions, less that portion of across-division correlation which is counted too often in the formation of this sum.

Finally, using (64) in (49) yields the expression

$$\text{(65)} \quad I(\omega) = \frac{\omega^2}{16\pi^2 \rho_o a_o^{\,3}} \frac{\cos^2\theta}{r^2} \overline{f_L^{\,2}}[(M+1)(L'-\overline{\gamma}_W)\ell_{c_W} - (M+1)(L'-\overline{\gamma}_A{}')\ell_{c_A}{}' + (L-\overline{\gamma}_A)\ell_{c_A}]$$

for the sound intensity radiated from a regularly divided cylinder.

The derivation of (65) assumed that periodic divisions only affected the phase of f_L. If, on the other hand,

cylinder-flow interactions causing amplitude variation in f_L are present as well, then (65) is not totally appropriate. Although this equation could still serve to approximate the radiated intensity, it should be used with great caution in such cases.

Sinusoidal Cylinders

The case of a cylinder with a sinusoidal surface (see Figure C-4a) is still more complicated. Variation of diameter with z implies variation of both the local Strouhal number and the local Reynolds number. Therefore, as lift coefficient is Reynolds number dependent, both the frequency and the amplitude of the local lift force vary along the cylinder's length. In addition, as in the previously considered cases, phase variation with z also occurs.

In order to reduce complexity somewhat, phase variation will be ignored in what follows; that is, the local lift forces at two cross sections of equal diameter (points A and B in Figure C-4a) will be assumed in phase. Similarly, in order to avoid consideration of where in the sinusoid the cylinder terminates, the cylinder will be assumed scaled so that it is of minimum diameter at each end. To simplify algebraic manipulation, the cylinder will be idealized in that the diameter will be permitted to be zero (Figure C-4b) but rigidity will remain postulated.

If the cylinder is considered to be divided into short segments (dz) over which the lift force is of constant frequency and amplitude, then the radiated sound should be

the superposition of the sound produced by each segment. That is, the sound should exhibit a frequency spectrum extending to the infinitely high frequency associated with zero diameter, with sound amplitude frequency dependent.

Mathematically,

$$(33) \qquad p = -\frac{1}{4\pi a_o}\frac{\cos\theta}{r}\int_{-L/2}^{L/2} \dot{f}_L(z,t)\,dz$$

applies. As f_L is assumed narrowband within any segment dz,

$$\dot{f}_L = i\,\omega\,f_{L_o}\,e^{i\omega t}$$

where f_{L_o} is the local lift force amplitude. Therefore, noting that ω itself is z dependent,

$$(66) \qquad p = -\frac{i}{4\pi a_o}\frac{\cos\theta}{r}\int_{-L/2}^{L/2} \omega\,f_{L_o}\,e^{i\omega t}\,dz.$$

Now,

$$\omega = \frac{2\pi\overline{U}S}{d} \qquad \text{and} \qquad f_{L_o} = C_L\,\frac{1}{2}\,\rho\,\overline{U}^2\,d$$

by the definitions of S and C_L.

Often C_L exhibits a power relation with Reynolds number. Assuming such a relation yields, with K and n serving as constants,

$$C_L = K\,R_e{}^n = K\,\overline{U}^n\,d^n/\nu^n$$

or

$$\omega\, f_{L_o} = \frac{\rho\, K\, \pi\, \overline{U}^{n+3}\, S}{\nu^n}\, d^n\ ,$$

and

$$(67)\qquad p = -\,\frac{i\,\rho\, K\, \overline{U}^{n+3}\, S}{4a_o\nu^n}\;\frac{\cos\,\theta}{r}\int_{-L/2}^{L/2} d^n e^{\,i\frac{2\pi\overline{U}St}{d}}\,dz$$

Now, the previous assumption was that $d = D\sin z$ where D is the maximum cylinder diameter. Thus,

$$(68)\qquad p = -\,\frac{i\,\rho\, K\, \overline{U}^{n+3}\, S}{4a_o\nu^n}\;\frac{\cos\,\theta}{r}\int_{-L/2}^{L/2} D^n\,\sin^n z\, e^{\,i\frac{2\pi\overline{U}S}{D\sin z}t}\,dz$$

To evaluate the integral, let $\omega = \dfrac{2\pi\overline{U}S}{D\sin z}$; then

$$(69)\qquad p = \frac{i\rho K}{a_o\nu^n D}\,2^{n-1}\pi^{n+1}(\overline{U}^2S)^{n+2}\int_{-\infty}^{\infty}\frac{e^{i\omega t}\,d\omega}{\omega^{n+1}\sqrt{\omega^2-\left(\frac{2\pi\overline{U}S}{D}\right)^2}}$$

where positive ω actually varies from $\dfrac{2\pi\overline{U}S}{D}$ to infinity.

Examination of the integral in (69) immediately reveals that it is an inverse Fourier transform.[50] As such, the integrand, less the $e^{i\omega t}$ factor, provides the frequency spectrum of p. This spectrum is plotted in Figure C-5 as a function of the parameter n which relates lift coefficient

to Reynolds number. The infinite frequency, present in this idealized case corresponds to zero cylinder diameter, while the minimum frequency is the Strouhal frequency of maximum diameter.

Evaluation of the integral to obtain a closed form expression for p as a time function involves using the appropriate transform tables.[50,51] Cursory examination of these tables indicates that the resulting p is a summation of Hankel functions of varying frequency, each term of which in the asymptotic limit of time is a sinusoid.

However, the algebraic details of this process are not included herein for two reasons. First, (69) describes an idealized case; it ignores phase variation, represents a rigid cylinder with zero diameter and specified end conditions, and is dependent upon a constant power relation between lift coefficient and Reynolds number. Second and more important, observations reported later in this paper indicate that non-uniform diameter cylinders may not be treated in terms of superposition of independent segments. The non-uniformity introduces shadowing and other effects which cause interdependence between similar cylinder sections as well as relatively unpredictable cylinder-flow interactions. In these cases, mathematical models based upon independence serve poorly for both lift force and sound field predictions, and therefore, the lengthy algebraic manipulation required for complete evaluation of the integral in (69) is not an appropriate effort.

The best fit value, .201, is only slightly lower than the .205 to .21 mean reported in the literature. This agreement lends confidence to the experimental configuration used, particularly to the effectiveness of the end caps.

Initially, the various measurements discussed in the preceding two sections were attempted with no end caps; the loss of base pressure suction caused by spanwise flow[21,45] resulted in catastrophic reduction of both Strouhal frequency and total lift force. Addition of end caps, on the other hand, reduced spanwise flow as evidenced by the present Strouhal frequency being within 4 percent of the mean value obtained in closed test sections with sealed cylinder penetrations at the side walls. As such, lift forces herein obtained similarly should be only slightly less than those reported previously.

Correlation length (ℓ_c) and the centroid of the one-sided correlation curve ($\bar{\gamma}$) were calculated per equations (40) and (41) from measured $R(\gamma)$ curve values. All integrations were performed numerically using one diameter abscissa intervals. Results are listed in Tables B-1 through B-3 and are plotted in Figure C-49.

Figure C-50 compares the current values with those reported in the literature.[2,25,32,33,36-42] Although the present results are somewhat higher than the previous mean, high confidence nevertheless may be placed in them.

As noted in Section I, ℓ_c is an approximate measure of twice the physical distance over which f_L is of relatively

constant phase. Accordingly, visual observations[2,32,33,38,41] are indicative of $\ell_c/2$, and the corresponding reported values have been doubled on the figure for comparison.

Several observers[40,49] question the measurements of Prendegast[39] and El Baroudi.[42] The latter were among the first obtained, and they contradict the concept of correlation length not increasing as vortex turbulence increases with Reynolds number. In addition, Prendegast's results were based on measured $R(\gamma)$ values which remained non-zero at extremely large γ.

As noted in the last section, the effect of measurement difficulty is to decrease $R(\gamma)$, thereby causing a similar decrease in calculated ℓ_c and $\bar{\gamma}$. Therefore, the location of current values at or above already reported magnitudes adds to their credibility. Moreover, these values agree rather well with the recent careful measurements of Ballou[36] and Leehey and Hansen.[25] These two observations, then, coupled with the consistency herein obtained over several cylinder diameters, support the high confidence assigned.

Total lift force was calculated by modifying the raw voltage data listed in Tables B-1 to B-3 and B-5 to account for impedance head calibration and F_L-electronics gain factors. This process yielded F_L in pounds. Then equations (44) and (47) as well as the already obtained ℓ_c and $\bar{\gamma}$ values were used to compute the local lift forces (f_L) and local lift coefficients (C_L) listed in these same tables.

Local lift coefficients are plotted in Figure C-51. As observed in the last section, small magnitude lift force amplitudes associated with low velocities are highly uncertain. With one exception, the values obtained over the entire range appear independent of cylinder and diameter variation. The apparent C_L decrease characterizing 1" cylinder data may be attributable to inadequacy of the 3:1 ratio of tunnel size to cylinder diameter.

The best fit to the data of Figure C-51 is duplicated and compared to reported C_L values[6,21,25,43,44,55-57] in Figure C-52. The current data exhibit the C_L increase with Reynolds number common to the other observations. The sharp knee at $R = 2.1 \times 10^4$ may be an artifact or may be attributable to the 3" tunnel width becoming more significant as vortex strength increased.

The previously reported data exhibit considerable scatter. Gerrard partially explained this scatter by clarifying the increase of lift force with the turbulence level of the incoming flow.[43,44] His explanation reconciled his results with those of Schwage,[56] Keefe,[21] and Bishop and Hassen;[57] however, the greater of the two low turbulence C_L values reported by Leehey and Hansen[25] is too large to fit Gerrard's pattern.

All results shown except the current values and that of Koopmann[6] are for closed test sections. Koopmann's point represents synchronization, with accompanying lift force amplification, and a 3 percent incoming flow turbulence

level. The small magnitude lift force exhibited again is an exception to the other data.

In view of this scatter of reported data, as well as similar scatter in data reported for higher Reynolds numbers,[55] the present results appear credible. If they deviate from previous values, such deviation is downward, and corresponds in direction to the slight Strouhal number decrease discussed above.

Predicted sound field intensities, listed in Tables B-1 to B-3 and B-5, were calculated by inserting already obtained F_L and ω data into equation (49). Measured sound intensities from Tables B-18 to B-20 and B-22 are compared with these predicted values in Figures C-53 to C-55. Agreement is not only excellent, but so consistent that a best fit line could be drawn to both predicted and measured intensities for two different $\frac{1}{2}$" cylinders in Figure C-54.

NON-UNIFORM CYLINDERS

Except for the irregular multinotched cylinder (Figure C-33e), both total lift force and radiated sound were measured for all non-uniform cylinders. Only radiated sound was measured for the exception. Values of total lift force and of predicted sound intensities obtained by using these F_L values in Equation (49) are listed in Tables B-4 and B-5 to B-17. Measured sound intensities are listed in Tables B-21 and B-23 to B-35. Predicted and measured values are compared in Figures C-56 through C-67 where, for

reference, the best fit line for $\frac{1}{2}$" uniform cylinders from Figure C-54 is repeated.

Agreement between predicted and measured sound is excellent except for the skewed cylinder at zero skew angle. In this anomalous case, measured sound is not only lower than predicted but also lower than the reference. This unexplainable shortfall, unfortunately not discovered until after the wind tunnel was disassembled, is assumed to be a transitory systematic measurement error.

Disregarding this single exception, the overwhelming consistent agreement exhibited on the other eleven figures totally confirms the theory of aerodynamic sound. Regardless of the specific non-uniformity of each particular cylinder, be it roughness, fins, splitter plates, skew or notches, and regardless of the relation between each sound intensity and the corresponding $\frac{1}{2}$" uniform cylinder reference intensity, predicted and radiated sound values agree completely.

The extent of this agreement is particularly significant in view of the current naval and oceanographic applications noted in the introduction. It demonstrates that F_L and I now may be used almost interchangeably as their direct Equation (49) relationship has been validated experimentally. Moreover, this agreement shows that reduction of lift force, by any means, leads to a corresponding reduction in radiated sound, with the correspondence quantitatively described by Equation (49).

Having accomplished this confirmation of Lighthill's theory and having noted the implications of this confirmation, the primary objective of this research has been satisfied. Examination of lift force and correlation length variation thus becomes the focus of remaining interest.

Roughened cylinder C_L and ℓ_c values, calculated in the usual manner and listed in Table B-4, are plotted on Figures C-68 and C-69 respectively. These figures, together with Figure C-56 indicate that roughening reduces total lift force by adding sufficient three dimensionality to decrease the correlation factor, $(L - \overline{\gamma})\ell_c$ (see Equation (44)). Local lift force also may be reduced, but the measured reduction is too slight to clarify any substantial effect. Similarly, unplotted Strouhal number data fall within the scatter measured for uniform cylinders (Figure C-48) and average .198, only slightly below the .201 measured reference.

Correlation factors for the four-finned cylinder were calculated by applying Equation (64) to measured $R(\gamma)$ curves, using one diameter abscissa intervals for numerical integration. Results appear in Table B-7 and on Figure C-63. The uniform $\frac{1}{2}$" cylinder correlation factor, $(L - \overline{\gamma})\ell_c$, also is shown as a reference.

As recorded on the $R(\gamma)$ curves, the vortex wake behind a cylinder section bounded by adjacent fins was highly two dimensional, exhibiting nearly constant phase between adjacent fins and some phase correlation across fins. Nevertheless, the resulting correlation factor, when compared to the

no fin case, showed a decrease. This indicates that the increase in local two-dimensionality did not compensate for the reduction in large γ axial coherence caused by the introduction of fins.

Correlation data were not recorded for the two-finned cylinder. Therefore, the approximate correlation factor shown in the figure was obtained by averaging four fin and uniform cylinder values.

Strouhal numbers for these finned cylinders again fell within the uniform cylinder scatter shown in Figure C-48. Average values were .205 and .197 for the two and four fin cases respectively. The latter figure perhaps should be larger in view of the measured increased in wake two dimensionality. However, the amount of data recorded for the four-finned case together with the appearance of the expected result for the two-finned cylinder mitigate this observed contradiction.

The expectation of local lift force remaining independent of wake two-dimensionality predicts, in view of decreased correlation factor, a decrease in total lift force. However, as indicated on Figures C-57 and C-58, F_L in fact increased. C_L values calculated from Equations (47) and (64) and plotted on Figure C-71 identify the cause of this increase. Local lift force indeed showed a dependence on the local two-dimensionality of the flow. This initially unexpected phenomenon will be discussed further later in this subsection.

For the cylinder with splitter plates, ℓ_c and C_L values, calculated in the usual manner, are listed in Tables B-8 and B-9 and plotted in Figures C-72 and C-73. These figures indicate that the reduction in total lift force shown on Figure C-59 resulted from decreases in both local lift force and correlation values. Figures C-59 and C-73 also indicate that the decrease is greater for the larger plate, particularly at lower Reynolds numbers. The contrary trend shown for low Re on Figure C-72 is based on uncertain data, in view of the poor anomometer probe signal-to-noise ratios discussed in the previous section. As such, this contra-indication is considered insubstantial.

The Reynolds number dependence is explainable in terms of Gerrard's formation length[44], which is defined as the distance in back of the cylinder where fluid from outside the wake first crosses the wake axis. This length, in effect, is that over which virtually no interaction occurs between opposite vorticity regions of the wake. Therefore, insertion of a splitter plate of length less than the formation length should have little effect on the flow. Formation length decreases as Reynolds number increases.[44]

For the present case, the large splitter plate extended past the uniform cylinder formation length at all Reynolds numbers considered. The small plate similarly exceeded the less than 2d[44] formation length characterizing Reynolds numbers above 8×10^3. However, below this Re, formation length increased almost to the 3d extent of the smaller

plate, minimizing the plate's influence on the vortex formation process.

Observed Strouhal numbers averaged 68 and 46 percent of the .201 uniform cylinder value for the small and large plate respectively. These values, compare favorably with the 76 and 36 percent figures reported by Apelt and West[54] for similarly scaled but more precisely mounted plates.

Skewed cylinder measurements herein reported were made to determine the applicability of superposition to flow over a cylinder in the presently considered Reynolds number regime. This determination was motivated by verbal reports that superposition, in spite of the non-linearity of the governing Navier-Stokes equation, nevertheless predicted correct experimental values.

To accomplish this portion of the experiment, the usual quantities were measured for skew angles, β, of zero and 45 degrees and at four intermediate angles of about 10, 21, 31 and 39 degrees. Results obtained then were compared with those for uniform cylinders, with appropriate modified parameters such as $U^* = \overline{U} \cos \beta$, $Re^* = \frac{U^*d}{\nu}$ and $S^* = \frac{\omega d}{2\pi U^*}$ used to provide a reasonable corresponding basis. In general, these results confirmed the applicability of superposition at small skew angles, but they also indicated an attenuation of ℓ_c, $\overline{\gamma}$, S^*, C_L, and F_L which grew more significant as skew angle was increased.

This conclusion is exemplified by the sound intensity curves of Figures C-61 through C-65 and by the average

Strouhal numbers listed in Table B-36. Moreover, it may be applicable to the ℓ_c and $\overline{\gamma}$ values of Figures C-74 to C-79, which were computed from measured $R(\gamma)$ values using Equations (40) and (41). On the other hand, the results shown for ℓ_c and $\overline{\gamma}$ also were attenuated by poor signal-to-noise ratios as discussed in Section III, and therefore, the magnitude of the shortfall attributable to superposition is not clear.

If these correlation values in fact had been larger, then the C_L values listed in Tables B-12 through B-17 and plotted in Figures C-80 through C-85 would have been smaller than shown (see Equations (44) and (47)). As such, the indicated C_L values represent upper bounds and thus affirm the previously stated conclusion.

Further consideration of the Strouhal number values of Table B-36 motivated additional comparison. Recognizing that the factor ω/ω_s was consistently about equal to or less than cos β dictated examination of the resultant data with ω/ω_s replacing cos β as the factor for computing effective normal flow velocity. Accordingly, the previous C_L and I results were replotted against $U^{**} = \overline{U}\ \omega/\omega_s$ and $Re^{**} = \frac{U^{**}d}{\nu}$ as shown in Figures C-86 through C-95. On the other hand, the previously mentioned measurement uncertainty obviated the necessity to replot ℓ_c and $\overline{\gamma}$ values.

As the figures indicate, employment of this new effective skew angle, $\cos^{-1}\ \omega/\omega_s$, postpones the apparent introduction

of the departure from superposition, but it does not alter the basic conclusion. Application of superposition predicts experimentally correct results at small skew angles but is increasingly inappropriate as skew becomes more severe.

The two-notched cylinder (Figure C-33c), as indicated in the previous section, is essentially two 5 inch long cylinders with different diameters. As such, the total lift force measured for the $\frac{1}{2}$" section should be lower than that of the 10 inch reference. Figure C-66 exhibits this result and also indicates reasonable 3/8" section lift force magnitude.

Although correlation quantities were not measured for this cylinder, ℓ_c and $\bar{\gamma}$ values appropriate to each diameter were determined from the uniform normal cylinder curves of Figure C-49. These values then were used, together with the 5" length, in Equations (44) and (47) to calculate the C_L values listed in Table B-10 and plotted in Figure C-96. Results agree with those already obtained for 10" cylinders. Similarly, measured Strouhal numbers averaged .201, the previous uniform cylinder mean value.

Results for the regular multi-notched cylinder, on the other hand, are not so amenable to direct interpretation. Although radiated sound again agreed with predicted values (see Figure C-67), the magnitudes of both F_L and I as well as those of correlation parameters and S, as discussed in detail below, were smaller than expected for $\frac{1}{2}$" sections. The 3/8" sections showed similar agreement between predicted

and measured sound intensity, but the strong shadowing effect precluded measurement of correlation function.

Nevertheless, Strouhal frequencies, based upon wake measurements as well as lift force and sound field data, were measured for 3/8" sections. The values obtained matched those measured on this same cylinder for $\frac{1}{2}$" sections, with neither set exhibiting any more scatter than the corresponding data of Figure C-48. The average Strouhal number of .183 was 10 percent less than the uniform cylinder value.

An estimate of the effect of shadowing was obtained by comparing the f_L predicted from uniform cylinder C_L with the F_L measured for 3/8" sections. The comparison assumed that 3/8" sections were phase independent, a reasonable assumption in view of the failure to observe other than random phase relationships during the shadowing – aborted attempt to measure 3/8" section $R(\gamma)$. As enumerated in Table B-11, the square of the effective length was obtained by dividing the square of measured F_L by five times the square of predicted f_L (see Equation (64)). The result was an effective length averaging .3d per 1" long section, with a standard deviation of about .05d. Therefore, because of shadowing, each 1" long, 3/8" diameter section radiated sound as if it was an unshadowed section about 1/8" in length.

The $\frac{1}{2}$" section $R(\gamma)$ values of .25 at minimum probe separation and the similarly weak but consistently 180° out-of-phase values between separated sections are subject

to two interpretations. The first treats the intervening 3/8" sections as periodic divisions (see Figure C-44 (a) and (b)) and applies Equation (64) to compute a correlation factor of 2.865. The second assumes that shadowing effectively causes the lift force to be applied along the entire cylinder. Then, sketching in the unmeasured portion of the $R(\gamma)$ curve (Figure C-44(c)) permits calculation of ℓ_c and $\bar{\gamma}$. The resulting correlation factor, $\sqrt{(L-\bar{\gamma})\ell_c}$, of 2.5 agrees relatively well with that obtained by the first method.

C_L values based upon measured F_L and the above 2.865 correlation factor are listed in Table B-11 and plotted in Figure C-97. As indicated, they are only 40% of uniform cylinder values, a reduction which corresponds mathematically to the two orders of magnitude decrease in radiated sound shown in Figure C-67. Moreover, this decrease is unaffected by any $R(\gamma)$ measurement inaccuracies caused by poor signal-to-noise ratios and spanwise flow between $\frac{1}{2}$" sections. As for previous cylinders for which $R(\gamma)$ measurement difficulties were encountered, underestimating correlation factors implies that C_L values based upon these factors are upper bounds.

To obtain reasonable lengths of unshadowed 3/8" sections, as noted earlier, the irregular multinotched cylinder was fabricated toward the end of this experiment, and for this cylinder, only radiated sound was measured. Results, plotted

in Figure C-98 were used together with an estimate of correlation factor to obtain an estimate of C_L.

For the four 1 3/4" long, 3/8"d sections two estimates of correlation factor were made. Both assumed phase independence between sections as well as an unshadowed length of about 2d within each section, with the latter value inferred from the shadowed length computation for the regular multinotched cylinder. The first estimate, 4.47, followed from Equation (64) and the stipulation that within each section, correlation was identical to the $R_W(\gamma)$ curve characterizing $\frac{1}{2}$" sections of the regular multinotched cylinder. The second estimate, 6.76, resulted from the assumption of a within-section effective length identical to the .65L value obtained for uniform $\frac{1}{2}$" cylinders.

Substitution of these estimates and measured I values into Equations (44), (47) and (49) provided the 3/8" section C_L values listed in Table B-37 and plotted in Figure C-99. As shown, lift coefficients still are slightly below uniform cylinder results.

Similarly, these same two methods were used to obtain correlation factor estimates for the three 1" long, $\frac{1}{2}$"d sections. However, in this case inter-section phase independence was not an assumption but was determined from crude wake measurements which indicated no phase relationships between separated sections. Values obtained are listed in Table B-37 together with resultant C_L values, and the latter are also plotted in Figure C-92. Again, a slight decrease

from uniform cylinder results is indicated, but comparison with Figure C-97 reveals that this decrease is not nearly so severe as that measured for the regular multinotched cylinder.

Finally, the proximity of irregular multinotched and uniform cylinder C_L values is paralleled by the .204 mean Strouhal number measured for the former.

The difference in lift force attenuation between these two multinotched cylinders may be understood in terms of the mechanism of vortex shedding as explained by Gerrard.[44]

"The growing vortex continues to be fed by circulation from the shear layer until the vortex becomes strong enough to draw the other shear layer across the wake. The approach of oppositely-signed vorticity in sufficient concentration cuts off further supply of circulation to the vortex, which then ceases to increase in strength. We may speak of the vortex as being shed from the body at this stage."[44]

On both irregular multinotched and uniform cylinders, this mechanism applied. Their Strouhal numbers agreed, and C_L differentials between these cylinders were small. Moreover, as discussed below, small decreases in vortex wake two-dimensionality in back of the 2d lengths of $\frac{1}{2}$" sections on the irregular multinotched cylinder may have caused the small f_L reduction observed.

On the regular multi-notched cylinder, however, where $\frac{1}{2}$" sections were not phase independent, Gerrard's mechanism apparently was modified. The same 180° phase reversal

existed between $\frac{1}{2}$" sections as existed between opposite cylinder sides on a uniform cylinder. In addition, the Strouhal number decrease observed implied the presence of spanwise flow. Therefore, one may conclude that in Gerrard's description the oppositely-signed vorticity, which caused shedding, flowed to the top of one $\frac{1}{2}$" section from the bottom of that section and, in lesser quantity, from the top of adjacent sections as well. This between-section flow interaction, similar to the usual opposite-side-of-the-cylinder interaction, thus disrupted the vortex shedding process and caused lift force attenuation.

This significant magnitude effect, wherein strong spanwise interaction introduced large lift force attenuation, may be generalized, in view of the previously reported results for other cylinders, to the observation that the magnitude of local lift force is dependent upon the two-dimensionality of the vortex wake.

On the irregular multinotched cylinder, f_L attenuation, although small, was nevertheless present. Moreover, the L/d ratio of two for each section was hardly large enough to justify considering each section as an infinitely long uniform cylinder. As such, some wake three-dimensionality must have been present.

In addition, some lift force attenuation accompanied increased three-dimensionality for both the roughened and the skewed cylinder, particularly at large skew angles for the latter. Although the magnitude of the observed attenuation

could be considered to fall within experimental error, the trend nevertheless exhibited supports the above generalization.

More importantly, the greatly increased wake two-dimensionality observed for finned cylinders was accompanied by large lift force amplification. This large magnitude result together with above discussed regular multinotched cylinder measurements clearly indicates that f_L is monotonic with local two-dimensionality in the vortex wake.

This conclusion, although previously not stated so explicitly, nevertheless is supported by several reports in the literature. Among those reporting lift force amplification, Keefe[21] mounted 5d fins on an otherwise uniform cylinder and varied fin spacing between 25 and 3d. At large separation, the fins had virtually no effect on f_L, but as separation was decreased, f_L was amplified, with the amount of amplification per unit separation decrease more significant at small spacing. Amplification factors of 1.2 and 1.5 were observed at 5 and 3d separation respectively.

Other researchers[8,27-30,58-62] also noted an increase in f_L with increasing two-dimensionality, but such increase accompanied synchronization. Nevertheless, the reports of lift force amplification were so numerous that Schmidt[63] suggested the necessity for a correction to measured local lift force to account for the relationship between correlation length and the finite extent of the force transducers used for f_L measurement. This correction is not applicable to the current experiment wherein F_L, not f_L, is measured.

In general, reports of lift force attenuation[6,21,25] pertain to the previously addressed reduction of both f_L and S which accompanies the loss of base pressure suction. In turn, this loss is well known to be caused by spanwise flow,[45] a three dimensional phenomenon. On the other hand, no reports of measurements such as those herein obtained for multinotched cylinders are known to this author. As such, it appears that the literature does not as completely support the coupling of lift force attenuation and increased wake three dimensionality as it does the lift force amplification phenomenon.

It appears, therefore, that measurement of local lift force is required to complement previously discussed results regarding this effect. For such measurement, a short-length cylindrical force transducer with equal diameter cylindrical attachments fabricated so as to provide finned and notched cylinders is required. The appropriate measurements then could be made by placing the cylinder/transducer body in flow and recording force transducer output.

Unfortunately, in the present case, time and funding limitations precluded pursuing this task which, while serving to quantify the observed effect, nevertheless is tangential to the already attained primary experimental objective of validating the theory of aerodynamic sound for cylinders in flow. On the other hand, a qualitative, yet expeditious and inexpensive confirmation of the above discussed effect was accomplished in the measurement discussed at the end of Section III.

This measurement of velocity variation, u', in the vortex wake, at a position fixed relative to different equal diameter cylinders, was made for two flow velocities, 48 and 88 feet per second. Results obtained indicated that u' was virtually identical for irregular multinotched and uniform cylinders; u' doubled with the addition of fins and decreased by forty percent from the uniform cylinder value for the regular multinotched cylinder.

As f_L and u' definitely are related monotonically, these data qualitatively agree with the previous results regarding amplification and attenuation of local lift force. The near quantitative agreement, however, may well be fortuitous as the exact numerical relation between f_L and u' is not clear.

Bernoulli's law is inapplicable to determination of this relation as the conditions for its use are not satisfied. Moreover, experimental data relating surface pressure to u' apparently appear in only a single reference. Goldstein's[64] report of data recorded by Schiller and Linke indicates that over the limited Reynold's number range 4 to 6 X 10^3, an increase in u' by a factor of 1.25 is accompanied by a corresponding 1.4 factor increase in C_L. Extrapolation of this linear relation to other Reynolds numbers is not clearly justifiable, particularly in view of the shadowing and other flow effects applicable to these multinotched cylinders; however, this limited information does support somewhat the one-to-one relationship obtained for the additional wake measurement herein reported.

In all, in spite of these uncertainties, the experimental evidence available, within the current results or synthesized from the literature, does support the existence of the effect. Local lift force indeed appears to increase monotonically with vortex wake two-dimensionality, or equivalently, with reduction of spanwise flow.

V. CONCLUSIONS

This experimental effort originally was focused toward validating the theory of aerodynamic sound. However, several tangential paths were explored in the course of the research, and therefore, the conclusions reached extend beyond the original scope.

1. The theory of aerodynamic sound as applied to cylinders is correct. Radiated sound predictions based on measured total lift force agree overwhelmingly with measured sound intensity.

2. Reduction of lift force, by any means, correspondingly reduces radiated sound intensity.

3. The herein derived extension of this theory to periodically divided cylinders also is correct. Lift coefficients calculated from measured total force and correlation values form a consistent pattern and agree with applicable results in the literature.

4. The magnitude of local lift force varies monotonically with the two-dimensionality of the vortex wake behind the cylinder. This effect is supported qualitatively by the results herein obtained and by reports in the literature.

5. Installing a microphone within a Helmholtz resonant cavity is a feasible method of measuring surface pressure variation at a point on a cylinder. Use of this method first requires careful calibration of both the phase and the amplitude of the microphone-cavity system.

6. Reports of incoming flow turbulence, cylinder end conditions, cylinder roughness, and vortex-wake two-dimensionality should accompany reports of measured lift force. The need for turbulence data first was addressed by Gerrard,[43,44] and several observers[21,45,54] showed the need for specification of end conditions. The additional requirements are indicated by the current results.

VI. SUGGESTED FURTHER RESEARCH

The present experiment opens a new area of inquiry, the study of the effect reported in Section IV and summarized in the fourth conclusion of Section V. Quantification of this effect requires simultaneous measurement of local lift force and correlation parameters for a variety of uniform, finned and notched cylinders, the fabrication of which was discussed in Section IV. However, exhaustive quantification further requires that the spacing of fins and notches, relative to the force transducer used, be variable.

In addition, information gained from searching the literature and from reading papers in related areas also suggests areas for further inquiry. First, although Lighthill's theory correctly predicts the magnitude of radiated sound, no clear understanding of the phase relationship between radiated sound pressure and surface pressure variation on the cylinder has been attained. Experimental determination of this phase relationship would be facilitated by use of a synchronized cylinder.

Similarly, a synchronized cylinder is necessary for study of the second related area, the effect of skew on synchronization. Little is known regarding the combination of these two phenomena.

Finally, $R(\gamma)$ traditionally has been determined using one of two techniques, the measurement of phase relations

in the vortex wake or the phase comparison of the outputs of two or more cylinder-mounted force transducers. Although these two distinct methods have resulted in values which exhibit general agreement, proof of their equivalence awaits the equality of experimental results obtained simultaneously with each method.

VII. REFERENCES

1. V. Strouhal 1878 Annalen Physik und Chemie Bd 5. 216-51

2. O. M. Phillips 1956 Journal of Fluid Mechanics 1. "The Intensity of Aeolian Tones"

3. Lord Rayleigh 1879 Philosophical Magazine 7. 149-62

4. Lord Rayleigh 1896 The Theory of Sound Vol. II. London: MacMillan

5. F. Allborn 1902 Agh Geb Naturwiss Bd 17.

6. G. H. Koopman 1969 Wind Induced Vibrations and their Associated Sound Fields. Washington, D.C.: Catholic University

7. H. Bénard 1908 Academie des Sciences Comptes Rendues T. 147. 839-42

8. G. H. Koopmann 1967 Journal of Fluid Mechanics 28. "The Vortex Wakes of Vibrating Cylinders at Low Reynolds Numbers"

9. T. Von Kármán 1912 Physikolische Zeitschrift Bd 13. "Über der Mechanismus des Flüssigkeitsund Luftwiderstandes"

10. W. F. Durand Ed. 1943 Aerodynamic Theory No. 1 Div. D. (Giacommelli and Pistolesi) : Durand Reprinting Committee

11. Lord Rayleigh 1915 Philosophical Magazine 29-6. "Aeolian Tones"

12. E. F. Relf 1921 Philosophical Magazine 42-6. "On the Sound Emitted by Wires of Circular Section when Exposed to Air Current"

13. L. S. G. Kovasznay 1949 Proceedings of the Royal Society A198. "Hot Wire Investigation of the Wake Behind Cylinders at Low Reynolds Numbers"

14. A. Roshko 1953 NACA TN2913. "On the Development of Turbulent Wakes from Vortex Streets"

15. J. H. Gerrard 1955 Proceedings of the Royal Society B68. "Measurement of the Sound from Circular Cylinders in an Air Stream"

16. E. Z. Stowell and A. F. Deming 1936 Journal of the Acoustic Society of America 7. "Vortex Noise from Rotating Cylindrical Rods"

17. E. Y. Yudin 1947 NACA TN1136. (Translation of Zhur Tekh Fiz 14,561 (1944))

18. M. J. Lighthill 1952 Proceedings of the Royal Society A211. "On Sound Generated Aerodynamically, I General Theory"

19. N. Curle 1955 Proceedings of the Royal Society A231. "The Influence of Solid Boundaries upon Aerodynamic Sound"

20. B. Etkin, G. K. Korbacher and R. T. Keefe 1956 UTIA Report 39. "Acoustic Radiation from a Stationary Cylinder in a Fluid Stream (Aeolian Tones)" Toronto: University of Toronto

21. R. T. Keefe 1961 UTIA Report 76. "An Investigation of the Fluctuating Forces Acting on a Stationary Circular Cylinder in a Subsonic Stream and of the Associated Sound Field" Toronto : University of Toronto

22. M. J. Lighthill 1962 Proceedings of the Royal Society A267. "The Bakerian Lecture 1961, Sound Generated Aerodynamically"

23. H. M. Fitzpatrick and M. Strassberg 1957 Naval Hydrodynamic Publication 515 National Academy of Science. "Hydrodynamic Sources of Sound" Washington, D.C.

24. F. N. Frenkiel 1959 Advances in Applied Mechanics Vol. III. "Turbulent Diffusion" New York Academic Press

25. P. Leehey and C. E. Hanson 1971 Journal of Sound and Vibration 13. "Aeolian Tones Associated with Resonant Vibrations"

26. H. Schlicting 1968 Boundary Layer Theory New York: McGraw Hill

27. O. M. Griffen and C. W. Votaw 1972 Journal of Fluid Mechanics 51. "The Vortex Sheet in the Wake of a Vibrating Cylinder"

28. O. M. Griffen, R. A. Skop and G. H. Koopmann 1973 Journal of Sound and Vibration 31. "The Vortex Excited Resonant Vibrations of Circular Cylinders"

29. O. M. Griffin 1973 Journal of Sound and Vibration 27. "A Model for the Vortex-Excited Resonant Response of Bluff Cylinders"

30. N. Ferguson and G. V. Parkinson 1967 American Society of Mechanical Engineers Paper 67, Vibration - 31. "Surface and Wake Flow Phenomena of the Vortex-Excited Oscillation of a Circular Cylinder"

31. N. Ferguson and G. V. Parkinson 1967 Journal of Engineering for Industry. "Surface and Wake Flow Phenomena of the Vortex Excited Oscillation of A Circular Cylinder"

32. J. H. Gerrard 1961 Journal of Fluid Mechanics 11. "An Experimental Investigation of the Oscillating Lift and Drag of a Circular Cylinder Shedding Turbulent Vortices"

33. J. S. Humphreys 1960 Journal of Fluid Mechanics 9. "On a Circular Cylinder in a Steady Wind at Transition Reynold Numbers"

34. R. L. Goldman 1958 Shock and Vibration Bulletin Part II. Washington, D.C. : Naval Research Laboratory

35. Y. C. Fung 1960 Journal of Aerospace Sciences 27. "Fluctuating Lift and Drag acting on a Cylinder in Flow at Supercritical Reynolds Numbers"

36. C. L. Ballou 1967 MIT Engineering Projects Laboratory Report 76028-2. "Investigation of the Wake Behind a Cylinder at Coincidence of a Natural Frequency of Vibration of the Cylinder and the Vortex Shedding Frequency" Boston : Massachusetts Institute of Technology

37. J. H. Gerrard 1958 ARC 19,844 "Measurements of the Fluctuating Pressure on the Surface of a Circular Cylinder, Part I - Cylinder of 1" Diameter"

38. F. R. Hama 1957 Journal of Aeronautical Sciences 24. "Three Dimensional Vortex Patterns Behind a Circular Cylinder"

39. V. Prendegast 1958 UTIA TN23. "Measurement of Two-Point Correlations of the Surface Pressure on a Circular Cylinder" Toronto : University of Toronto

40. L. V. Schmidt 1965 Journal of Aircraft 2. "Measurement of Fluctuating Air Loads on a Circular Cylinder"

41. M. S. Macovsky 1958 David Taylor Model Basin Report 1190. "Vortex-Induced Vibration Studies" Carderock, Maryland: US Navy

42. M. Y. El Baroudi 1960 UTIA TN31. "Measurement of Two-Point Correlations of Velocity Near a Circular Cylinder Shedding a Karman Vortex Street" Toronto : University of Toronto

43. J. H. Gerrard 1965 Journal of Fluid Mechanics 22. "A Disturbance - Sensitive Reynolds Number Range of the Flow Past a Circular Cylinder"

44. J. H. Gerrard 1966 Journal of Fluid Mechanics 25. "The Mechanics of the Vortex Formation Region of Vortices Behind Bluff Bodies"

45. P. W. Bearman 1965 Journal of Fluid Mechanics 21. "Investigation of the Flow Behind a Two-Dimensional Model with a Blunt Trailing Edge and Fitted with Splitter Plates"

46. J. A. Stratton 1941 Electromagnetic Theory. New York: McGraw Hill

47. P. T. Laird and H. Cohen 1952 Journal of the Acoustic Society of America 24. "Directionality Patterns for Acoustic Radiation from a Source on a Rigid Cylinder"

48. W. R. Morgans 1930 Philosophical Magazine 9-7. "The Kirchhoff Formula Extended to a Moving Surface"

49. C. Graham 1966 MIT Engineering Projects Laboratory Report 76028-1. "A Survey of Correlation Length Measurements of the Vortex Shedding Process Behind a Circular Cylinder" Boston : Massachusetts Institute of Technology

50. G. A. Campbell and R. M. Foster 1948 Fourier Integrals. Princeton : D. Van Nostrand

51. 1965 Handbook of Mathematical Functions. U. S. Department of Commerce National Bureau of Standards

52. L. E. Kinsler and A. R. Frey 1962 Fundamentals of Acoustics. New York : John Wiley and Sons

53. N. Minorsky 1962 Non-Linear Oscillations. Princeton : D. Van Nostrand

54. C. J. Apelt and G. S. West 1975 Journal of Fluid Mechanics 71. "The Effects of Wake Splitter Plates on Bluff-Body Flow in the Range $10^4 < R < 5 \times 10^4$, Part 2"

55. J. H. Lienhard 1966 WSU Technical Extension Service Bulletin 300. "Synopsis of Lift, Drag and Vortex Frequency Data for Rigid Circular Cylinders" : Washington State University

56. W. Weaver Jr. 1961 ASCE Proceedings 87 No. EM-1. "Wind Induced Bivrations of Antenna Members"

57. R. E. D. Bishop and A. Y. Hassan 1964 Proceedings of the Royal Society A277. "The Lift and Drag Forces on a Circular Cylinder in a Flowing Fluid"

58. R. E. D. Bishop and A. Y. Hassan 1964 Proceedings of the Royal Society A277. "The Lift and Drag Forces on a Circular Cylinder Oscillating in a Flowing Fluid"

59. O. M. Griffen 1972 Journal of Engineering for Industry, May. "Flow Near Self-Excited and Forced Vibrating Circular Cylinders"

60. O. M. Griffen 1971 Journal of Applied Mechanics, Dec. "The Unsteady Wake of an Oscillating Cylinder at Low Reynolds Number"

61. V. C. Mei and I. G. Curie 1969 Physics of Fluids 12. "Flow Separation on a Vibrating Circular Cylinder"

62. G. H. Toebes 1969 Journal of Basic Engineering, Sept. "The Unsteady Flow and Wake Near an Oscillating Cylinder"

63. L. V. Schmidt 1970 Journal of Spacecraft and Rockets 7. "Influence of Spatial Correlation upon Load Resolution"

64. S. Goldstein Ed. 1938 Modern Developments in Fluid Dynamics, Vol. II. Oxford Press

APPENDIX A: GLOSSARY

A	Cross-sectional area of cylinder
$A(t)$	Anemometer output voltage: first probe
a_o	Speed of sound
$B(t)$	Anemometer output voltage: second probe
C_L	Root-mean-square local lift coefficient
d	Cylinder diameter
D	Maximum diameter — sinusoidal cylinder
F_i	Total force on cylinder in i direction
F_L	Total lift force on cylinder
f_i	Local force in i direction
f_L	Local lift force
f_{L_1}	Local lift force at $z = z_1$
f_{L_2}	Local lift force at $z = z_2$
f_{L_o}	Local lift force amplitude-sinusoidal cylinder
I	Radiated Sound intensity
k	Spring constant
L	Cylinder length
L'	Length between divisions-periodically divided cylinder
$L_\perp$	Perpendicular distance between end caps - skewed cylinder
ℓ_i	Direction cosine of the outward normal from the fluid
ℓ'	Effective entrance length — Helmholtz resonant cavity
ℓ_c	Correlation length

ℓ_{c_W}	Intra-section correlation length — periodically divided cylinder
ℓ_{c_A}	Inter-section correlation length — periodically divided cylinder
ℓ_{c_A}'	Correlation length adjustment — periodically divided cylinder
M	Number of divisions — periodically divided cylinder
Ma	Mach Number
m	Cylinder mass
$\vec{n}$	Outward normal from the fluid
P_i	Force per unit area in the i direction exerted by the fluid on the cylinder
$P(\omega)$	Fourier transform of p — sinusoidal cylinder
P_{ij}	Compressive stress tensor
p	Acoustic pressure
Q	Quality factor of cylinder-spring system for synchronization
Q'	Quality factor of Helmholtz resonant cavity
$R(\gamma)$	Correlation function
$R_W(\gamma)$	Intra-section correlation function — periodically divided cylinder
$R_A(\gamma)$	Inter-section correlation function — periodically divided cylinder
$R_{AA}(\tau)$	Autocorrelation in time of first anemometer output
$R_{BB}(\tau)$	Autocorrelation in time of second anemometer output
$R_{AB}(\tau)$	Cross correlation in time of first and second anemometer outputs
R_e	Reynolds number
$R_e{}^*$	Reynolds number-skewed cylinder; modified for skew angle
$R_e{}^{**}$	Reynolds number-skewed cylinder; modified for effective skew angle

$\vec{r}$	$\vec{x} - \vec{y}$: Vector from body to field point
S	Strouhal number; also body surface as in an integral
S*	Strouhal number-skewed cylinder: modified for skew angle
s	Area of Helmholtz resonant cavity entrance
T_{ij}	Instantaneous applied stress
T	Duration of signal for correlation
t	Time
$\overline{U}$	Speed of undisturbed flow
U*	$\overline{U}$ modified for skew angle-skewed cylinder
U**	$\overline{U}$ modified for effective skew angle-skewed cylinder
U_i	Velocity of center of mass of the cylinder in i direction
U_L	Velocity of center of mass of the cylinder in the direction of lift
$u_i(z,t)$	Velocity of a dz section: non-rigid cylinder
u'	Root-mean square velocity variation in vortex wake
V	Cylinder volume
V'	Helmholtz resonant cavity volume
v_i	Fluid velocity vector
x_i	Vector from origin to field point
y_i	Vector from origin to a point in the source region; usually a body coordinate
z	x_3 direction or coordinate (along axis of cylinder)
α	Damping ratio for synchronization
β	Skew angle
γ	Separation distance along cylinder; $(z_2 - z_1)$
$\overline{\gamma}$	Centroid of area under one-sided $R(\gamma)$ curve

$\bar{\gamma}_W$	Centroid of area under one-sided $R_W(\gamma)$ curve
$\bar{\gamma}_A$	Centroid of area under one-sided $R_A(\gamma)$ curve
$\bar{\gamma}_A'$	Centroid adjustment to $\bar{\gamma}_A$
θ	Angle between x_2 direction and r
μ	Mass ratio for synchronization
ν	Kinematic viscosity
ρ	Fluid density
ρ_o	Mean fluid density
ρ_c	Cylinder density
τ	Time coordinate of correlator output
ϕ	Polar circumferential angle at center of cylinder
ω	Strouhal frequency; measured Strouhal frequency
ω_s	Predicted Strouhal frequency
ω_o	Resonant frequency of Helmoltz cavity
ω_i	Angular velocity vector for cylinder rotation

APPENDIX B

TABLES

TABLE B-1. AMPLIFIED IMPEDANCE HEAD OUTPUT ($F_L/2$), CORRELATION PARAMETERS, LIFT COEFFICIENT AND PREDICTED SOUND INTENSITY FOR THE UNIFORM 1/2" CYLINDER

$\bar{U}$ (ft/sec)	$\omega/2\pi$ (Hz)	$F_L/2$ (mV)	ℓ_c (d's)	$\bar{\gamma}$ (d's)	$f_L \times 10^{-3}$ (lbs/ft)	$C_L \times 10^{-2}$ -	Re$\times 10^3$ -	Predicted I (db re: 20μPa)
91.5	448	400	10.2	3.1	62.23	15.25	23.83	72.0
91.5	448	600	10.2	3.1	93.34	22.87	23.83	75.5
80.9	399	500	10.2	3.1	68.30	34.13	21.07	72.9
78.6	377	400	10.2	3.1	62.23	20.66	20.47	70.5
72.0	347	330	10.2	3.1	51.34	20.31	18.75	68.1
72.0	347	350	10.2	3.1	54.45	21.55	18.75	68.6
58.0	276	150	10.2	3.1	23.34	14.23	15.10	59.2
58.0	276	180	10.2	3.1	28.00	17.08	15.10	60.8
49.4	231	100	10.24	3.12	15.54	13.06	12.86	54.2
48.1	251	120	10.31	3.14	18.59	16.48	12.53	56.5
36.0	166	42	11.81	3.53	6.15	9.74	9.38	43.8
31.3	155	30	12.72	3.80	4.27	8.94	8.15	40.3
31.3	155	35	12.72	3.80	4.98	10.43	8.15	41.6
30.9	144	30	12.81	3.83	4.26	9.15	8.05	39.6
15.4	73	4.2	17.21	5.85	.55	4.75	4.01	16.6
15.4	73	5.25	17.21	5.85	.69	5.94	4.01	18.6
9.6	51	.5	19.98	7.29	.06	1.43	2.50	-5.0
9.6	51	1.5	19.98	7.29	.19	4.28	2.50	4.6

TABLE B-2. AMPLIFIED IMPEDANCE HEAD OUTPUT ($F_L/2$), CORRELATION PARAMETERS, LIFT COEFFICIENT AND PREDICTED SOUND INTENSITY FOR THE UNIFORM 1/4" CYLINDER

$\bar{U}$ (ft/sec)	$\omega/2\pi$ (Hz)	$F_L/2$ (mV)	ℓ_c (d's)	$\bar{\gamma}$ (d's)	$f_L \times 10^{-3}$ (lbs/ft)	$C_L \times 10^{-2}$ -	Re$\times 10^3$ -	Predicted I (db re: 20µPa)
105.9	907	210	10.2	3.1	44.22	16.18	13.8	72.5
105.9	907	157	10.2	3.1	33.06	12.09	13.8	70.0
100.0	853	160	10.25	3.11	33.61	13.79	13.0	69.6
91.5	837	125	10.43	3.19	26.06	12.77	11.91	67.3
73.7	643	58	11.68	3.51	11.48	8.67	9.60	58.3
73.1	667	60	11.72	3.51	11.85	9.10	9.52	59.0
55.8	520	50	13.46	4.12	9.29	12.25	7.27	55.2
55.8	520	35	13.46	4.12	6.51	8.57	7.27	52.1
52.8	462	32	13.82	4.29	5.88	8.66	6.88	50.3
52.8	462	39	13.82	4.29	7.17	10.55	6.88	52.0
48.9	464	20	14.35	4.50	3.62	6.21	6.37	46.3
48.9	464	30	14.35	4.50	5.43	9.32	6.37	49.8
35.8	305	8	16.37	5.40	1.37	4.40	4.66	34.7
35.8	305	12	16.37	5.40	2.06	6.59	4.66	38.2
35.1	336	8	16.48	5.49	1.37	4.56	4.57	35.5
35.1	336	12	16.48	5.49	2.06	6.85	4.57	39.0
31.0	303	5	17.20	5.83	.84	3.60	4.04	30.5
31.0	303	8	17.20	5.83	1.35	5.75	4.04	3 .
27.9	274	4.5	17.80	6.16	.75	3.95	3.63	28.7
27.9	274	5.5	17.80	6.16	.92	4.82	3.63	30.5
17.6	162	1.6	20.50	7.53	.25	3.36	2.29	15.2
12.1	119	.35	22.63	8.12	.05	1.49	1.58	-0.7
12.1	119	.70	22.63	8.12	.10	2.92	1.58	5.3
11.8	103	<1	22.82	8.21	<.15	<4.47	1.54	<7.2
9.3	90	@.225	24.31	9.42	.03	1.60	1.21	<-7.0
6.5	64	<.1	26.30	10.41	<.01	<1.42	.85	<-17.0

TABLE B-3. AMPLIFIED IMPEDANCE HEAD OUTPUT ($F_L/2$), CORRELATION PARAMETERS, LIFT COEFFICIENT AND PREDICTED SOUND INTENSITY FOR THE 1" CYLINDER

$\overline{U}$ (ft/sec)	$\omega/2\pi$ (Hz)	$F_L/2$ (mV)	ℓ_c (d's)	$\overline{\gamma}$ (d's)	$f_L \times 10^{-3}$ (lbs/ft)	$C_L \times 10^{-2}$ -	Re$\times 10^3$ -	Predicted I (db re: 20μPa)
113.8	296	700	10.2	3.1	85.22	6.75	59.27	73.2
103.6	286	500	10.2	3.1	60.87	5.82	53.96	70.0
103.6	286	700	10.2	3.1	85.22	8.14	53.96	72.9
101.6	249	620	10.2	3.1	75.48	7.50	52.90	70.7
90.3	235	500	10.2	3.1	60.87	7.66	47.03	68.3
90.3	235	700	10.2	3.1	85.22	10.72	47.03	71.2
83.7	216	440	10.2	3.1	53.56	7.84	43.60	66.5
74.0	184	400	10.2	3.1	48.69	9.12	38.50	64.2
74.0	184	325	10.2	3.1	39.56	7.41	38.50	62.4
61.0	153	260	10.2	3.1	31.65	8.72	31.77	58.9
61.0	153	200	10.2	3.1	24.35	6.71	31.77	56.6
57.0	137	250	10.2	3.1	30.43	9.61	29.70	57.6
42.2	108	170	10.2	3.1	20.70	11.92	22.00	52.2
32.9	76	80	10.2	3.1	9.74	9.23	17.10	42.6
32.9	76	40	10.2	3.1	4.87	4.61	17.10	36.6
32.0	81	45	10.2	3.1	5.48	5.49	16.70	38.1
32.0	81	80	10.2	3.1	9.74	9.75	16.70	43.1
17.9	47	20	11.83	3.55	2.34	7.48	9.32	26.4
11.7	30	8	14.60	4.61	.92	6.90	6.09	14.5
11.7	30	6	14.60	4.61	.69	5.65	6.09	12.0

TABLE B-4. AMPLIFIED IMPEDANCE HEAD OUTPUT ($F_L/2$), CORRELATION PARAMETERS, LIFT COEFFICIENT AND PREDICTED SOUND INTENSITY FOR THE ROUGHENED 1/2" CYLINDER

$\bar{U}$ (ft/sec)	$\omega/2\pi$ (Hz)	$F_L/2$ (mV)	ℓ_c (d's)	$\bar{\gamma}$ (d's)	$f_L \times 10^{-3}$ (lbs/ft)	$C_L \times 10^{-2}$ -	$Re \times 10^3$ -	Predicted I (db re: 20μPa)
103.0	440	800	6.0	2.21	158.2	30.58	26.82	77.9
103.0	440	675	6.0	2.21	133.4	25.80	26.82	76.4
88.4	376	425	6.02	2.27	84.03	22.06	23.02	71.0
80.6	354	330	6.05	2. 6	66.39	20.96	20.99	68.3
65.3	310	180	6.20	2.37	35.17	16.92	17.01	61.9
56.0	236	110	6.41	2.43	21.17	13.85	14.58	55.2
43.9	201	62	6.83	2.56	11.60	12.35	11.42	48.8
40.4	167	52	6.99	2.61	9.63	12.11	10.52	45.7
32.8	145	27	7.70	2.97	4.82	9.18	8.54	38.8
22.2	97	10	9.23	3.59	1.66	6.91	5.78	26.7
22.2	97	7.5	9.23	3.59	1.24	5.18	5.78	24.2
13.2	63	4	12.08	4.58	.60	7.05	3.44	15.0
13.2	63	2	12.08	4.58	.30	3.52	3.44	8.9
11.5	46	3	12.92	4.88	.44	6.80	2.99	9.7
11.5	46	0.5	12.92	4.88	.07	1.13	2.99	-5.8

TABLE B-5. AMPLIFIED IMPEDANCE HEAD OUTPUT ($F_L/2$), CORRELATION PARAMETERS, LIFT COEFFICIENT AND PREDICTED SOUND INTENSITY FOR THE 1/2" FINNED CYLINDER WITH NO FINS ATTACHED

$\bar{U}$ (ft/sec)	$\omega/2\pi$ (Hz)	$F_L/2$ (mV)	ℓ_c (d's)	$\bar{\gamma}$ (d's)	$f_L \times 10^{-3}$ (lbs/ft)	$C_L \times 10^{-2}$ -	$Re \times 10^3$ -	Predicted I (db re: 20μPa)
110.0	526	500	10.2	3.1	77.79	13.19	28.65	75.3
93.2	479	475	10.2	3.1	73.90	17.83	24.01	74.0
84.3	383	300	10.2	3.1	46.67	13.47	21.95	67.5
82.8	358	600	10.2	3.1	93.34	27.93	21.56	74.1
64.8	318	225	10.2	3.1	35.00	17.10	16.87	64.0
64.8	318	300	10.2	3.1	46.67	22.80	16.87	66.5
57.0	275	150	10.2	3.1	23.34	14.73	14.84	59.2
57.0	275	180	10.2	3.1	28.00	17.68	14.84	60.8
29.2	140	28	13.21	3.99	3.93	9.46	7.60	38.8
17.7	85	<10	16.41	5.45	<1.32	<8.65	4.61	<25.5
12.0	58	1	18.76	6.59	.13	1.83	3.12	2.2
12.0	58	3	18.76	6.59	.39	5.50	3.12	13.7
10.5	50*	1	19.51	6.99	.13	2.39	2.73	0.9
10.5	50*	3	19.51	6.99	.38	7.16	2.73	10.4

*Uncertain

TABLE B-6. AMPLIFIED IMPEDANCE HEAD OUTPUT ($F_L/2$), CORRELATION PARAMETERS, LIFT COEFFICIENT AND PREDICTED SOUND INTENSITY FOR THE FINNED CYLINDER WITH TWO FINS

$\bar{U}$ (ft/sec)	$\omega/2\pi$ (Hz)	$F_L/2$ (mV)	Correlation Factor (d^2)	$C_L \times 10^{-2}$ -	Rex10^3 -	Predicted I (db re: 20μPa)
104.0	486	820	135.9	27.25	27.08	78.9
92.2	438	620	136.1	26.21	24.01	75.6
87.8	400	500	136.3	23.28	22.86	73.0
69.7	334	300	138.0	22.02	18.15	67.0
60.1	272	250	138.9	24.61	15.65	63.6
60.1	272	200	138.9	19.68	15.65	61.6
41.6	200	120	149.9	23.73	10.83	54.5
41.6	200	80	149.9	15.82	10.83	51.0
32.0	158	45	159.6	14.57	8.33	44.0
28.7	143	30	163.8	11.92	7.47	39.6
24.1	125	19	170.0	10.51	6.28	34.5
21.4	91	18	174.8	12.46	5.57	31.2
21.4	91	11	174.8	7.61	5.57	26.9
19.5	105	9	178.1	7.43	5.08	26.4
19.5	105	7	178.1	5.78	5.08	24.3
13.1	61	.5	193.2	.88	3.41	-3.4
13.1	61	10	193.2	17.57	3.41	22.6

TABLE B-7. AMPLIFIED IMPEDANCE HEAD OUTPUT ($F_L/2$), CORRELATION PARAMETERS, LIFT COEFFICIENT AND PREDICTED SOUND INTENSITY FOR THE FINNED CYLINDER WITH FOUR FINS

$\bar{U}$ (ft/sec)	$\omega/2\pi$ (Hz)	$F_L/2$ (mV)	Correlation Factor (d^2)	$C_L \times 10^{-2}$ -	Re$\times 10^3$ -	Predicted I (db re: 20μPa)
107.1	482	850	97.0	31.52	27.89	79.2
94.3	443	750	99.8	35.37	24.56	77.4
90.1	407	720	100.1	37.14	23.46	76.3
89.3	382	700	100.2	36.74	23.26	75.5
84.3	347	667	102.0	38.94	21.95	74.4
84.3	347	467	102.0	27.26	21.95	71.1
64.0	292	473	106.9	46.80	16.67	69.7
64.0	292	273	106.9	27.01	16.67	65.0
57.0	254	245	109.1	30.25	14.84	62.8
50.6	229	210	111.8	32.50	13.18	60.6
45.7	208	120	113.7	22.58	11.90	54.9
45.7	208	150	113.7	28.22	11.90	56.8
40.3	180	120	115.8	28.77	10.49	53.6
37.7	173	95	116.5	25.95	9.82	51.3
33.6	157	70	119.0	23.81	8.75	47.8
27.2	135	42	123.2	21.43	7.08	42.0
23.0	108	20	126.1	14.11	5.99	33.6
14.8	75	5	134.3	8.25	3.85	18.4
14.8	75	7	134.3	11.55	3.85	21.3
10.9	42	<2	140.2	<5.96	2.84	<5.4
7.3	35-40*	<2	148.1	<12.92	1.90	<9.8

*Uncertain

TABLE B-8. AMPLIFIED IMPEDANCE HEAD OUTPUT ($F_L/2$), CORRELATION PARAMETERS, LIFT COEFFICIENT AND PREDICTED SOUND INTENSITY FOR THE 1/2" CYLINDER FITTED WITH THE SMALL SPLITTER PLATE

$\overline{U}$ (ft/sec)	$\omega/2\pi$ (Hz)	$F_L/2$ (mV)	ℓ_c (d's)	$\overline{\gamma}$ (d's)	$f_L \times 10^{-3}$ (lbs/ft)	$C_L \times 10^{-2}$ -	Rex10^3 -	Predicted I (db re: 20μPa)
92.3	283	50	6.23	1.96	9.63	2.32	24.04	50.0
85.6	268	40	6.23	1.96	7.71	2.16	22.29	48.6
82.6	252	38.3	6.23	1.96	7.38	2.22	21.51	46.6
67.6	237	24	6.23	1.96	4.62	2.08	17.60	42.0
67.6	237	30	6.23	1.96	5.78	2.59	17.60	44.0
63.0	175	27	6.24	1.96	5.20	2.69	16.41	40.4
54.6	150	20	6.40	1.96	3.80	1.81	14.22	38.0
49.4	166	12	6.58	1.99	2.25	1.89	12.86	32.2
46.5	139	12	6.70	2.01	2.23	2.12	12.11	31.4
38.7	130	11.5	7.18	2.14	2.07	2.94	10.08	30.4
32.8	120	9	8.10	2.47	1.55	2.78	8.54	27.6
26.6	87	6*	9.78	3.10	.97*	2.84*	6.93	21.3*
26.6	87	10*	9.78	3.10	1.62*	4.73*	6.93	25.7*
18.2	60	7*	12.85	4.25	1.00*	6.28*	4.74	19.5*
18.2	60	10*	12.85	4.25	1.43*	8.88*	4.74	22.6*
11.1	48	<4	16.82	5.75	<.53	<8.79	2.89	<12.6

*Uncertain

TABLE B-9. AMPLIFIED IMPEDANCE HEAD OUTPUT ($F_L/2$), CORRELATION PARAMETERS, LIFT COEFFICIENT AND PREDICTED SOUND INTENSITY FOR THE 1/2" CYLINDER FITTED WITH THE LARGE SPLITTER PLATE

$\bar{U}$ (ft/sec)	$\omega/2\pi$ (Hz)	$F_L/2$ (mV)	ℓ_c (d's)	$\bar{Y}$ (d's)	$f_L \times 10^{-3}$ (lbs/ft)	$C_L \times 10^{-2}$ -	$Re \times 10^3$ -	Predicted I (db re: 20μPa)
97.1	215	42.5	4.80	1.60	9.24	2.01	25.29	46.2
97.1	215	56	4.80	1.60	12.17	2.65	25.29	48.6
90.3	202	41	4.80	1.61	8.91	2.24	23.52	45.3
82.6	179	37.5	4.80	1.63	8.16	2.45	21.51	43.5
65.1	155	20	4.80	1.69	4.36	2.11	16.95	36.8
57.9	142	17	4.83	1.70	3.69	2.26	15.08	34.6
51.7	126	14	5.08	1.71	2.97	2.28	13.46	31.9
37.2	73	9	6.49	1.97	1.70	2.52	9.69	23.3
30.1	69	6	7.76	2.53	1.05	2.38	7.84	19.3
30.1	69	8	7.76	2.53	1.40	3.18	7.84	21.8
23.6	55	4	9.77	3.50	.64	2.37	6.15	13.8
23.6	55	8	9.77	3.50	1.29	4.74	6.15	19.8
16.7	38*	<3*	12.66	4.89	<.44*	<3.26*	4.35	<8.1*
11.2	25*	<2*	16.00	6.47	<.28*	<4.54*	2.92	<0.9*

*Uncertain

TABLE B-10a. AMPLIFIED IMPEDANCE HEAD OUTPUT ($F_L/2$), CORRELATION PARAMETERS, LIFT COEFFICIENT AND PREDICTED SOUND INTENSITY FOR THE TWO-NOTCHED CYLINDER: 1/2" SECTION

$\overline{U}$ (ft/sec)	$\omega/2\pi$ (Hz)	$F_L/2$ (mV)	Uniform Cylinder ℓ_c (d's)	$\overline{\gamma}$ (d's)	$f_L \times 10^{-3}$ (lbs/ft)	$C_L \times 10^{-2}$ -	$Re \times 10^3$ -	Predicted I (db re: 20μPa)
104.0	444	433	10.2	3.1	105.4	19.99	27.08	72.6
104.0	444	650	10.2	3.1	158.3	30.01	27.08	76.1
90.1	388	370	10.2	3.1	90.08	22.76	23.46	70.1
84.3	346	280	10.2	3.1	68.17	19.68	21.95	66.7
70.6	310	200	10.2	3.1	48.69	20.04	18.39	62.8
62.2	280	120	10.2	3.1	29.22	15.49	16.20	57.5
62.2	280	145	10.2	3.1	35.30	18.72	16.20	59.1
57.2	271	120	10.2	3.1	29.22	18.32	14.90	57.2
51.8	242	80	10.2	3.1	19.48	14.90	13.49	52.7
42.1	201	34	10.9	3.28	8.11	9.39	10.96	42.7
39.6	182	30	11.4	3.39	7.06	9.23	10.31	41.7
33.2	154	22	12.4	3.70	5.08	9.46	8.65	37.5
31.4	143	15	12.7	3.81	3.46	7.19	8.18	33.6
26.6	120	10	13.8	4.28	2.29	6.66	6.93	28.5
24.8	125	9	14.3	4.46	2.07	6.89	6.46	28.0
24.1	111	9	14.4	4.52	2.07	7.31	6.28	26.9
22.8	103	4.5	14.8	4.69	1.04	4.09	5.94	20.3
16.8	86	3.25	16.8	5.59	.77	5.61	4.38	15.9
16.7	83	2.75	16.8	5.62	.65	4.82	4.35	14.1
9.0	43	<3.5	20.0*	5.00*	<.71	<18.1	2.34	<10.5

*If $(L-\overline{\gamma})\ell_c > L^2$, use L^2 as the correlation factor.

TABLE B-10b. AMPLIFIED IMPEDANCE HEAD OUTPUT ($F_L/2$), CORRELATION PARAMETERS, LIFT COEFFICIENT AND PREDICTED SOUND INTENSITY FOR THE TWO-NOTCHED CYLINDER: 3/8" SECTION

$\bar{U}$ (ft/sec)	$\omega/2\pi$ (Hz)	$F_L/2$ (mV)	Uniform Cylinder ℓ_c (d's)	$\bar{\gamma}$ (d's)	$f_L \times 10^{-3}$ (lbs/ft)	$C_L \times 10^{-2}$ -	Rex10^3 -	Predicted I (db re: 20μPa)
104.0	613	250	10.2	3.1	66.64	16.85	20.31	70.6
104.0	613	350	10.2	3.1	93.30	23.59	20.31	73.6
90.1	532	200	10.2	3.1	53.28	17.98	17.60	67.5
90.1	532	300	10.2	3.1	79.92	26.97	17.60	71.0
84.3	478	163	10.2	3.1	43.45	16.72	16.46	64.8
84.3	478	203	10.2	3.1	54.11	20.83	16.46	66.7
70.6	430	100	10.2	3.1	26.66	14.63	13.79	59.6
62.2	392	84	10.4	3.14	22.22	15.71	12.15	57.3
57.2	382	60	10.8	3.25	15.66	13.09	11.17	54.1
51.8	311	45	11.4	3.41	10.36	10.74	10.12	49.9
42.1	253	26	12.7	3.79	6.44	9.92	8.22	43.3
39.6	243	20	13.1	3.95	4.91	8.57	7.73	40.7
33.2	211	14	14.3	4.45	3.38	8.40	6.48	37.3
31.4	236	8	14.6	4.60	1.93	5.35	6.13	32.5
26.6	181	8	15.6	5.09	1.92	7.43	5.20	30.2
24.8	179	6	16.1	5.29	1.44	6.39	4.84	27.6
24.1	163	6	16.3	5.38	1.44	6.76	4.71	26.7
22.8	146	3	16.7	5.55	.72	3.77	4.45	19.8
16.8	123	1.5	18.5	6.48	.36	3.52	3.28	12.3
16.7	109	1.3	18.5	6.50	.31	3.05	3.26	10.0
9.0	58	<3.25	26.7*	6.67*	<.66	<22.41	1.76	<12.4

*If $(L-\bar{\gamma})\ell_c > L^2$, use L^2 as the correlation factor.

TABLE B-11a. AMPLIFIED IMPEDANCE HEAD OUTPUT ($F_L/2$), CORRELATION PARAMETERS, LIFT COEFFICIENT AND PREDICTED SOUND INTENSITY FOR THE REGULAR MULTI-NOTCHED CYLINDER: 1/2" SECTIONS

$\overline{U}$ (ft/sec)	$\omega/2\pi$ (Hz)	$F_L/2$ (mV)	Correlation Factor (d^2)	$f_L \times 10^{-3}$ (lbs/ft)	$C_L \times 10^{-2}$ -	Rex10^3 -	Predicted I (db re: 20μPa)
115.0	494	42	2.865	50.7	7.86	30.0	53.3
115.0	494	50	2.865	60.3	9.36	30.0	54.8
115.0	449	34.3	2.865	41.4	6.42	30.0	50.7
98.0	460	32.5	2.865	39.2	8.38	25.5	50.4
88.9	420	29.0	2.865	35.0	9.08	23.2	48.7
85.4	380	22.5	2.865	27.15	7.64	22.6	45.6
*62.9	277	13.3	2.865	16.02	8.32	16.4	38.3
*61.2	248	10.0	2.865	12.07	6.61	15.9	34.8
*61.2	248	7.5	2.865	9.05	4.96	15.9	32.3
*60.1	280	8	2.865	9.65	5.48	15.7	33.9
*60.1	280	11	2.865	13.27	7.54	15.7	36.7
*60.1	234	8.75	2.865	10.56	6.00	15.7	33.2
*60.1	271	8	2.865	9.65	5.48	15.7	33.7
*60.1	271	12	2.865	14.50	8.22	15.7	37.2
**49.4	235	5	2.865	6.03	5.07	12.9	28.3
**46.4	225	4.5	2.865	5.43	5.17	12.1	27.0
**46.4	225	3.0	2.865	3.62	3.45	12.1	23.5
**37.9	178	2.25	2.865	2.72	3.88	9.9	19.0
**29.2	147	1	2.865	1.21	2.90	7.6	10.3
**29.2	147	2.5	2.865	3.02	7.26	7.6	18.2
**23.5	111	1.1	2.865	1.33	4.93	6.1	8.7
**10.9	46	≤1	2.865	1.21	<20.8	2.8	<0.2

*Uncertain entries in this row

**Very uncertain entries in this row

TABLE B-11b. AMPLIFIED IMPEDANCE HEAD OUTPUT ($F_L/2$), UNIFORM CYLINDER C_L, CALCULATED EFFECTIVE LENGTH AND PREDICTED SOUND INTENSITY FOR THE REGULAR MULTINOTCHED CYLINDER: 3/8" SECTIONS

$\bar{U}$ (ft/sec)	$\omega/2\pi$ (Hz)	$F_L/2$ (mV)	$Re \times 10^3$	Uniform Cylinder $C_L \times 10^{-2}$	Effective Length (d)	Predicted I (db re: 20 μPa)
115	617	21	22.5	22.5	.30	49.2
98	600	15	19.1	21.0	.31	46.0
88.9	521	12.2	17.4	19.1	.34	43.0
88.9	556	11	17.4	19.1	.31	42.7
85.4	522	6.25	16.7	18.3	.20	37.2
* 62.9	368	3.5	12.3	13.8	.27	29.1
* 61.2	359	3.5	12.0	13.6	.29	28.9
* 60.1	350	3	11.7	13.3	.26	27.4
* 60.1	350	4	11.7	13.3	.35	29.9
* 49.4	332	3	9.6	11.2	.46	26.9
* 46.4	300	2	9.1	10.5	.37	22.5
* 46.4	300	4	9.1	10.5	.74	28.5
* 37.9	233	1	7.4	8.65	.34	14.3
* 37.9	233	2	7.4	8.65	.67	20.3
* 29.2	180	.6	5.7	6.85	.43	7.6
* 29.2	180	1	5.7	6.85	.72	12.0
* 23.5	149	≤1	4.6	5.6	<.77	≤10.4
**10.9	+	<1	2.1	2.7	<13.1	+

* Entries in this row are uncertain

** Extremely uncertain

\+ Cannot be determined

TABLE B-12. AMPLIFIED IMPEDANCE HEAD OUTPUT ($F_L/2$), CORRELATION PARAMETERS, LIFT COEFFICIENT AND PREDICTED SOUND INTENSITY FOR THE SKEWED CYLINDER AT NORMAL ($\beta = 0°$) INCIDENCE

$\overline{U}$ (ft/sec)	$\omega/2\pi$ (Hz)	$F_L/2$ (mV)	ℓ_c (d's)	$\overline{Y}$ (d's)	$C_L \times 10^{-2}$ -	$Re \times 10^3$ -	Predicted I (db re: 20μPa)
90.9	466	500	8.9	2.83	20.51	23.67	74.3
70.6	338	270	8.9	2.83	18.36	18.39	66.1
50.9	241	120	8.9	2.83	15.70	13.26	56.2
35.8	169	42	10.4	3.20	10.39	9.32	44.0
17.7	88	5.5	14.0	4.59	5.01	4.61	20.6
17.7	81	2	14.0	4.59	1.82	4.61	11.1

TABLE B-13. FORCE, CORRELATION AND FREQUENCY PARAMETERS, AND PREDICTED I FOR SKEWED CYLINDERS: $\beta = 10.9°$

$\bar{U}$ (ft/sec)	$\bar{U} \cos\beta$ (ft/sec)	$Re x 10^3 \cdot \cos\beta$	$\omega/2\pi$ (Hz)	ω/ω_s –	$\bar{U} \cdot \omega/\omega_s$ (ft/sec)	$Re x 10^3 \cdot \omega/\omega_s$ –
99.2	97.4	25.37	472	.991	96.3	25.11
82.3	80.8	21.05	402	1.018	79.9	21.09
70.6	69.3	18.05	333	.983	68.6	17.72
53.3	52.3	13.63	286	1.118	51.8	15.11
53.3	52.3	13.63	209	.817	51.8	11.30
42.9	42.1	10.97	172	.835	41.7	9.32
34.3	33.7	8.77	171	1.039	33.3	9.30
24.8	24.4	6.34	115	.966	24.1	6.24
17.7	17.4	4.53	90	1.059	17.2	4.79
17.7	17.4	4.53	48	.565	17.2	2.61

		Measured			Skewed Cylinder Normal Incidence			Predicted
$\bar{U}$ (ft/sec)	$F_L/2$ (mV)	ℓ_c (d's)	$\bar{\gamma}$ (d's)	$C_L x 10^{-2}$ –	ℓ_c (d's)	$\bar{\gamma}$ (d's)	$C_L x 10^{-2}$ –	I (db re: 20μPa)
99.2	500	7.6	2.8	19.31	2.83	17.86	74.4	8.9
82.3	320	7.6	2.8	17.96	2.83	16.61	69.1	8.9
70.6	250	7.7	2.8	18.95	2.83	17.64	65.3	8.9
53.3	105	7.75	2.8	13.93	2.83	13.01	56.5	8.9
53.3	150	7.75	2.8	19.90	2.83	18.59	56.9	8.9
42.9	85	7.85	2.8	17.29	2.99	15.89	50.2	9.4
34.3	40	8.4	3.1	12.39	3.48	11.15	43.6	10.6
24.8	20	9.5	3.35	11.19	3.90	10.00	34.2	12.3
17.7	1	10.5	3.55	1.05	4.59	.94	6.0	14.0
17.7	6	10.5	3.55	6.32	4.59	5.65	15.8	14.0

TABLE B-14. FORCE, CORRELATION AND FREQUENCY PARAMETERS, AND PREDICTED I FOR SKEWED CYLINDERS; $\beta = 21.2°$

$\bar{U}$ (ft/sec)	$\bar{U}\cos\beta$ (ft/sec)	$Re \times 10^3 \cdot \cos\beta$ -	$\omega/2\pi$ (Hz)	ω/ω_s -	$\bar{U} \cdot \omega/\omega_s$ (ft/sec)	$Re \times 10^3 \cdot \omega/\omega_s$ -
85.8	80.0	20.83	328	.796	76.4	17.75
61.6	57.4	14.96	259	.876	54.8	14.05
48.6	45.3	11.80	229	.982	43.3	12.41
39.6	36.9	9.62	171	.900	35.3	9.29
32.2	30.0	7.82	130	.841	28.7	7.06
32.2	30.0	7.82	130	.841	28.7	7.06
23.4	21.8	5.68	112	.997	20.8	6.07
15.4	14.4	3.74	55	.744	13.7	2.95
15.4	14.4	3.74	55	.744	13.7	2.95

		Measured			Skewed Cylinder Normal Incidence			Predicted I
$\bar{U}$ (ft/sec)	$F_L/2$ (mV)	ℓ_c (d's)	$\bar{\gamma}$ (d's)	$C_L \times 10^{-2}$ -	ℓ_c (d's)	$\bar{\gamma}$ (d's)	$C_L \times 10^{-2}$ -	(db re: 20μPa)
85.8	350	6.3	2.3	20.57	2.83	17.54	68.1	8.9
61.6	142	6.4	2.4	16.12	2.83	13.82	58.2	8.9
48.6	95	6.5	2.4	17.18	2.90	14.88	53.7	8.9
39.6	60	6.5	2.4	16.36	3.00	13.53	47.2	9.8
32.2	20	6.5	2.5	8.27	3.79	6.61	35.2	10.9
32.2	25	6.5	2.5	10.34	3.79	8.26	37.2	10.9
23.4	9	6.7	2.6	6.96	4.02	5.27	27.0	12.6
15.4	3.75	6.8	2.7	6.61	4.82	4.77	13.2	14.7
15.4	7.5	6.8	2.7	13.23	4.82	9.54	19.2	14.7

TABLE B-15. FORCE, CORRELATION AND FREQUENCY PARAMETERS, AND PREDICTED I FOR SKEWED CYLINDERS: $\beta = 30.4°$

$\bar{U}$ (ft/sec)	$\bar{U}\cos\beta$ (ft/sec)	$Re \times 10^3 \cdot \cos\beta$ –	$\omega/2\pi$ (Hz)	ω/ω_s –	$\bar{U}\cdot\omega/\omega_s$ (ft/sec)	$Re \times 10^3 \cdot \omega/\omega_s$ –
88.0	75.9	19.76	336	.795	69.4	18.21
80.9	69.8	18.16	285	.734	63.8	15.49
68.1	58.7	15.29	255	.780	53.7	13.82
54.3	46.8	12.19	190	.729	42.8	10.30
42.8	36.9	9.61	155	.754	33.8	8.41
39.6	34.1	8.89	149	.784	31.2	8.09
39.6	34.1	8.89	149	.784	31.2	8.09
32.2	27.8	7.23	127	.822	25.4	6.89
25.7	22.2	5.77	104	.843	20.3	5.64
25.7	22.2	5.77	104	.843	20.3	5.64
17.7	15.3	3.97	73	.859	14.0	3.96
17.7	15.3	3.97	73	.859	14.0	3.96

	Measured				Skewed Cylinder Normal Incidence			Predicted I
$\bar{U}$ (ft/sec)	$F_L/2$ (mV)	ℓ_c (d's)	$\bar{\gamma}$ (d's)	$C_L \times 10^{-2}$ –	ℓ_c (d's)	$\bar{\gamma}$ (d's)	$C_L \times 10^{-2}$ –	(db re: 20µPa)
88.0	200	5.15	1.88	13.63	2.83	10.60	63.5	8.9
80.9	140	5.15	1.88	11.28	2.83	8.77	59.0	8.9
68.1	65	5.15	1.88	7.41	2.83	5.76	51.3	8.9
54.3	60	5.15	1.88	10.75	2.83	8.36	48.1	8.9
42.8	50	5.15	1.88	14.42	2.99	10.95	44.7	9.4
39.6	30	5.15	1.88	10.13	3.00	7.54	39.9	9.8
39.6	45	5.15	1.88	15.19	3.00	11.30	43.5	9.8
32.2	19	5.15	1.88	9.65	3.79	6.94	34.6	10.9
25.7	6	5.15	1.88	4.78	3.83	3.27	22.8	12.1
25.7	17	5.15	1.88	13.54	3.83	9.25	31.9	12.1
17.7	0.8	5.15	1.88	1.34	4.59	.87	2.3	14.0
17.7	1.2	5.15	1.88	2.01	4.59	1.30	5.8	14.0

TABLE B-16. FORCE, CORRELATION AND FREQUENCY PARAMETERS, AND PREDICTED I FOR SKEWED CYLINDERS: β = 38.8°

$\overline{U}$ (ft/sec)	$\overline{U}\cos\beta$ (ft/sec)	Rex10^3 · $\cos\beta$ -	$\omega/2\pi$ (Hz)	ω/ω_s -	$\overline{U}\cdot\omega/\omega_s$ (ft/sec)	Rex10^3 · ω/ω_s -
92.4	72.1	18.77	288	.649	57.7	15.61
85.1	66.4	17.28	261	.639	53.1	14.13
85.1	66.4	17.28	261	.639	53.1	14.13
79.6	62.1	16.17	259	.678	49.7	14.02
79.6	62.1	16.17	259	.678	49.7	14.02
62.2	48.5	12.63	189	.633	38.8	10.25
62.2	48.5	12.63	189	.633	38.8	10.25
52.8	41.2	10.72	158	.623	32.9	8.56
52.8	41.2	10.72	158	.623	32.9	8.56
34.7	27.1	7.05	91	.546	21.7	4.94
34.7	27.1	7.05	91	.546	21.7	4.94
22.3	17.4	4.53	63	.589	13.9	2.67
22.3	17.4	4.53	63	.589	13.9	2.67
15.4	12.0	3.13	47	.636	9.6	2.54

	Measured				Skewed Cylinder Normal Incidence			Predicted I
$\overline{U}$ (ft/sec)	$F_L/2$ (mV)	ℓ_c (d's)	$\overline{\gamma}$ (d's)	C_Lx10^{-2} -	ℓ_c (d's)	$\overline{\gamma}$ (d's)	C_Lx10^{-2} -	(db re: 20μPa)
92.4	115	4.9	1.76	8.88	2.83	6.75	57.3	8.9
85.1	100	4.9	1.76	9.10	2.83	6.92	55.3	8.9
85.1	140	4.9	1.76	12.74	2.83	9.69	58.2	8.9
79.6	75	4.9	1.76	7.81	2.83	5.94	52.7	8.9
79.6	110	4.9	1.76	11.45	2.83	8.71	56.0	8.9
62.2	40	4.9	1.76	6.83	2.83	5.19	44.5	8.9
62.2	80	4.9	1.76	13.65	2.83	10.38	50.5	8.9
52.8	35	4.9	1.76	8.28	2.83	6.29	41.8	8.9
52.8	50	4.9	1.76	11.82	2.83	8.99	44.9	8.9
34.7	10	4.9	1.76	5.47	3.45	3.87	26.1	10.6
34.7	20	4.9	1.76	10.93	3.45	7.73	32.1	10.6
22.3	4.4	4.9	1.76	5.83	4.14	3.82	15.8	12.8
22.3	8.8	4.9	1.76	11.67	4.14	7.64	21.8	12.8
15.4	<4	4.9	1.76	<11.15	4.82	< 6.93	<12.4	14.7

TABLE B-17. FORCE, CORRELATION AND FREQUENCY PARAMETERS, AND PREDICTED I FOR SKEWED CYLINDERS: $\beta = 45°$

$\overline{U}$ (ft/sec)	$\overline{U}\cos\beta$ (ft/sec)	$Re \times 10^3 \cdot \cos\beta$ —	$\omega/2\pi$ (Hz)	ω/ω_s —	$\overline{U} \cdot \omega/\omega_s$ (ft/sec)	$Re \times 10^3 \cdot \omega/\omega_s$ —
100.0	70.7	18.41	320	.667	59.4	17.36
92.4	65.3	17.01	264	.595	54.9	14.31
92.4	65.3	17.01	264	.595	54.9	14.31
71.4	50.5	13.15	214	.624	42.4	11.59
71.4	50.5	13.15	214	.624	42.4	11.59
61.6	43.6	11.34	173	.585	36.6	9.39
61.6	43.6	11.34	173	.585	36.6	9.39
51.8	36.6	9.54	138	.555	30.8	7.48
51.8	36.6	9.54	138	.555	30.8	7.48
36.2	25.6	6.67	102	.587	21.5	5.54
36.2	25.6	6.67	102	.587	21.5	5.54
22.8	16.1	4.20	60	.548	13.5	3.26
22.8	16.1	4.20	60	.548	13.5	3.26
16.3	11.5	3.00	40	.511	9.7	2.29

	Measured				Skewed Cylinder Normal Incidence			Predicted I
$\overline{U}$ (ft/sec)	$F_L/2$ (mV)	ℓ_c (d's)	$\overline{\gamma}$ (d's)	$C_L \times 10^{-2}$ —	ℓ_c (d's)	$\overline{\gamma}$ (d's)	$C_L \times 10^{-2}$ —	(db re: 20μPa)
100.0	70	3.4	1.38	6.17	2.83	3.92	53.9	8.9
92.4	60	3.6	1.41	6.03	2.83	3.94	50.9	8.9
92.4	90	3.6	1.41	9.04	2.83	5.91	54.5	8.9
71.4	40	3.9	1.82	6.50	2.83	4.39	45.6	8.9
71.4	45	3.9	1.82	7.32	2.83	4.94	46.6	8.9
61.6	25	3.9	1.82	5.45	2.83	3.68	39.7	8.9
61.6	30	3.9	1.82	6.54	2.83	4.42	41.2	8.9
51.8	10	3.9	1.82	3.10	2.83	2.09	29.7	8.9
51.8	15	3.9	1.82	4.64	2.83	3.13	33.3	8.9
36.2	4	3.9	1.82	2.53	3.19	1.60	19.2	10.3
36.2	8	3.9	1.82	5.06	3.19	3.20	25.2	10.3
22.8	3	3.9	1.82	4.80	4.05	2.78	12.0	12.7
22.8	6	3.9	1.82	9.60	4.05	5.56	18.1	12.7
16.3	<3	3.9	1.82	<9.41	4.73	<5.19	<8.5	14.4

TABLE B-18. MEASURED SOUND INTENSITY FOR THE UNIFORM 1/2" CYLINDER

$\bar{U}$ (ft/sec)	$\omega/2\pi$ (Hz)	Recorded I (db)	Microphone Sensitivity (db re: 1V/10^5 μPa)	I Radiated from Cylinder (db re: 20μPa)
102.3	463	-31.0	-75.1	78.1
88.9	396	-41.0	-75.3	68.3
80.3	367	-39.3	-75.4	70.1
51.5	247	-48.5	-75.8	61.3
44.7	209	-61.5	-75.9	48.4
33.7	167	-70.4	-76.9	40.5
21.4	120	-76.0	-78.5	36.5
19.0	104	-92.4	-79.1	20.7
16.1	80*	<-90	-80.6*	<24.6*

*Uncertain

TABLE B-19. MEASURED SOUND INTENSITY FOR THE 1/4" CYLINDER

$\bar{U}$ (ft/sec)	$\omega/2\pi$ (Hz)	Recorded I (db)	Microphone Sensitivity (db re: 1V/10^5 μPa)	I Radiated from Cylinder (db re: 20 μPa)
94.1	956	-42.0	-74.4	66.4
88.9	867	-42.0	-74.6	66.6
80.3	787	-48.3	-74.7	60.4
75.7	761	-51.0	-74.7	57.7
63.8	640	-55.0	-74.9	53.9
48.9	501	-66.5	-75.1	42.6
31.1	307	-68.0*	-75.7	41.7*
21.8	212*	<-91*	-75.9*	<18.9
15.5	144*	<-87*	-77.6*	<24.6*
11.7	104*	<-96*	-79.1*	<17.1*
9.2	92*	<-91*	-79.6*	<22.6*

*Uncertain

TABLE B-20. MEASURED SOUND INTENSITY FOR THE 1" CYLINDER

$\bar{U}$ (ft/sec)	$\omega/2\pi$ (Hz)	Recorded I (db)	Microphone Sensitivity (db re: 1V/10^5 μ Pa)	I Radiated from Cylinder (db re: 20 μPa)
91.5	249	-34.0	-75.9	75.9
84.0	219	-39.0	-76.0	71.0
66.9	181	-46.0	-76.6	64.6
57.9	150	-52.5	-77.3	59.2
33.0	87	-72.0	-80.0	42.0
21.4	55	<-76*	-84.7	<42.7*
13.3	32*	<-83*	-93.0*	<44*

*Uncertain

TABLE B-21. MEASURED SOUND INTENSITY FOR THE ROUGHENED 1/2" CYLINDER

$\bar{U}$ (ft/sec)	$\omega/2\pi$ (Hz)	Recorded I (db)	Microphone Sensitivity (db re: 1V/10^5 μPa)	I Radiated from Cylinder (db re: 20 μPa)
90.2	435	-36.7	-75.2	72.9
79.2	384	-44.0	-75.4	65.4
57.9	249	-50.8	-75.8	59.0
45.9	184	-62.8	-76.6	47.8
28.0	120	-76.0	-78.5	36.5
14.2	94	<-80*	-79.7	<33.7*

*Uncertain

TABLE B-22. MEASURED SOUND INTENSITY FOR THE FINNED CYLINDER WITH NO FINS ATTACHED

$\bar{U}$ (ft/sec)	$\omega/2\pi$ (Hz)	Recorded I (db)	Microphone Sensitivity (db re: $1V/10^5$ μPa)	I Radiated from Cylinder (db re: 20 μPa)
88.9	428	-35.6	-75.2	73.8
74.5	377	-40.6	-75.3	68.7
50.2	247	-49.2	-75.9	60.7
34.3	182	-64.0	-76.6	46.6
21.4	123	-74.0	-78.4	38.4
9.2	46*	<-91*	-87.2*	<30.2*

*Uncertain

TABLE B-23. MEASURED SOUND INTENSITY FOR THE CYLINDER WITH 2 FINS

$\overline{U}$ (ft/sec)	$\omega/2\pi$ (Hz)	Recorded I (db)	Microphone Sensitivity (db re: 1V/10^5 μPa)	I Radiated from Cylinder (db re: 20 μPa)
88.9	421	-34.1	-75.3	75.2
79.2	361	-39.0	-75.4	70.4
49.7	237	-51.0	-75.9	58.9
37.5	187	-61.9	-76.3	48.4
21.6	126	-77.0	-78.3	35.3
10.1	52	<-86*	-85.1	<33.1*

*Uncertain

TABLE B-24. MEASURED SOUND INTENSITY FOR THE CYLINDER WITH FOUR FINS

$\bar{U}$ (ft/sec)	$\omega/2\pi$ (Hz)	Recorded I (db)	Microphone Sensitivity (db re: $1V/10^5$ μPa)	I Radiated from Cylinder (db re: 20 μPa)
90.2	418	-33.0	-75.3	76.3
81.5	363	-35.5	-75.4	73.9
53.2	244	-47.8	-75.8	62.0
37.1	179	-61.1	-76.6	49.5
28.3	133	-71.0	-78.0	41.0
16.1	81	<-90*	-80.4	≤21.4*

*Uncertain

TABLE B-25. MEASURED SOUND INTENSITY FOR THE 1/2" CYLINDER WITH SMALL SPLITTER PLATE

$\overline{U}$ (ft/sec)	$\omega/2\pi$ (Hz)	Recorded I (db)	Microphone Sensitivity (db re: 1V/10^5 μPa)	I Radiated from Cylinder (db re: 20 μPa)
102.3	363	-56	-75.3	53.3
91.5	322	-58	-75.6	51.6
88.9	292	-61	-75.7	48.7
86.4	280	-62	-75.7	47.7
68.0	232	-70	-75.9	39.9
50.6	179*	-73*	-76.7*	37.7*
43.1	135*	-78*	-77.9*	33.9*
26.2	86*	-89*	-80.1*	25.1*

*Uncertain

TABLE B-26. MEASURED SOUND INTENSITY FOR THE 1/2" CYLINDER WITH LARGE SPLITTER PLATE

$\bar{U}$ (ft/sec)	$\omega/2\pi$ (Hz)	Recorded I (db)	Microphone Sensitivity (db re: 1V/10^5 μPa)	I Radiated from Cylinder (db re: 20 μPa)
103.7	226	-62	-75.9	47.9
103.7	252	-62	-75.8	47.8
91.5	195	-64	-76.2	46.2
87.7	185	-67	-76.4	43.4
68.0	167	-72	-77.0	39.0
55.1	116	-78	-78.7	34.7
43.1	90	-86.5*	-79.9	27.4*

*Uncertain

TABLE B-27. MEASURED SOUND INTENSITY FOR THE TWO-NOTCHED CYLINDER

$\bar{U}$ (ft/sec)	$\omega/2\pi$ (Hz)	Recorded I (db)	Microphone Sensitivity (db re: 1V/10^5 μPa)	I Radiated from Cylinder (db re: 20 μPa)
(a) 1/2" SECTIONS				
90.2	441	-41.0	-75.3	68.3
74.5	373	-49.0	-75.5	60.5
43.1	246	-65.0	-75.9	44.9
20.7	90	-85.0*	-79.9	28.9*
(b) 3/8" SECTIONS				
90.2	597	-37.5	-75.0	71.5
74.5	507	-45.0	-75.1	64.1
43.1	330*	-66.0*	-75.6*	43.6*
20.7	130	<-92.0*	-77.6	<19.6*

*Uncertain

TABLE B-28. MEASURED SOUND INTENSITY FOR THE REGULAR MULTINOTCHED CYLINDER

$\bar{U}$ (ft/sec)	$\omega/2\pi$ (Hz)	Recorded I (db)	Microphone Sensitivity (db re: 1V/10^5 μPa)	I Radiated from Cylinder (db re: 20μPa)
(a) 1/2" SECTIONS				
99.5	484	-58.5	-75.1	50.6
91.5	437	-62.0	-75.2	47.2
85.2	384	-65.0	-75.3	44.3
(b) 3/8" SECTIONS				
99.5	600	-63	-75.0	46.0
91.5	549	-66	-75.0	43.0
85.2	528	<-71	-75.1	<38.1

TABLE B-29. MEASURED SOUND INTENSITY FOR THE IRREGULAR MULTINOTCHED CYLINDER

$\bar{U}$ (ft/sec)	$\omega/2\pi$ (Hz)	Recorded I (db)	Microphone Sensitivity (db re: 1V/10^5 μPa)	I Radiated from Cylinder (db re: 20 μPa)
(a) 1/2" SECTIONS				
90.8	484	-56	-75.1	53.1
87.1	439	-58	-75.2	51.2
74.5	385	-61	-75.3	48.3
57.9	241	-73	-75.9	36.9
(b) 3/8" SECTIONS				
90.8	633	-54	-74.9	54.9
87.1	575	-60	-75.0	49.0
74.5	498	-62	-75.1	47.1
57.9	325	-74	-75.6	35.6

TABLE B-30. MEASURED SOUND INTENSITY FOR THE SKEWED CYLINDER AT NORMAL INCIDENCE ($\beta = 0°$)

$\overline{U}$ (ft/sec)	$\omega/2\pi$ (Hz)	Recorded I (db)	Microphone Sensitivity (db re: $1V/10^5$ μPa)	I Radiated from Cylinder (db re: 20 μPa)
95.5	464	-42	-75.1	67.1
87.7	401	-45	-75.3	64.3
80.9	360	-49	-75.4	60.4
50.2	243	-59	-75.8	50.8
25.1	124	-81*	-78.4	31.4*
10.4	47*	<-88*	-86.8*	<32.8*

*Uncertain

TABLE B-31. MEASURED SOUND INTENSITY FOR THE SKEWED CYLINDER: $L_\perp$ = 9 7/16"; β = 9.8°

$\overline{U}$ (ft/sec)	$\omega/2\pi$ (Hz)	Recorded I (db)	Microphone Sensitivity (db re: 1V/10^5 μPa)	I Radiated from Cylinder (db re: 20 μPa)	$\overline{U}$ cos β (ft/sec)	$\overline{U}$ • (ω/ω_s) (ft/sec)
88.9	393	-38.0	-75.3	71.3	87.6	88.1
76.3	347	-41.0	-75.5	68.5	75.2	75.6
44.7	224	-59.0	-75.9	50.9	44.0	44.3
34.0	163	-66.7	-76.9	44.2	33.5	33.7
21.4	107	-83.0*	-79.0	30.0*	21.0	21.1
11.9	47*	<-87.0*	-86.8*	<33.8*	11.7	11.7

*Uncertain

TABLE B-32. MEASURED SOUND INTENSITY FOR THE SKEWED CYLINDER: $L_{\perp}$ = 9 9/16"; β = 22.1°

$\bar{U}$ (ft/sec)	$\omega/2\pi$ (Hz)	Recorded I (db)	Microphone Sensitivity (db re: 1V/$10^5\mu$Pa)	I Radiated from Cylinder (db re: 20 μPa)	$\bar{U}\cos\beta$ (ft/sec)	$\bar{U}\cdot(\omega/\omega_s)$ (ft/sec)
86.4	370	-40.5	-75.4	68.9	80.1	77.3
70.1	319	-46	-75.6	63.6	65.0	62.7
47.2	201	-56	-76.1	54.1	43.7	42.2
34.3	148	-68	-77.5	43.5	31.8	30.7
25.1	102	-79*	-79.3	34.3*	23.3	22.5
11.5	48	<-87*	-86.4	<33.4*	10.7	10.3

*Uncertain

TABLE B-33. MEASURED SOUND INTENSITY FOR THE SKEWED CYLINDER: $L_{\perp} = 9\ 3/8"$; $\beta = 32.6°$

$\bar{U}$ (ft/sec)	$\omega/2\pi$ (Hz)	Recorded I (db)	Microphone Sensitivity (db re: $1V/10^5\ \mu Pa$)	I Radiated from Cylinder (db re: 20 μPa)	$\bar{U} \cos \beta$ (ft/sec)	$\bar{U} \cdot (\omega/\omega_s)$ (ft/sec)
91.5	373	-46.5	-75.4	62.9	77.1	75.3
87.1	322	-48.0	-75.5	61.5	73.4	71.7
71.8	290	-52.5	-75.5	57.2	60.5	59.1
48.9	188	-65	-76.3	45.3	41.2	40.2
34.7	142	-74*	-77.7	37.7*	29.2	28.6
22.2	78	<-89*	-80.7	<25.7*	18.7	18.3

*Uncertain

TABLE B-34. MEASURED SOUND INTENSITY FOR THE SKEWED CYLINDER: $L_\perp = 9\ 3/8"$; $\beta = 39.6°$

$\overline{U}$ (ft/sec)	$\omega/2\pi$ (Hz)	Recorded I (db)	Microphone Sensitivity (db re: $1V/10^5\mu Pa$)	I Radiated from Cylinder (db re: $20\mu Pa$)	$\overline{U}\cos\beta$ (ft/sec)	$\overline{U}\cdot(\omega/\omega_s)$ (ft/sec)
93.5	305	-51	-75.6	58.6	72.1	63.8
85.2	264*	-55	-75.8*	54.8*	65.7	58.1
74.5	263*	-57	-75.8*	52.8*	57.4	39.2
49.7	162*	-71	-76.9*	39.9*	38.3	33.9
37.1	119*	-76*	-78.5*	36.5*	28.6	25.3
21.8	81*	<-89*	-80.4*	<25.4*	16.8	14.9

*Uncertain

TABLE B-35. MEASURED SOUND INTENSITY FOR THE SKEWED CYLINDER: $L_{\perp} = 9\ 3/4"$; $\beta = 45°$

$\bar{U}$ (ft/sec)	$\omega/2\pi$ (Hz)	Recorded I (db)	Microphone Sensitivity (db re: 1V/$10^5\mu$Pa)	I Radiated from Cylinder (db re: 20μPa)	$\bar{U}\cos\beta$ (ft/sec)	$\bar{U}\cdot(\omega/\omega_s)$ (ft/sec)
92.2	282	-56	-75.7	53.7	65.2	59.8
81.5	261	-59.5	-75.8	50.3	57.6	52.9
78.0	246	-62	-75.8	47.8	55.2	50.6
49.7	150	-74*	-77.6	37.6*	35.1	32.3
48.9	154	-73*	-77.2	38.2*	34.6	31.7
34.3	107*	<-82*	-79.0	<31.0*	24.3	22.3
21.8	75*	<-90*	-81.0	<25*	15.4	14.1

*Uncertain

TABLE B-36. COMPARISON OF ω/ω_s WITH cos β FOR SKEWED CYLINDERS

β (degrees)	cos β	ω/ω_s*	$(\omega/\omega_s)/\cos\beta$
9.8	.985	.991	1.006
10.9	.982	.971	.989
10.9	.982	.967	.985
21.2	.932	.890	.955
21.2	.932	.884	.948
22.1	.927	.895	.965
30.4	.863	.789	.914
30.4	.863	.734	.851
32.6	.842	.823	.977
38.8	.779	.624	.801
38.8	.779	.623	.800
39.6	.771	.682	.885
45.0	.707	.649	.918
45.0	.707	.594	.840
45.0	.707	.582	.823

*Average ω/ω_s for all recorded data in a set.

TABLE B-37. ESTIMATION OF C_L FROM MEASURED I FOR THE IRREGULAR MULTINOTCHED CYLINDER

$\bar{U}$ (ft/sec)	Rex10^3 —	Measured I (db re: 20 μPa)	$\omega/2\pi$ (Hz)	Correlation Factor(1) (d^2)	Correlation Factor (2) (d^2)	C_Lx10^{-2} from C.F.(1)	C_Lx10^{-2} from C.F.(2)
(a) 1/2" SECTIONS							
90.8	23.11	53.1	484	5.07	3.30	12.37	15.95
87.1	22.68	51.2	439	5.07	3.30	11.76	15.00
74.5	19.40	48.3	385	5.07	3.30	13.74	16.87
57.9	15.08	36.9	241	5.07	3.30	8.15	11.26
(b) 3/8" SECTIONS							
90.8	17.73	54.9	633	6.76	4.47	13.73	16.88
87.1	17.01	49.0	575	6.76	4.47	8.35	10.27
74.5	14.55	47.1	498	6.76	4.47	10.58	13.02
57.9	11.31	35.6	325	6.76	4.47	7.09	8.72

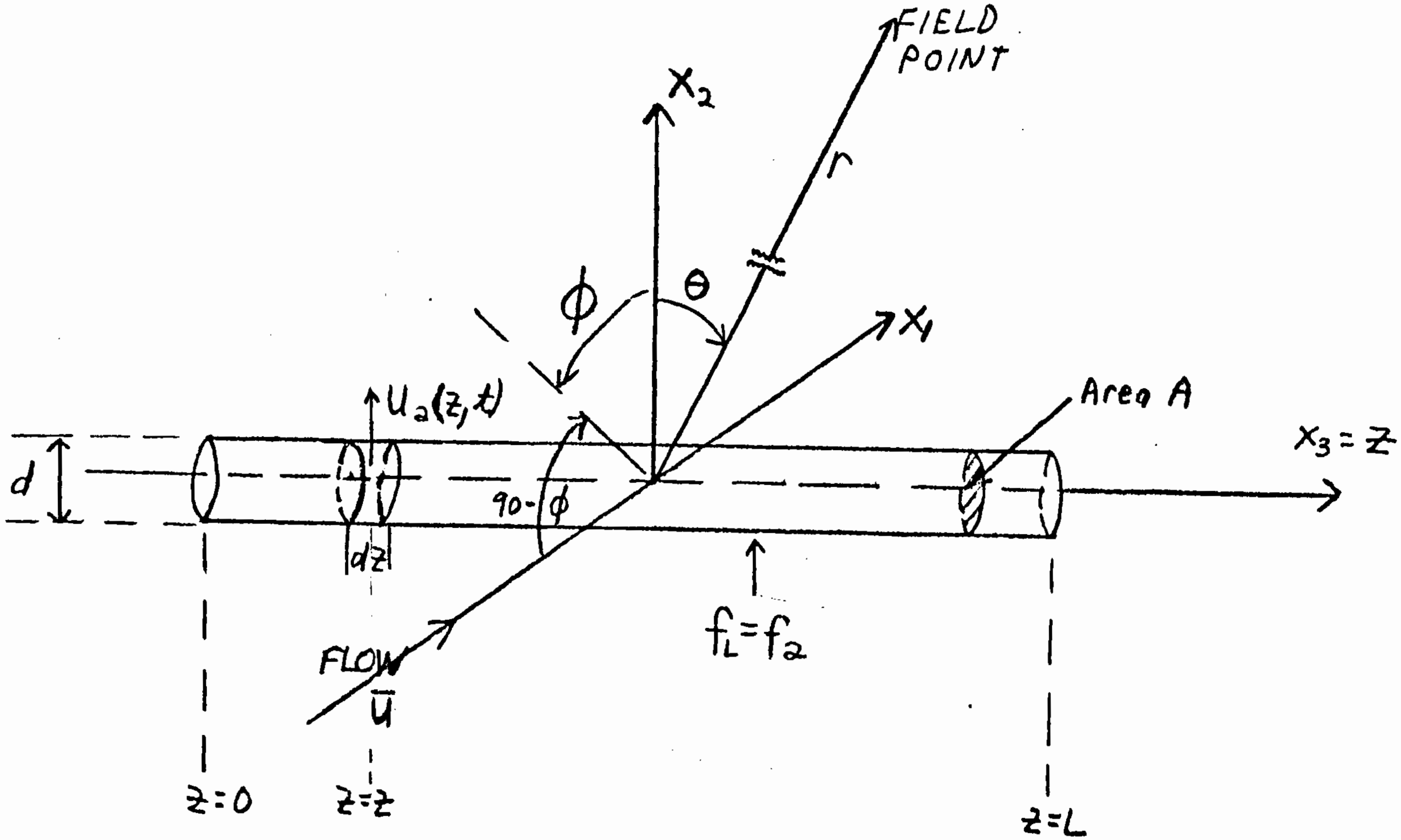

FIGURE C-1. CYLINDER COORDINATES

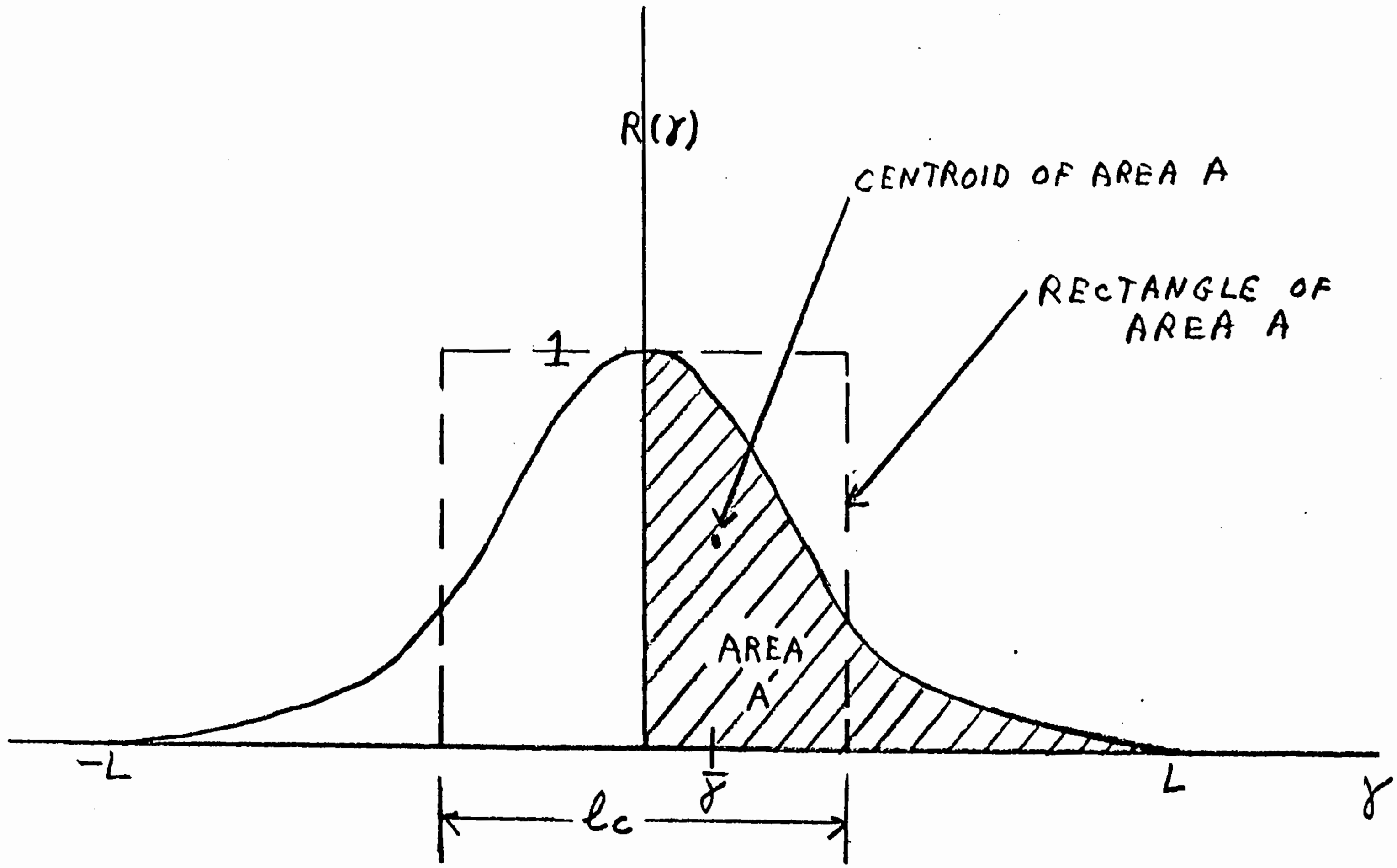

FIGURE C-2. CORRELATION FUNCTION

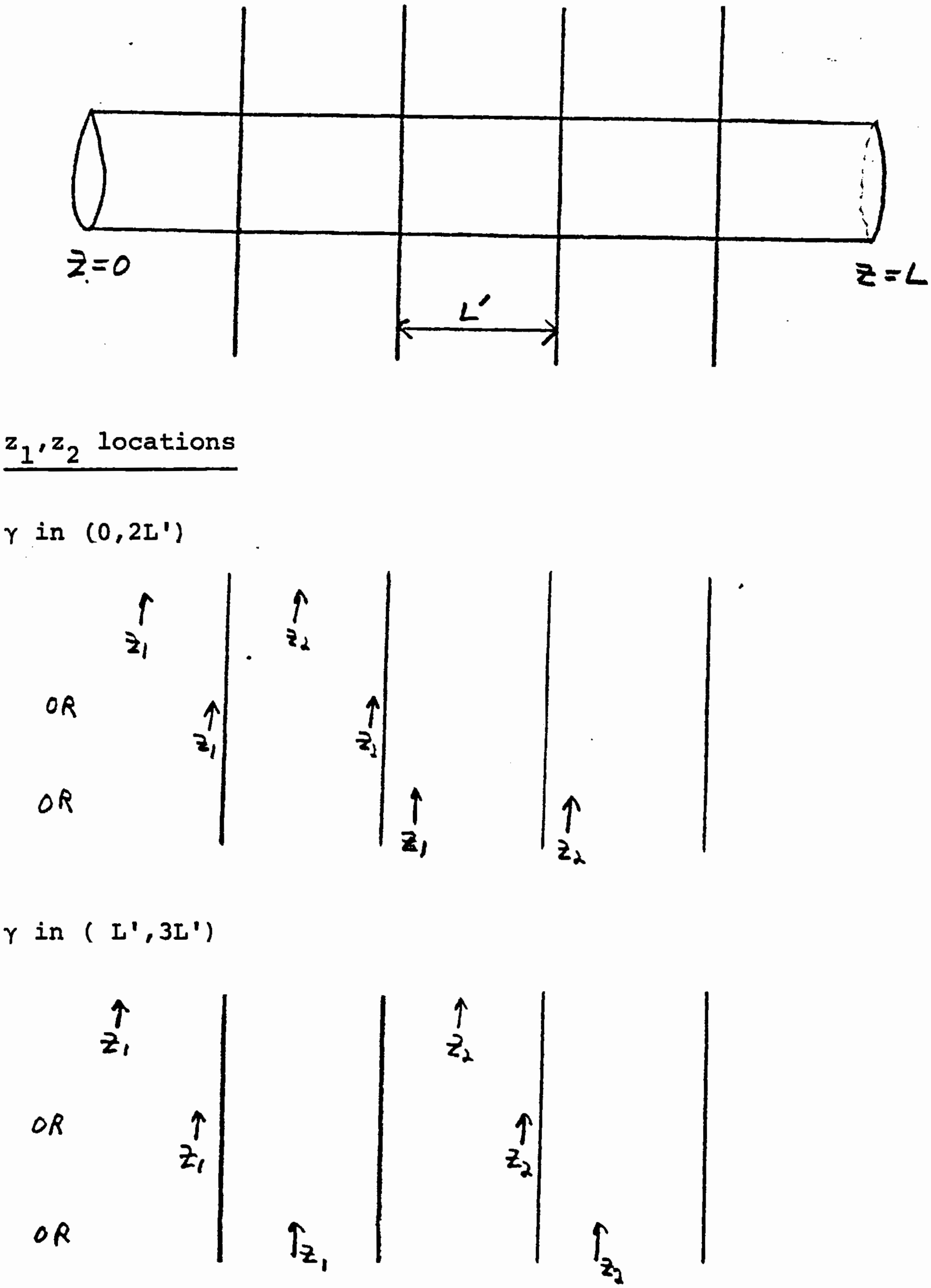

FIGURE C-3. PERIODICALLY DIVIDED CYLINDER
M = 4, L' = L/5

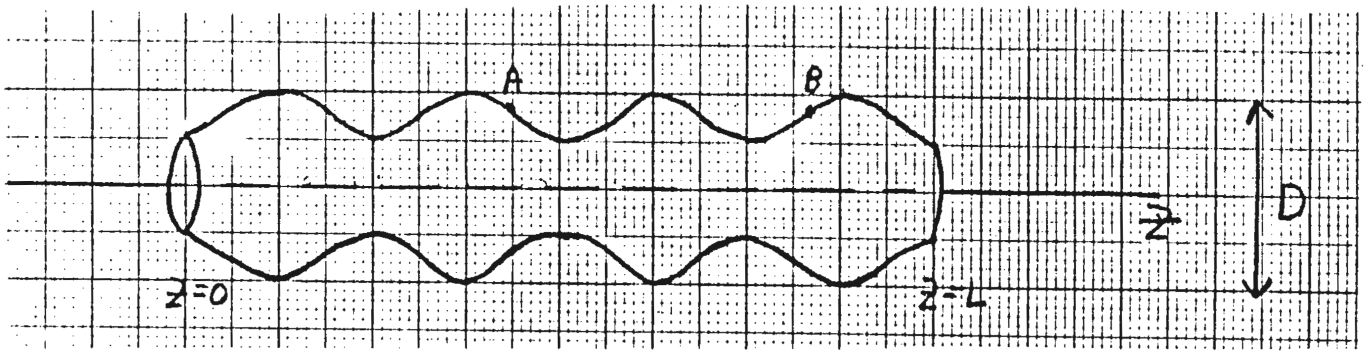

(a) ACTUAL

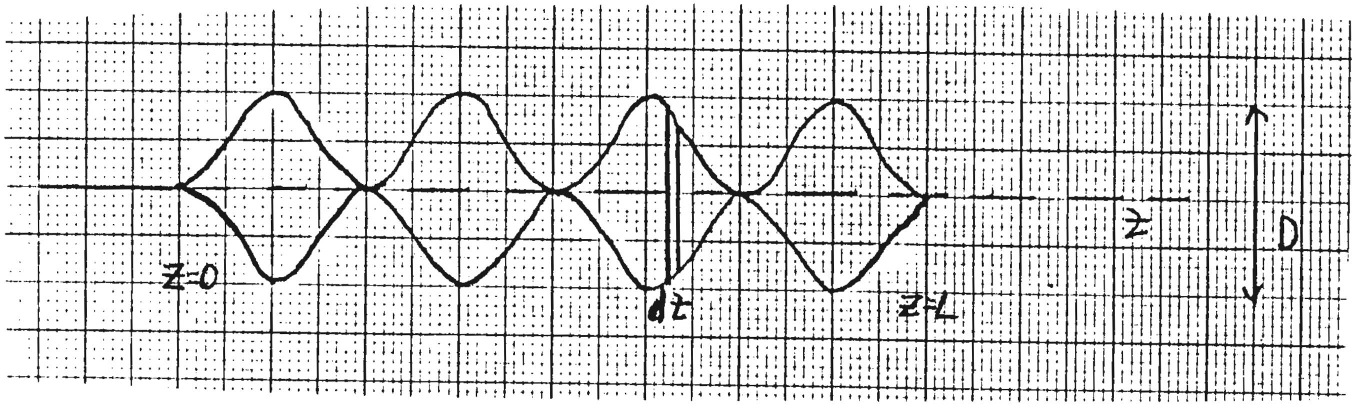

(b) IDEALIZED

FIGURE C-4. SINUSOIDAL CYLINDERS

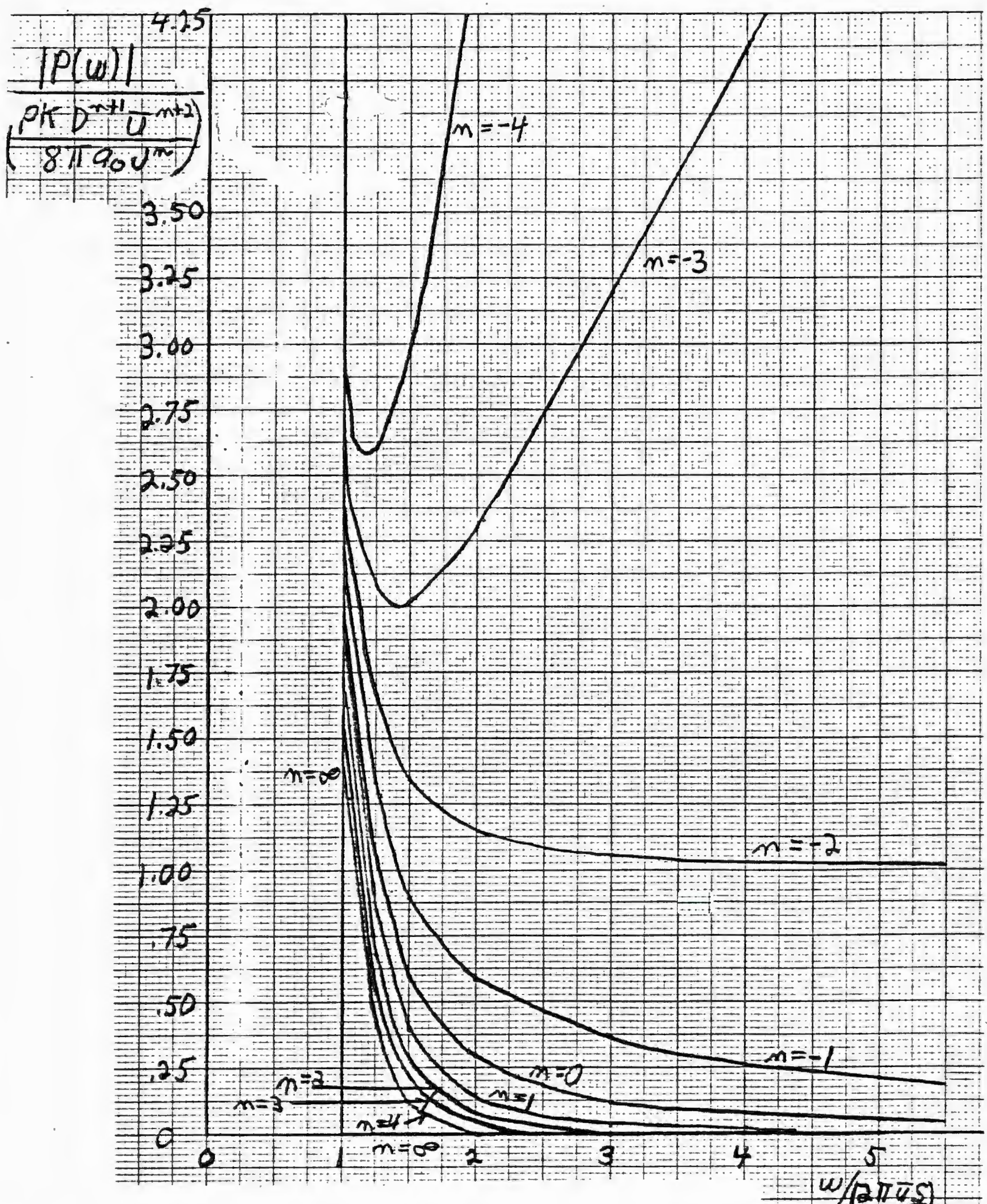

FIGURE C-5. FREQUENCY SPECTRUM OF SOUND PRESSURE RADIATED FROM IDEALIZED SINUSOIDAL CYLINDER

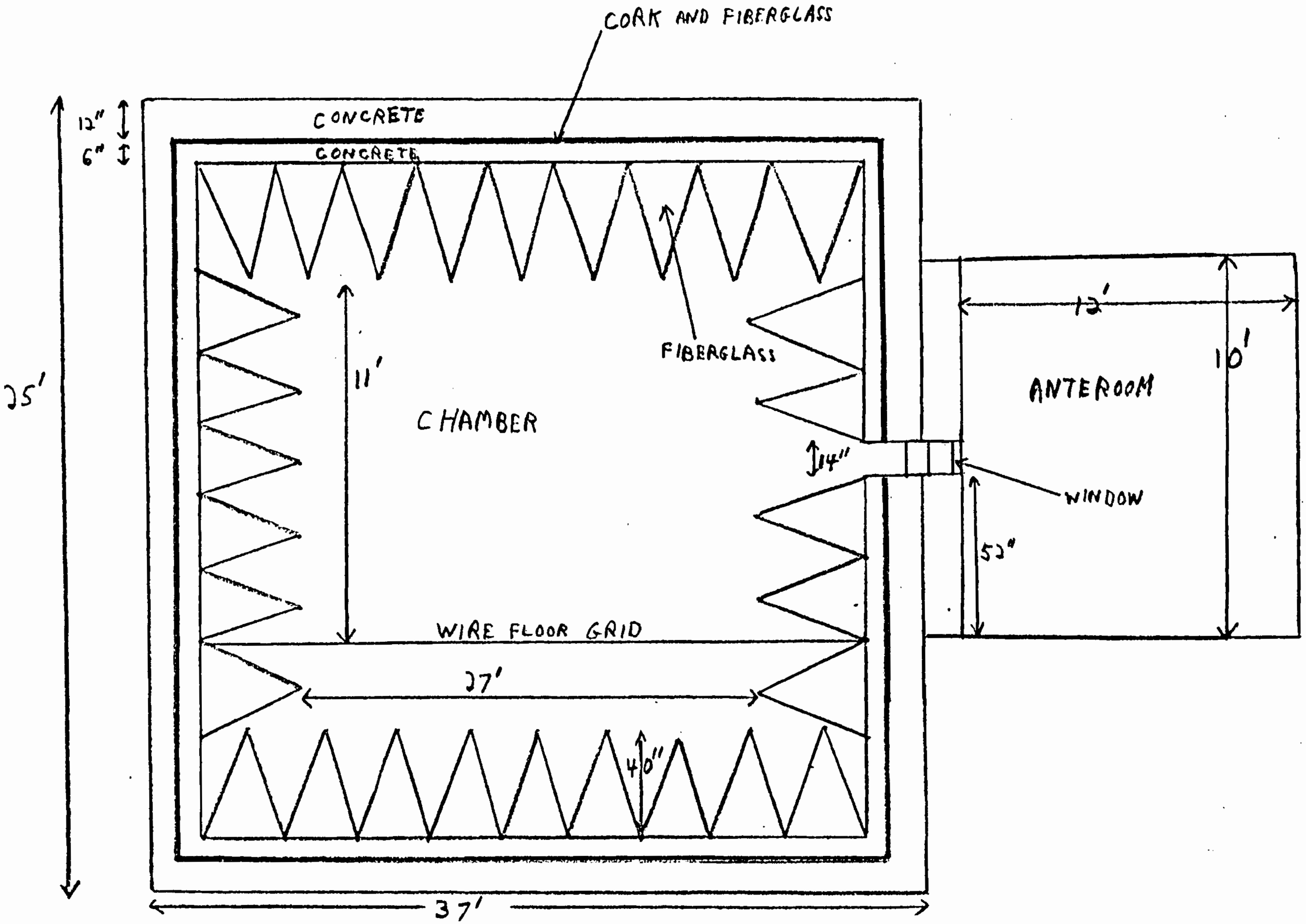

FIGURE C-6. ANECHOIC CHAMBER: SIDE VIEW

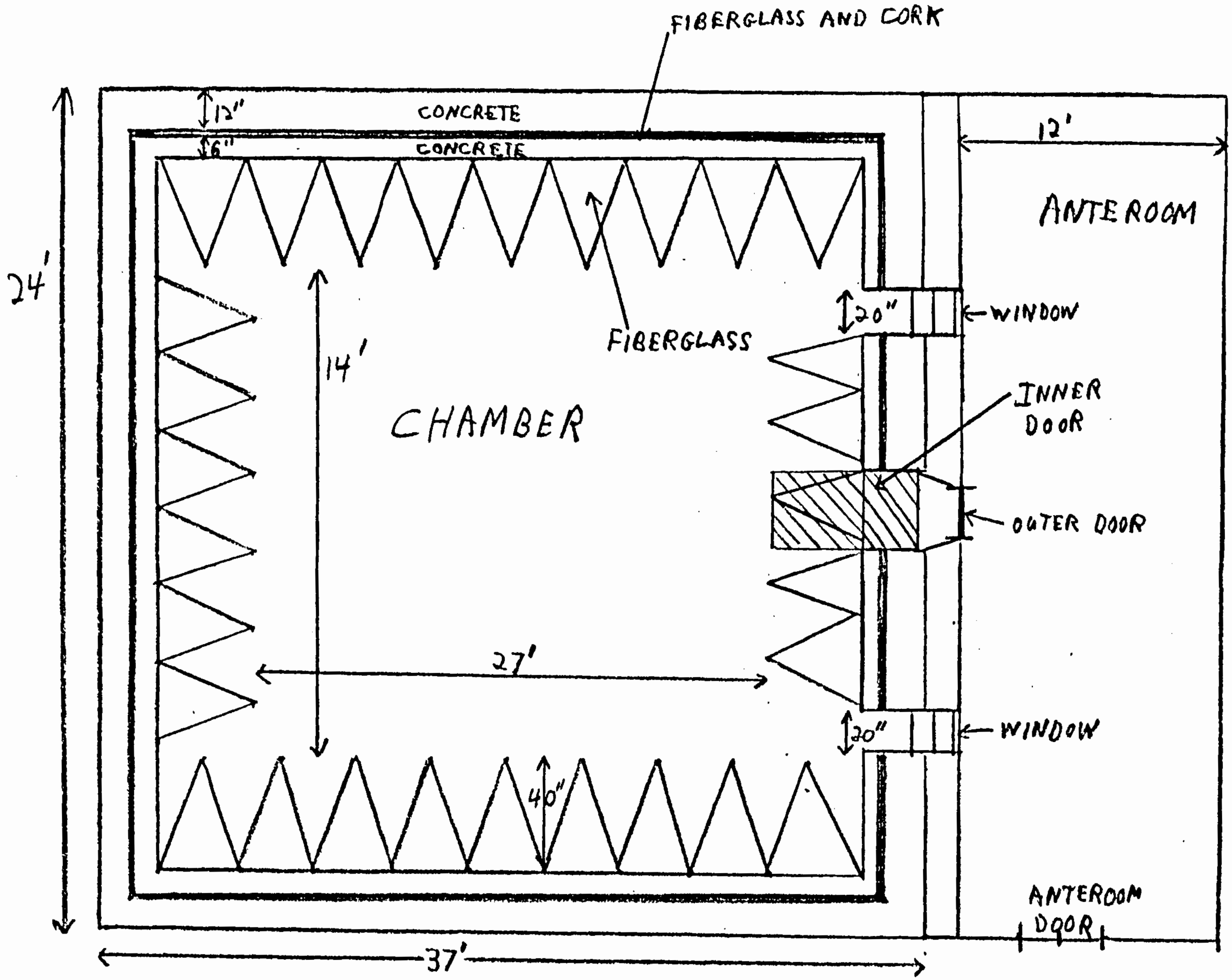

FIGURE C-7. ANECHOIC CHAMBER: TOP VIEW

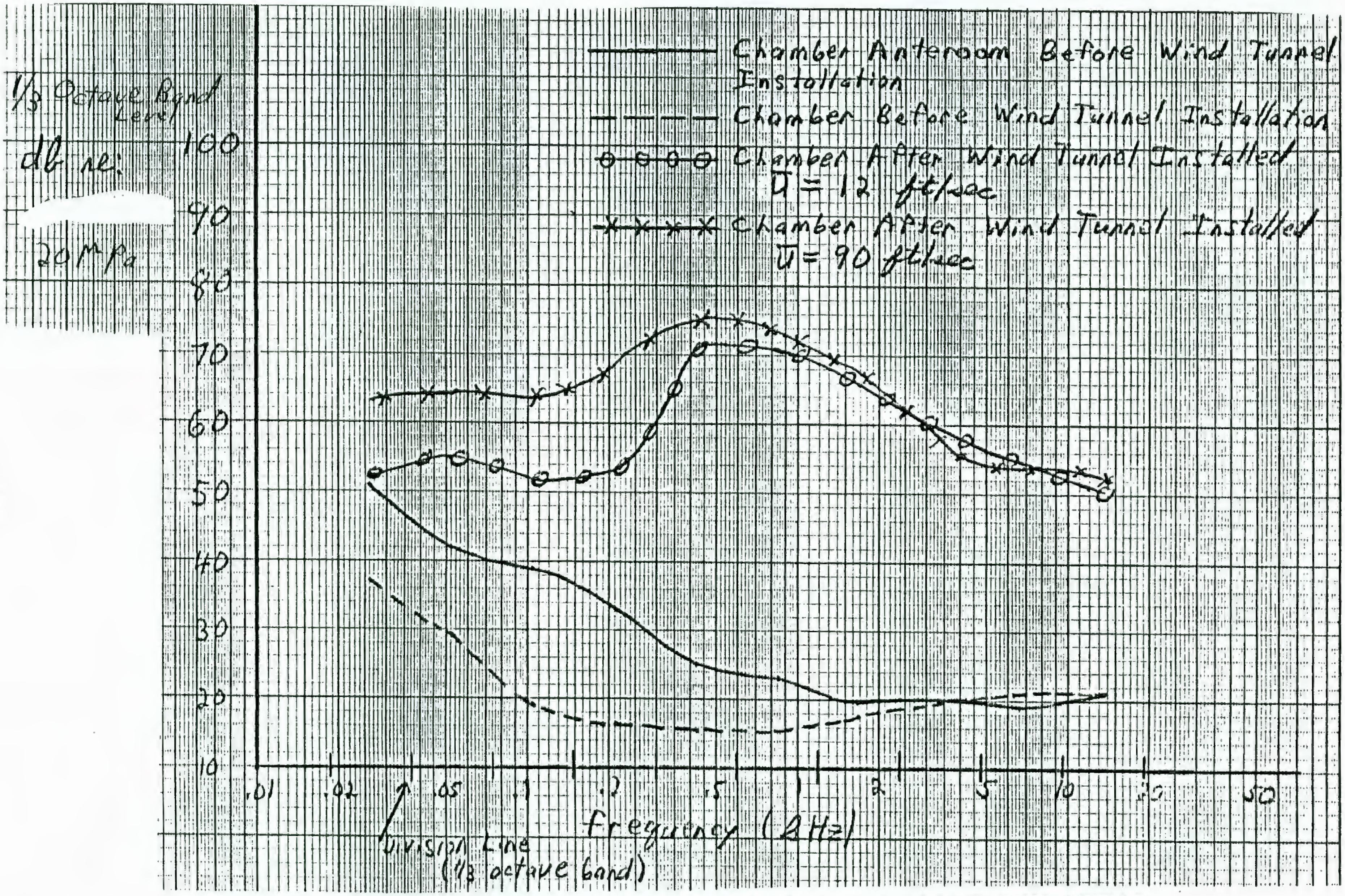

FIGURE C-8. ANECHOIC CHAMBER BACKGROUND NOISE IN 1/3 OCTAVE BAND LEVELS AS READ ON A SOUND LEVEL METER

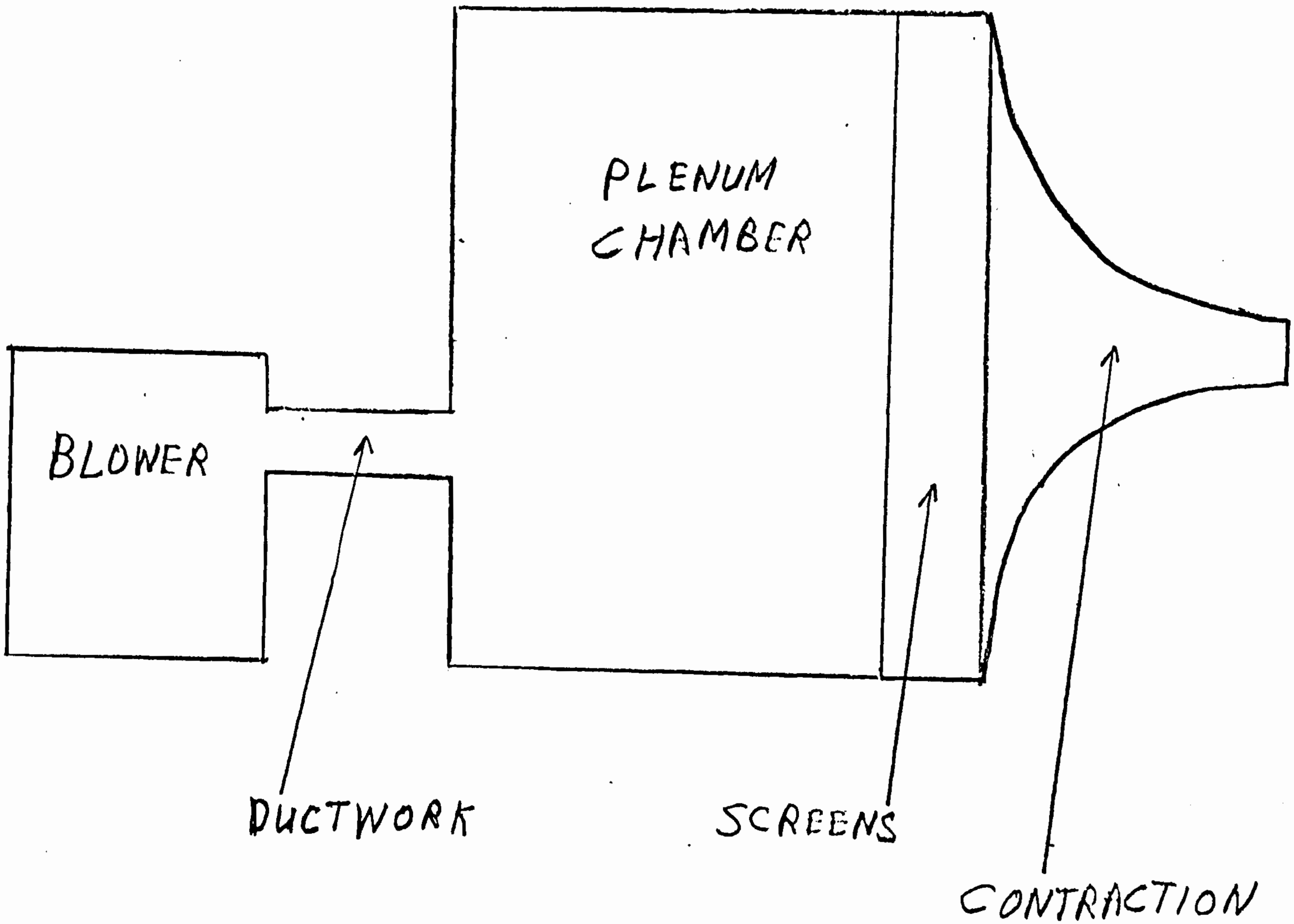

FIGURE C-9. WIND TUNNEL SCHEMATIC

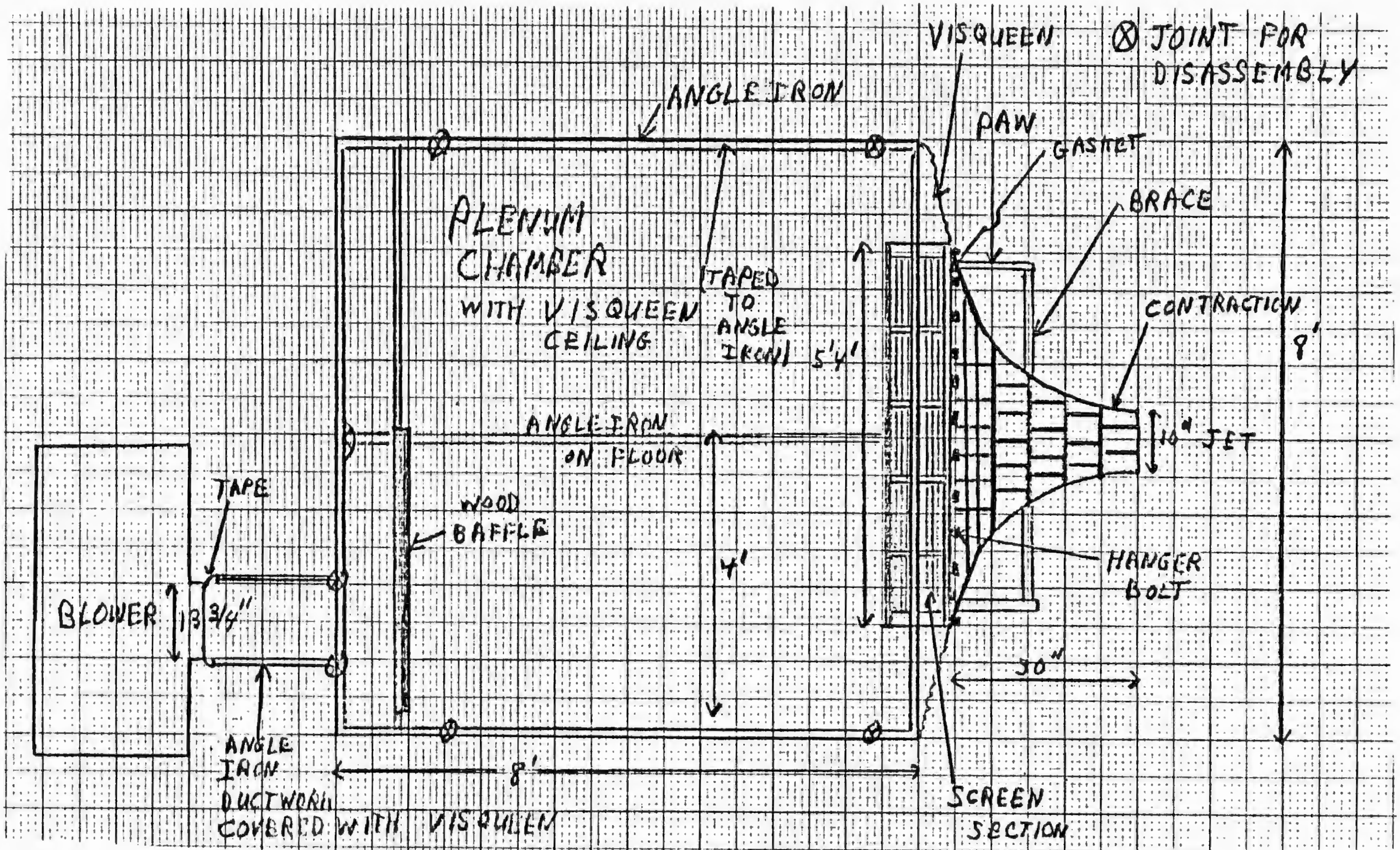

FIGURE C-10. WIND TUNNEL: TOP VIEW

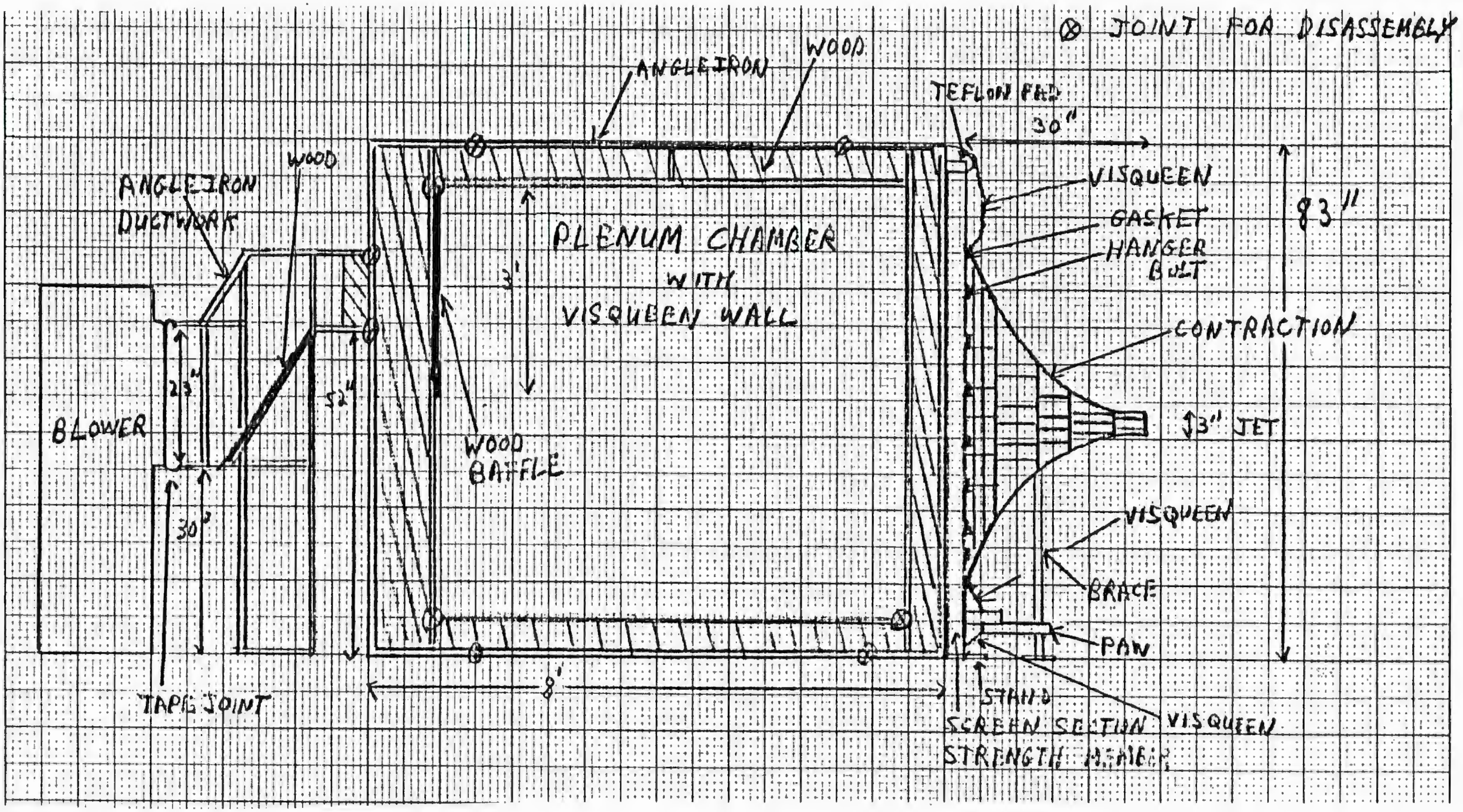

FIGURE C-11. WIND TUNNEL: SIDE VIEW

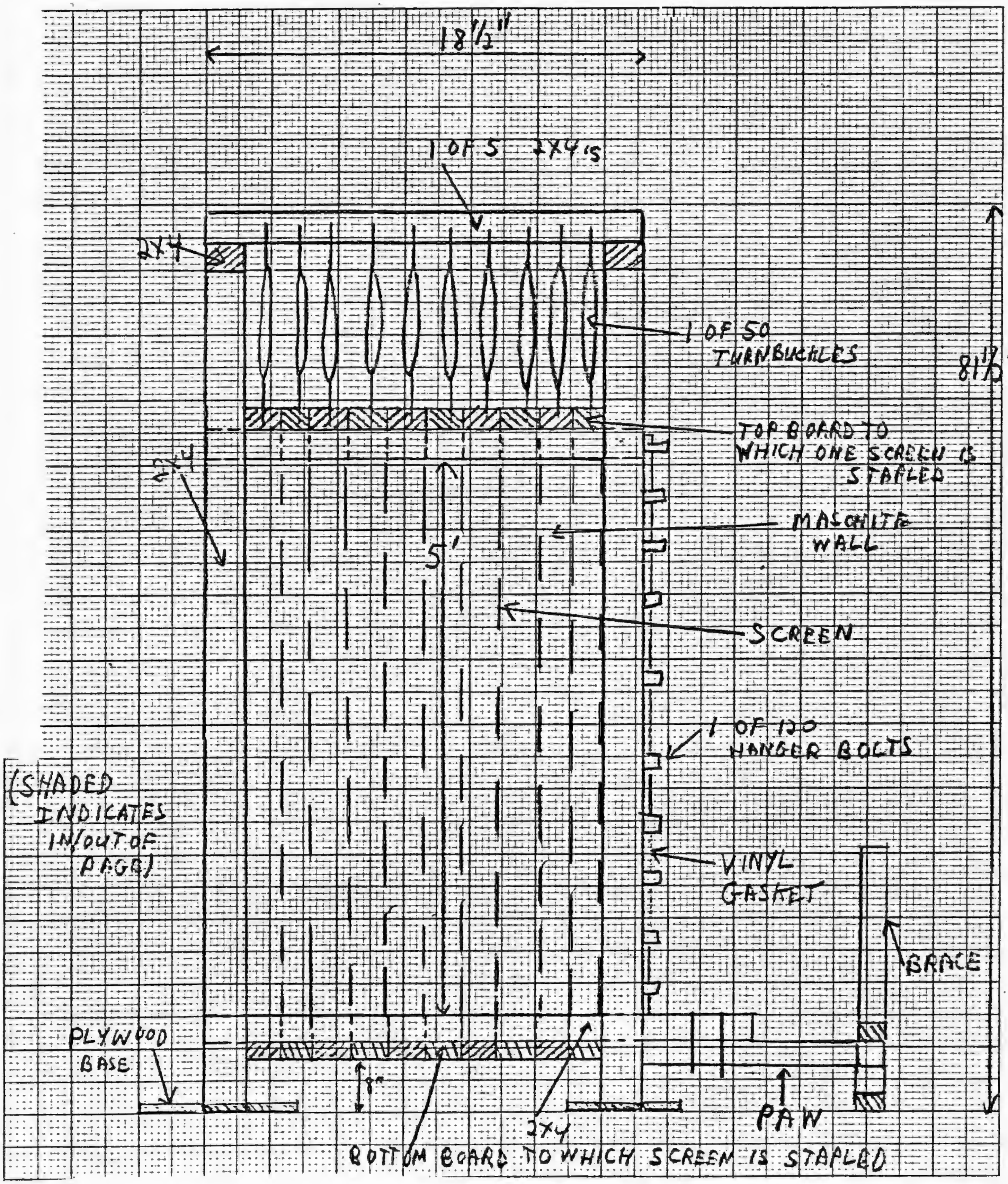

FIGURE C-12. SCREEN SECTION: SIDE VIEW

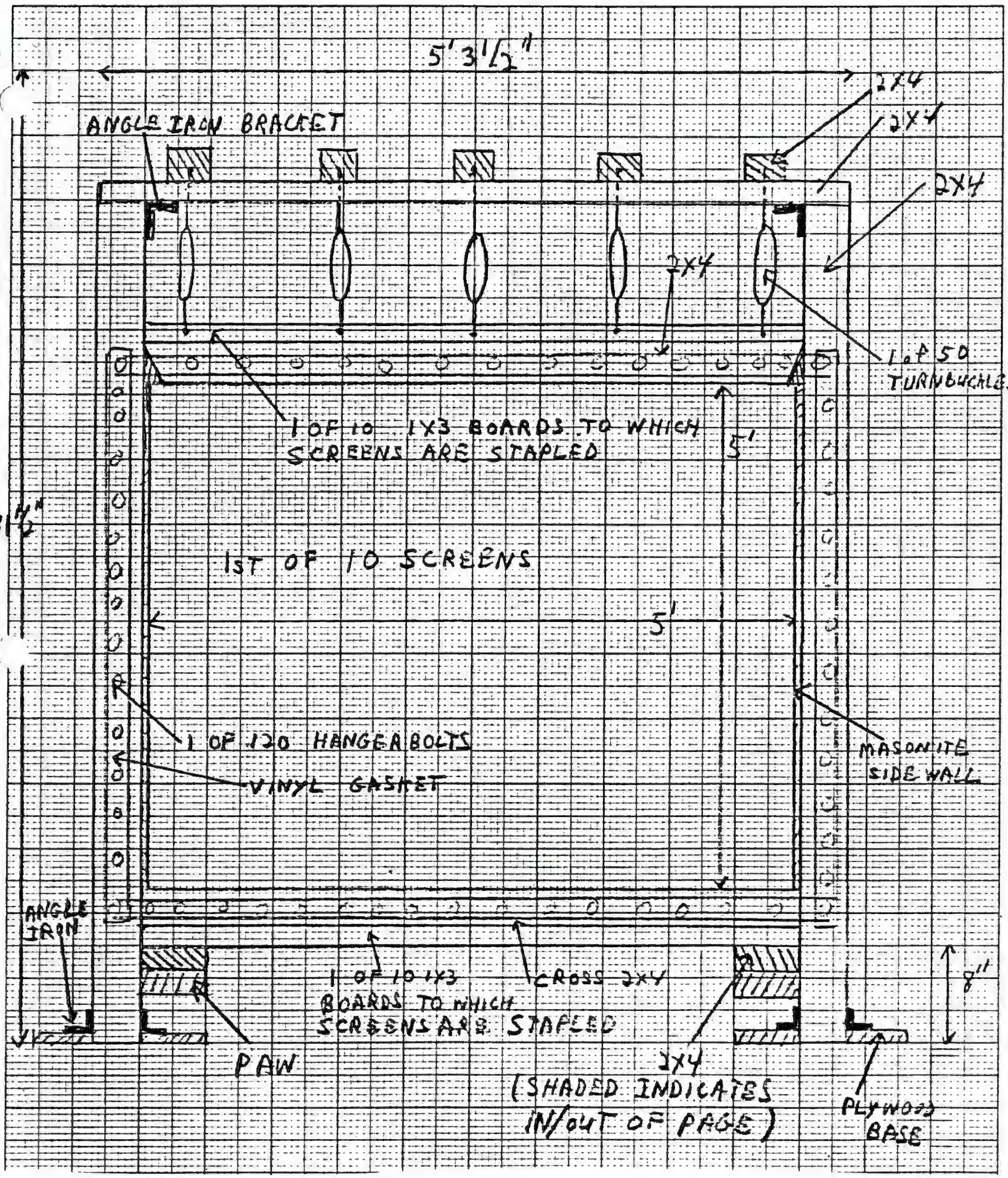

FIGURE C-13. SCREEN SECTION: FRONT VIEW

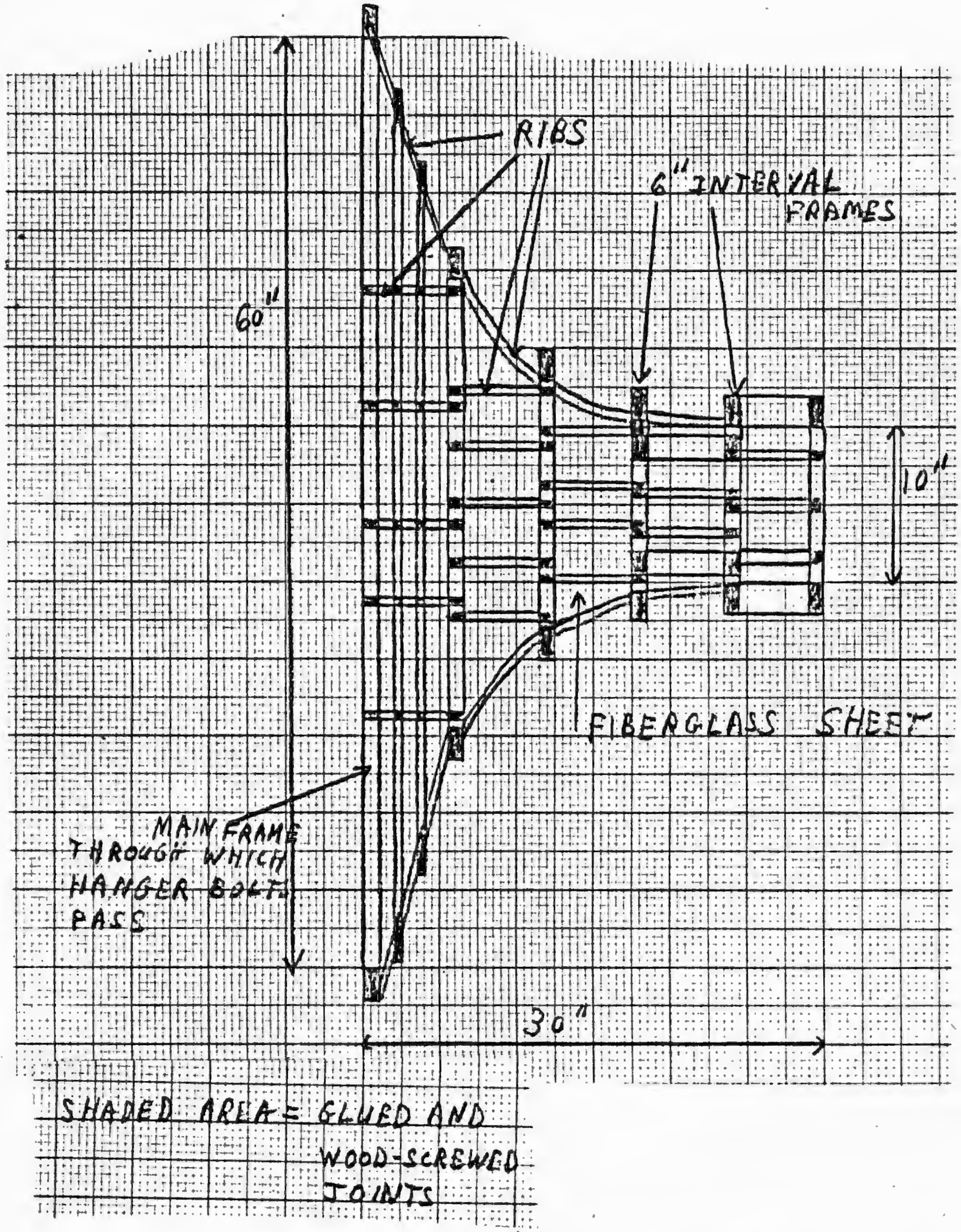

FIGURE C-14. WIND TUNNEL CONTRACTION: TOP VIEW

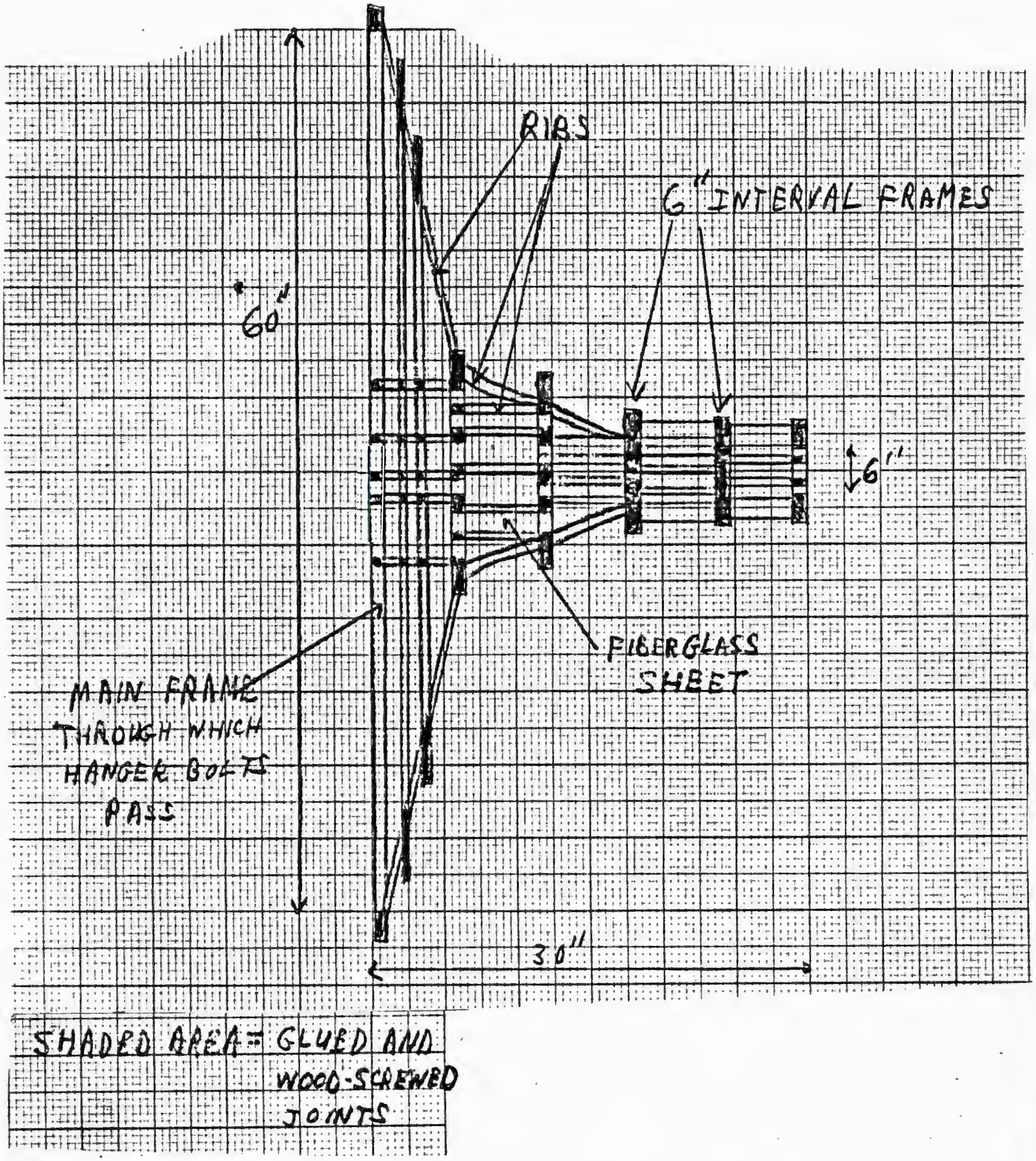

FIGURE C-15. WIND TUNNEL CONTRACTION: SIDE VIEW

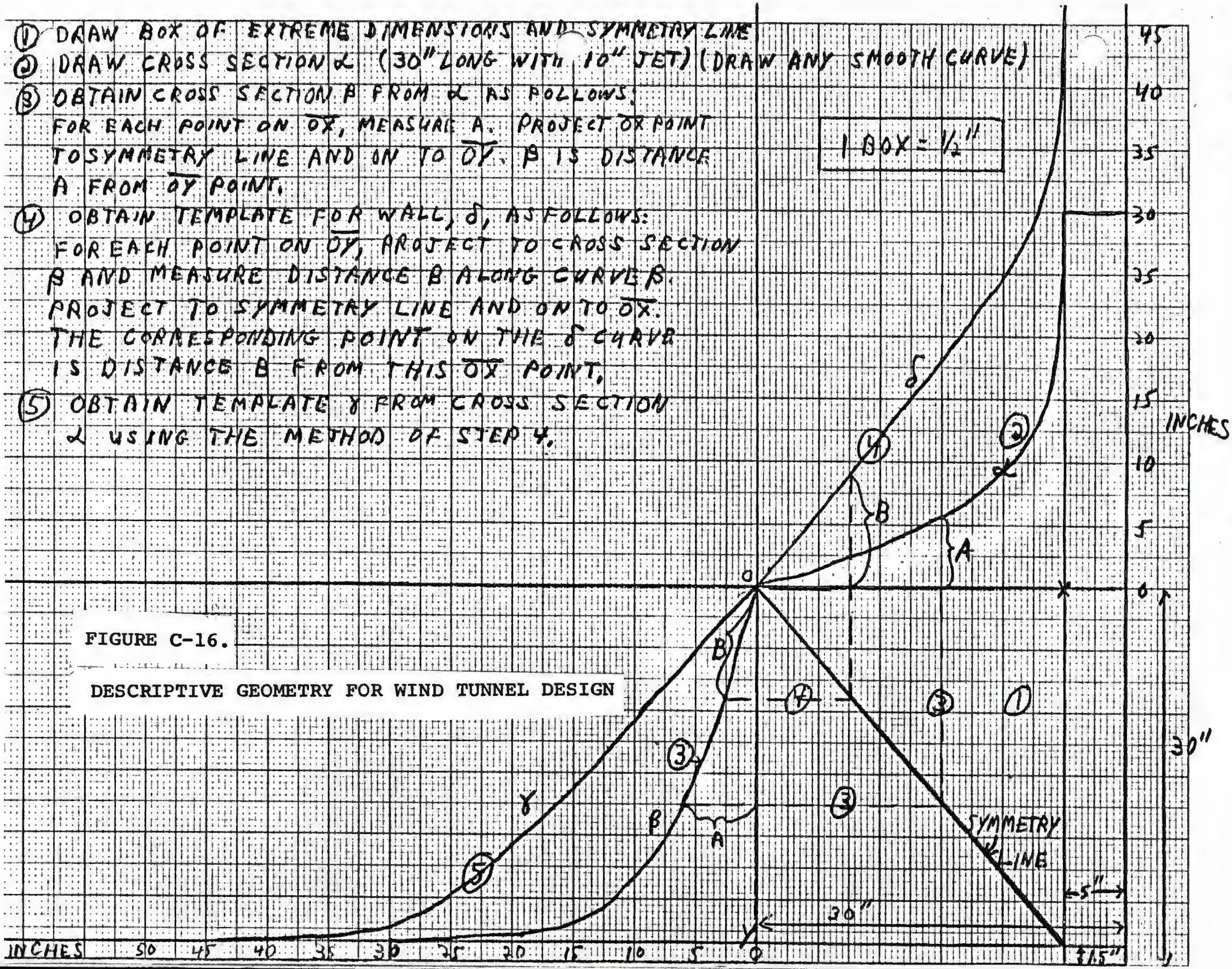

FIGURE C-16.

DESCRIPTIVE GEOMETRY FOR WIND TUNNEL DESIGN

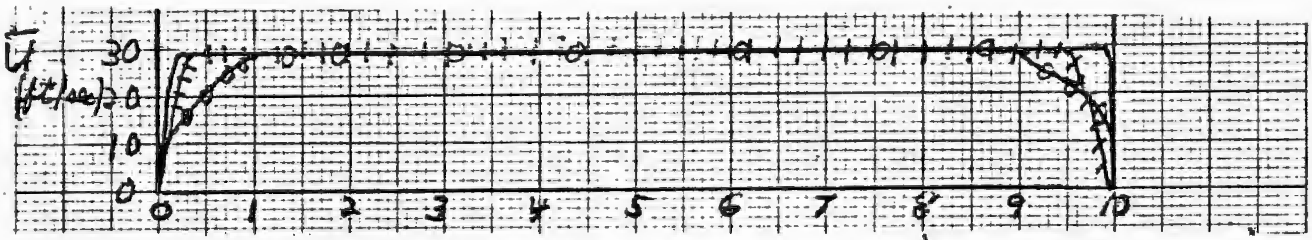

Distance across (inches)

(a) 1/8" FROM TOP OF JET

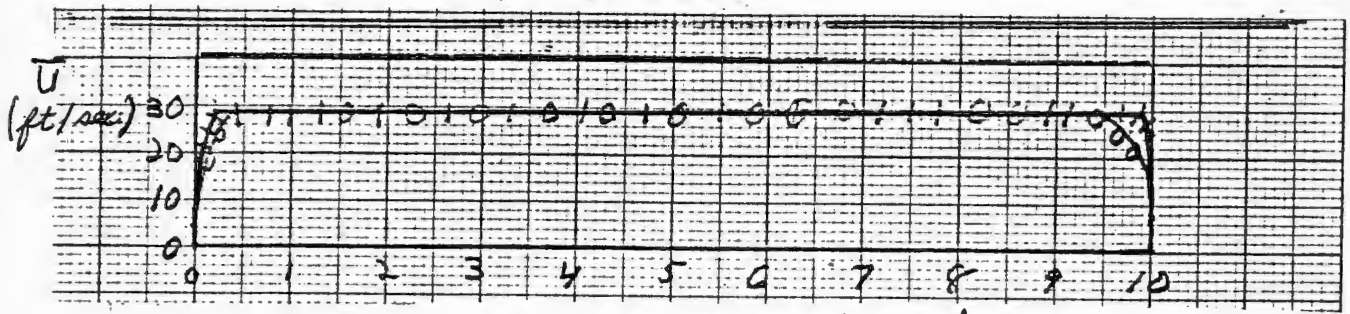

Distance across (inches)

(b) 1/2" FROM TOP OF JET

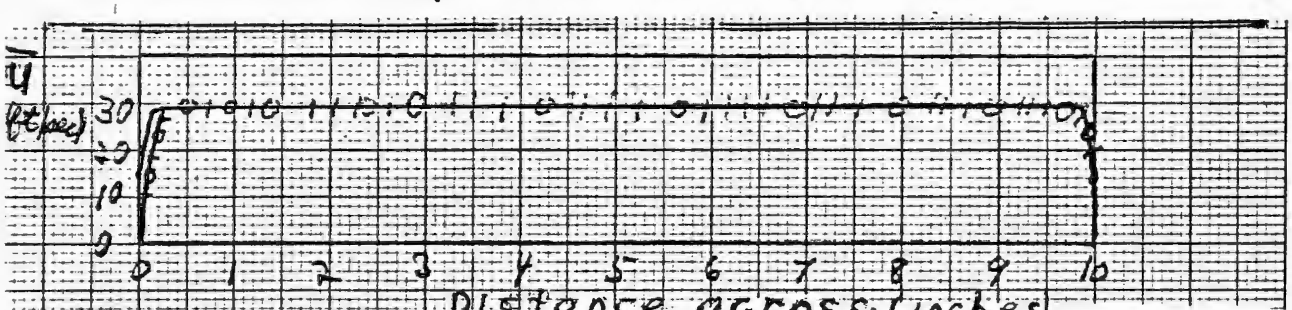

Distance across (inches)

(c) 1" FROM TOP OF JET

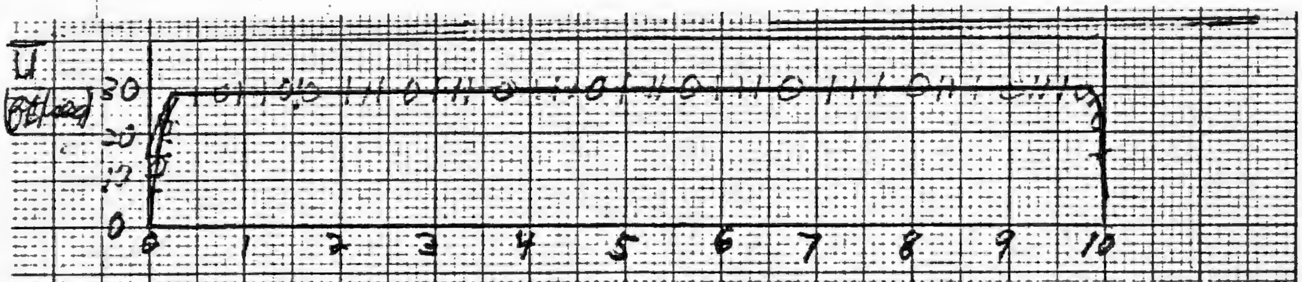

Distance across (inches)

(d) 1 1/2" FROM TOP OF JET

———	1/8" from mouth
+++	1" from mouth
-o-o-o-	2" from mouth

FIGURE C-17. WIND TUNNEL VELOCITY PROFILES FOR $\overline{U}$ = 29 FT/SEC

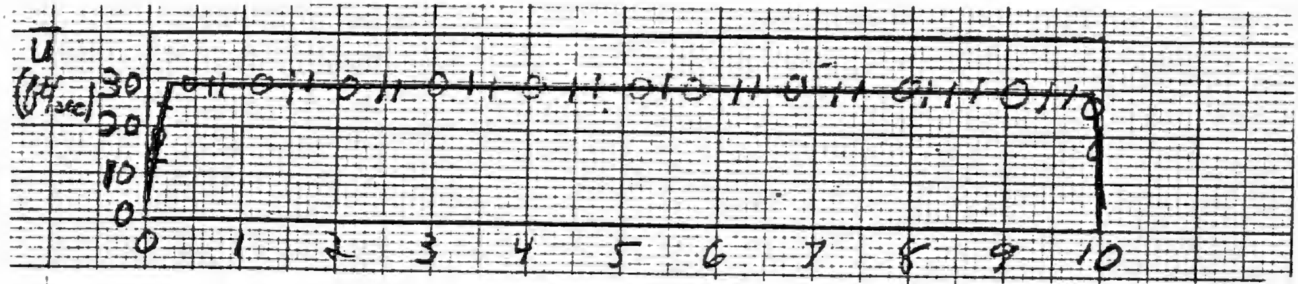

Distance across (inches)
(e) 2" FROM TOP OF JET

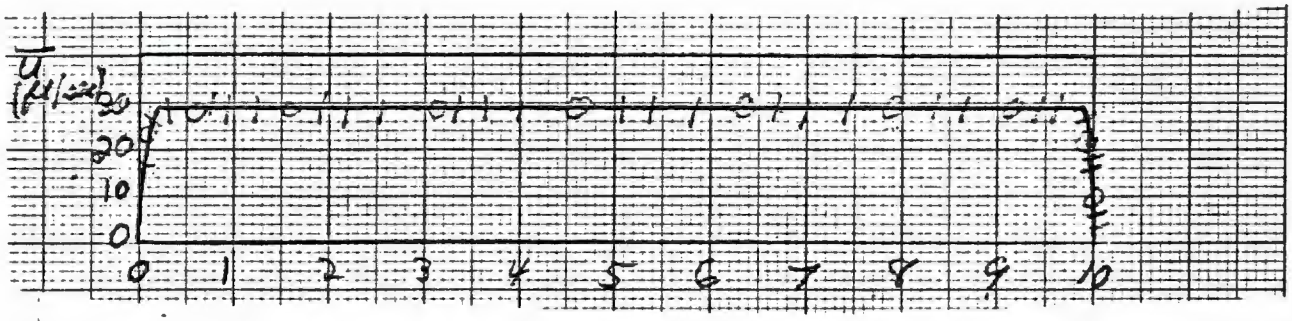

Distance across (inches)
(f) 2½" FROM TOP OF JET

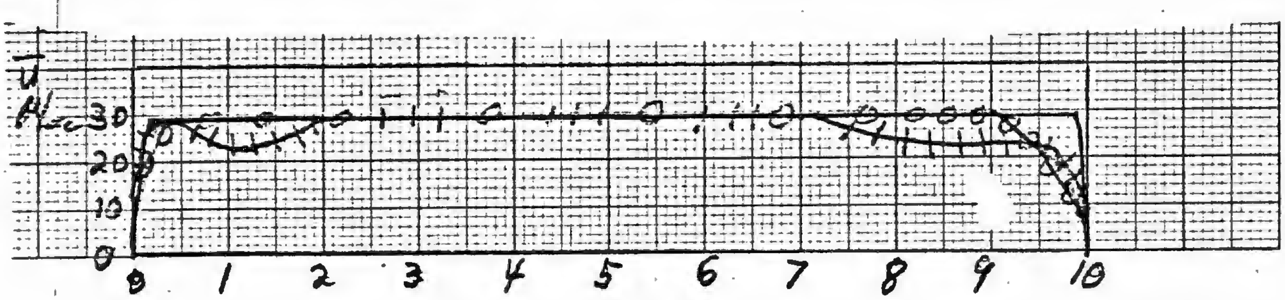

Distance across (inches)
(g) 2 7/8" FROM TOP OF JET

——— 1/8" from mouth
++++ 1" from mouth
-o-o-o- 2" from mouth

FIGURE C-17 (Continued)

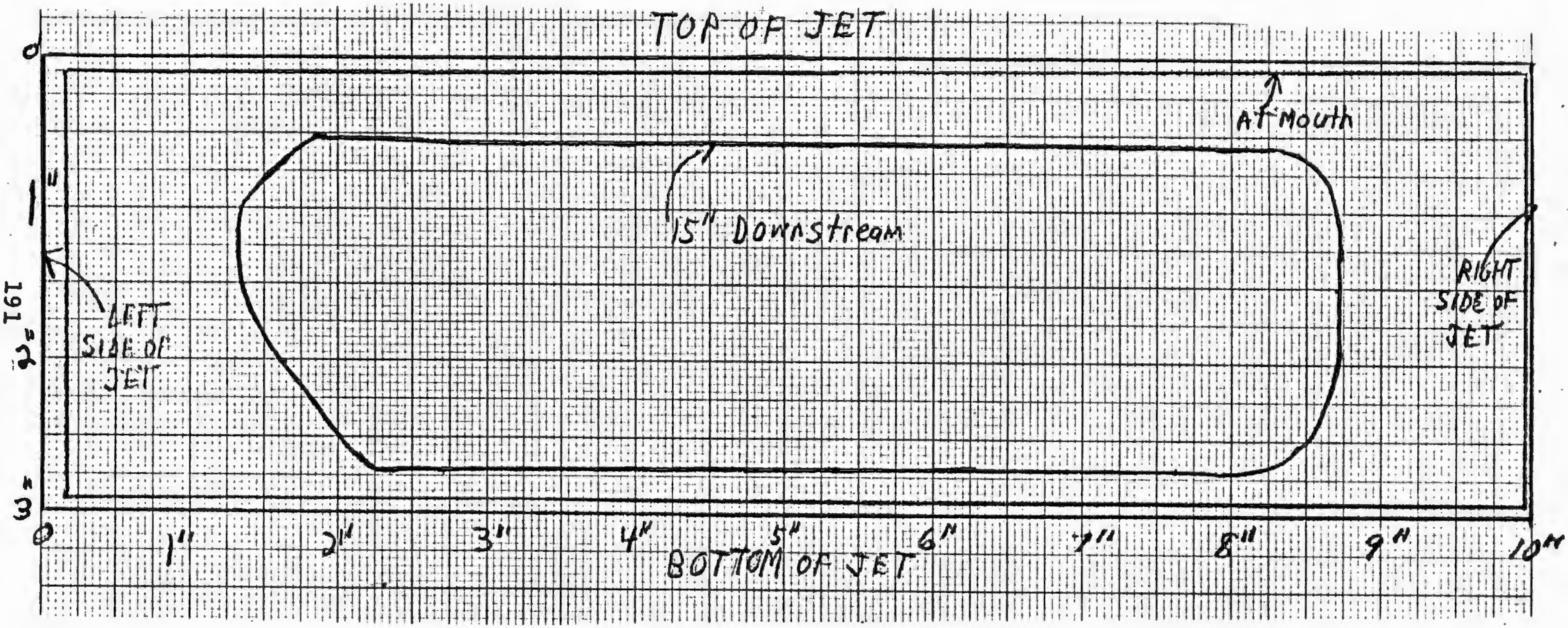

FIGURE C-18. WIND TUNNEL VELOCITY CONTOURS (BOUNDARY OF CONSTANT $\overline{U}$ AREA) AT $\overline{U}$ = 29 FT/SEC

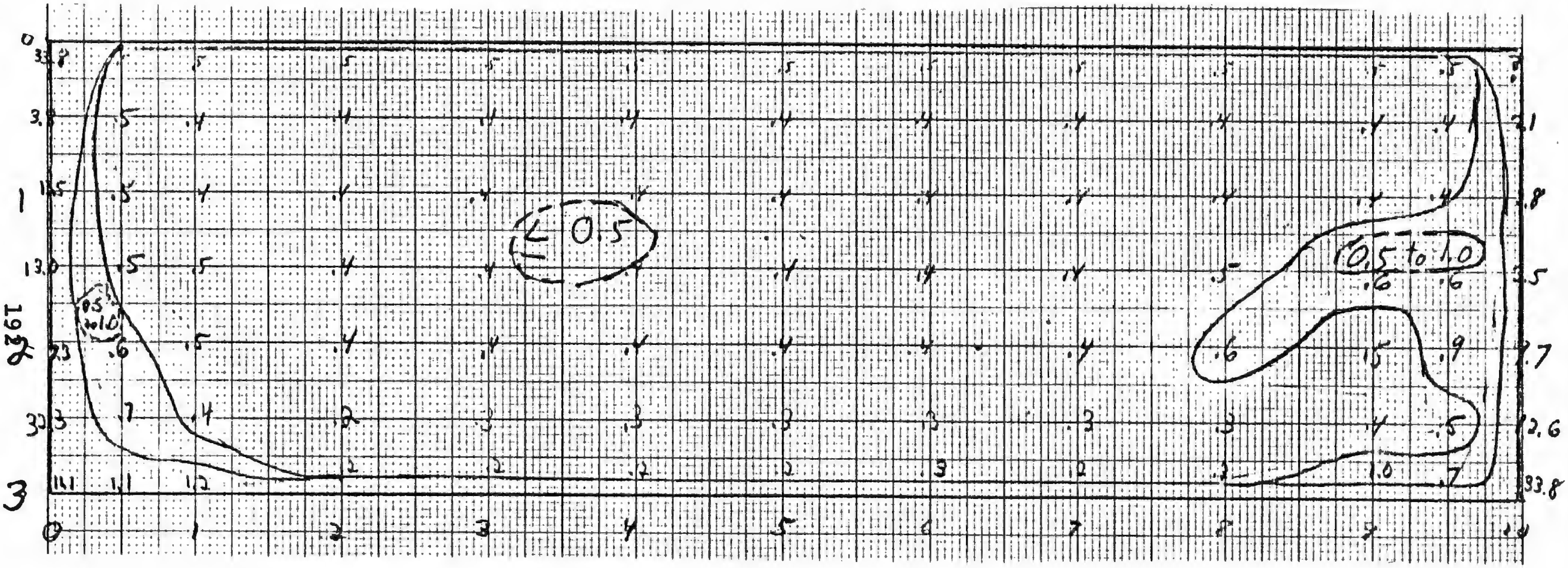

FIGURE C-19. WIND TUNNEL TURBULENCE
CONTOURS: 1/8" FROM MOUTH ($\overline{U}$ = 29 FT/SEC)
(numbers in percent)

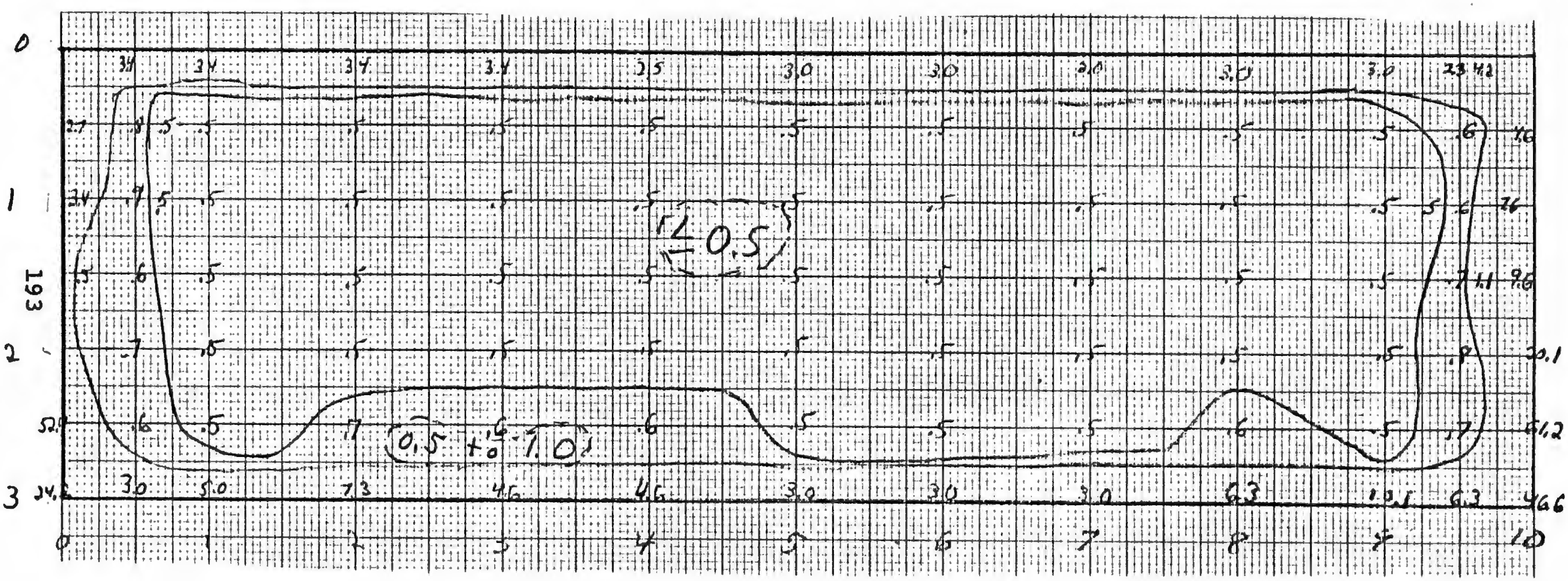

193

FIGURE C-20. WIND TUNNEL TURBULENCE CONTOURS:
1" FROM MOUTH ($\overline{U}$ = 29 FT/SEC)
(numbers in percent)

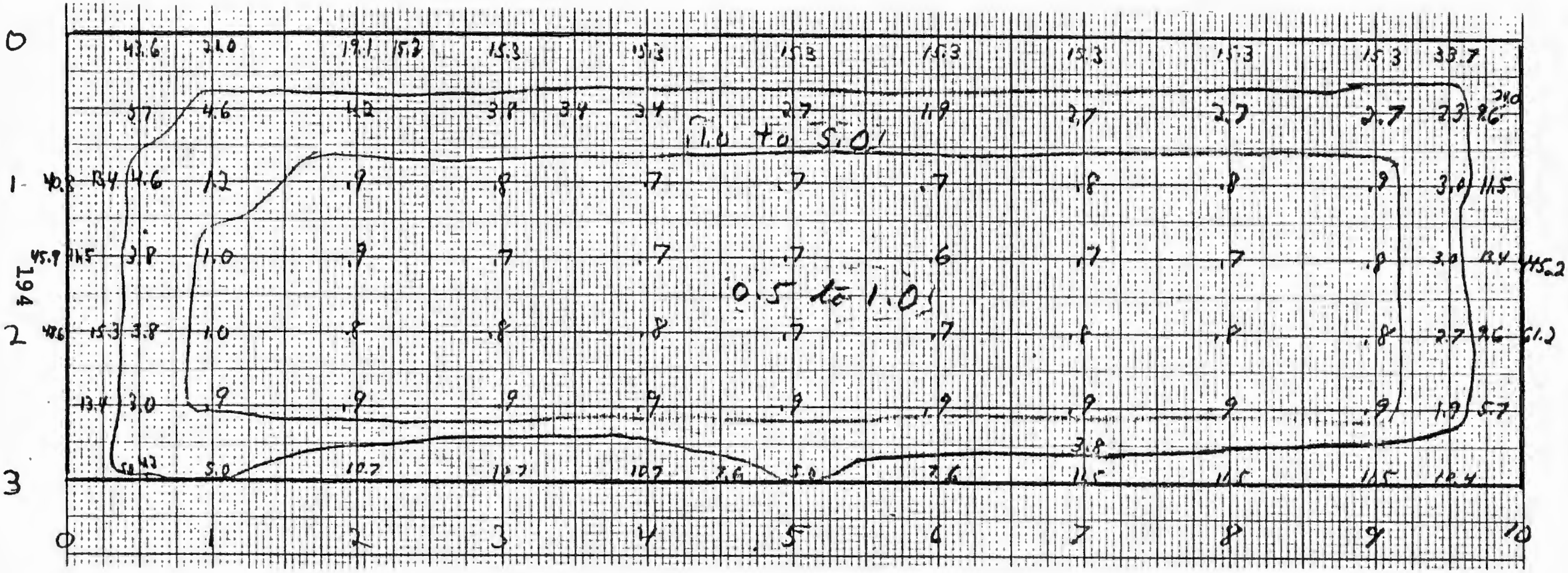

FIGURE C-21. WIND TUNNEL TURBULENCE CONTOURS:
2" FROM MOUTH ($\overline{U}$ = 29 FT/SEC)
(numbers in percent)

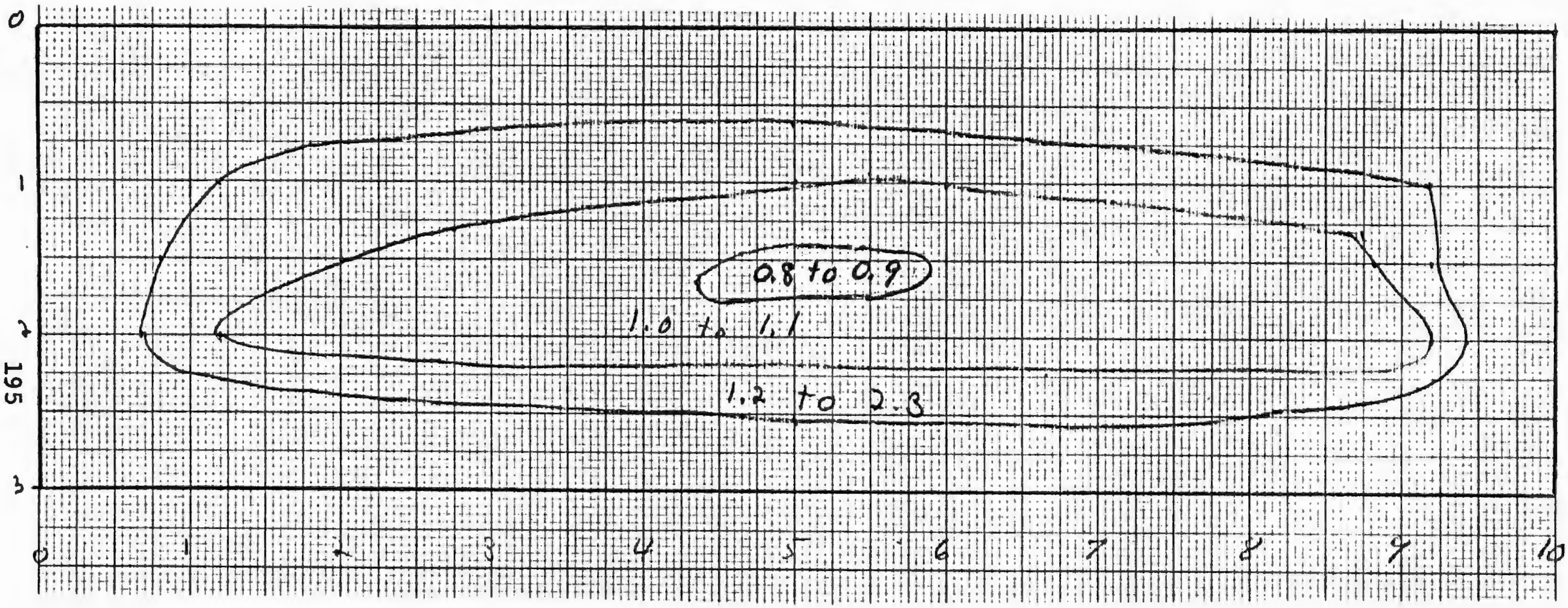

FIGURE C-22. WIND TUNNEL TURBULENCE CONTOURS:
3" FROM MOUTH ($\overline{U}$ = 29 FT/SEC)
(numbers in percent)

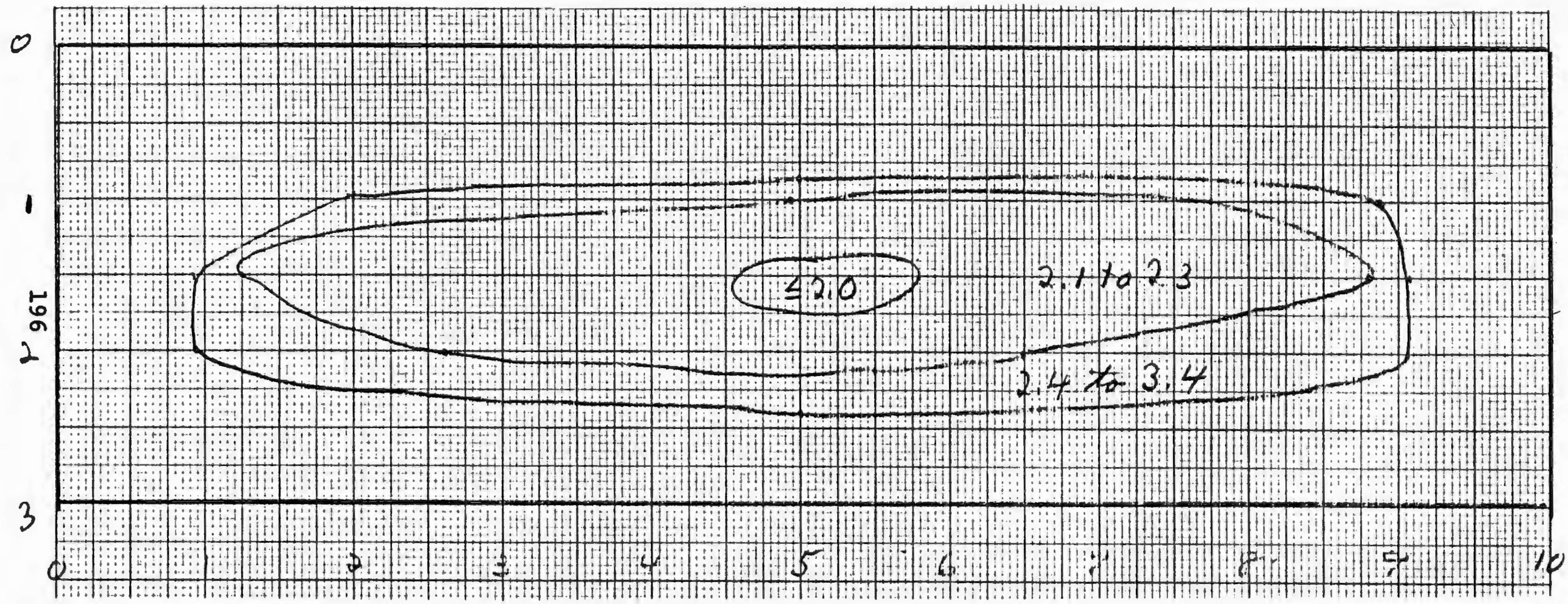

FIGURE C-23. WIND TUNNEL TURBULENCE CONTOURS:
5" FROM MOUTH ($\overline{U}$ = 29 FT/SEC)
(numbers in percent)

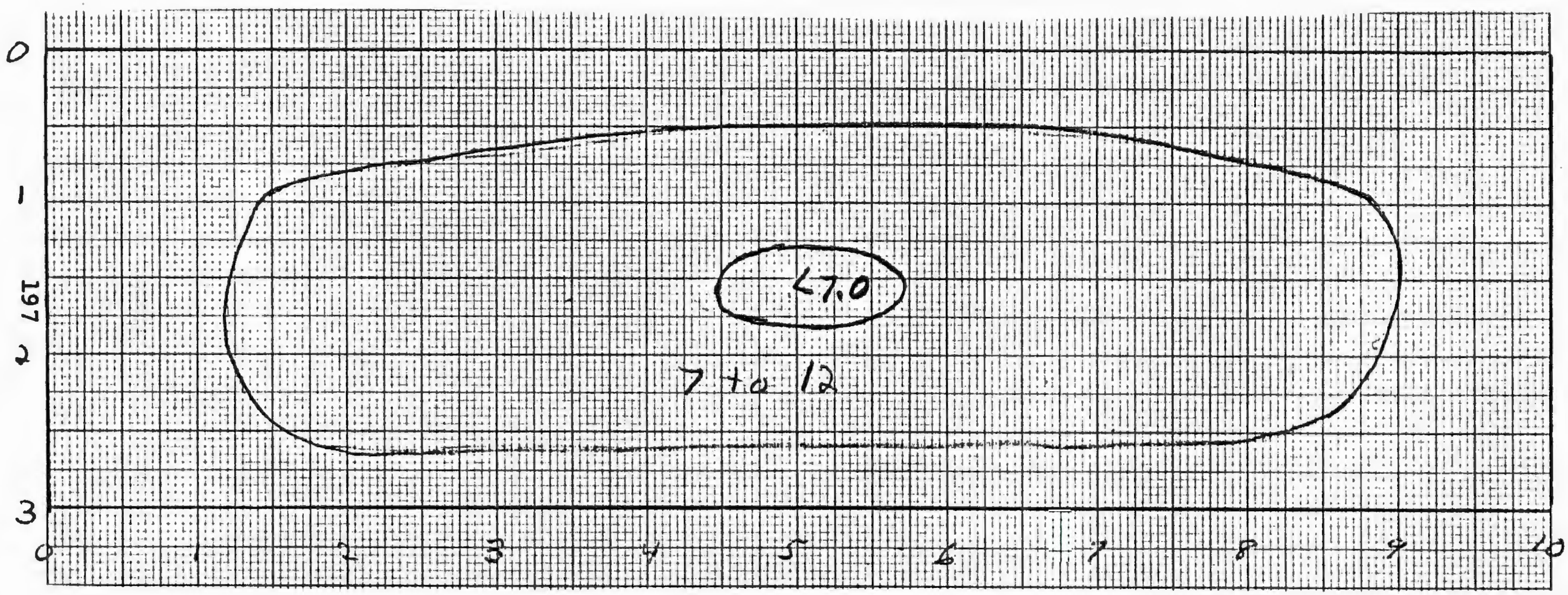

FIGURE C-24. WIND TUNNEL TURBULENCE CONTOURS (APPROXIMATE): 15" FROM MOUTH ($\overline{U}$ = 29 FT/SEC) (numbers in percent)

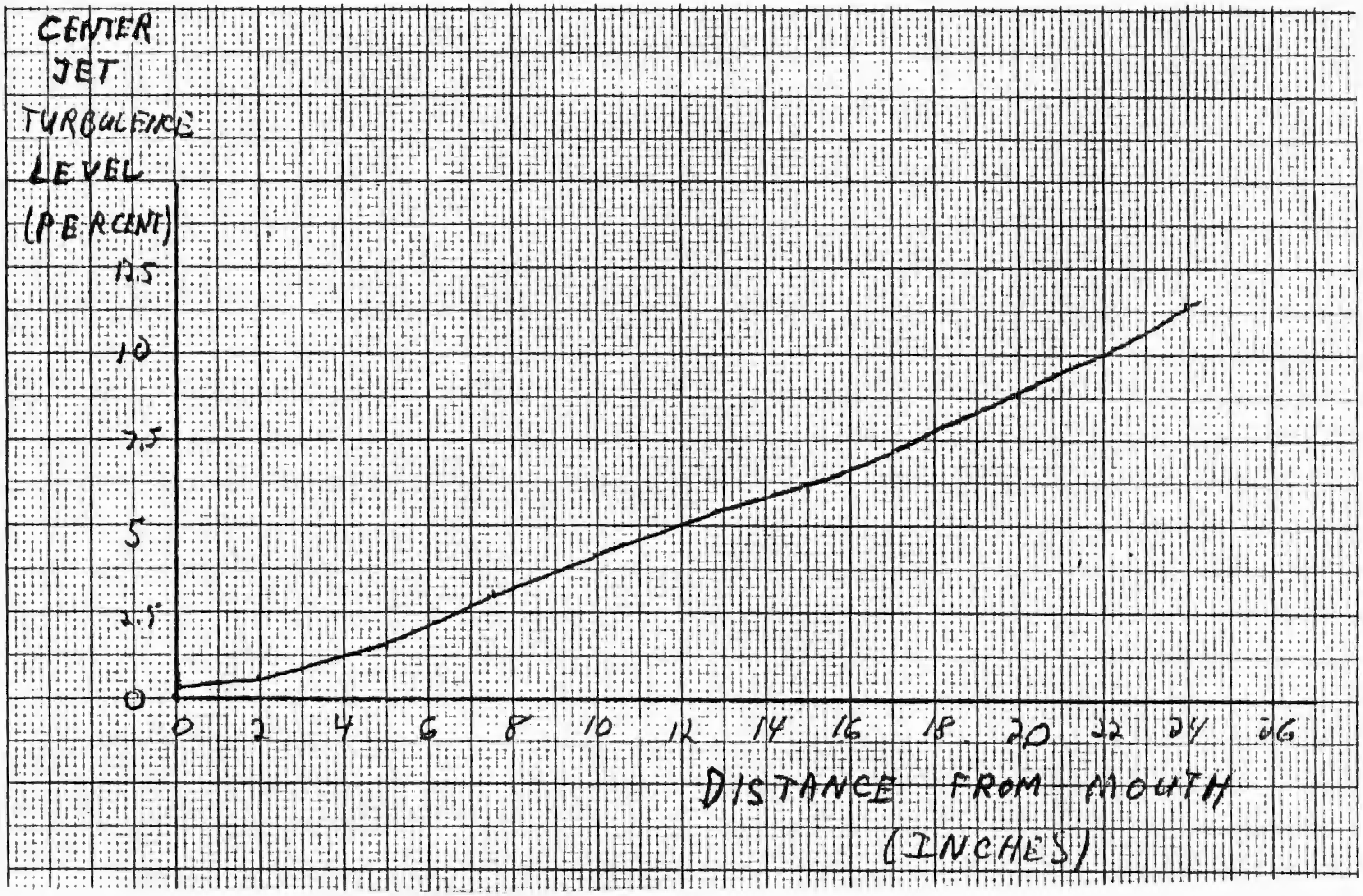

FIGURE C-25. WIND TUNNEL TURBULENCE LEVEL AT CENTER JET

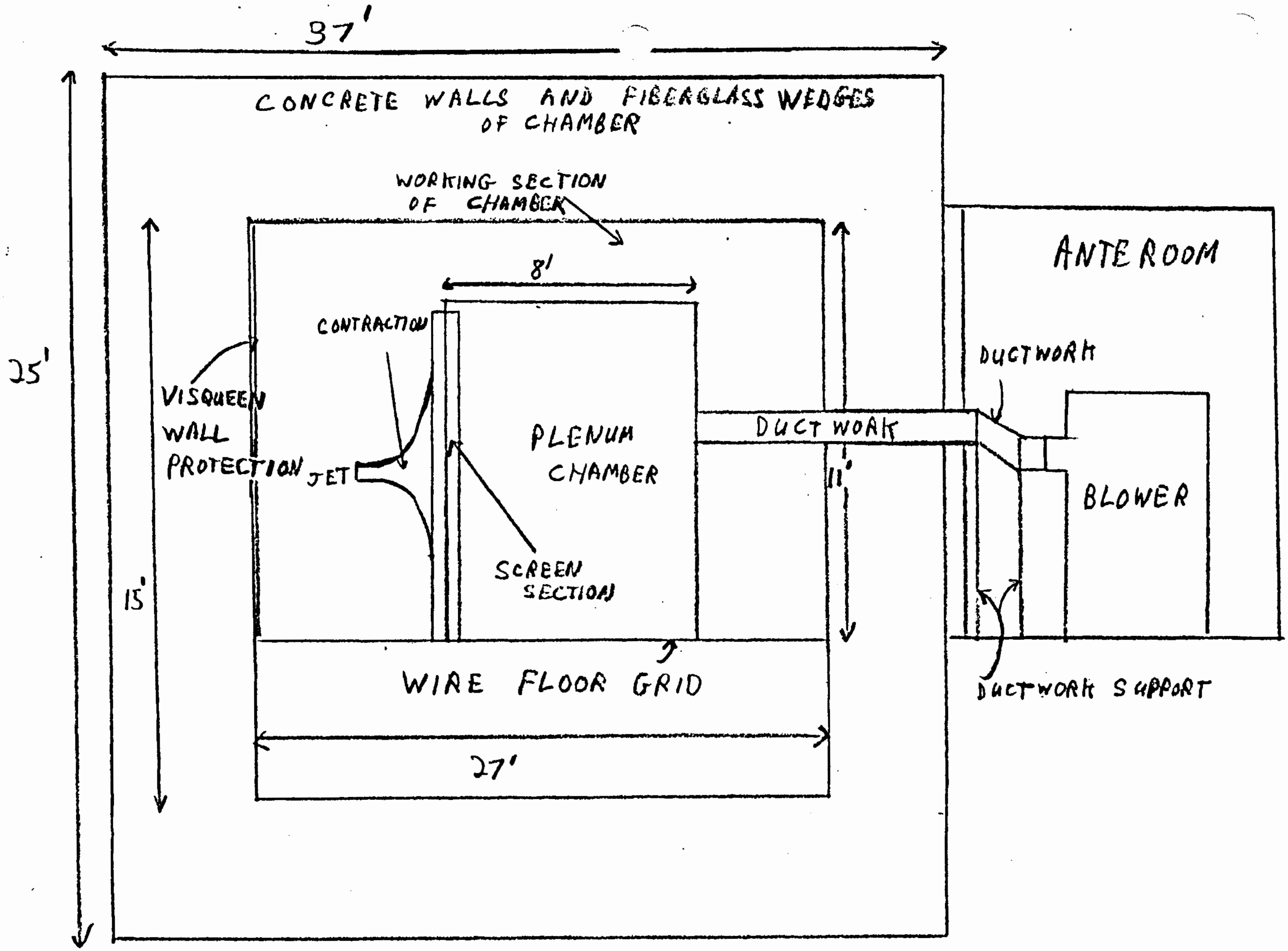

FIGURE C-26. WIND TUNNEL IN ANECHOIC CHAMBER: SIDE VIEW

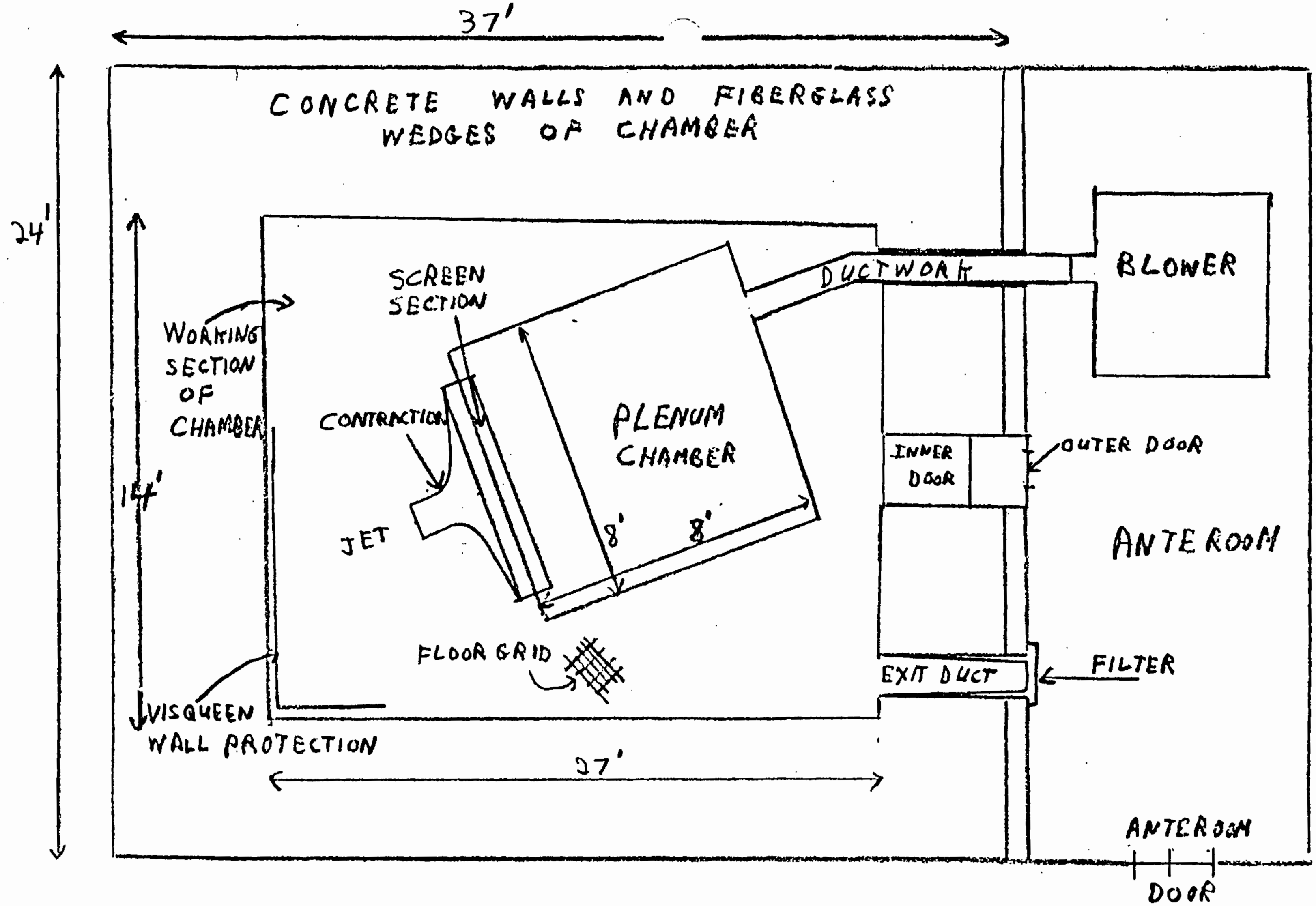

FIGURE C-27. WIND TUNNEL IN ANECHOIC CHAMBER: TOP VIEW

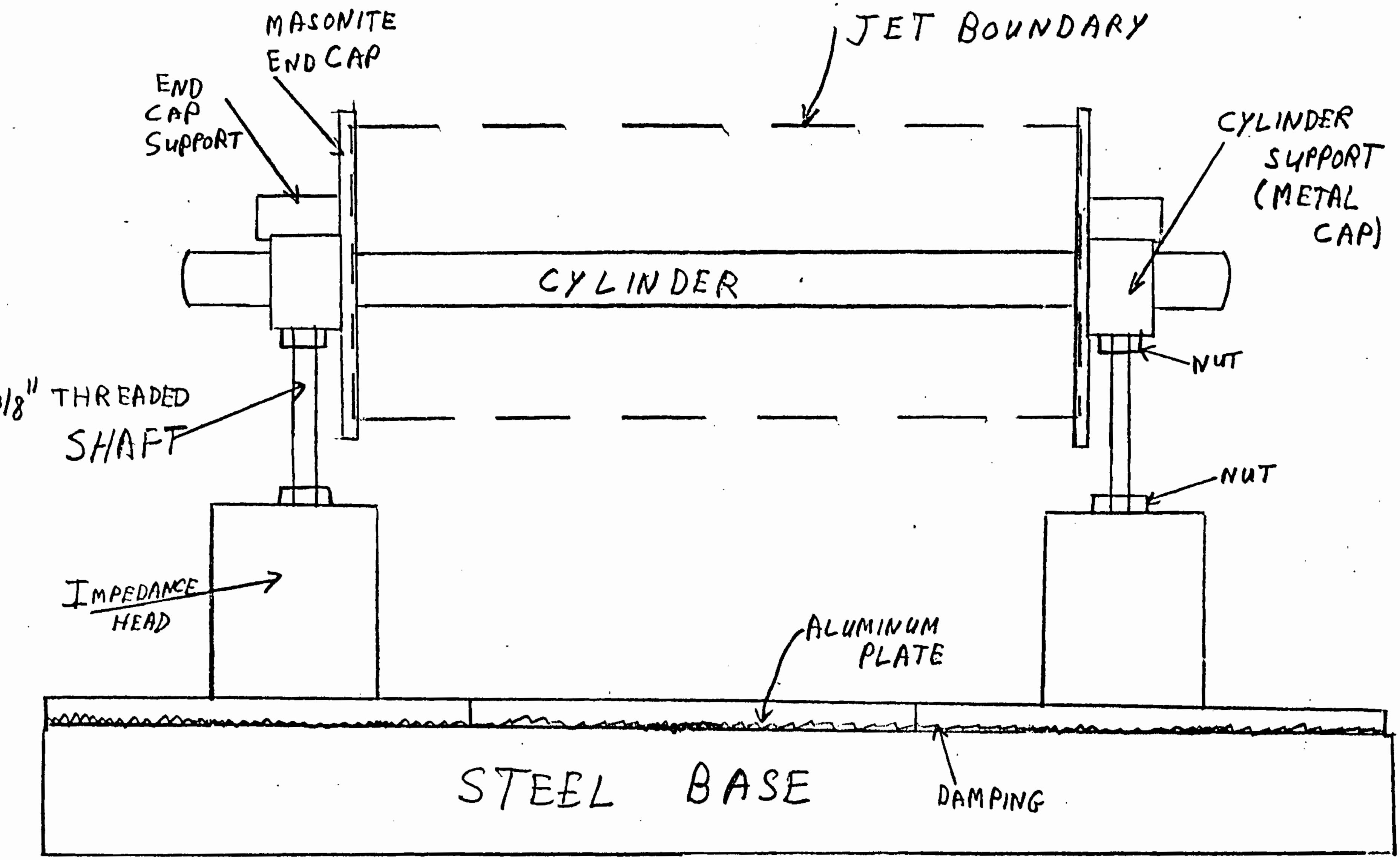

FIGURE C-28. CYLINDER SUPPORT STAND

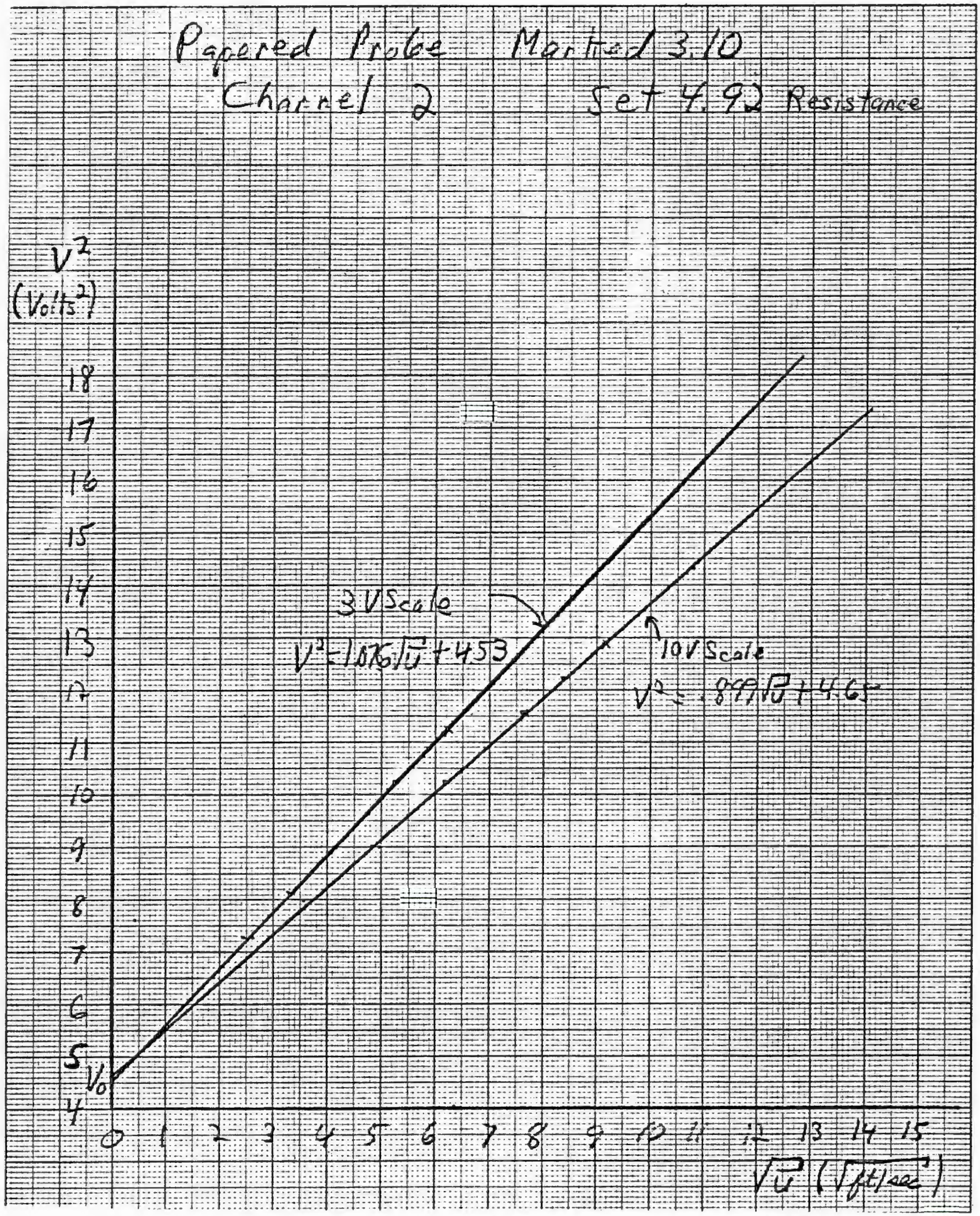

FIGURE C-29. HOT WIRE ANEMOMETER CALIBRATION CURVE

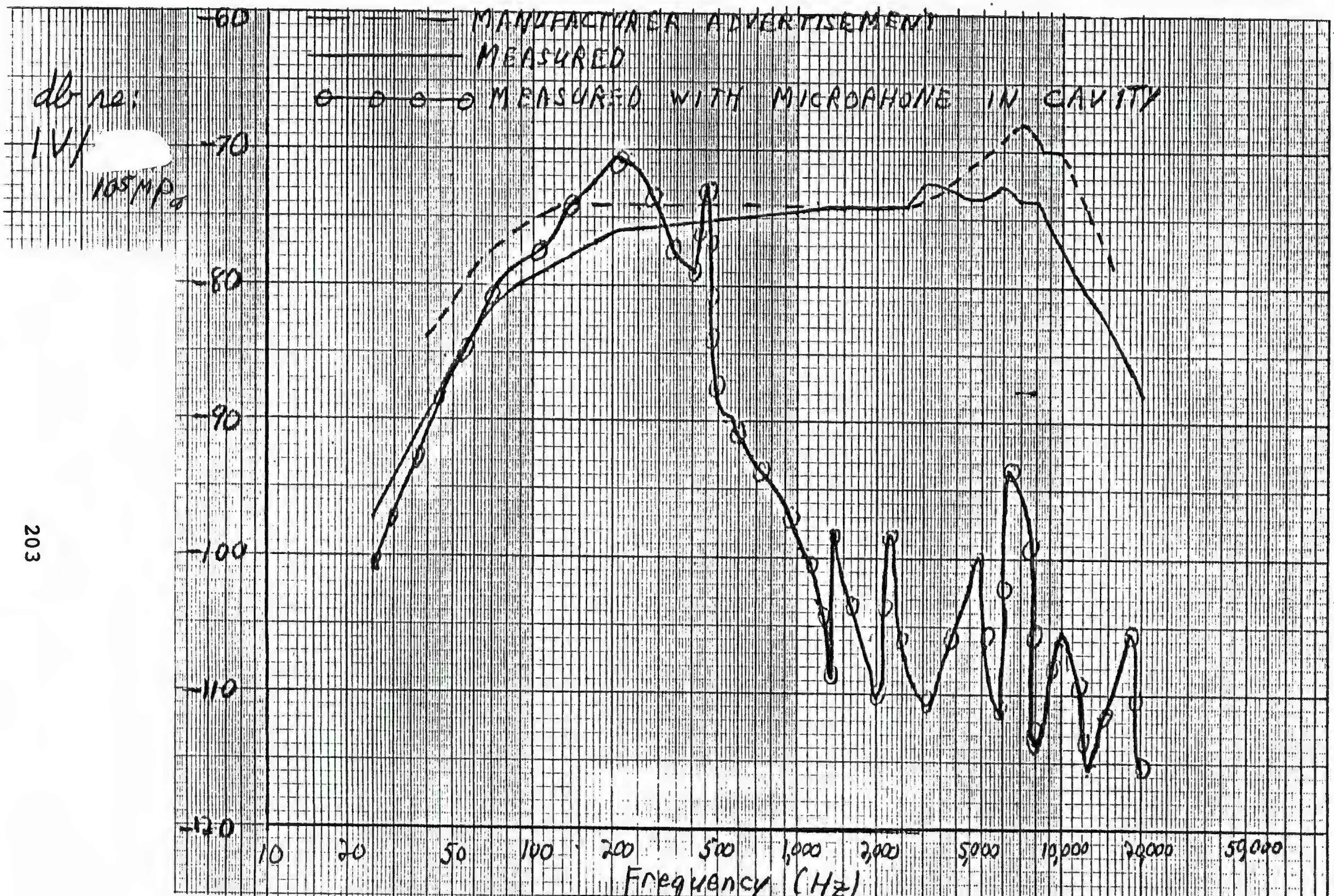

FIGURE C-30. MICROPHONE SENSITIVITY

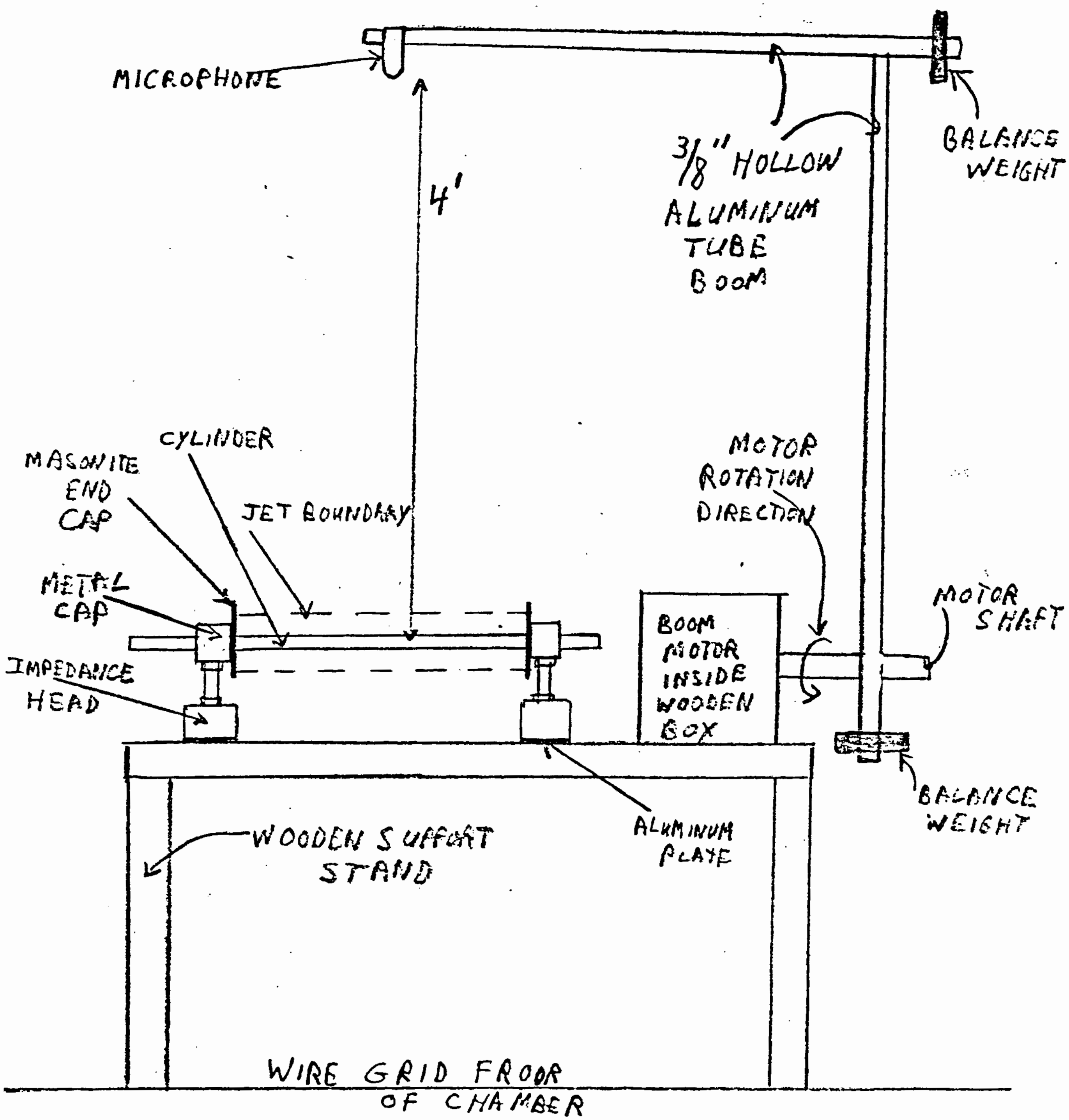

FIGURE C-31. MICROPHONE AND MOUNTING BOOM IN ANECHOIC CHAMBER

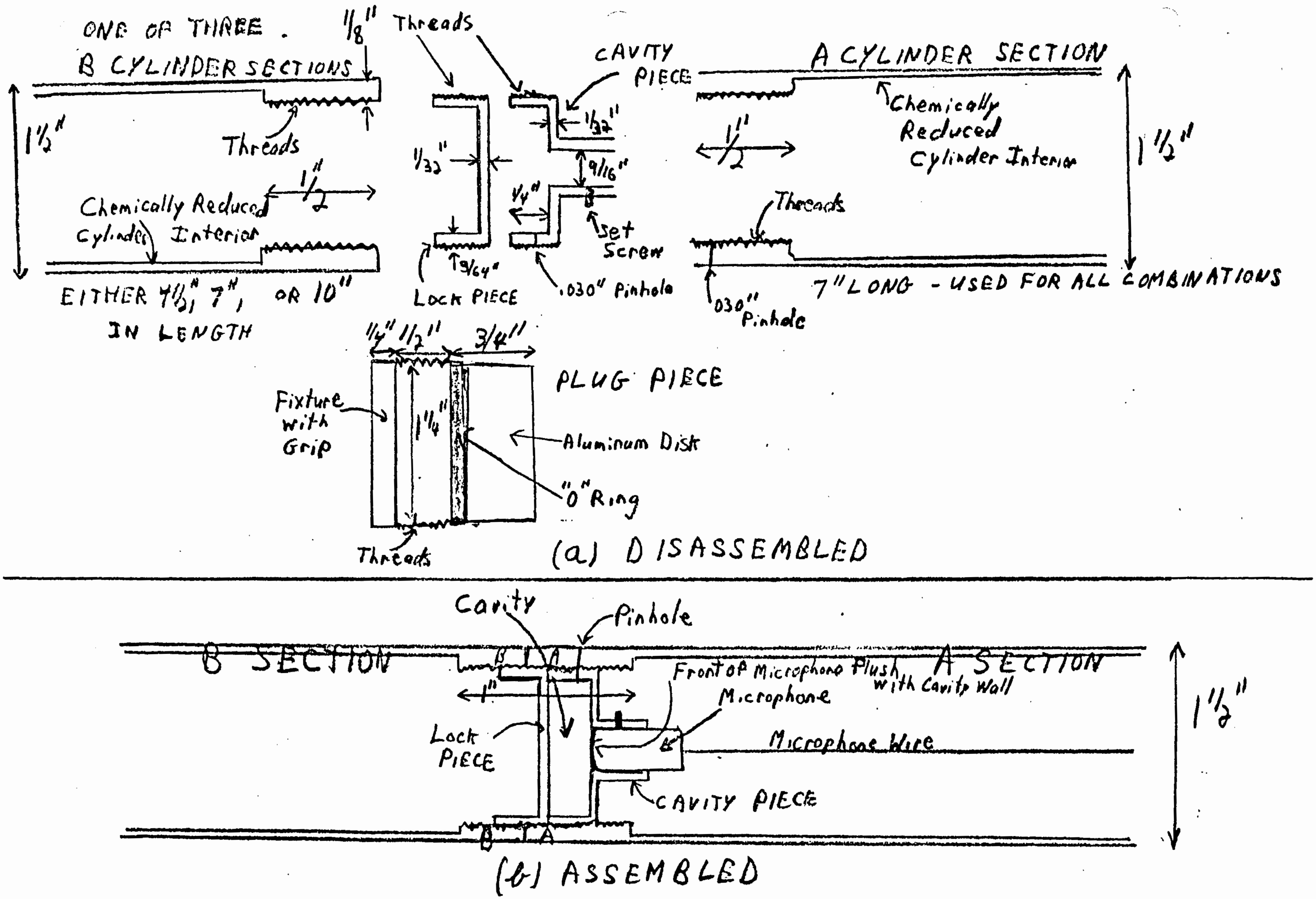

FIGURE C-32. MICROPHONE IN CAVITY INTERIOR TO CYLINDER

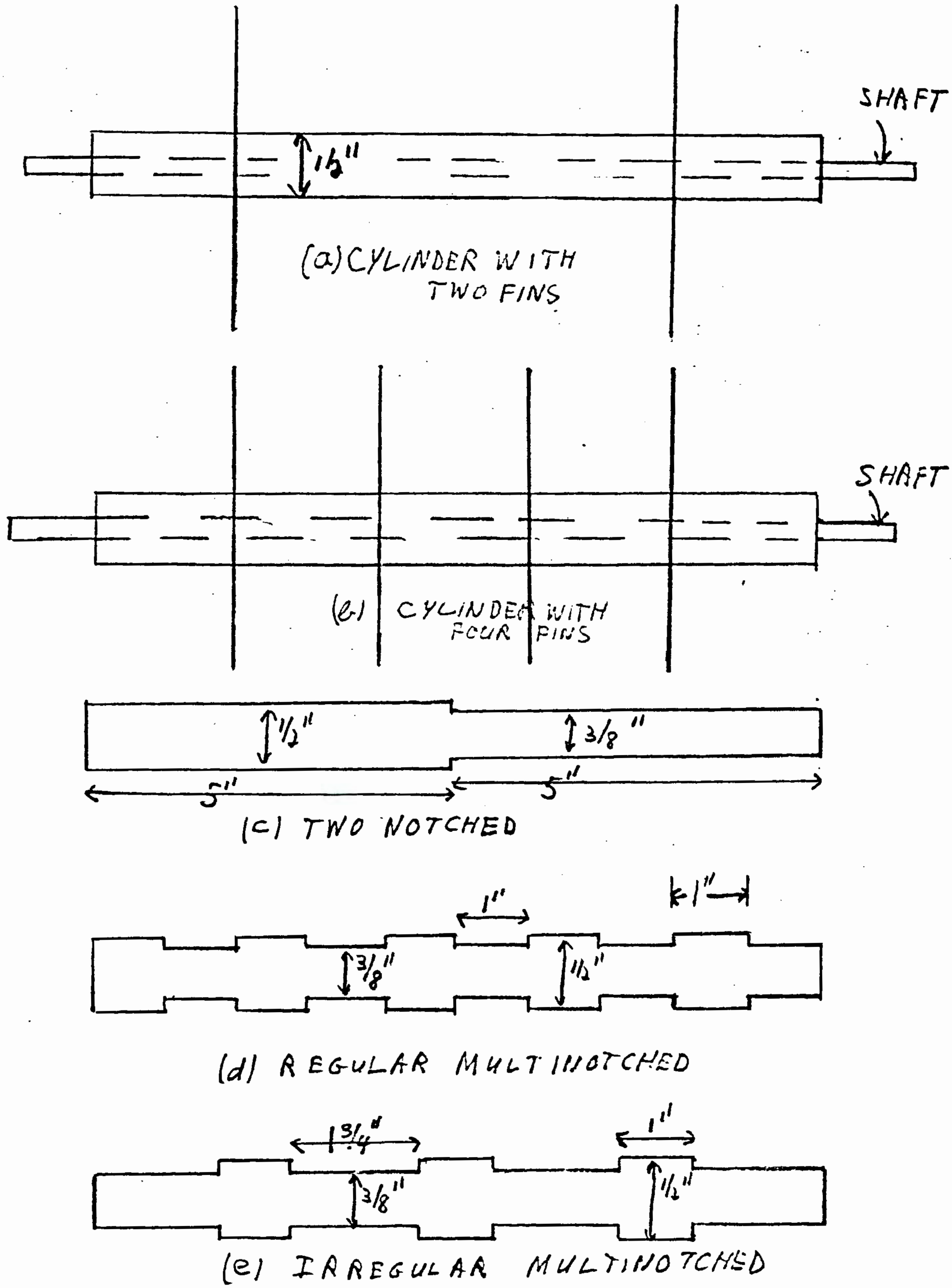

FIGURE C-33. CYLINDERS

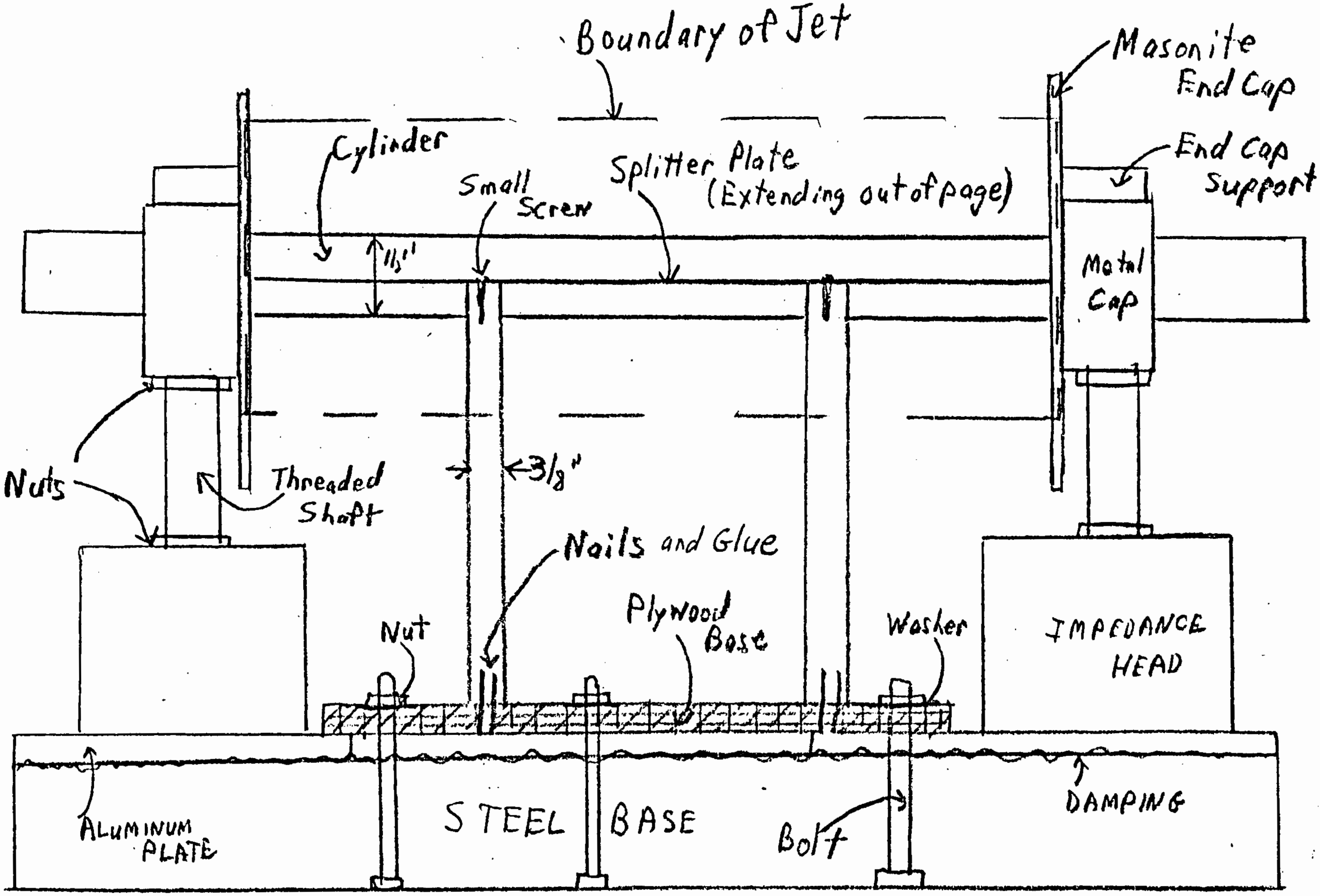

FIGURE C-34. SPLITTER PLATE SUPPORT

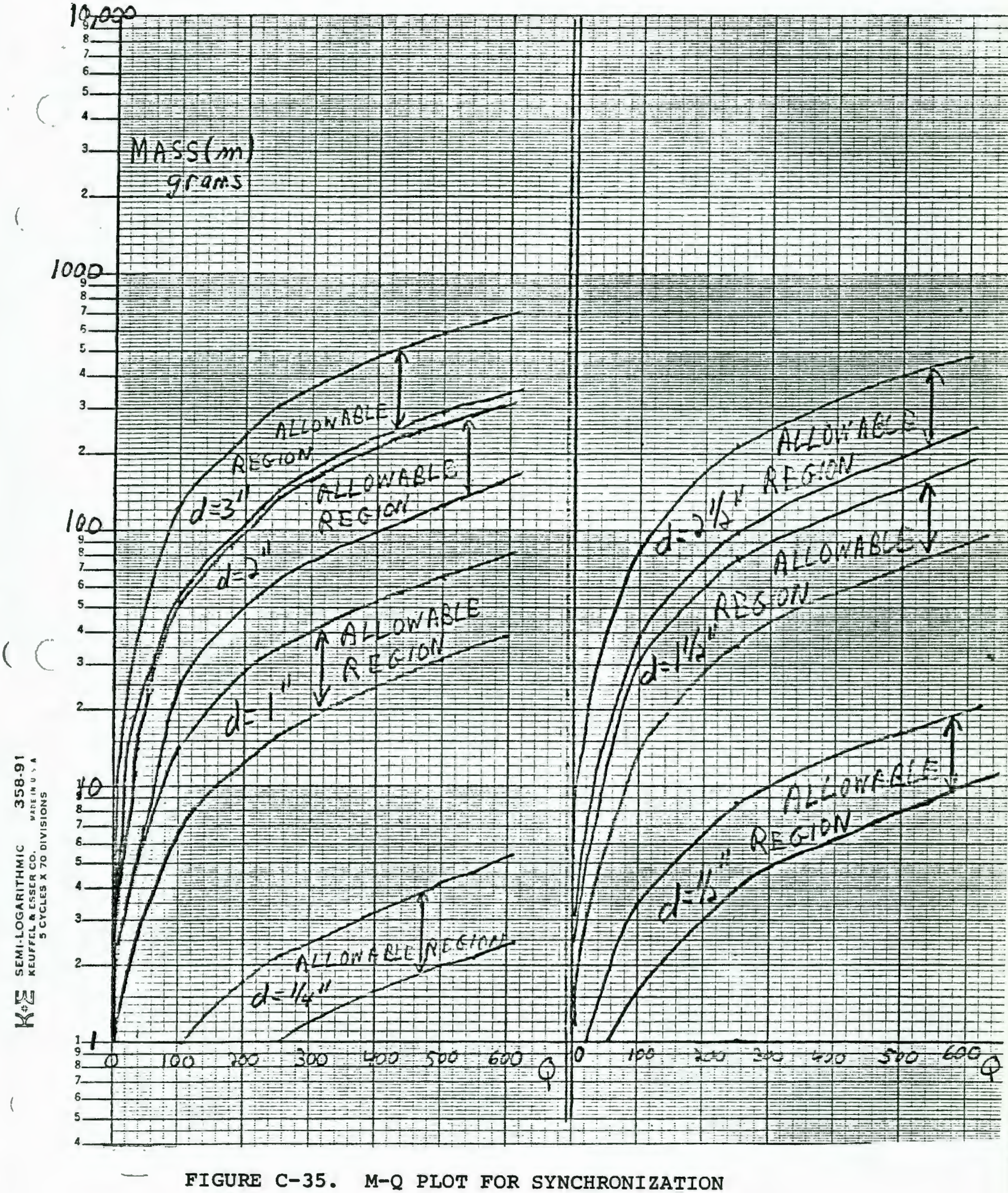

FIGURE C-35. M-Q PLOT FOR SYNCHRONIZATION

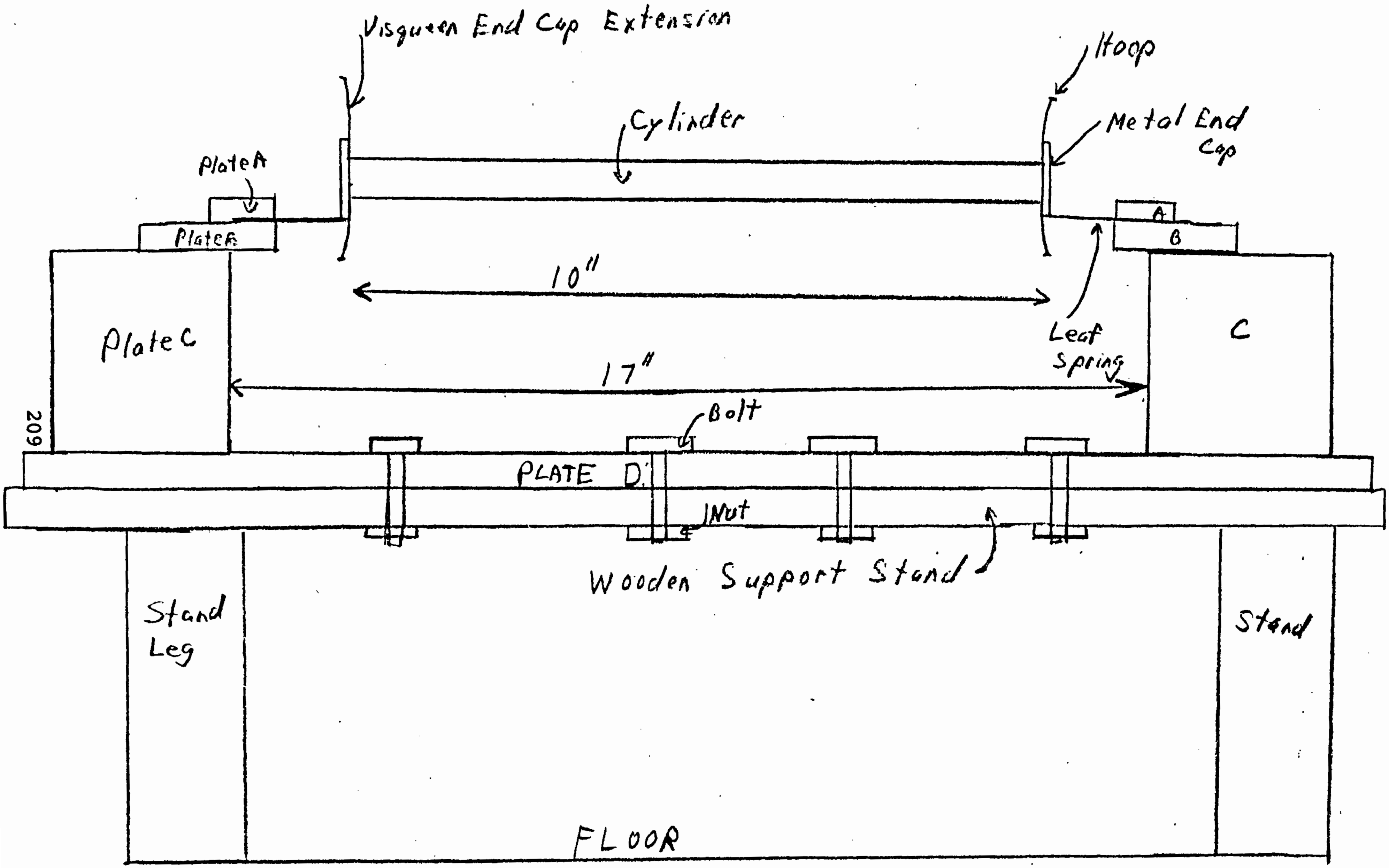

FIGURE C-36. CYLINDER SUPPORT FOR SYNCHRONIZATION

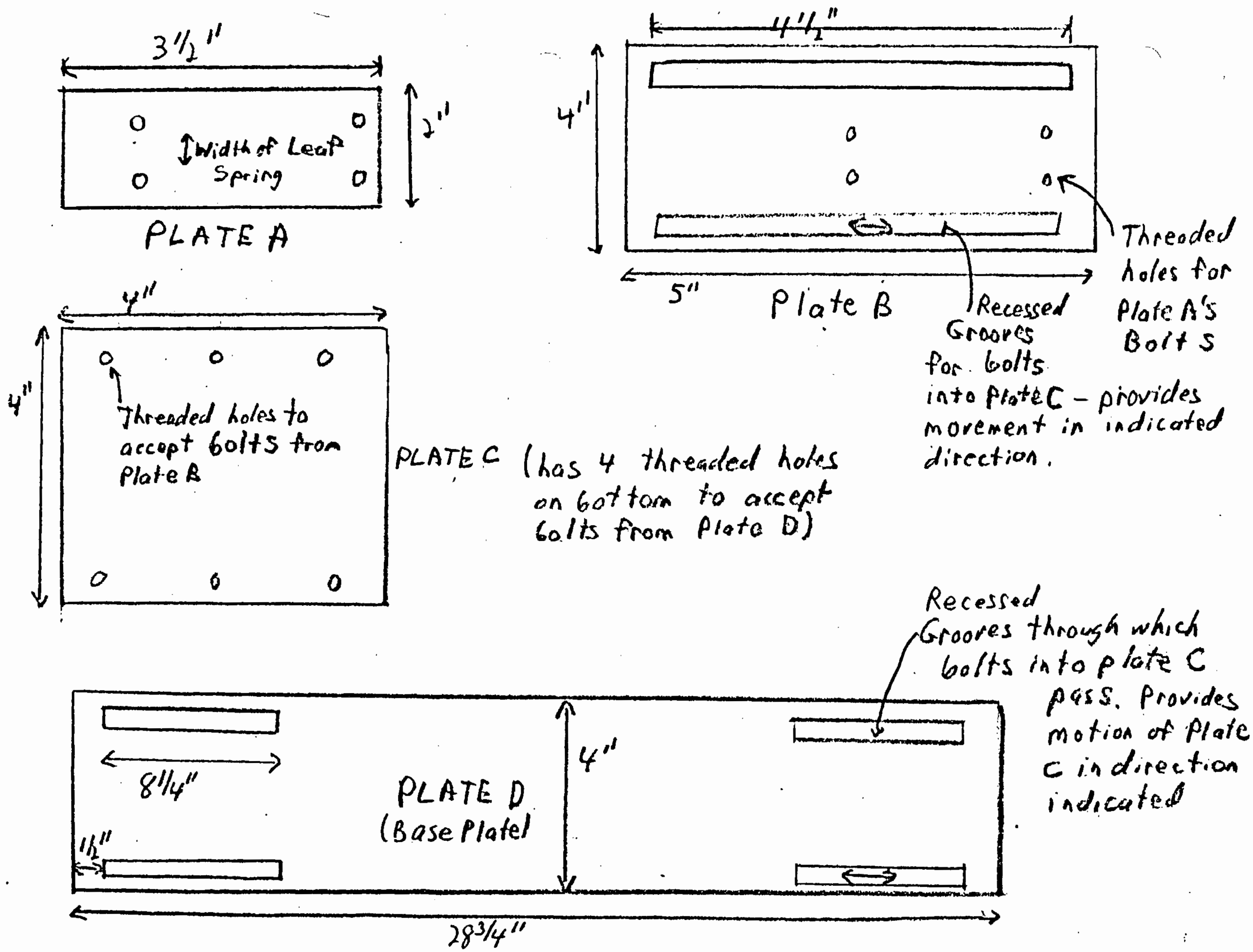

(a) Aluminum Plates - Disassembled: Top View

FIGURE C-37. STAND FOR SYNCHRONIZATION: DETAIL

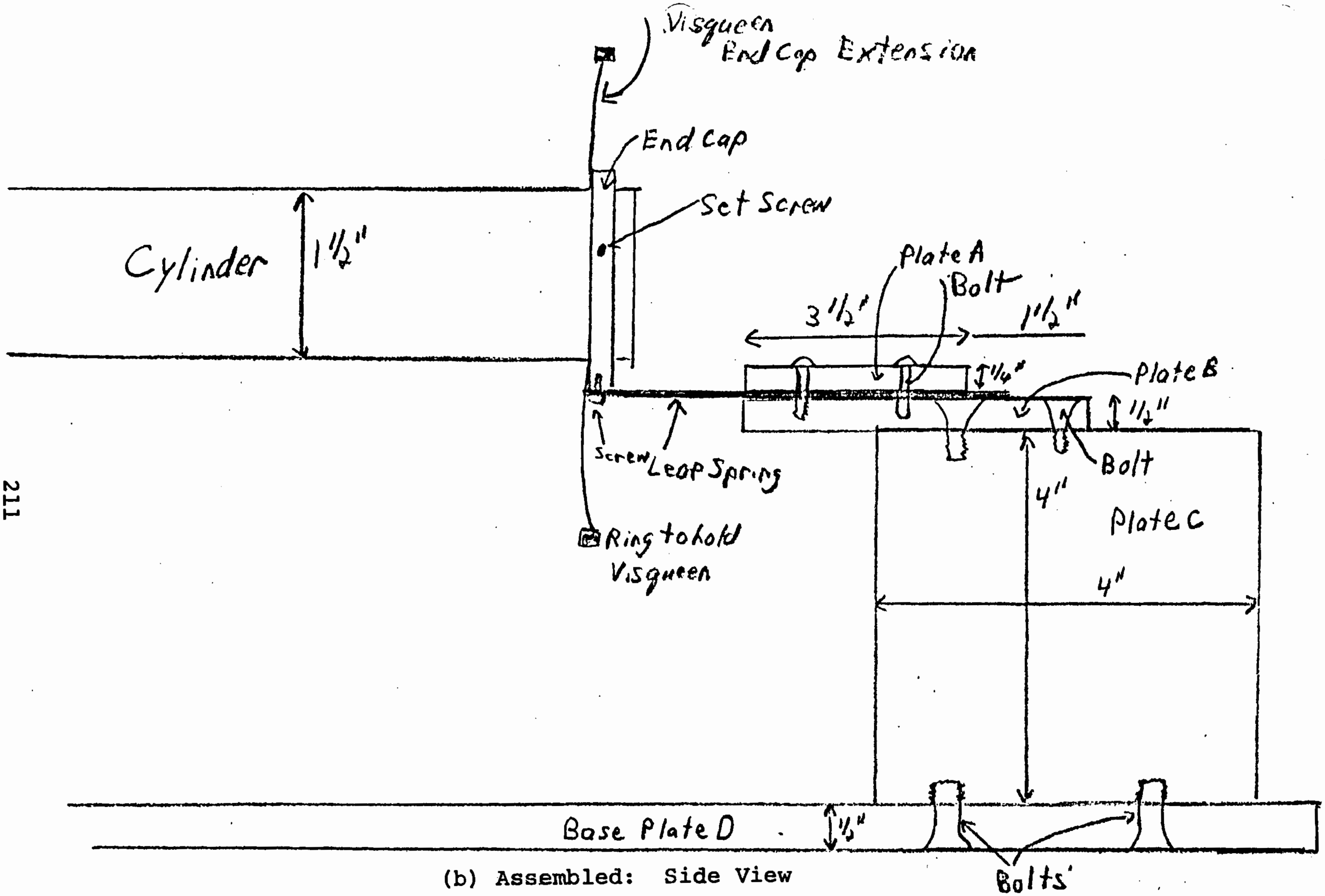

(b) Assembled: Side View

FIGURE C-37 (Continued)

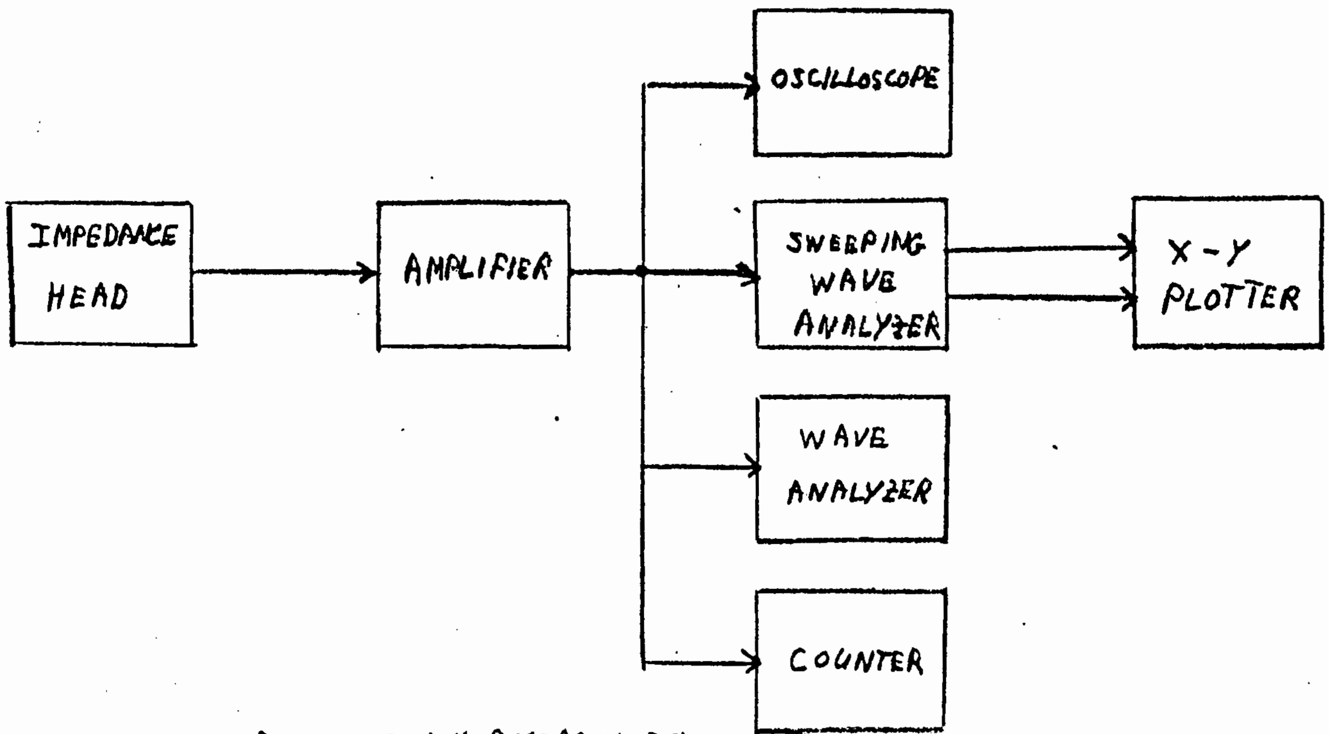

IMPEDANCE HEAD:	WILCOXON RESEARCH Z820
AMPLIFIER:	H/P 465A
OSCILLOSCOPE:	H/P 120A
WAVE ANALYZER:	H/P 3590A
SWEEPING LOCAL OSCILLATOR:	H/P 3594A
WAVE ANALYZER:	H/P 302A
COUNTER:	H/P 521C
X-Y PLOTTER:	VARIAN F120

FIGURE C-38. ELECTRONICS FOR TOTAL LIFT FORCE MEASUREMENT

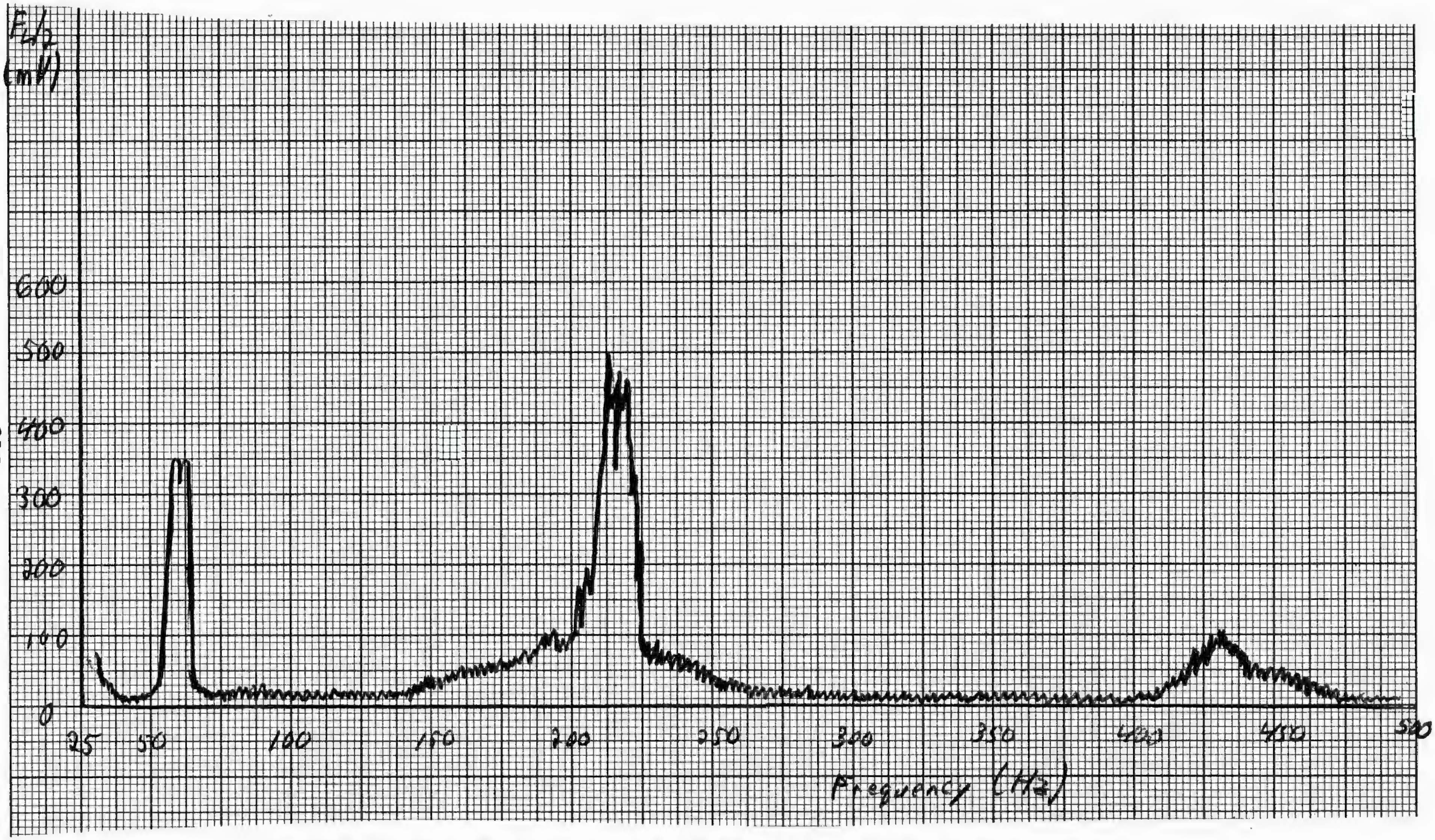

FIGURE C-39. VOLTAGE OUTPUT REPRESENTING $F_L/2$ VS FREQUENCY
$\overline{U}$ = 83.7 FT/SEC; 1" CYLINDER

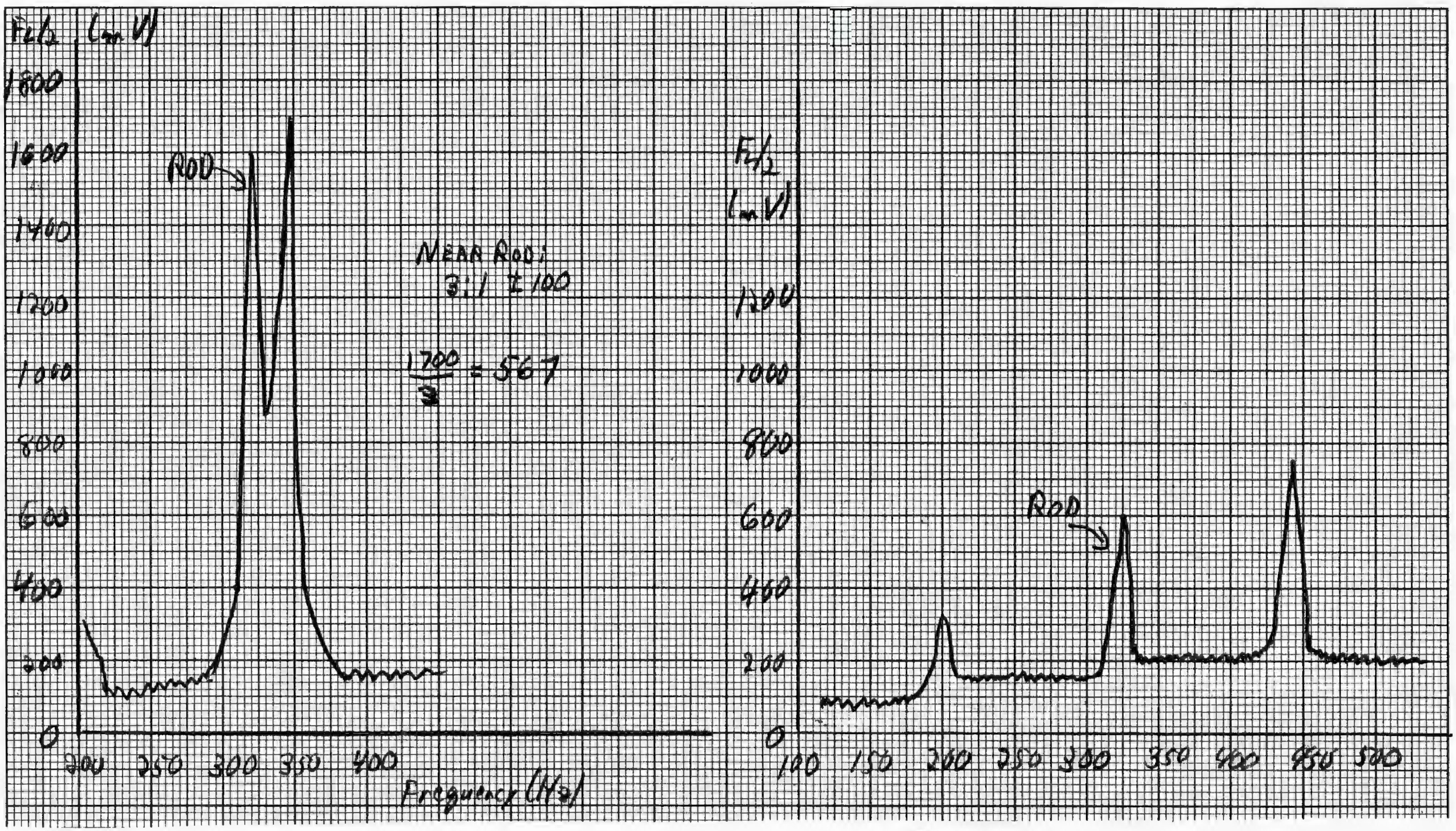

(a) $\overline{U}$ = 84.3 FT/SEC

(b) $\overline{U}$ = 94.3 FT/SEC

FIGURE C-40. VOLTAGE OUTPUT REPRESENTING $F_L/2$ VS FREQUENCY: CYLINDER WITH FOUR FINS

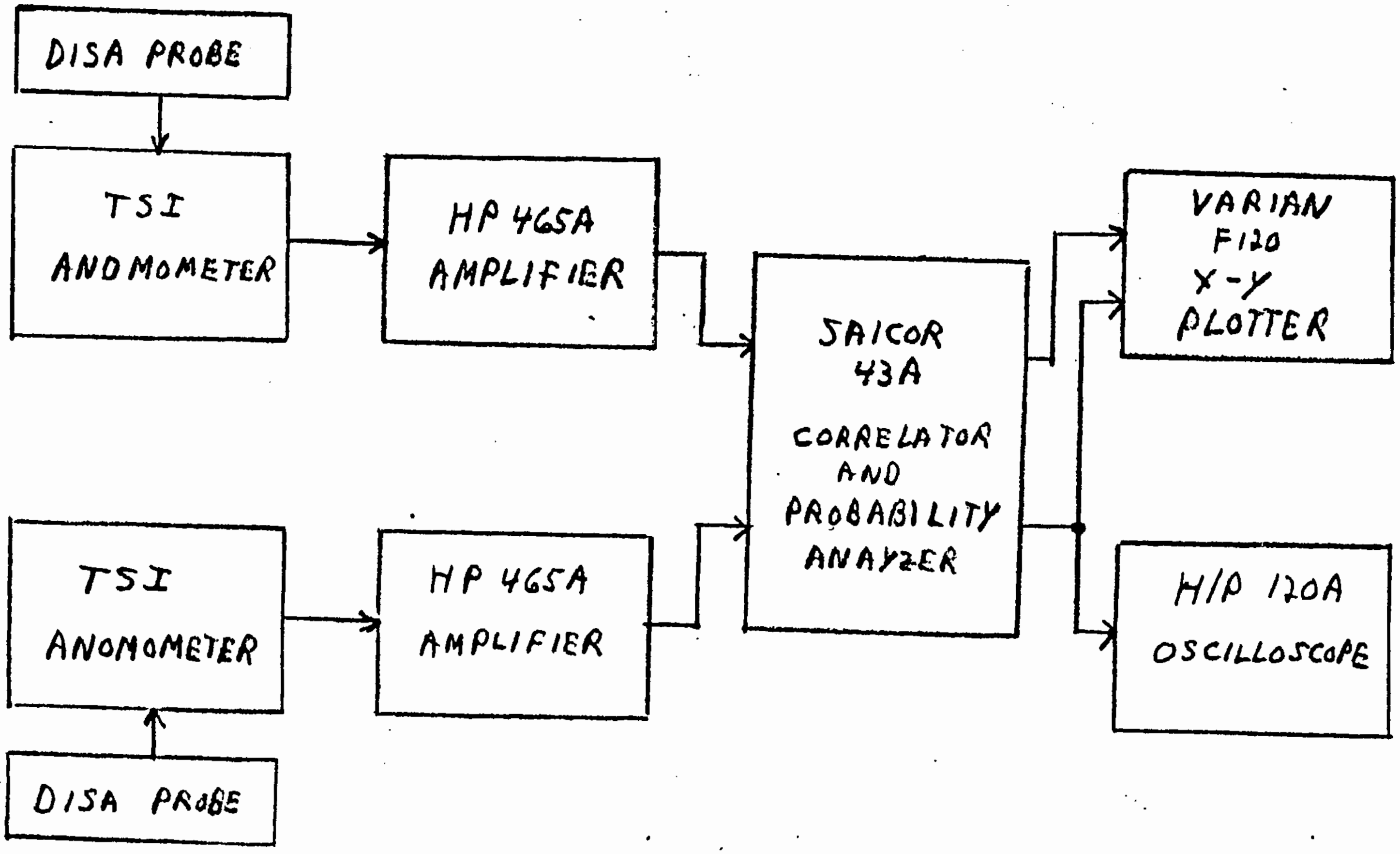

FIGURE C-41. ELECTRONICS FOR WAKE CORRELATION MEASUREMENT

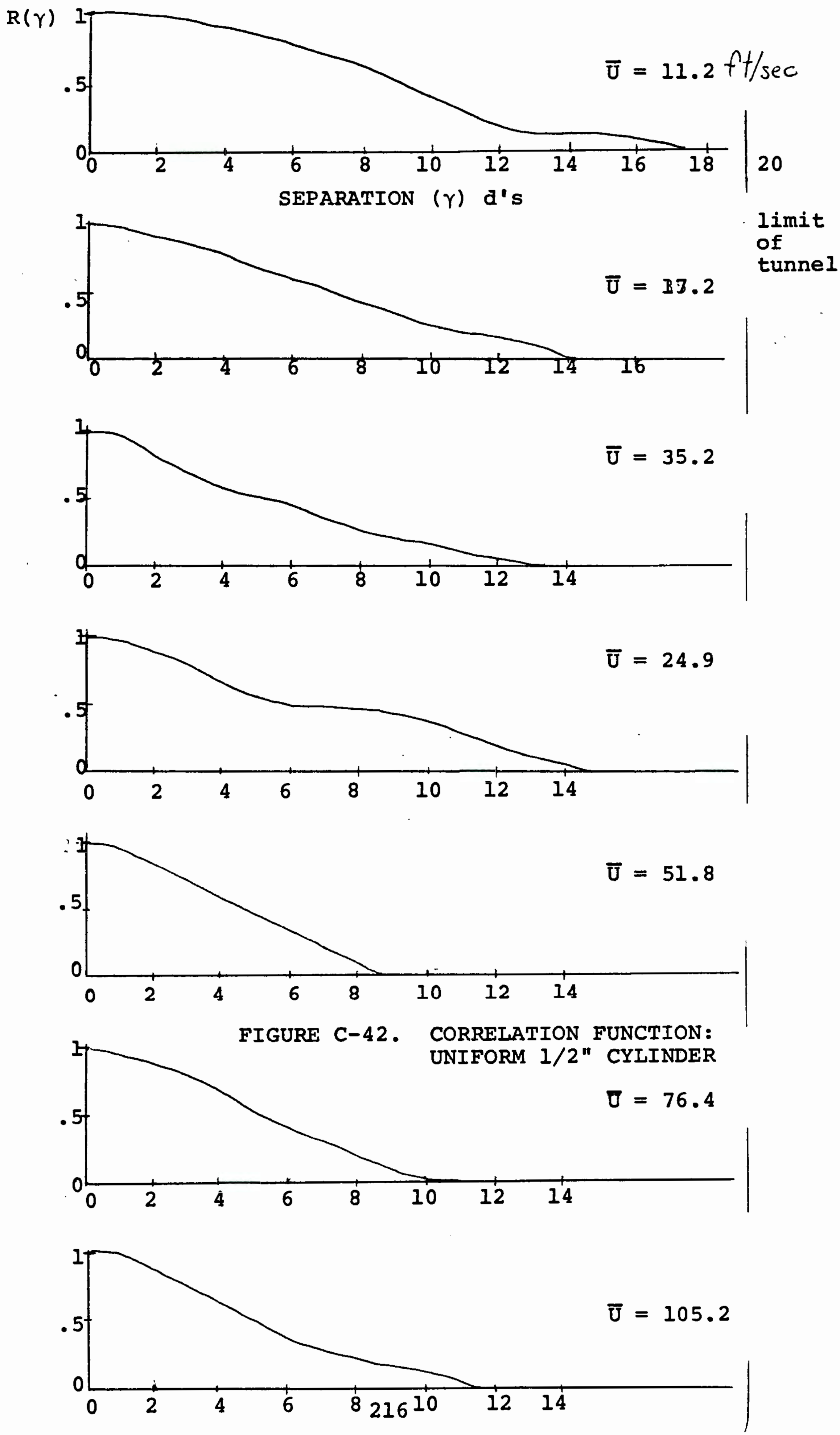

FIGURE C-42. CORRELATION FUNCTION: UNIFORM 1/2" CYLINDER

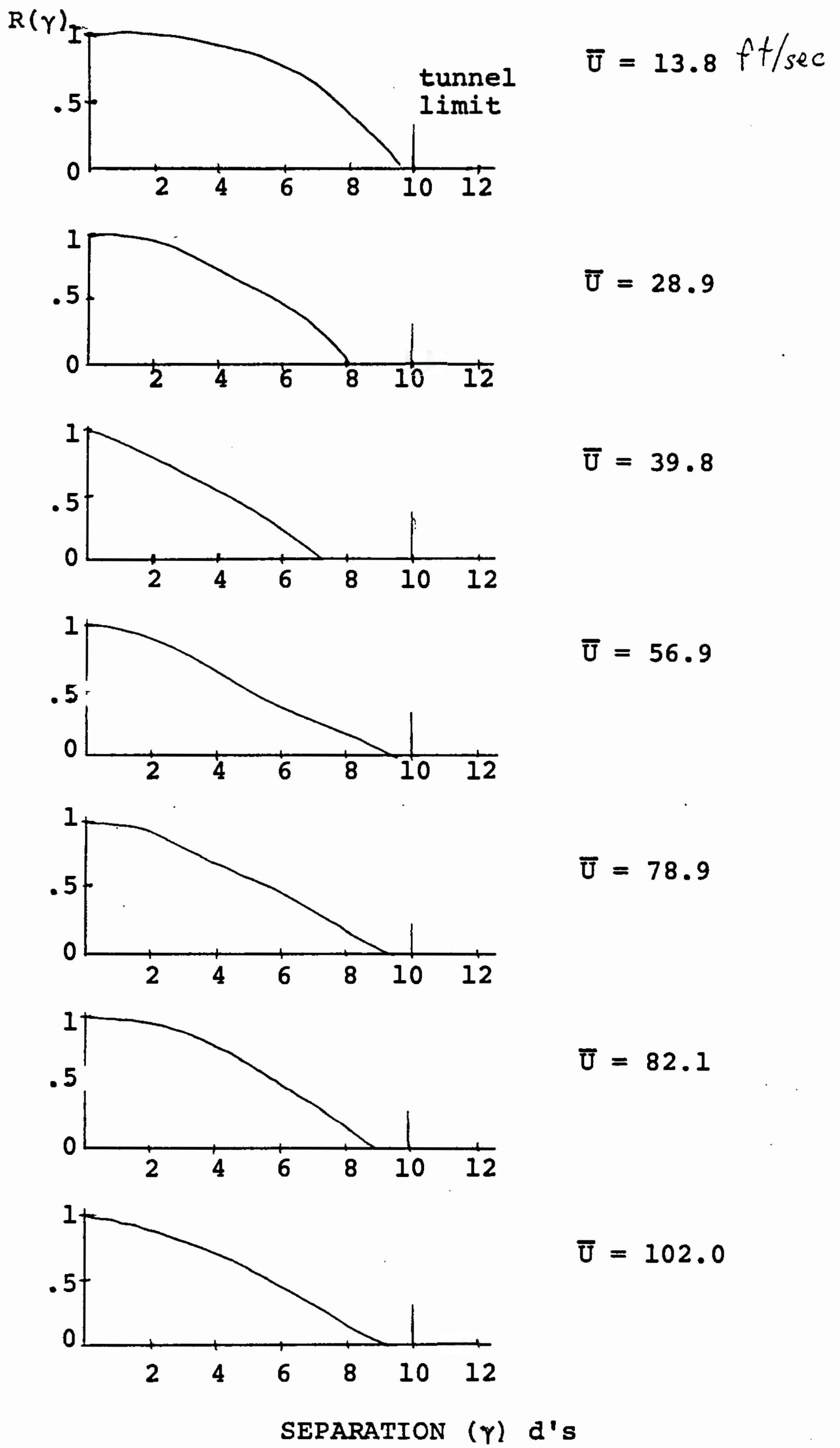

FIGURE C-43. CORRELATION FUNCTION: UNIFORM 1" CYLINDER

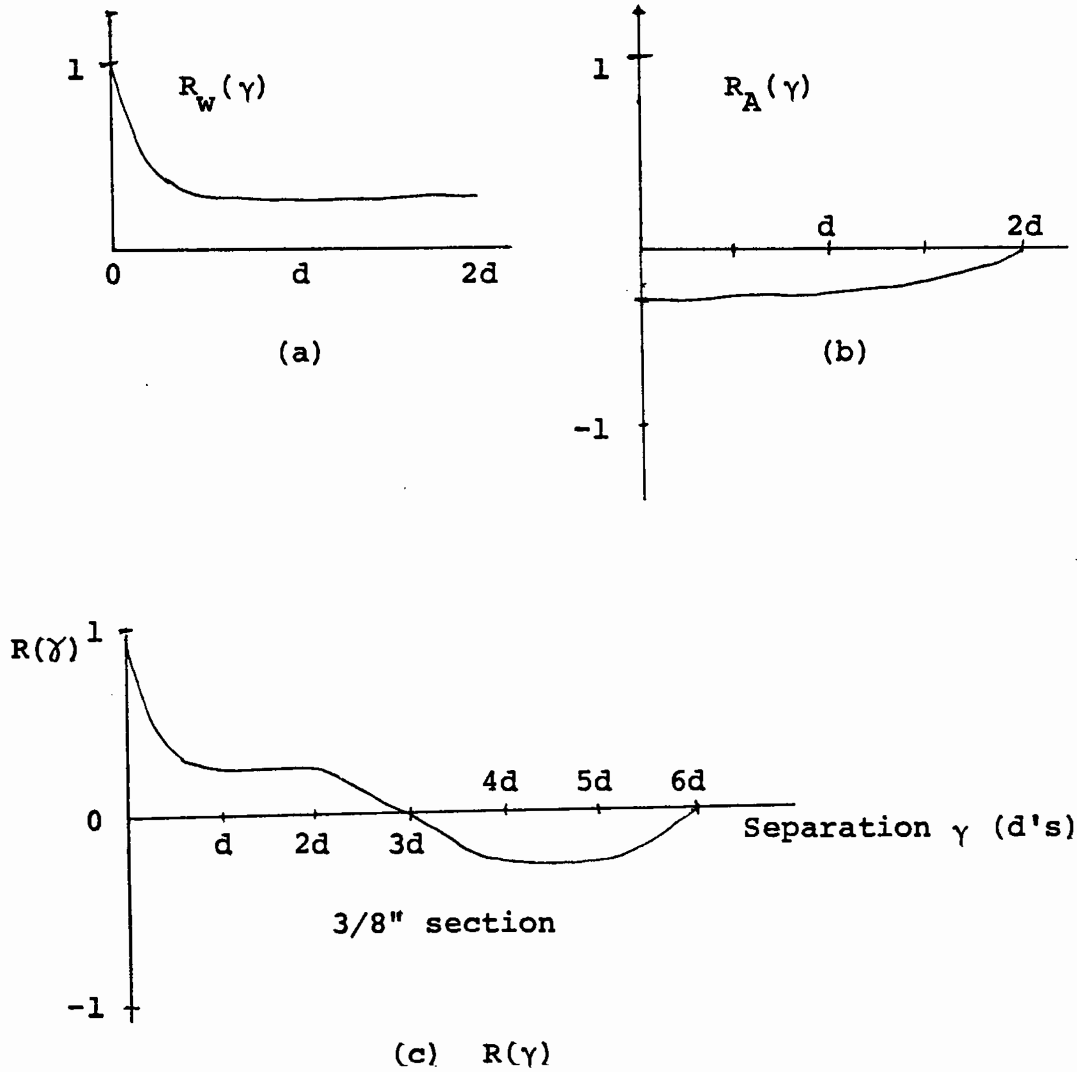

FIGURE C-44. CORRELATION FUNCTIONS: REGULAR MULTINOTCHED CYLINDER: 1/2" SECTIONS $\overline{U}$ = 75 FT/SEC

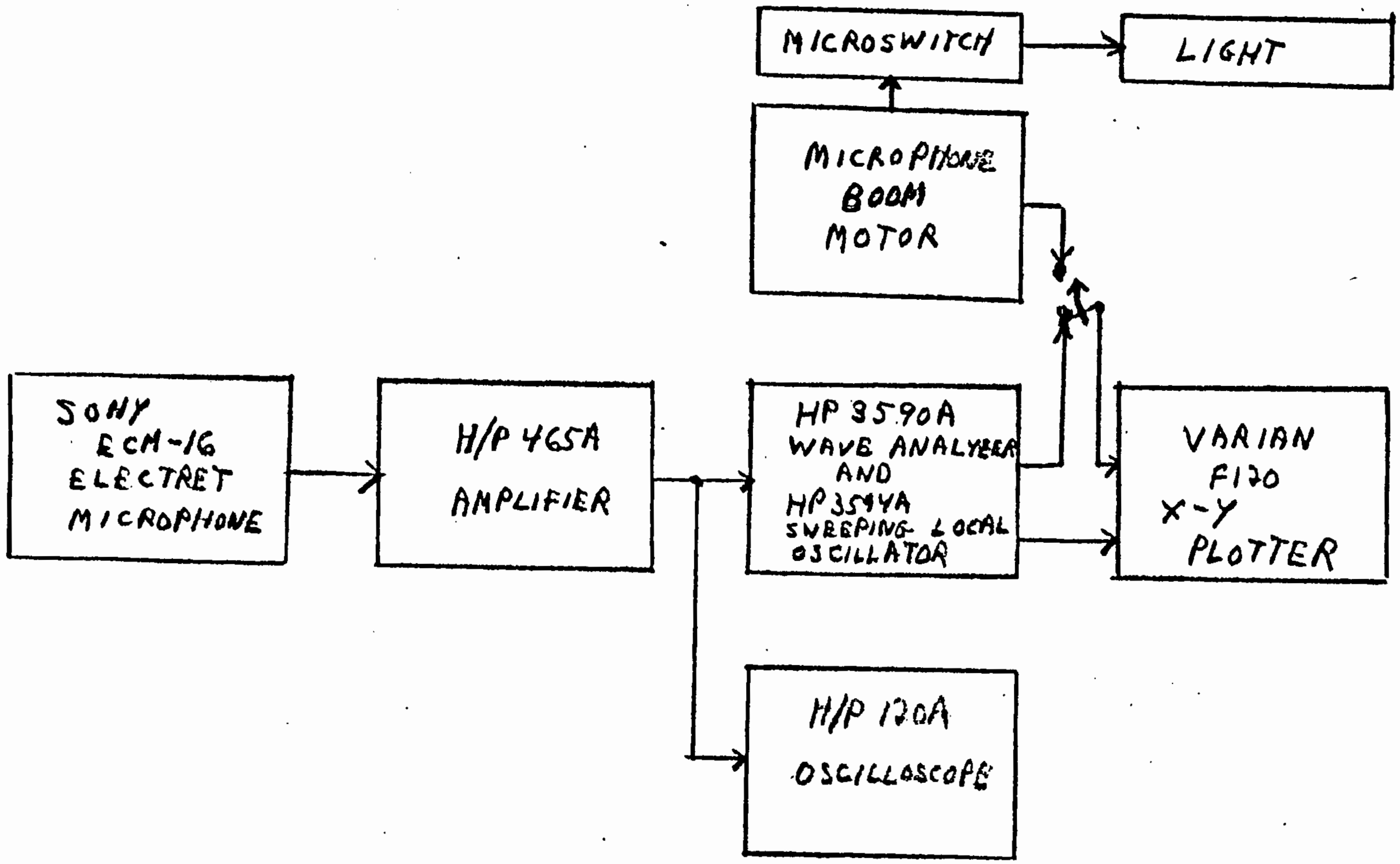

FIGURE C-45. ELECTRONICS FOR SOUND INTENSITY MEASUREMENT

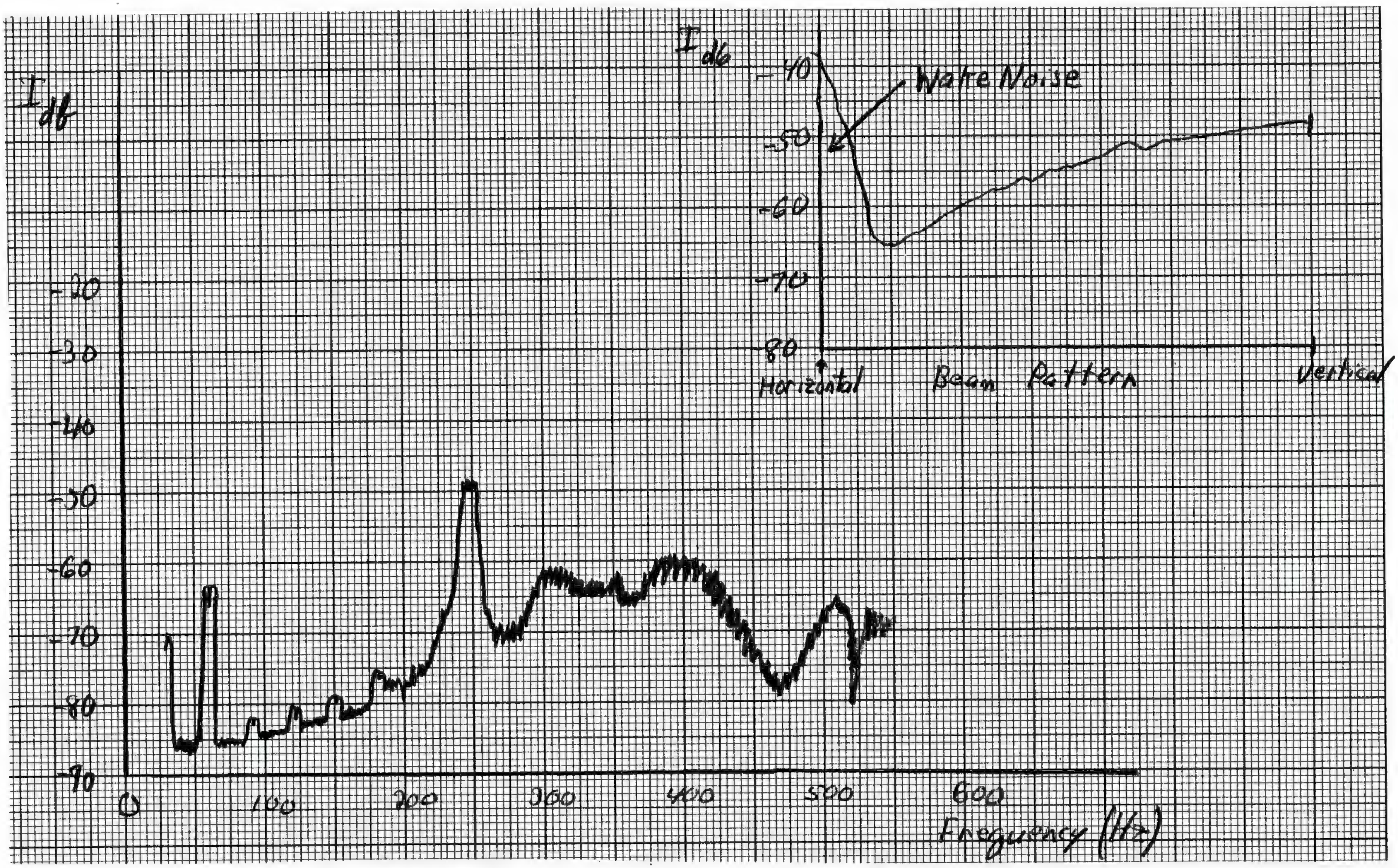

FIGURE C-46. MEASURED I: UNIFORM 1/2" CYLINDER; $\overline{U}$ = 51.5 FT/SEC

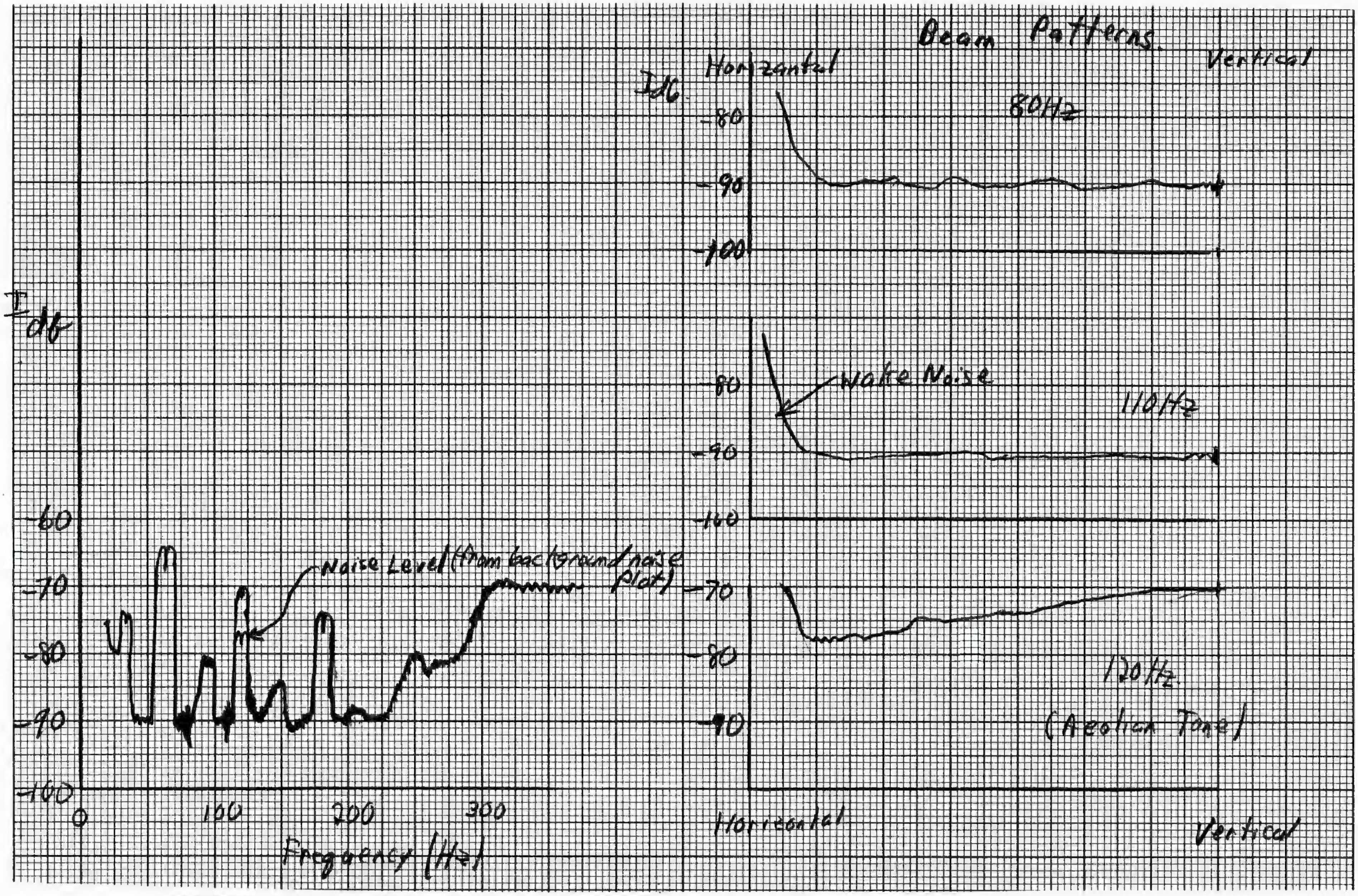

FIGURE C-47. MEASURED I: ROUGHENED 1/2" CYLINDER: $\overline{U}$ = 28 FT/SEC

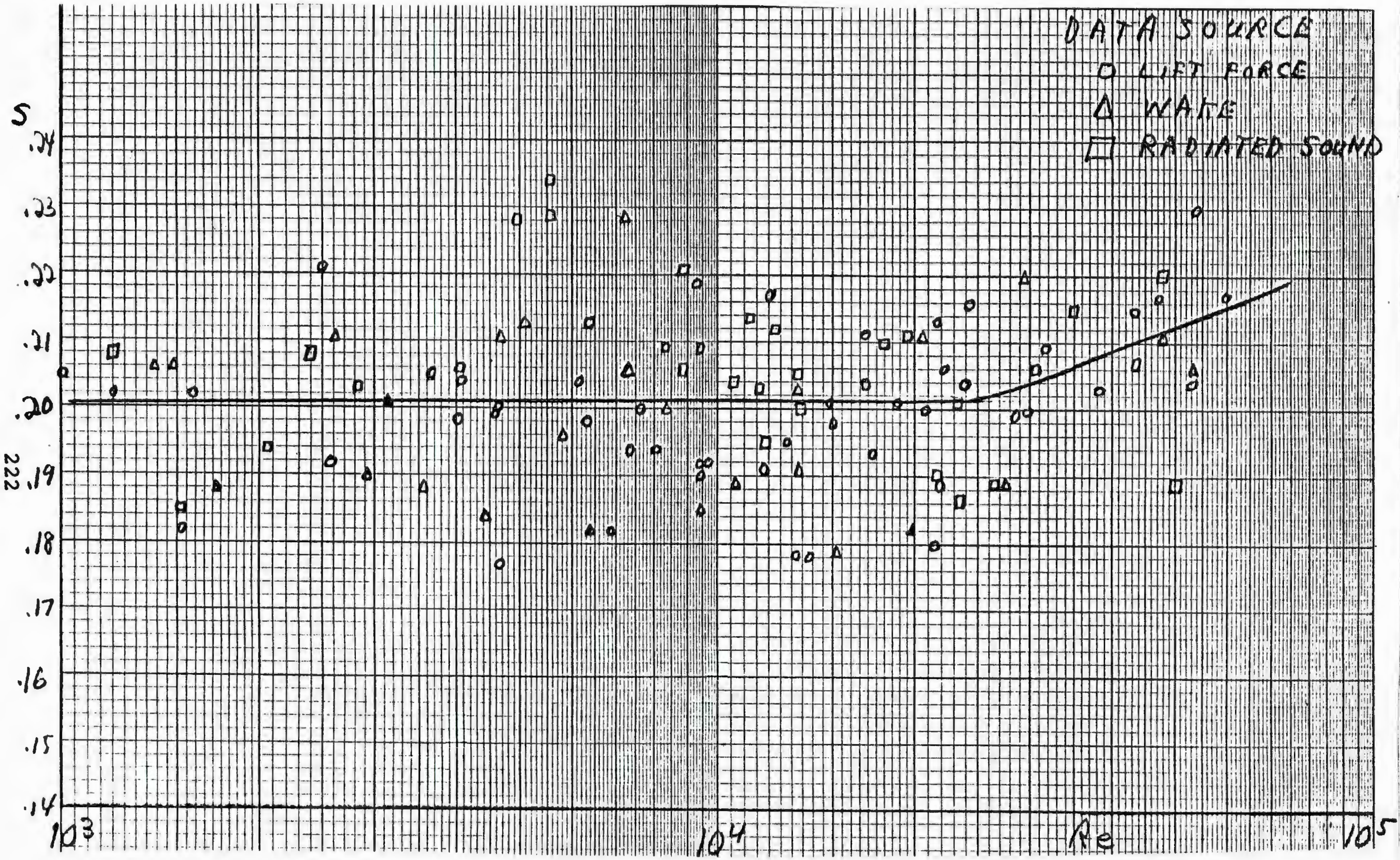

FIGURE C-48. STROUHAL NUMBER(S) VS REYNOLDS NUMBER (Re) FOR UNIFORM CYLINDER

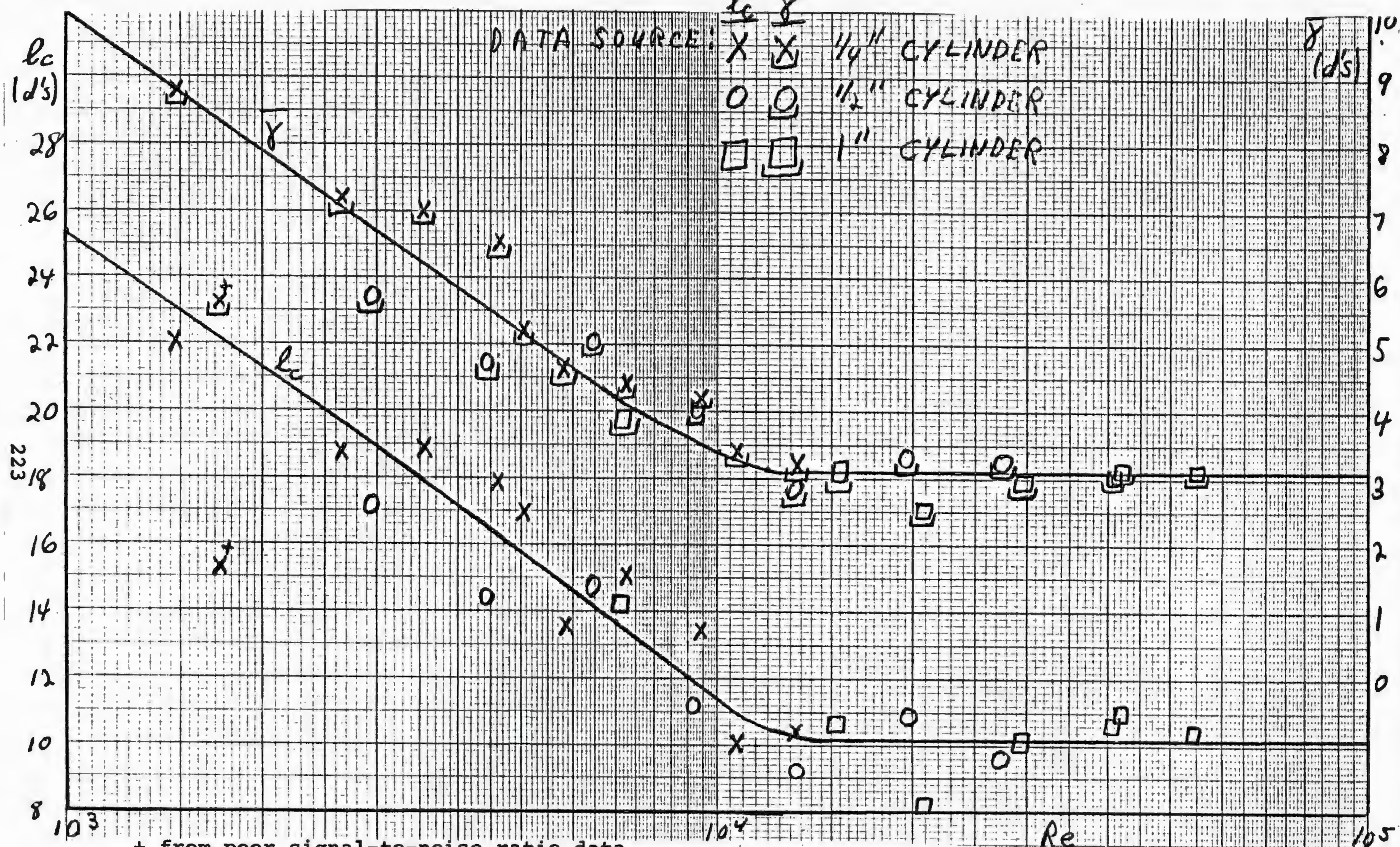

+ from poor signal-to-noise ratio data

FIGURE C-49. CORRELATION LENGTH AND CENTROID OF ONE-SIDED CORRELATION CURVE VS REYNOLDS NUMBER FOR UNIFORM CYLINDERS

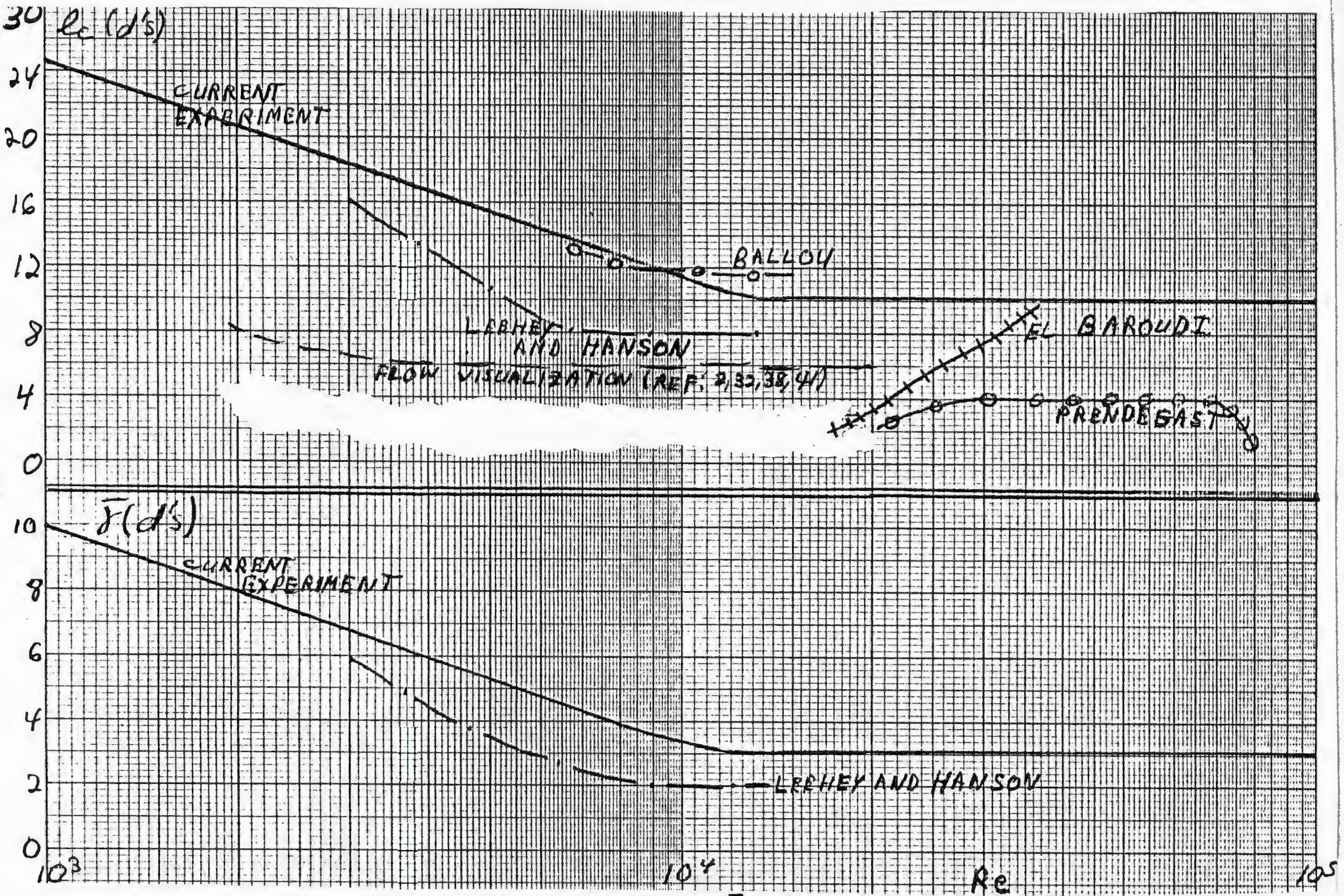

FIGURE C-50. COMPARISON OF CURRENT ℓ_c AND $\bar{\gamma}$ VALUES WITH PREVIOUS REPORTS

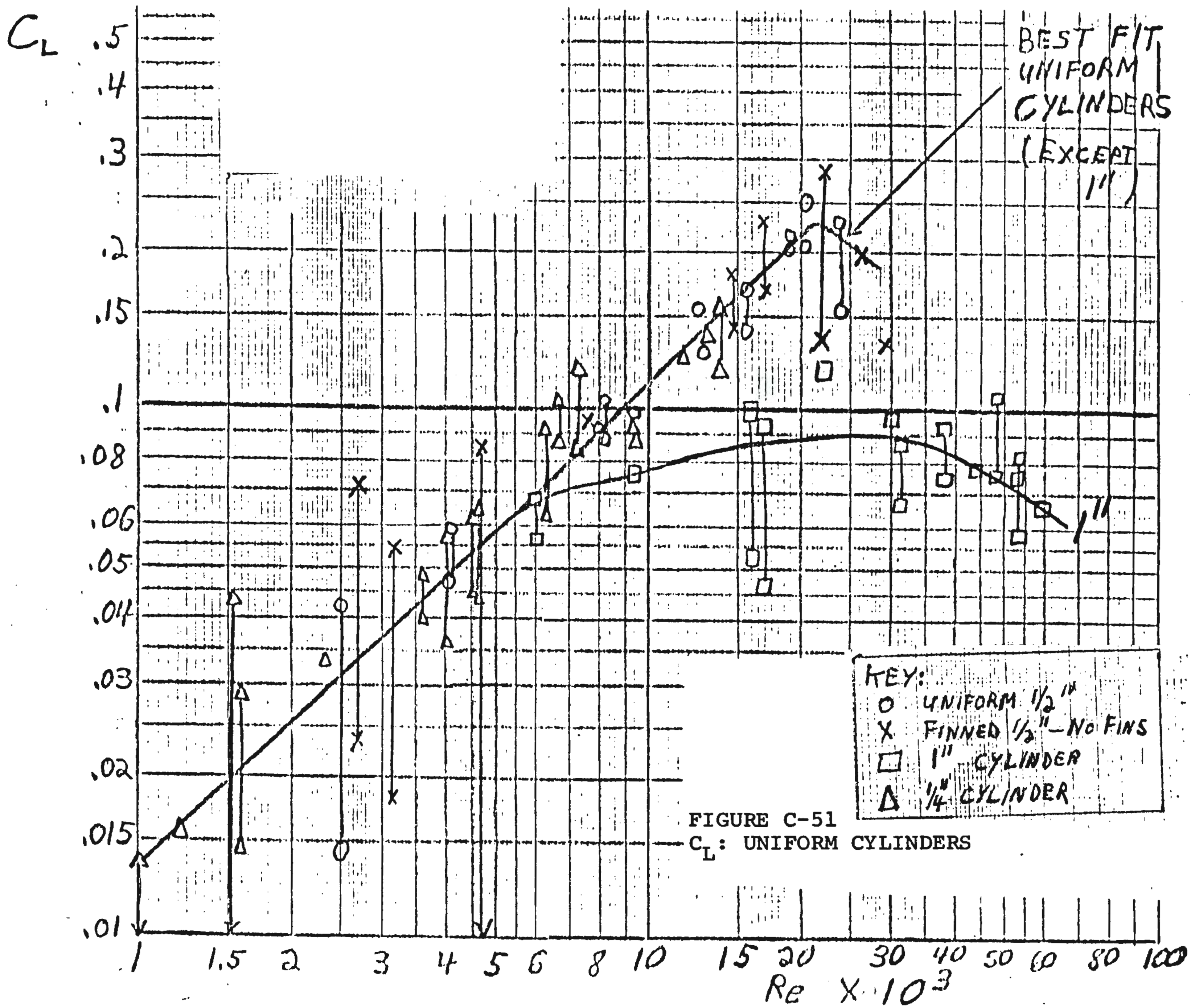

FIGURE C-51
C_L: UNIFORM CYLINDERS

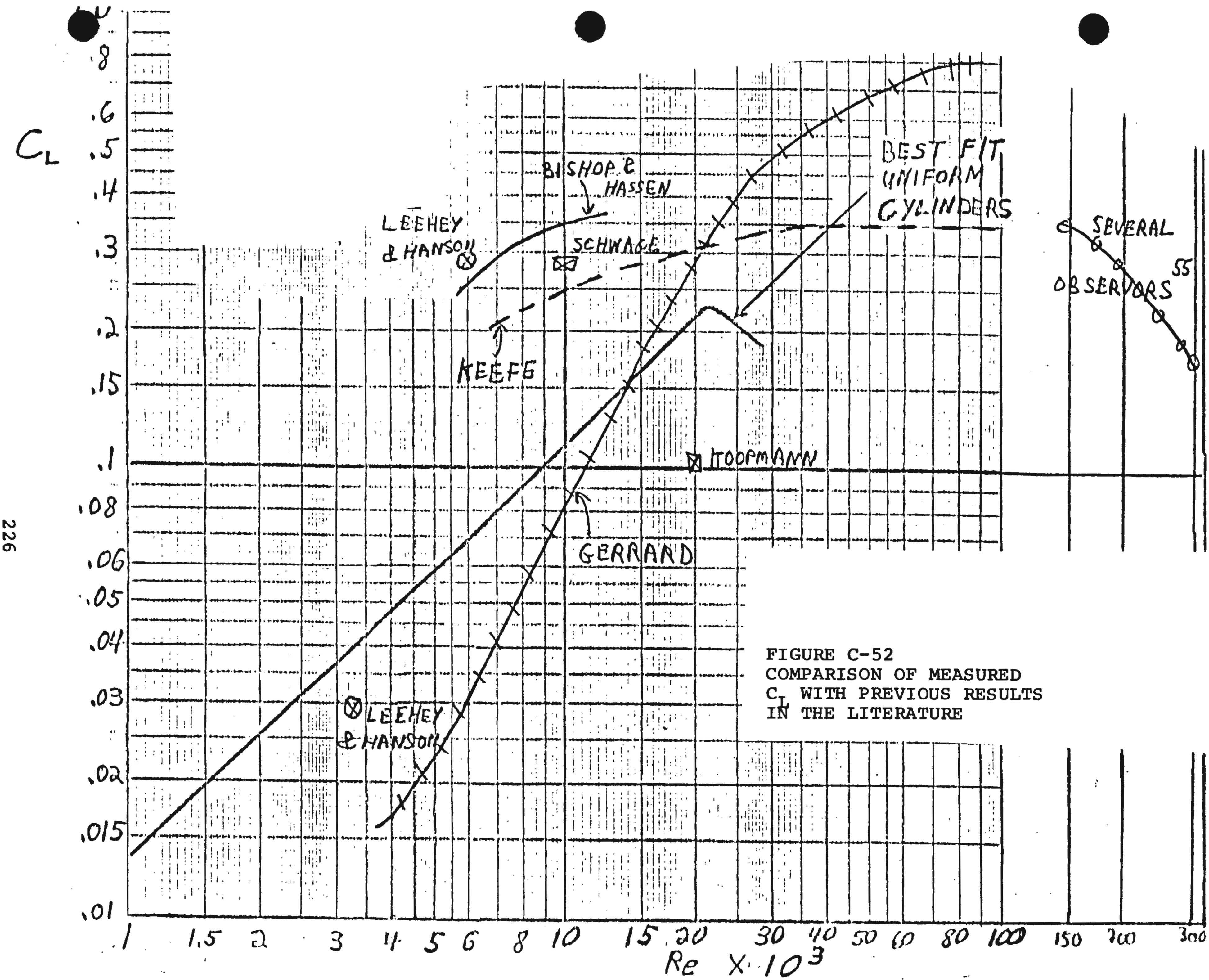

FIGURE C-52
COMPARISON OF MEASURED
C_L WITH PREVIOUS RESULTS
IN THE LITERATURE

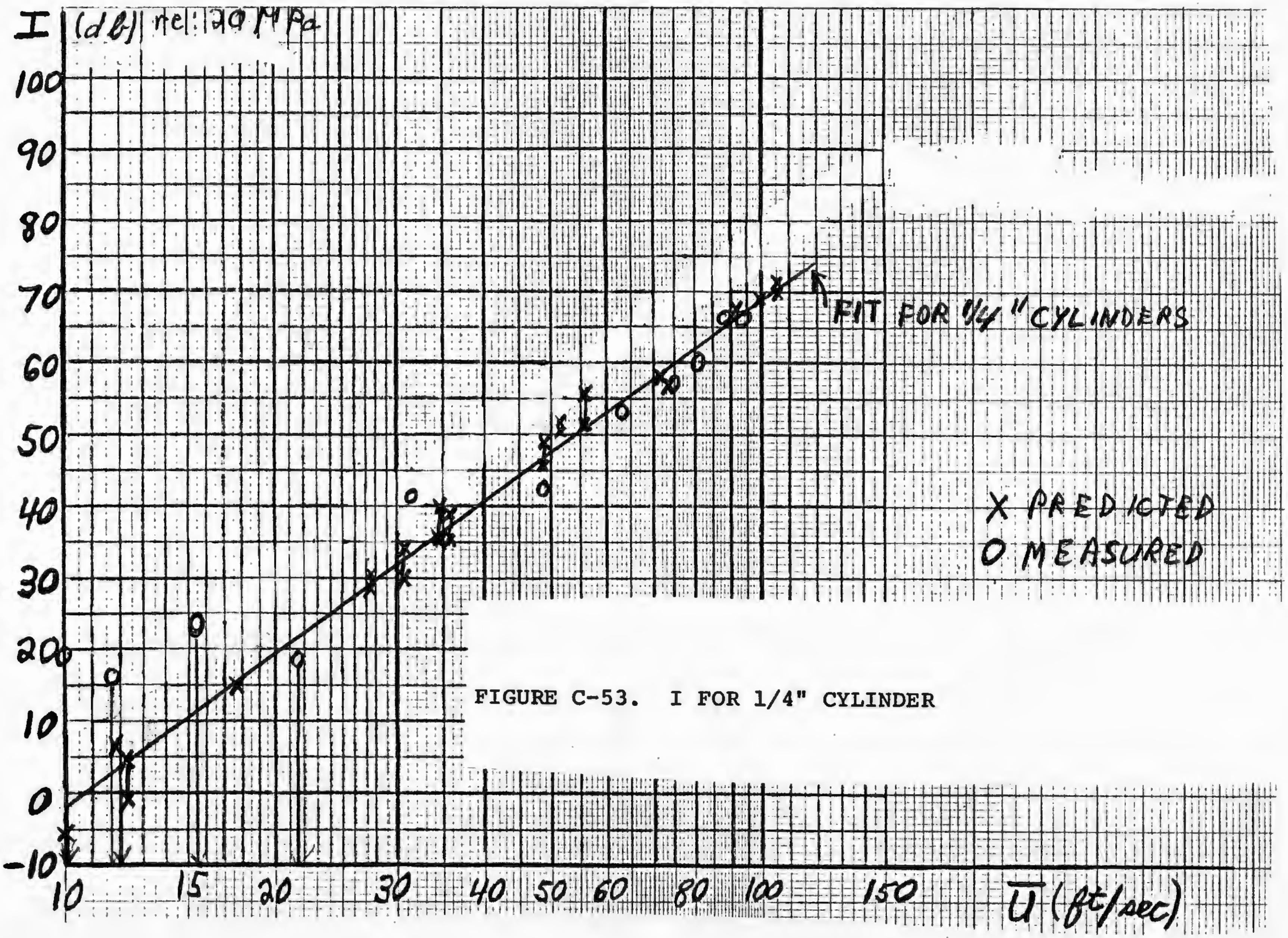

FIGURE C-53. I FOR 1/4" CYLINDER

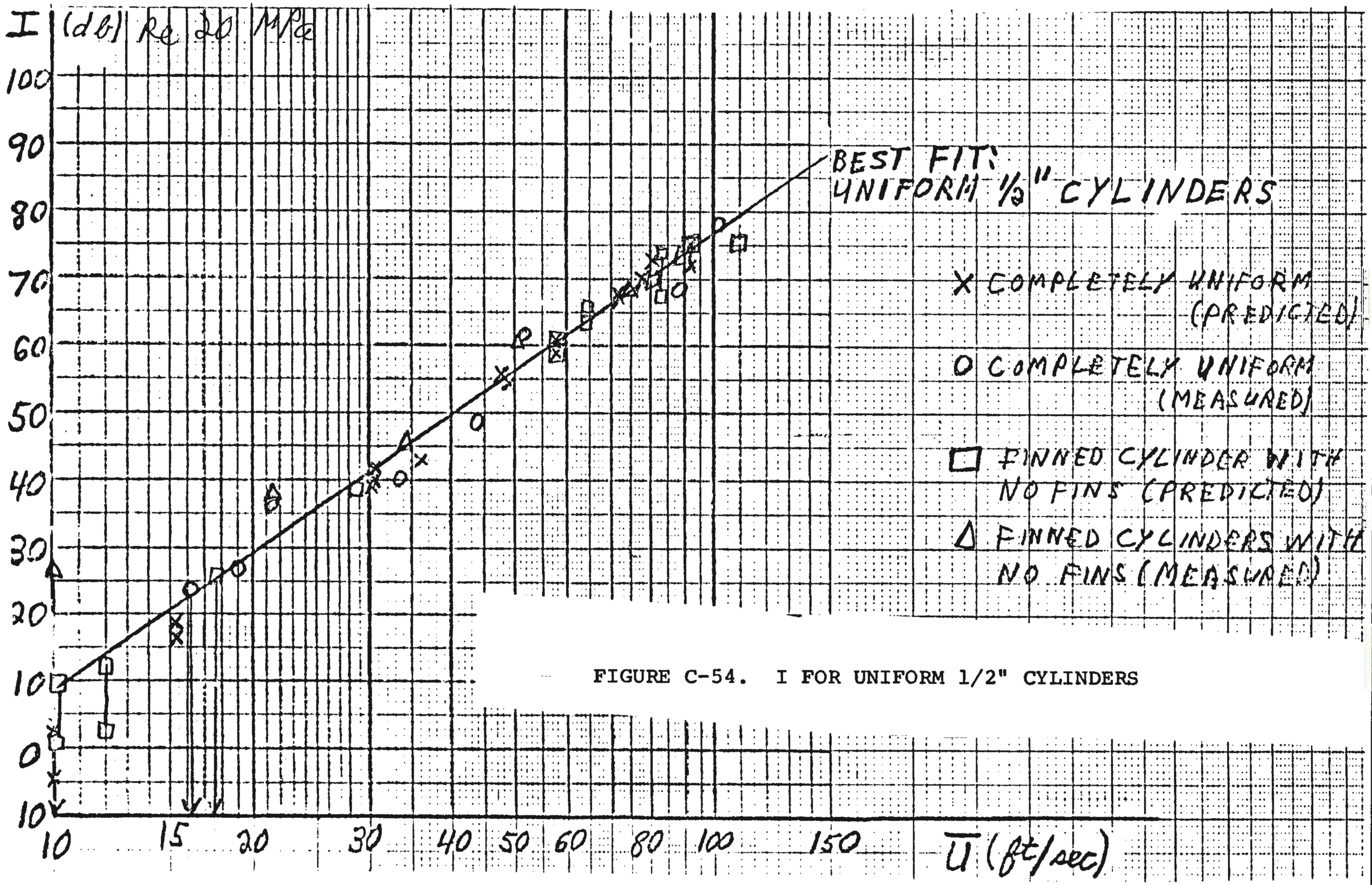

FIGURE C-54. I FOR UNIFORM 1/2" CYLINDERS

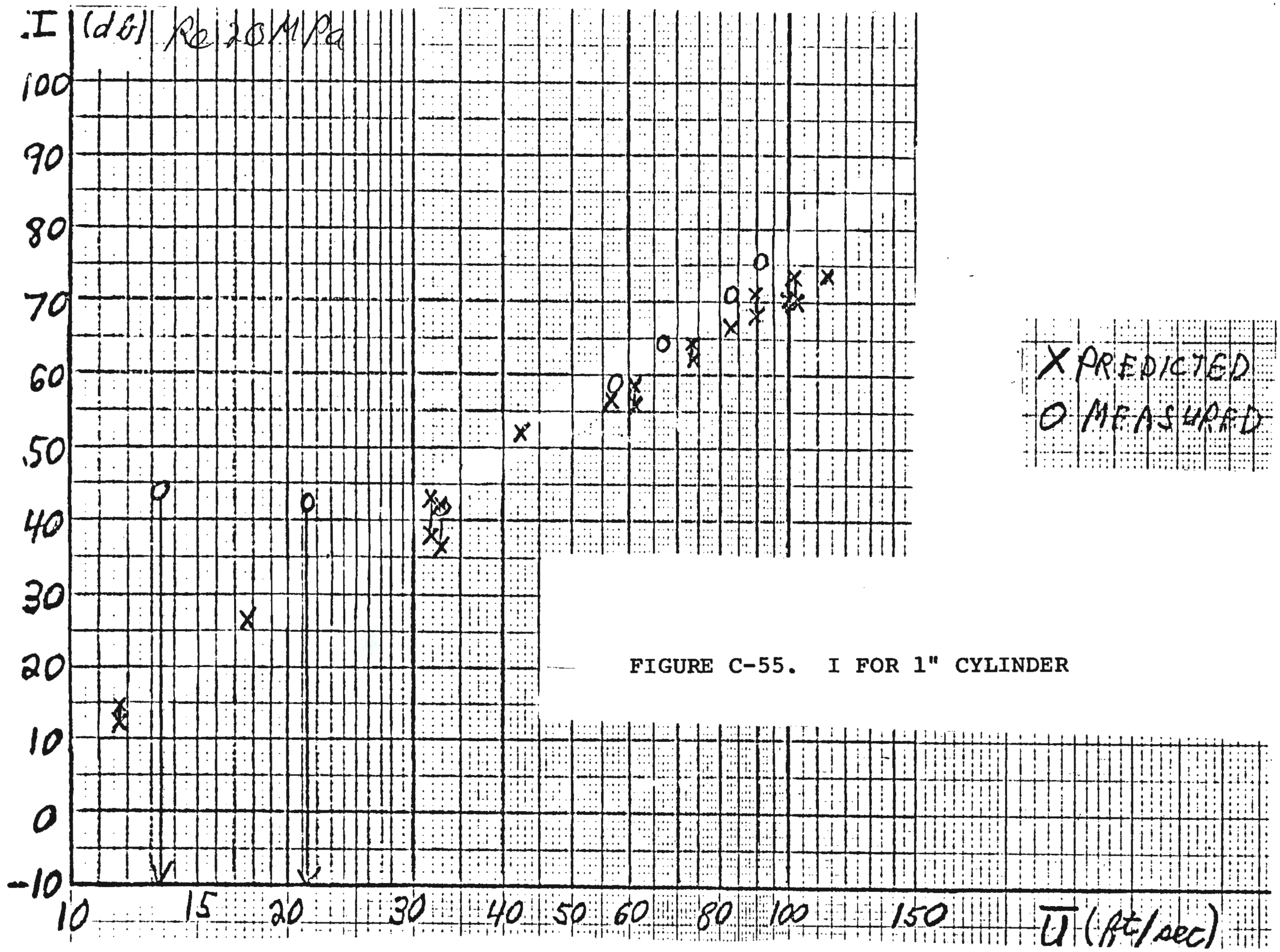

FIGURE C-55. I FOR 1" CYLINDER

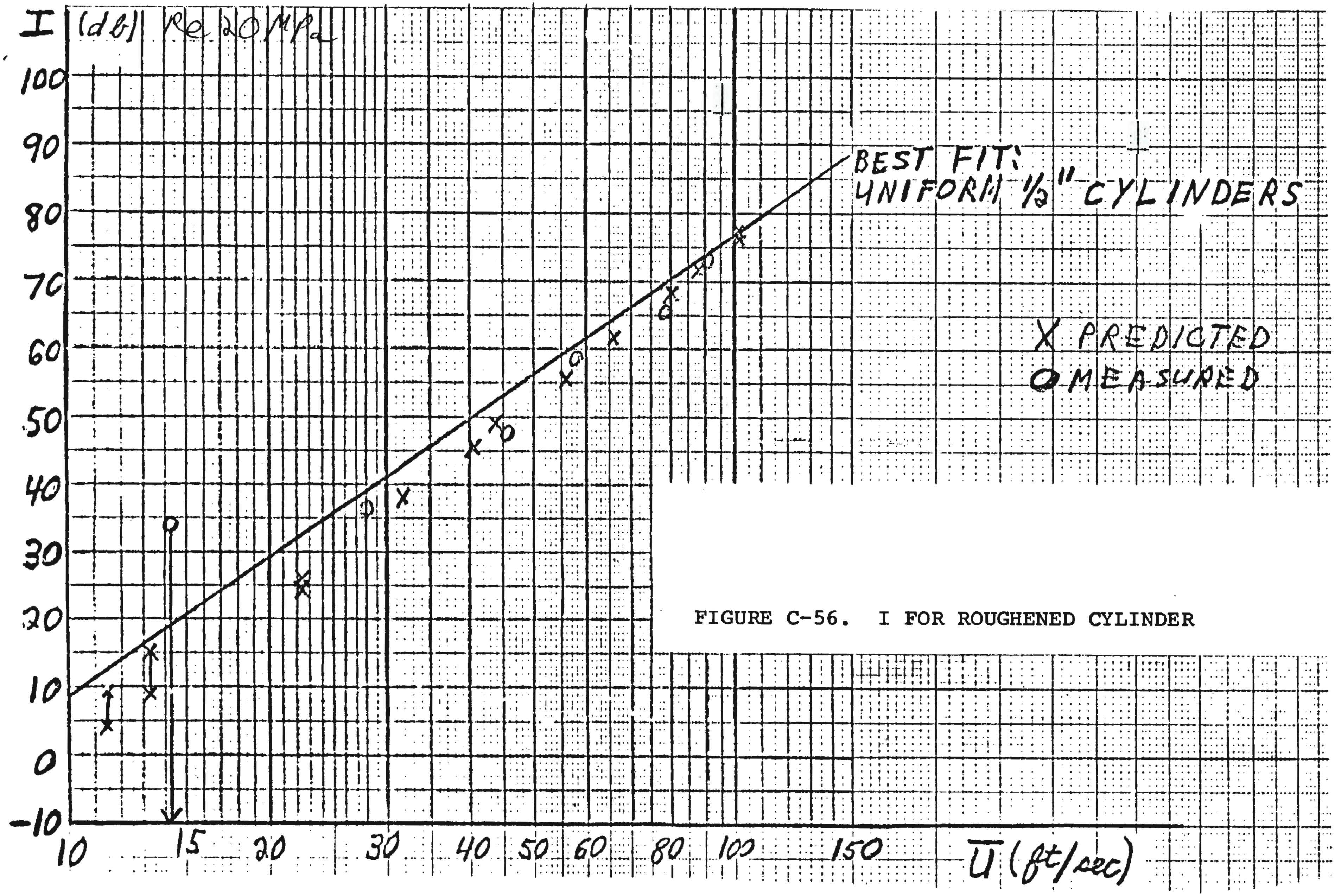

FIGURE C-56. I FOR ROUGHENED CYLINDER

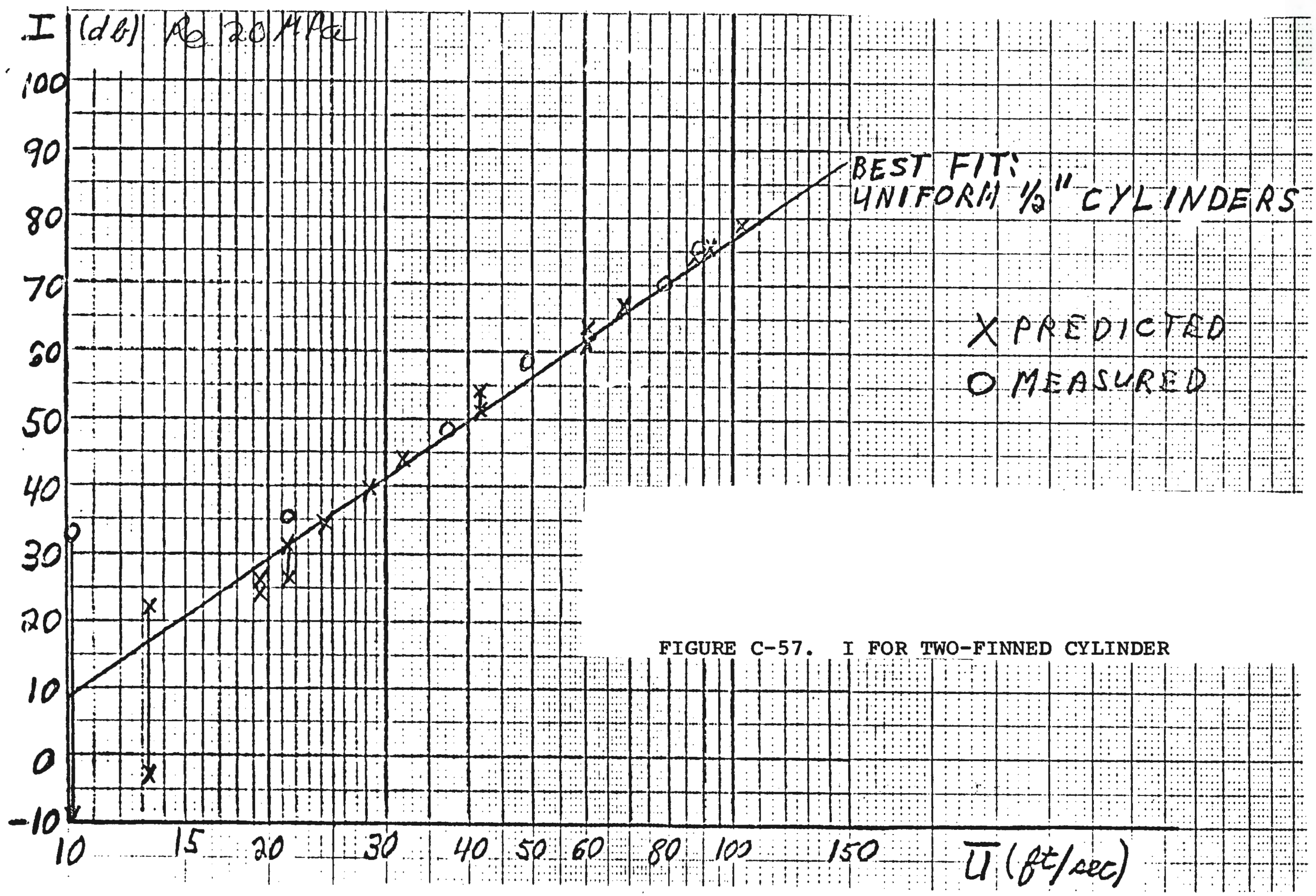

FIGURE C-57. I FOR TWO-FINNED CYLINDER

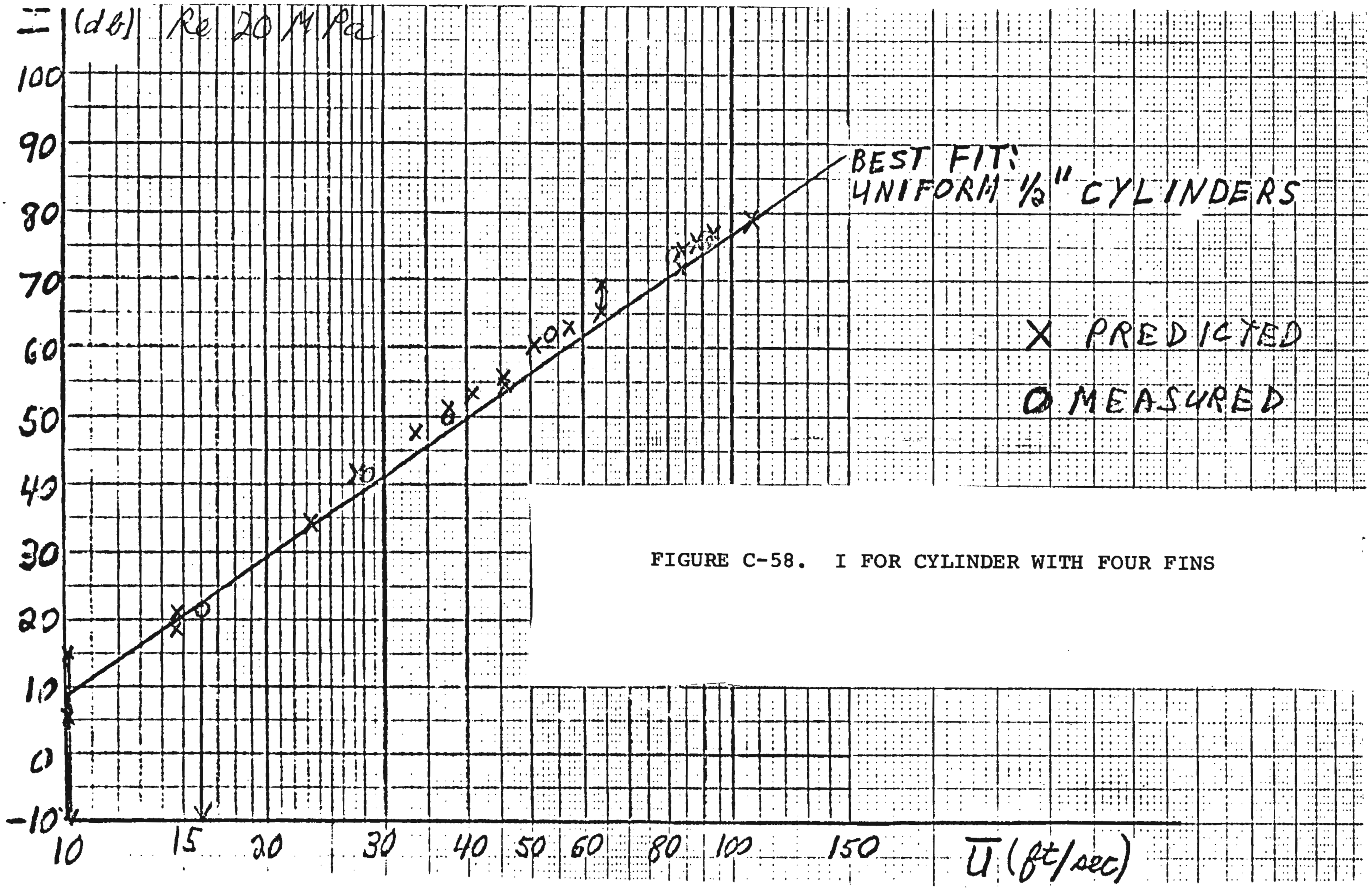

FIGURE C-58. I FOR CYLINDER WITH FOUR FINS

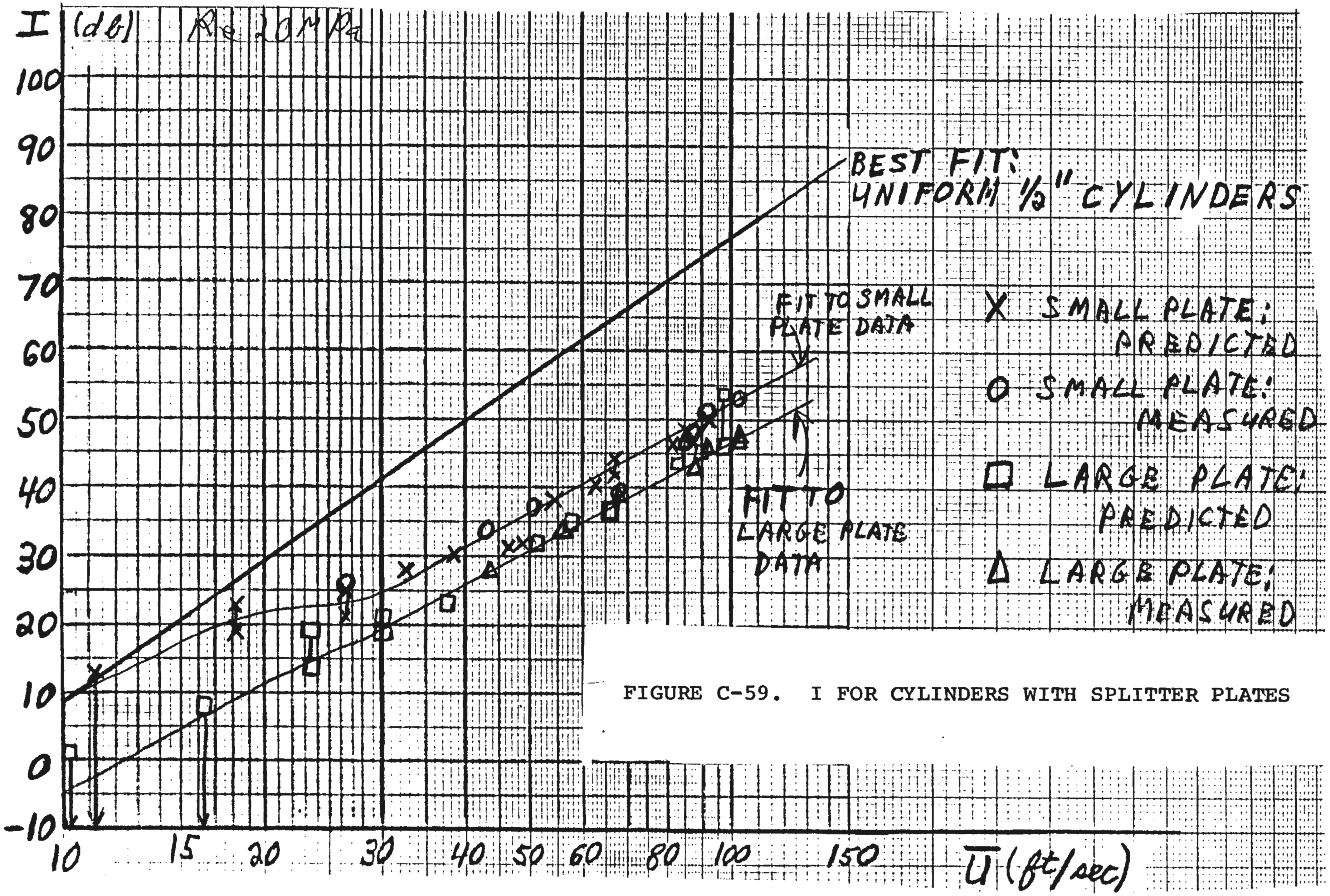

FIGURE C-59. I FOR CYLINDERS WITH SPLITTER PLATES

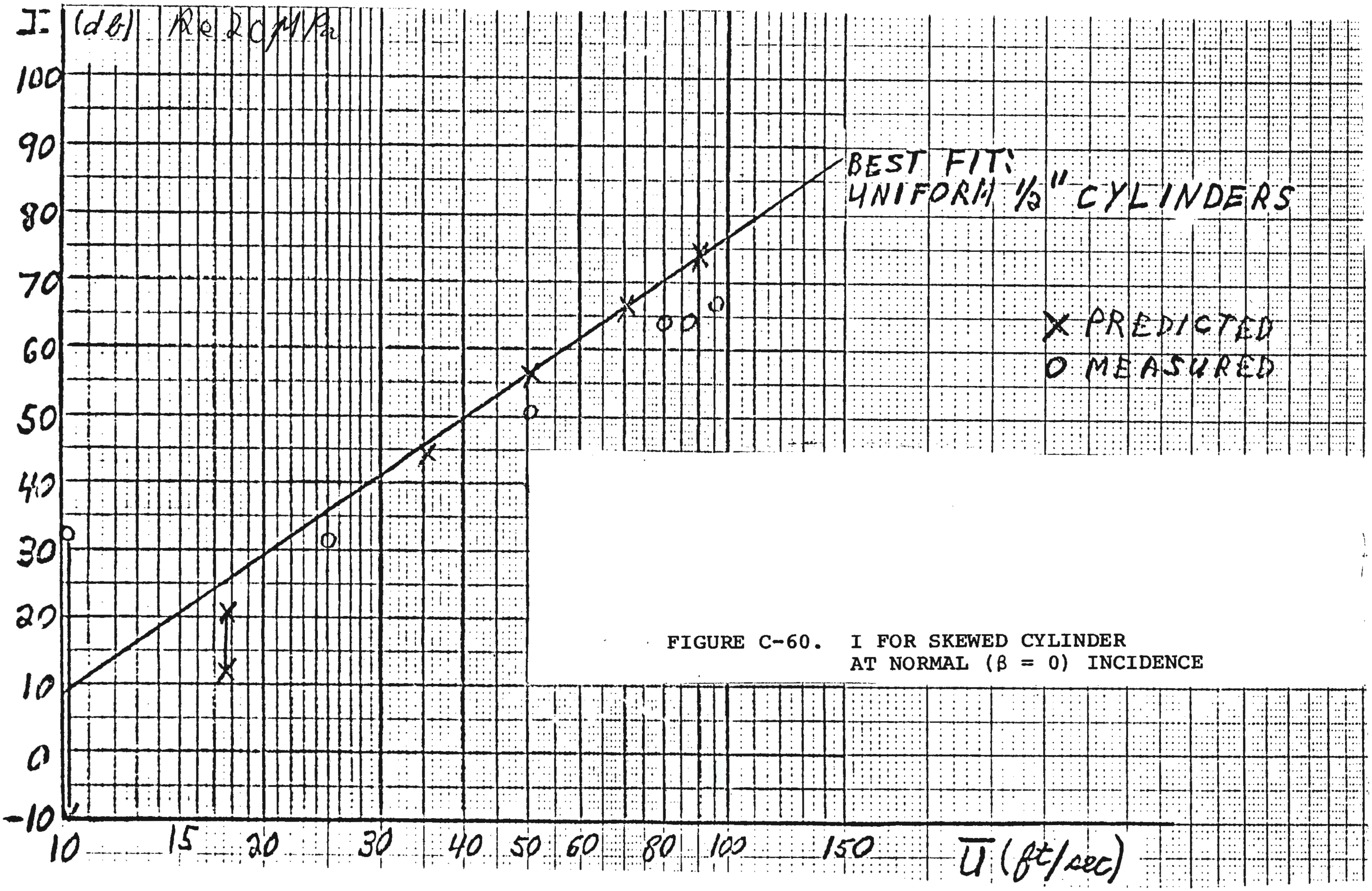

FIGURE C-60. I FOR SKEWED CYLINDER AT NORMAL (β = 0) INCIDENCE

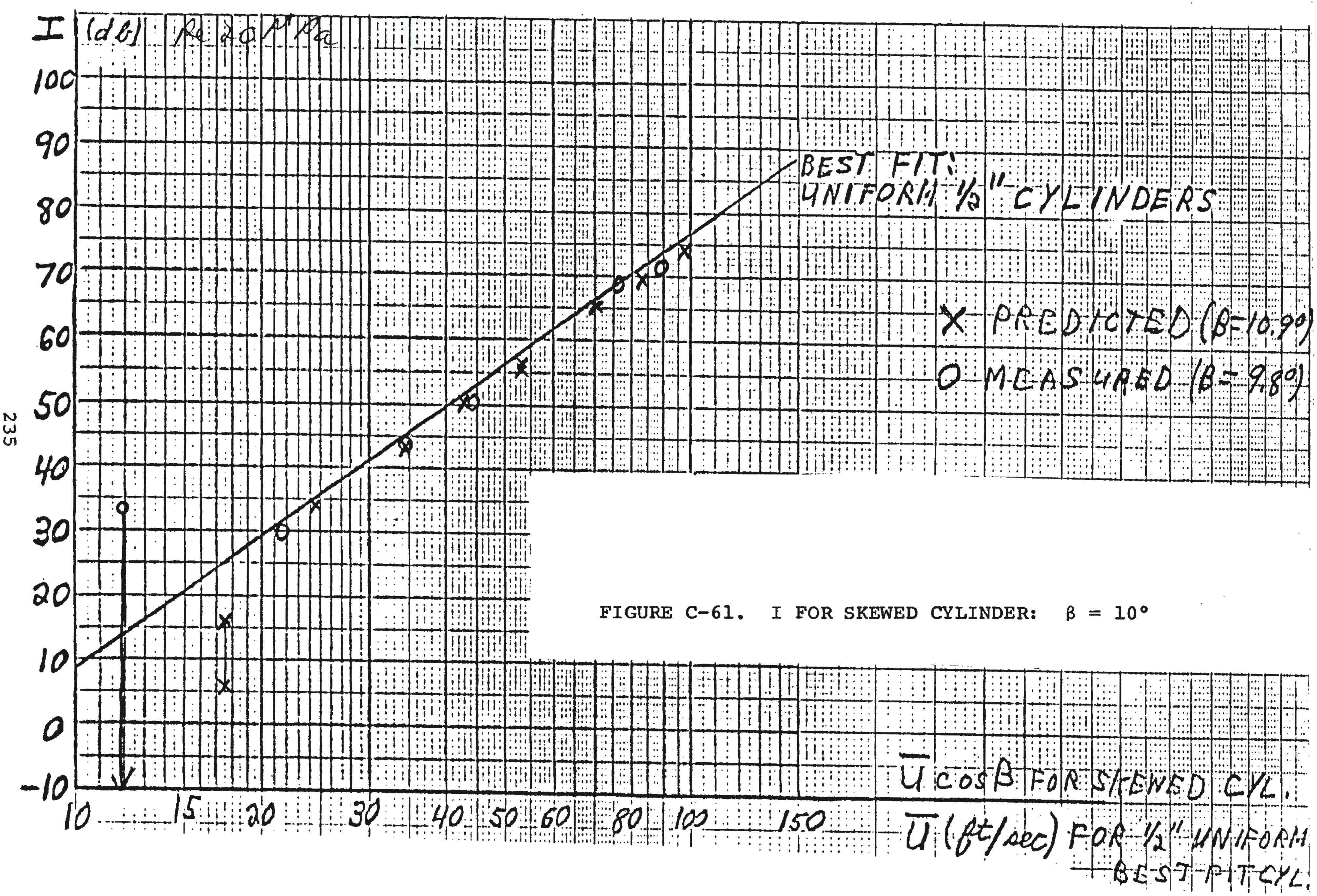

FIGURE C-61. I FOR SKEWED CYLINDER: β = 10°

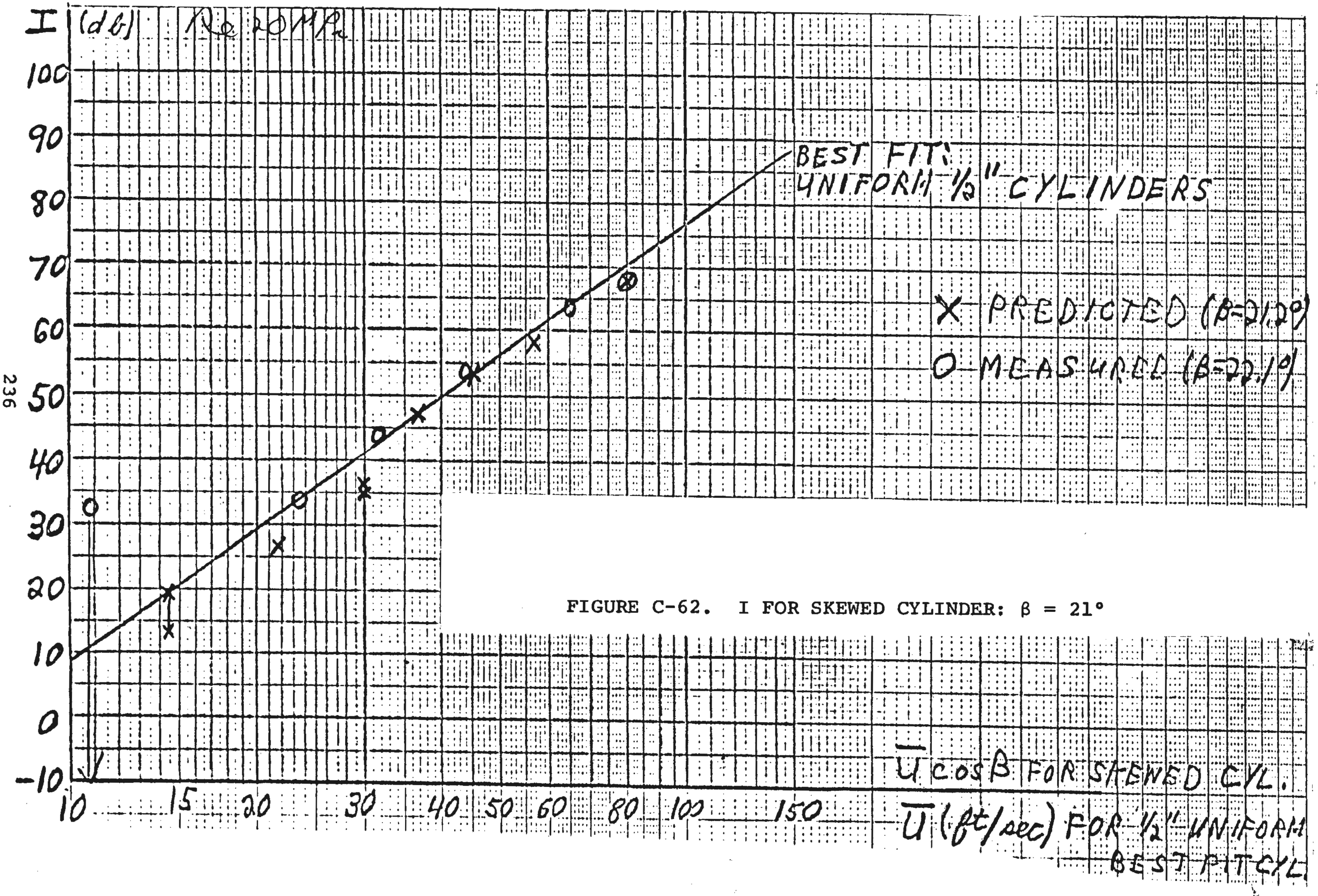

FIGURE C-62. I FOR SKEWED CYLINDER: β = 21°

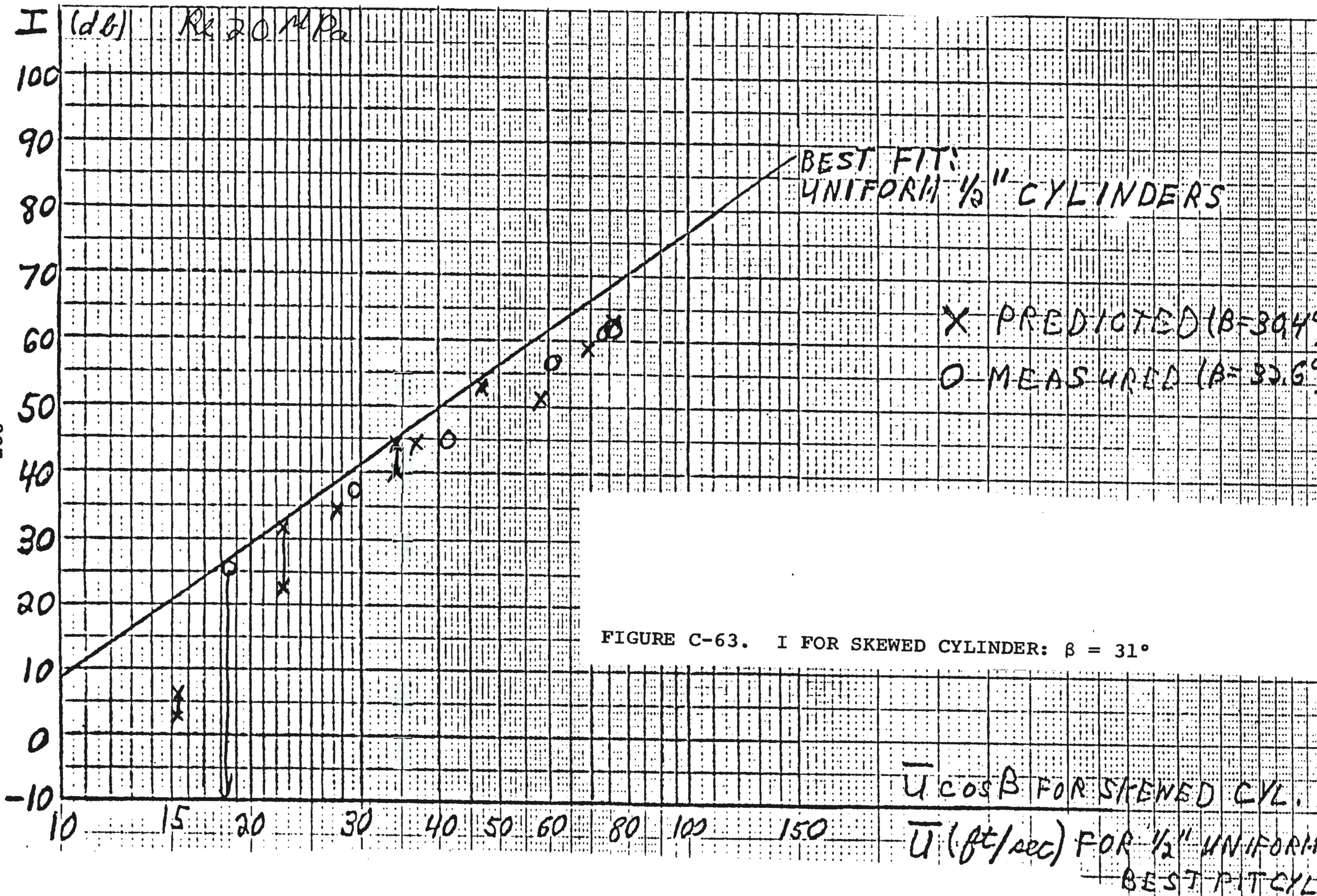

FIGURE C-63. I FOR SKEWED CYLINDER: β = 31°

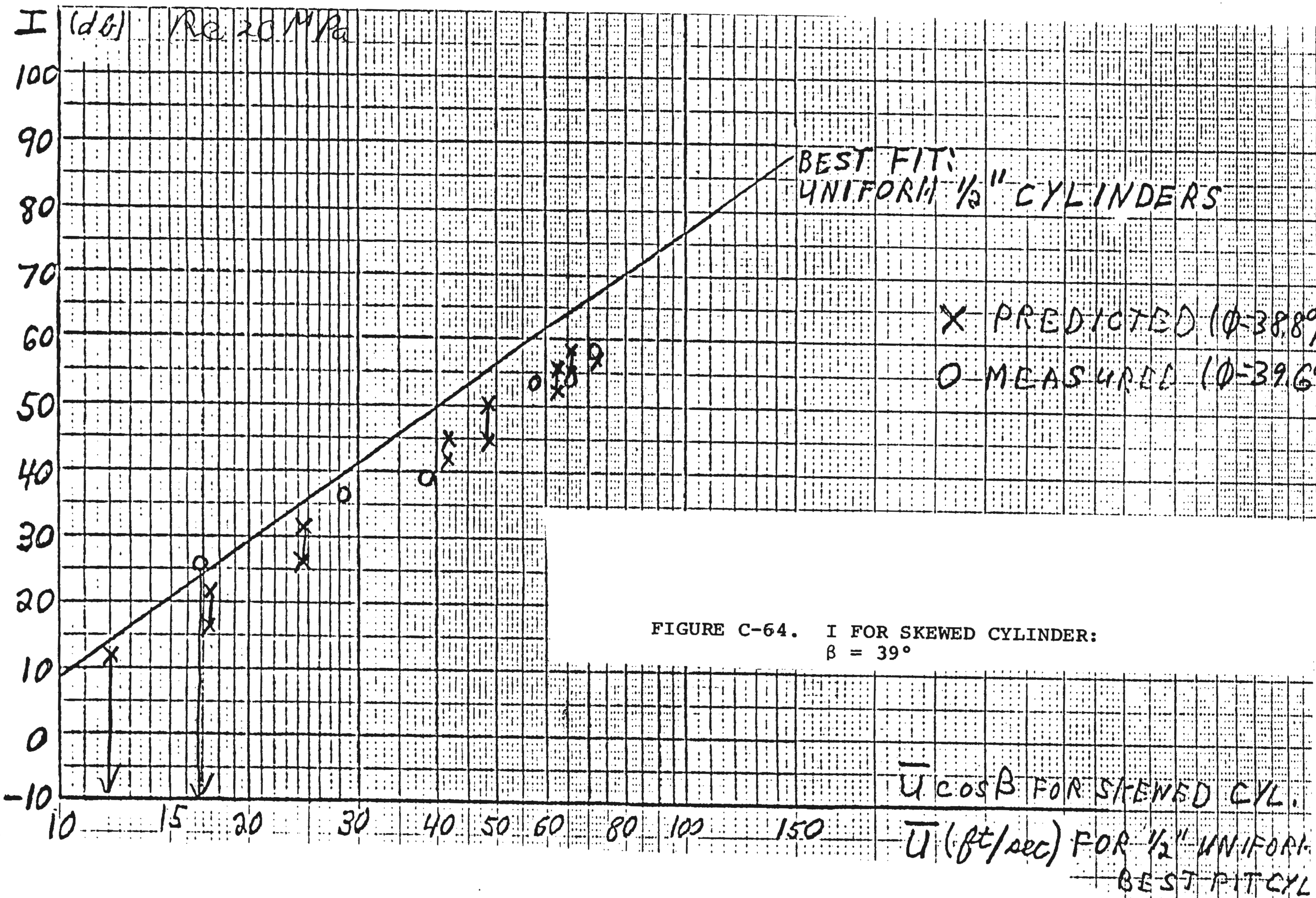

FIGURE C-64. I FOR SKEWED CYLINDER:
$\beta = 39°$

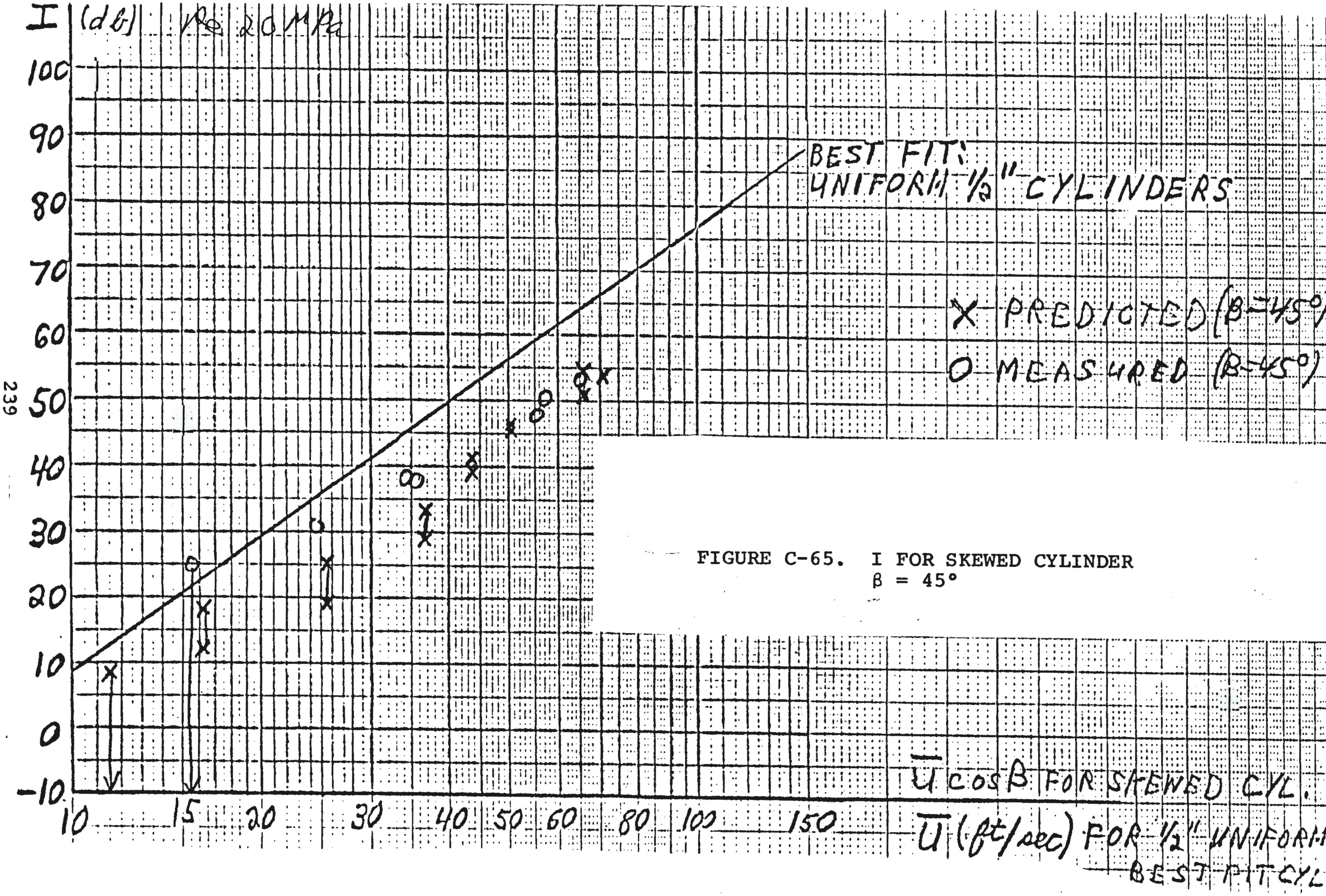

FIGURE C-65. I FOR SKEWED CYLINDER
β = 45°

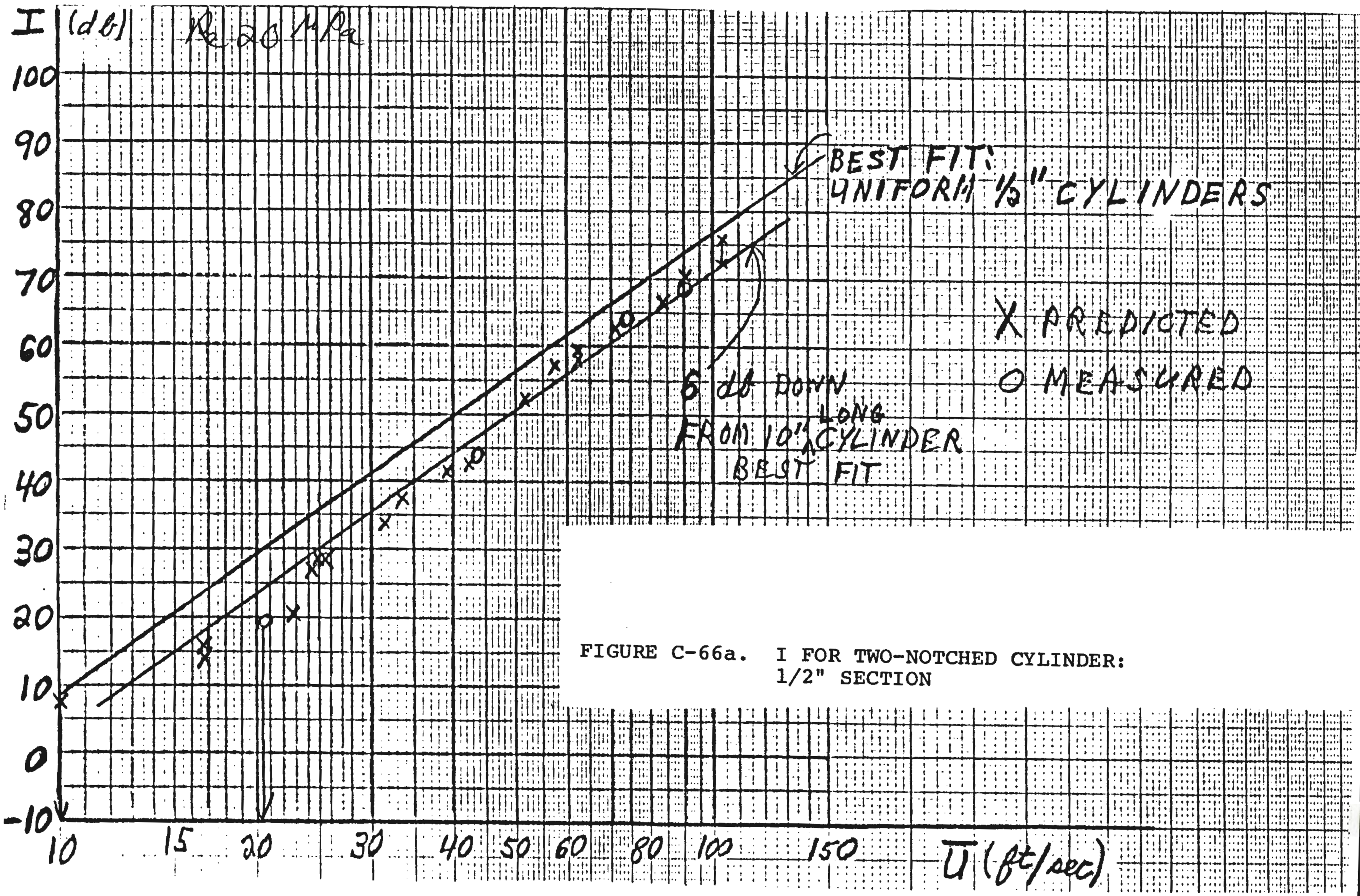

FIGURE C-66a. I FOR TWO-NOTCHED CYLINDER:
1/2" SECTION

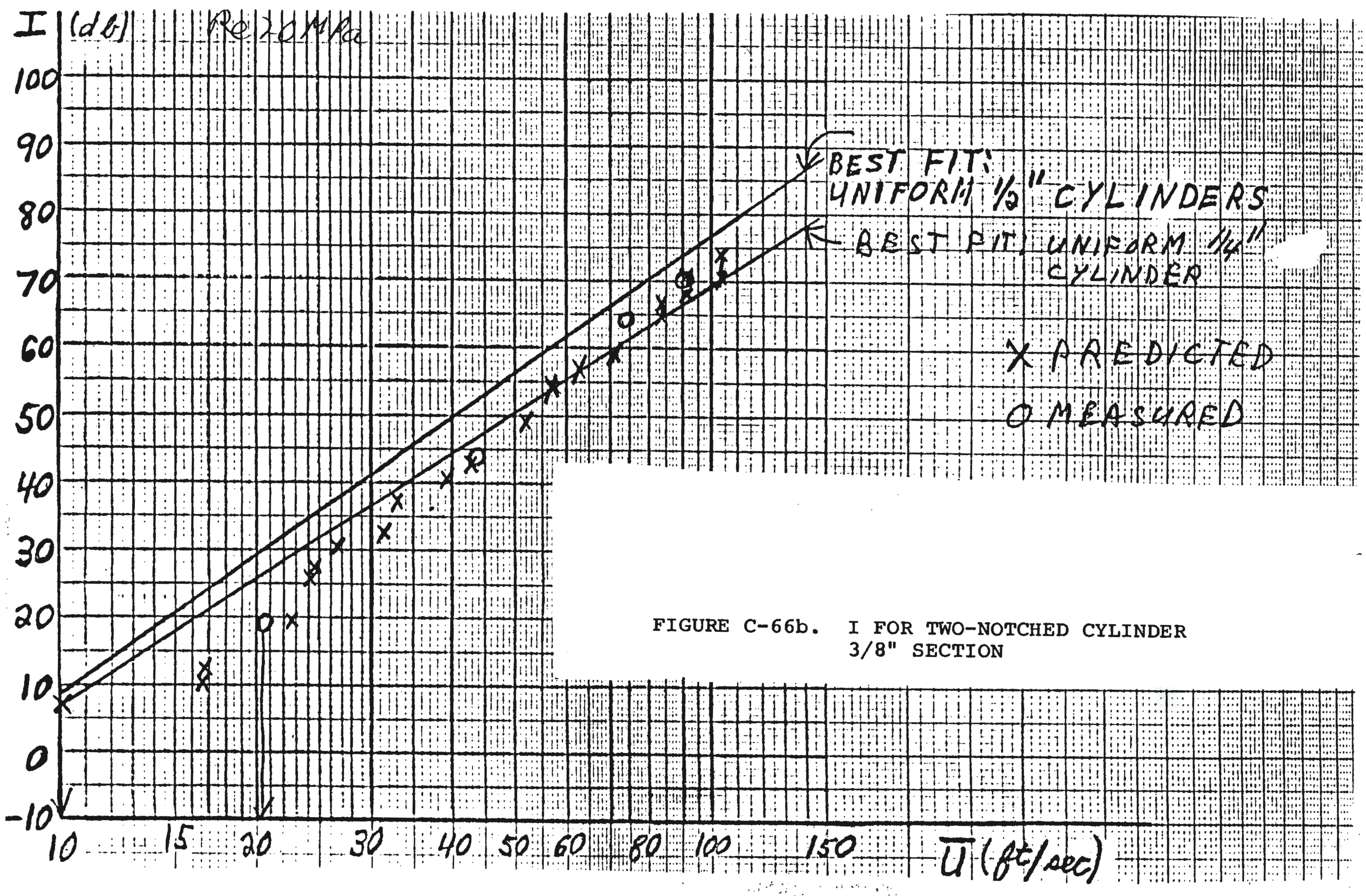

FIGURE C-66b. I FOR TWO-NOTCHED CYLINDER
3/8" SECTION

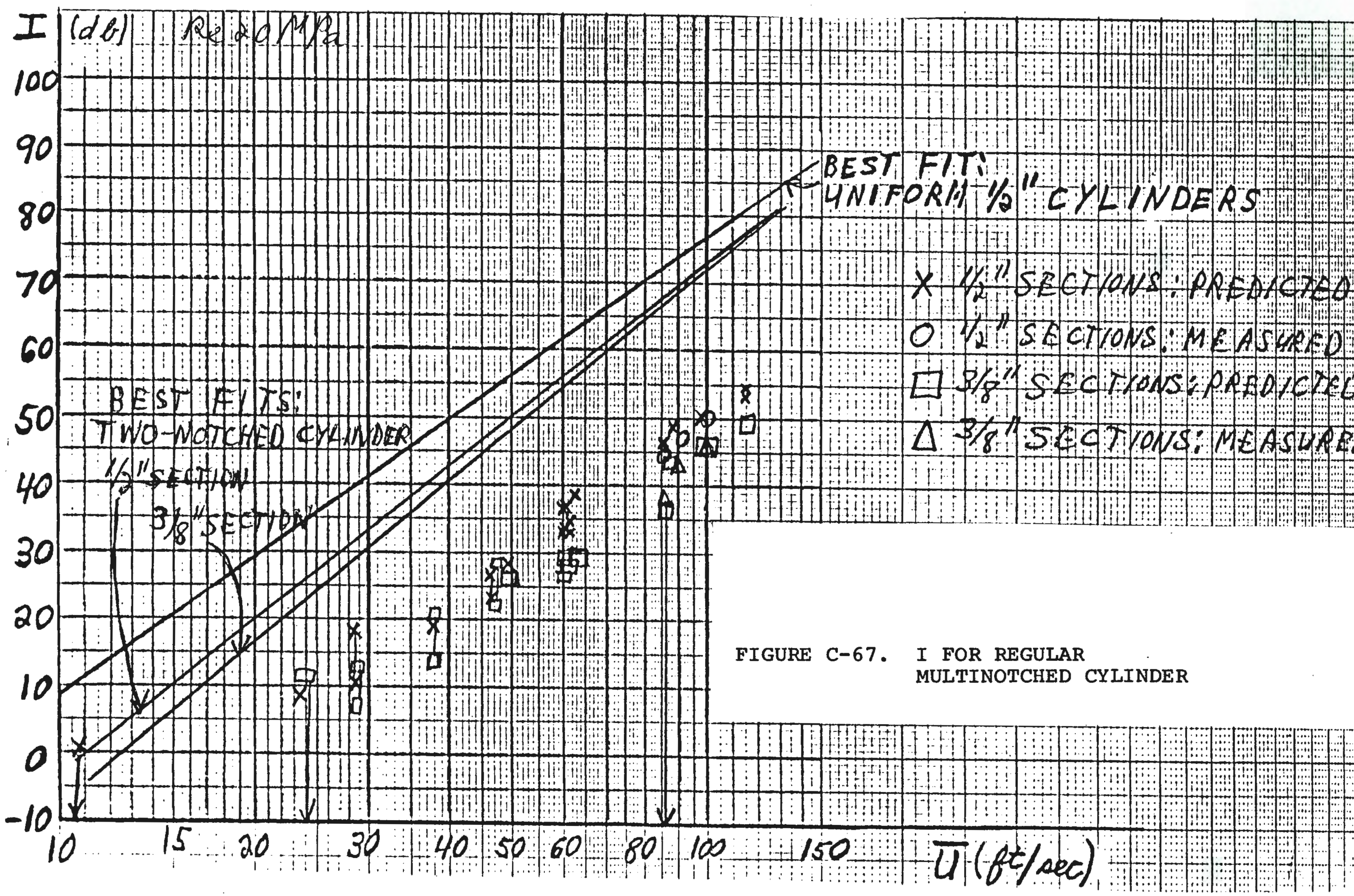

FIGURE C-67. I FOR REGULAR MULTINOTCHED CYLINDER

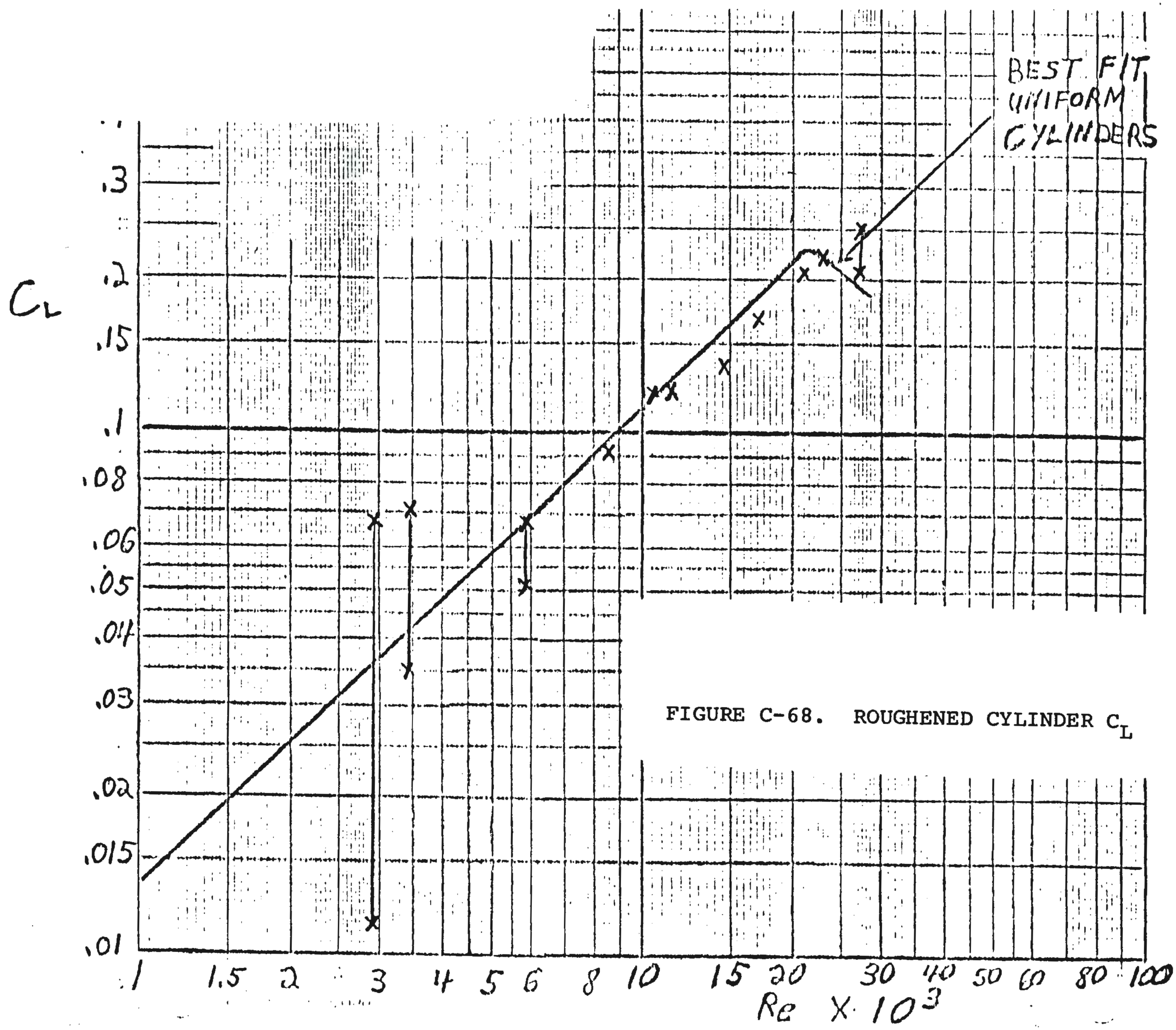

FIGURE C-68. ROUGHENED CYLINDER C_L

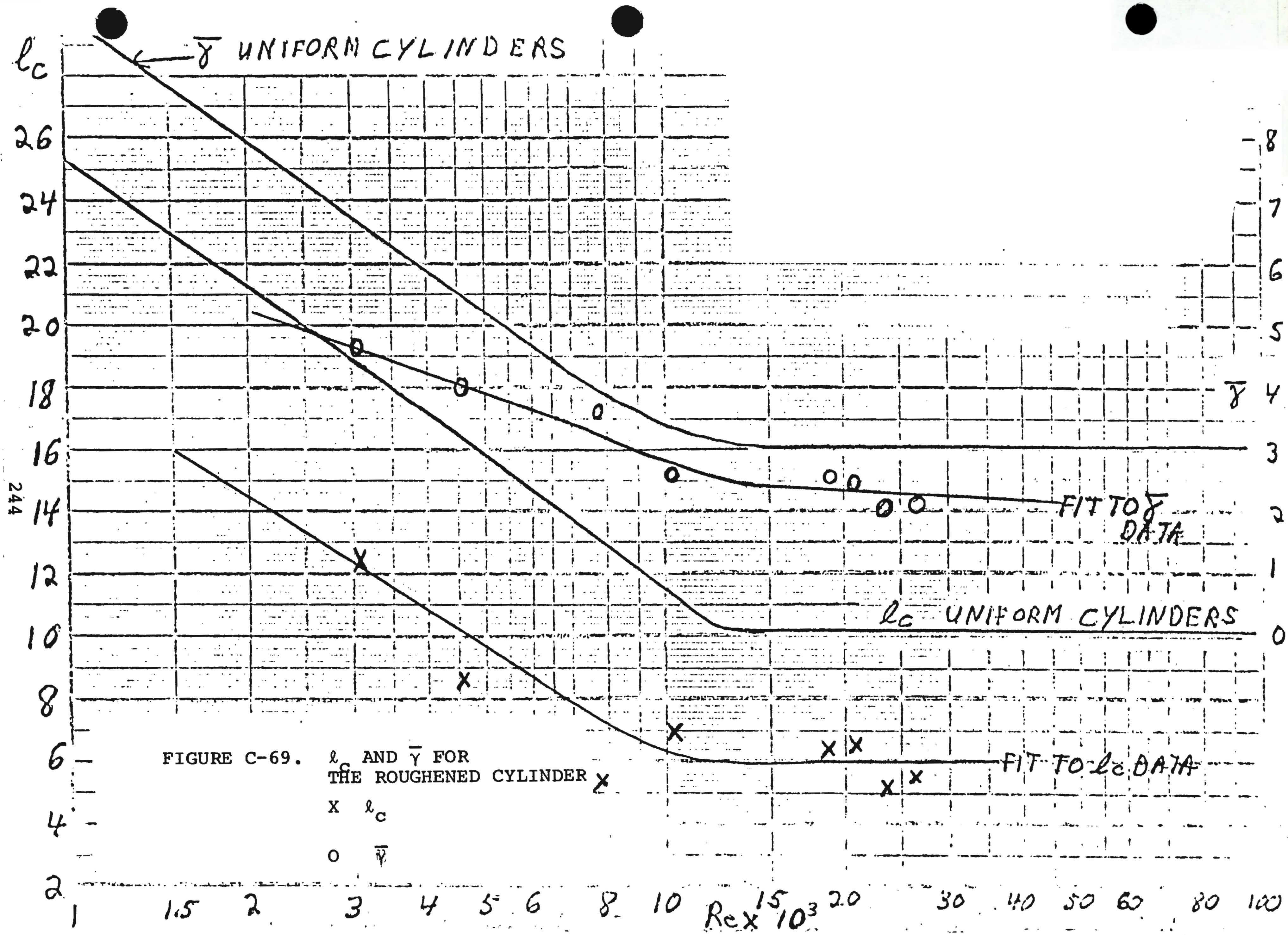

FIGURE C-69. ℓ_c AND $\bar{\gamma}$ FOR THE ROUGHENED CYLINDER

X ℓ_c

O $\bar{\gamma}$

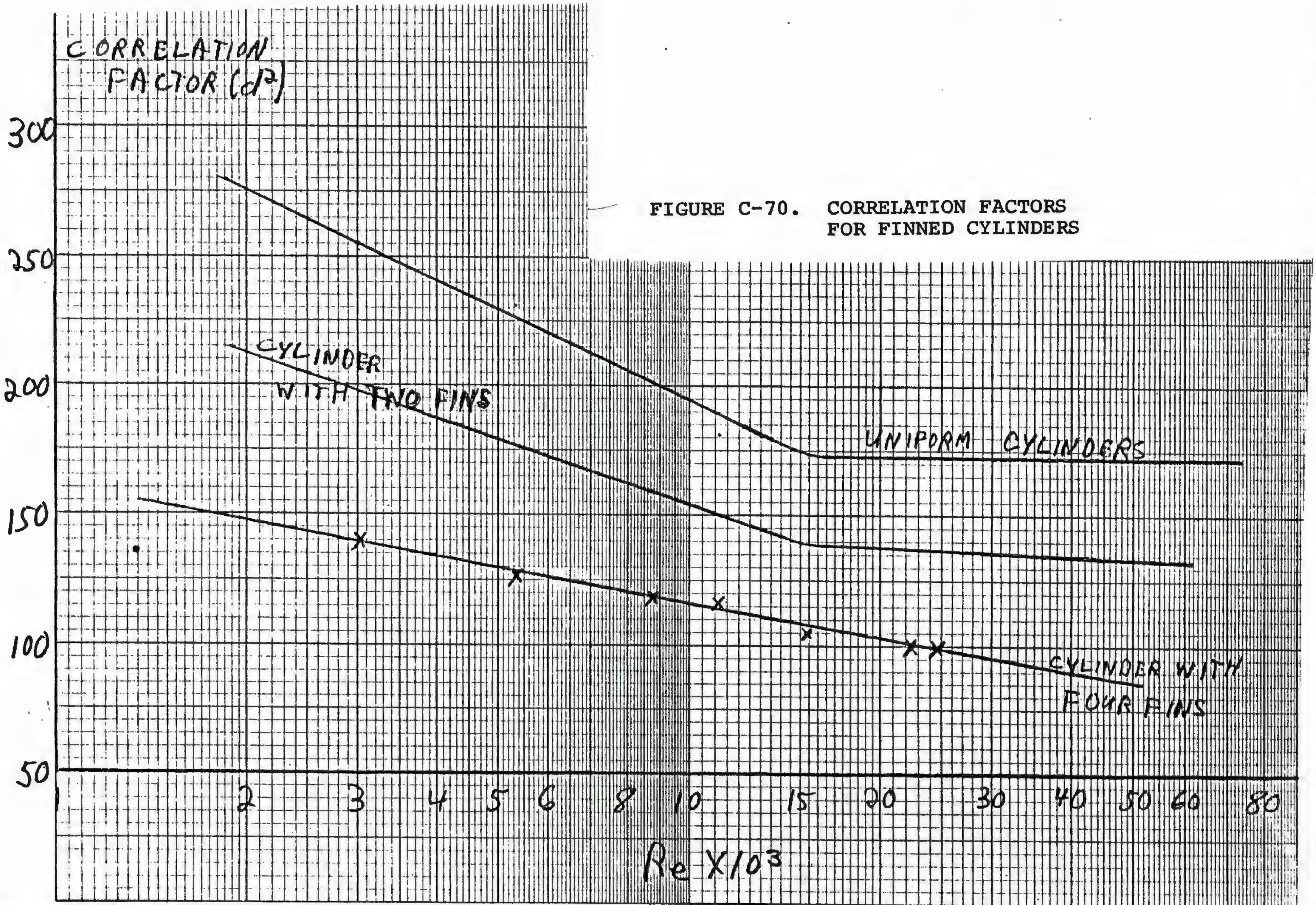

FIGURE C-70. CORRELATION FACTORS FOR FINNED CYLINDERS

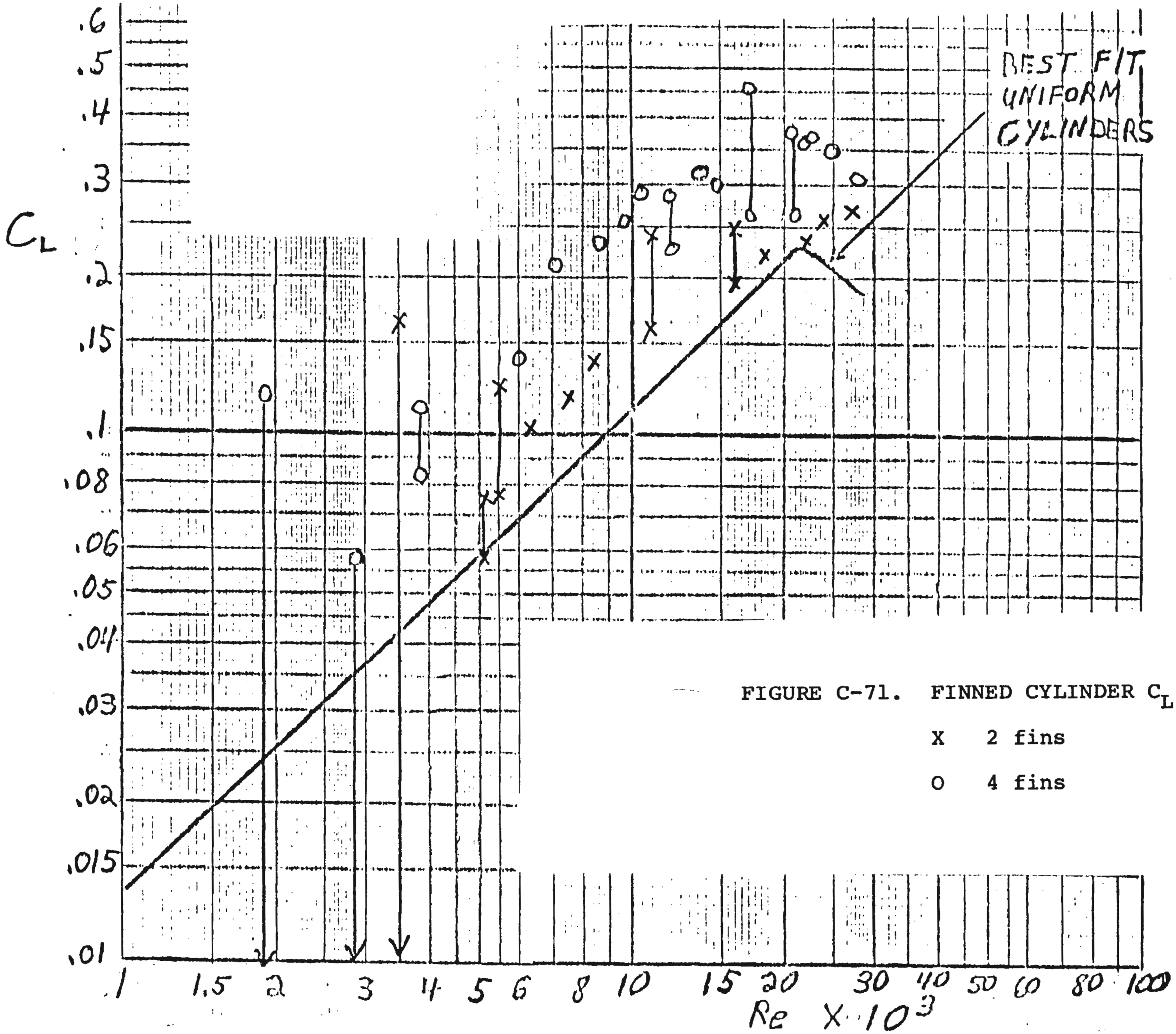

FIGURE C-71. FINNED CYLINDER C_L

X 2 fins

O 4 fins

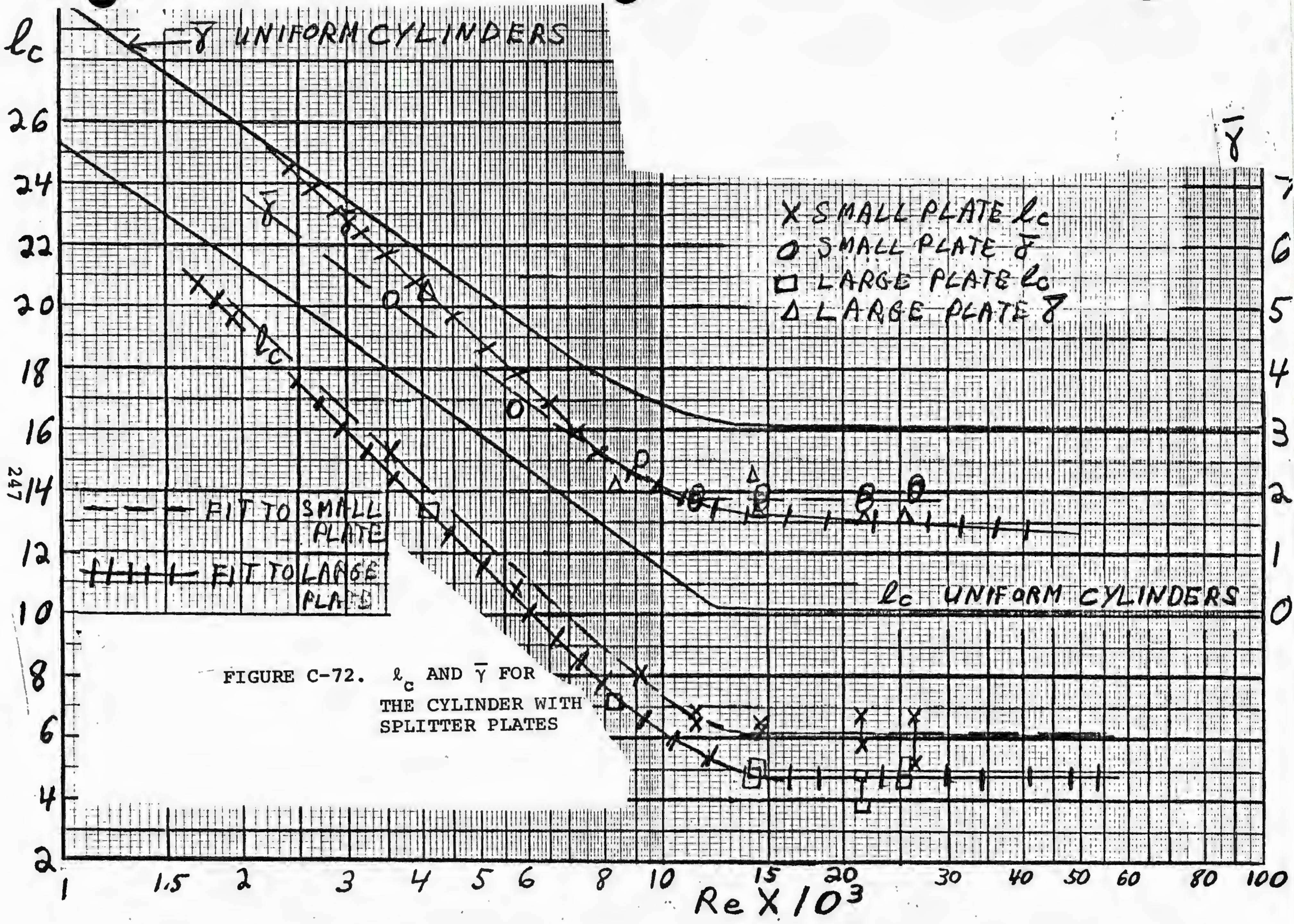

FIGURE C-72. ℓ_c AND $\bar{\gamma}$ FOR THE CYLINDER WITH SPLITTER PLATES

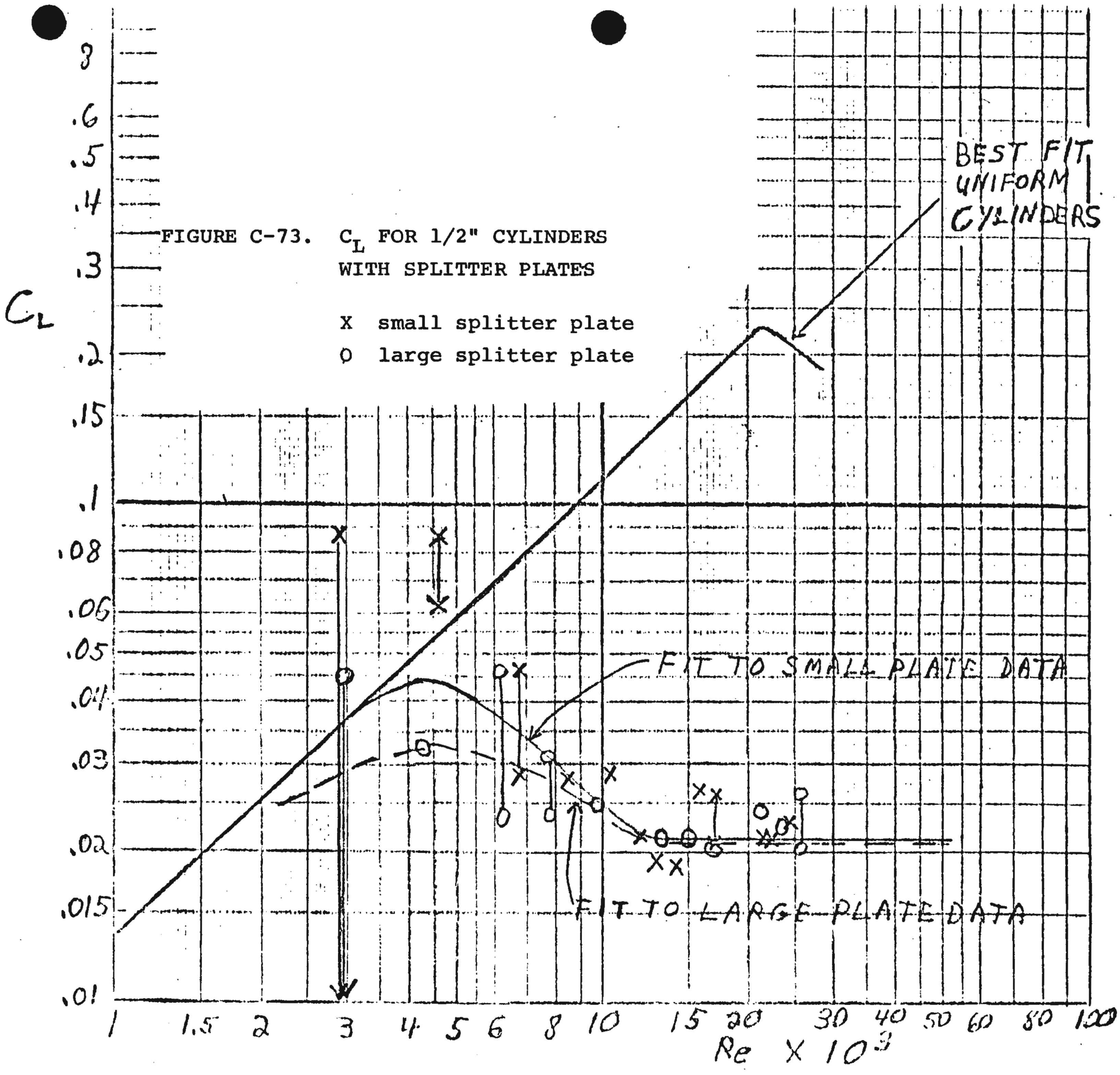

FIGURE C-73. C_L FOR 1/2" CYLINDERS WITH SPLITTER PLATES

X small splitter plate

O large splitter plate

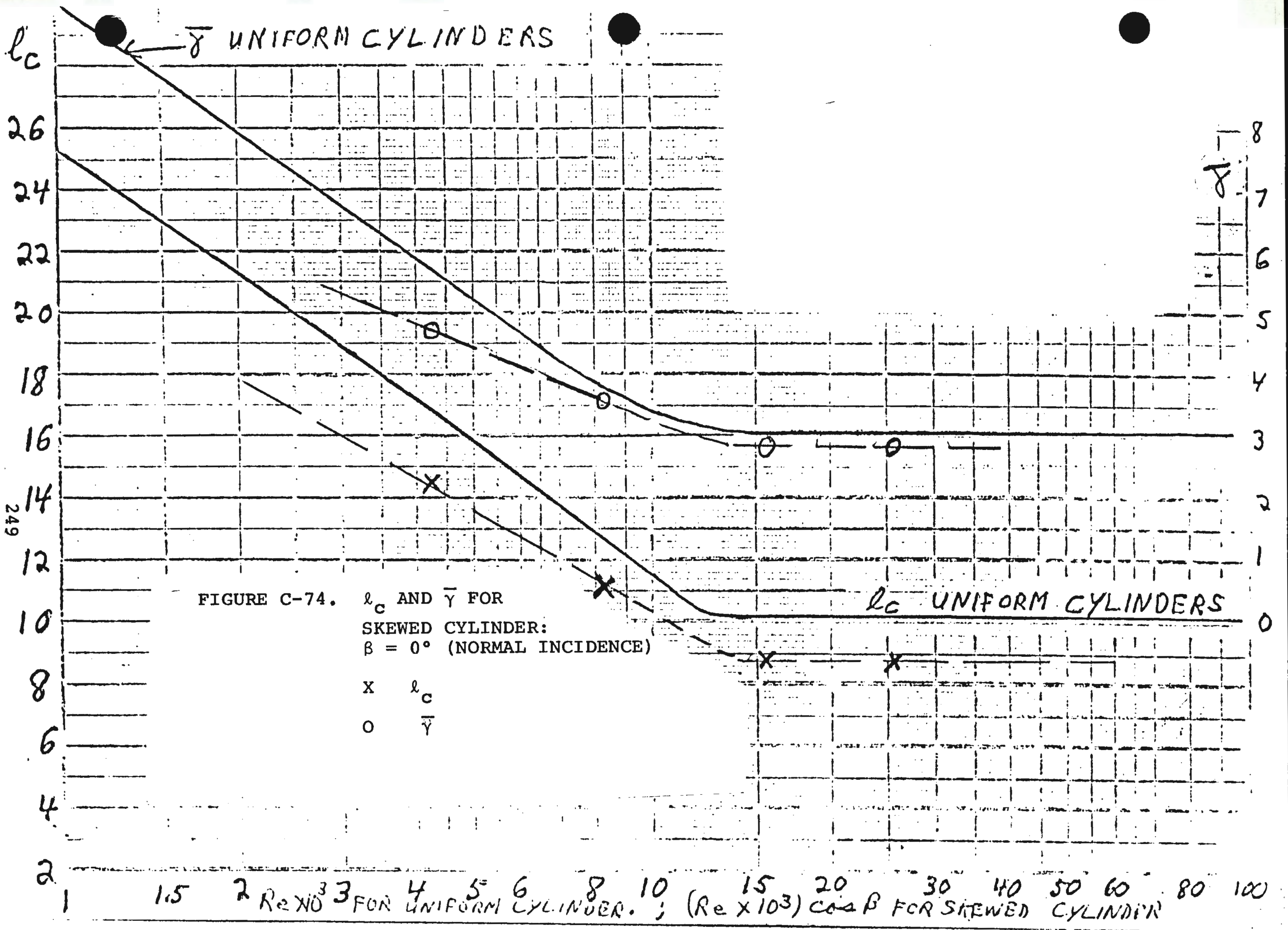

FIGURE C-74. ℓ_c AND $\bar{\gamma}$ FOR SKEWED CYLINDER: β = 0° (NORMAL INCIDENCE)

X ℓ_c

O $\bar{\gamma}$

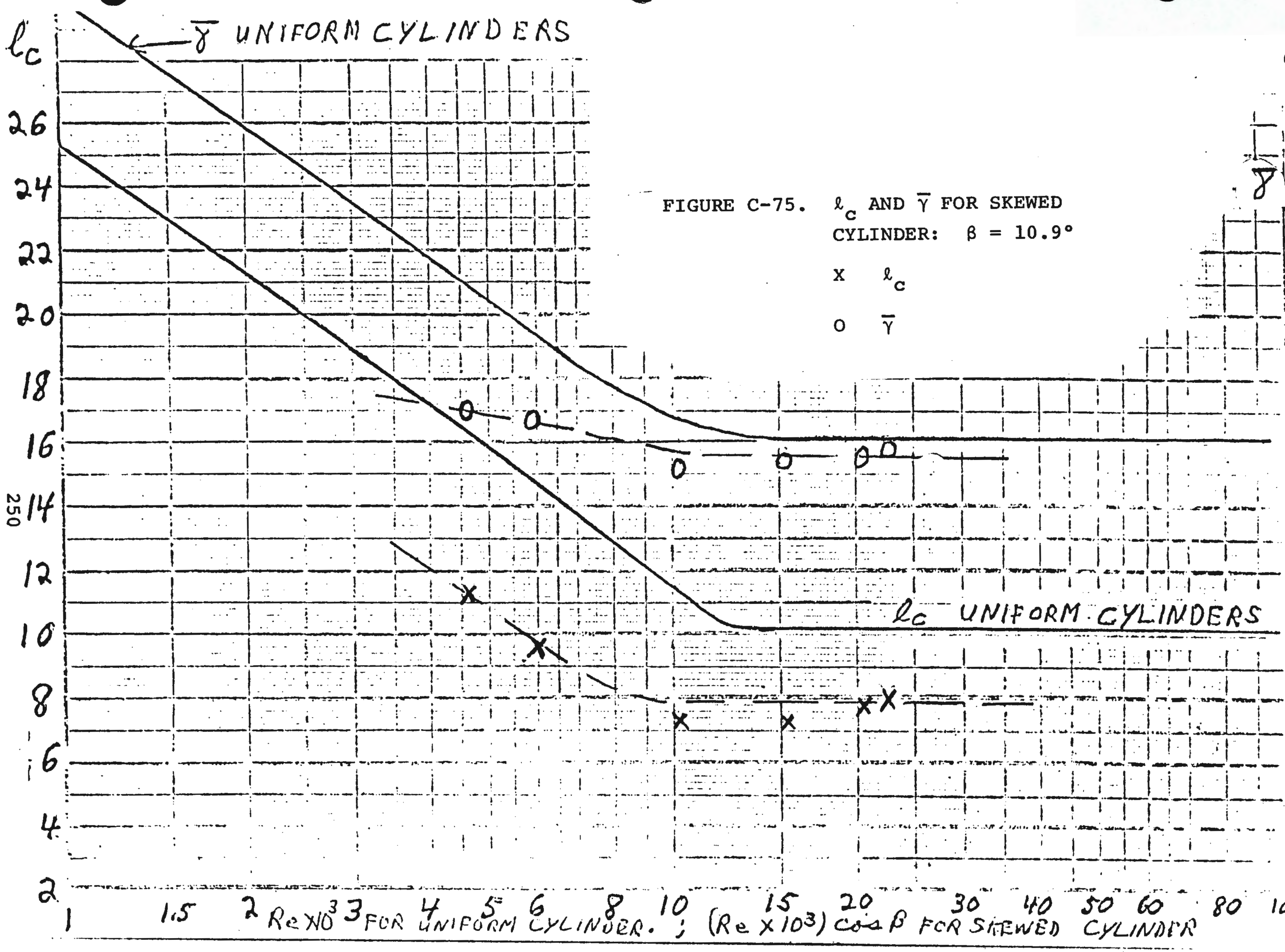

FIGURE C-75. ℓ_c AND $\bar{\gamma}$ FOR SKEWED CYLINDER: $\beta = 10.9°$

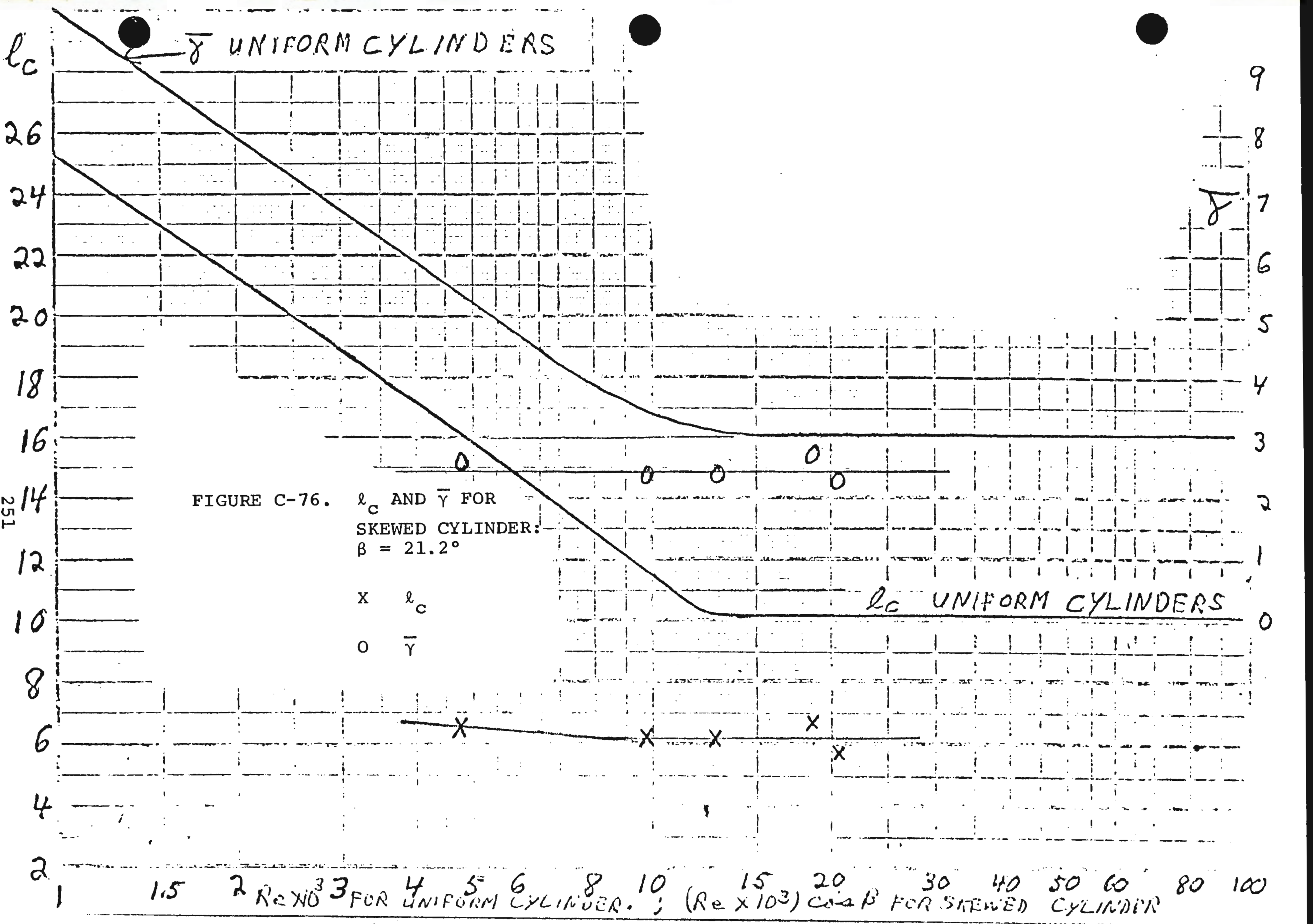

FIGURE C-76. ℓ_c AND $\bar{\gamma}$ FOR SKEWED CYLINDER: $\beta = 21.2°$

X ℓ_c

O $\bar{\gamma}$

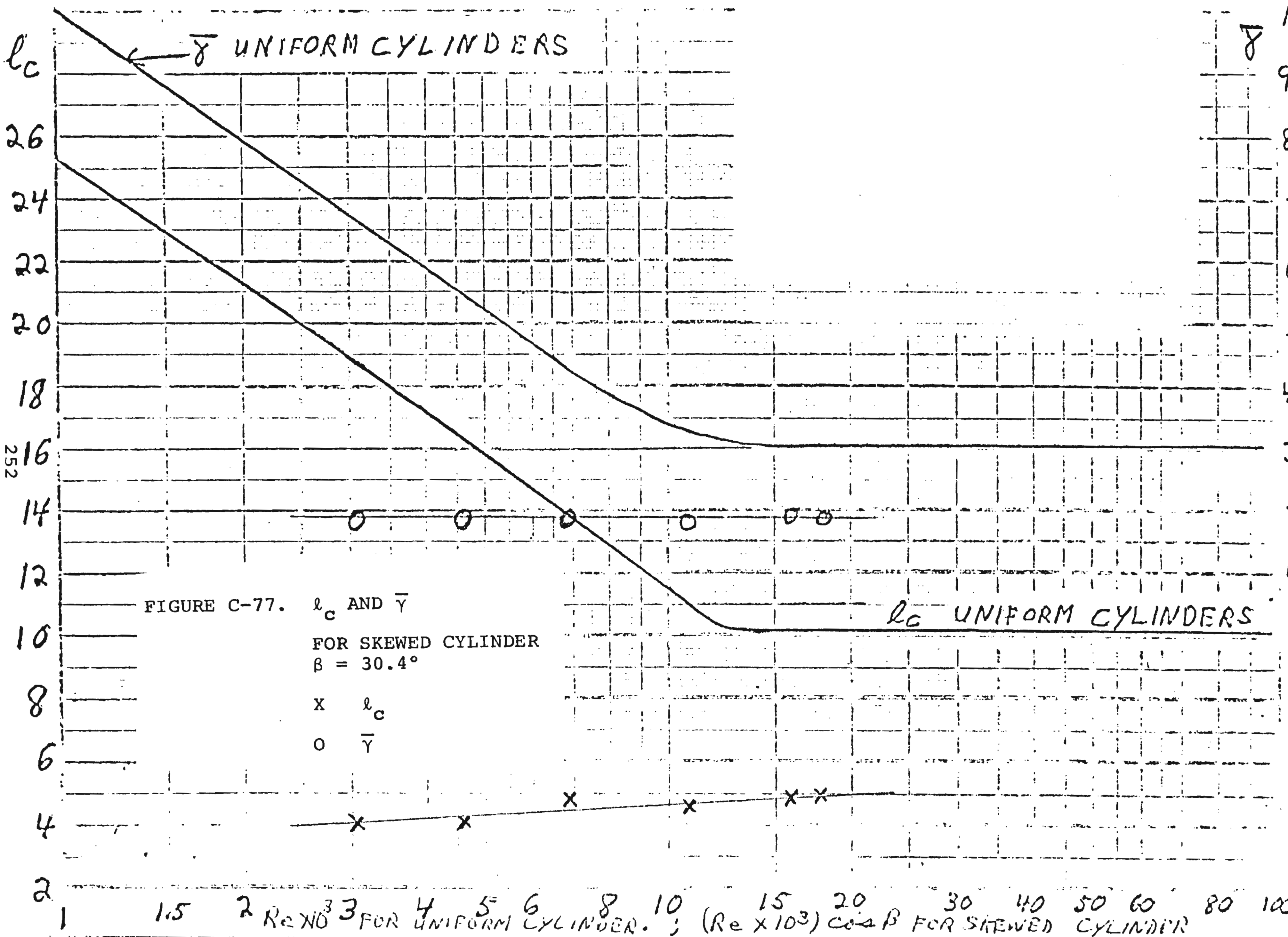

FIGURE C-77. ℓ_c AND $\bar{\gamma}$ FOR SKEWED CYLINDER $\beta = 30.4°$

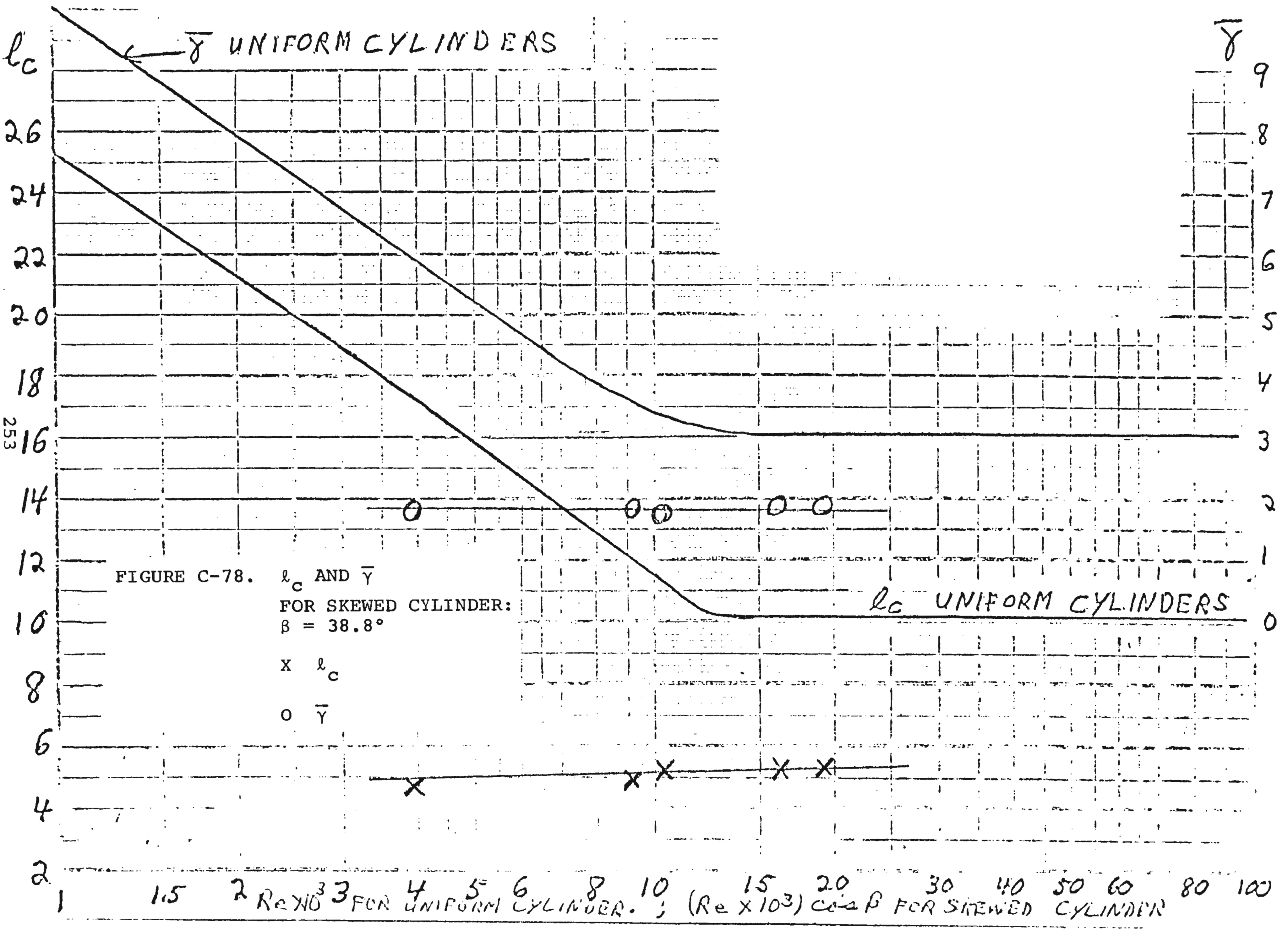

FIGURE C-78. ℓ_c AND $\bar{\gamma}$ FOR SKEWED CYLINDER: $\beta = 38.8°$

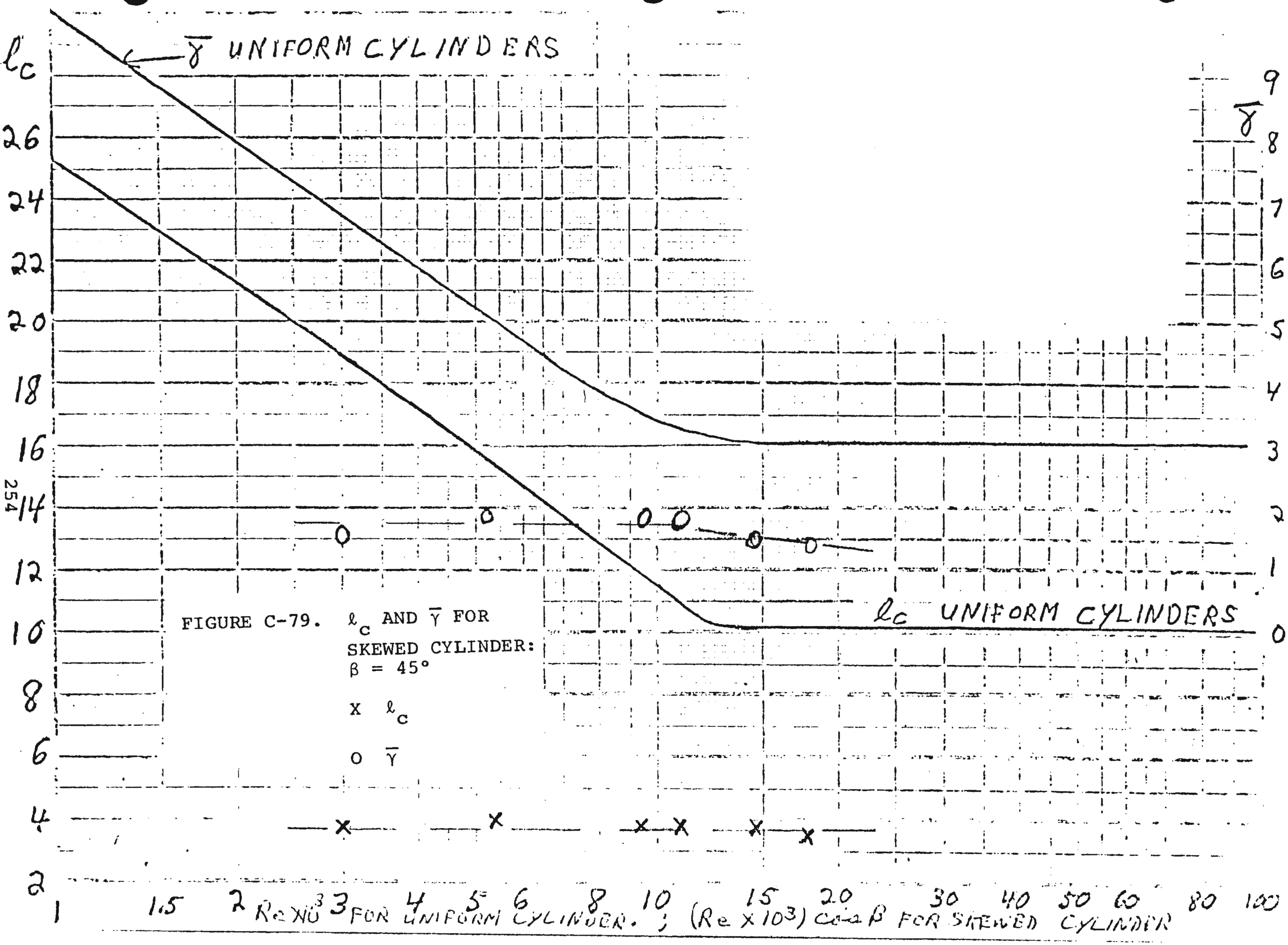

FIGURE C-79. ℓ_c AND $\bar{\gamma}$ FOR SKEWED CYLINDER: $\beta = 45°$

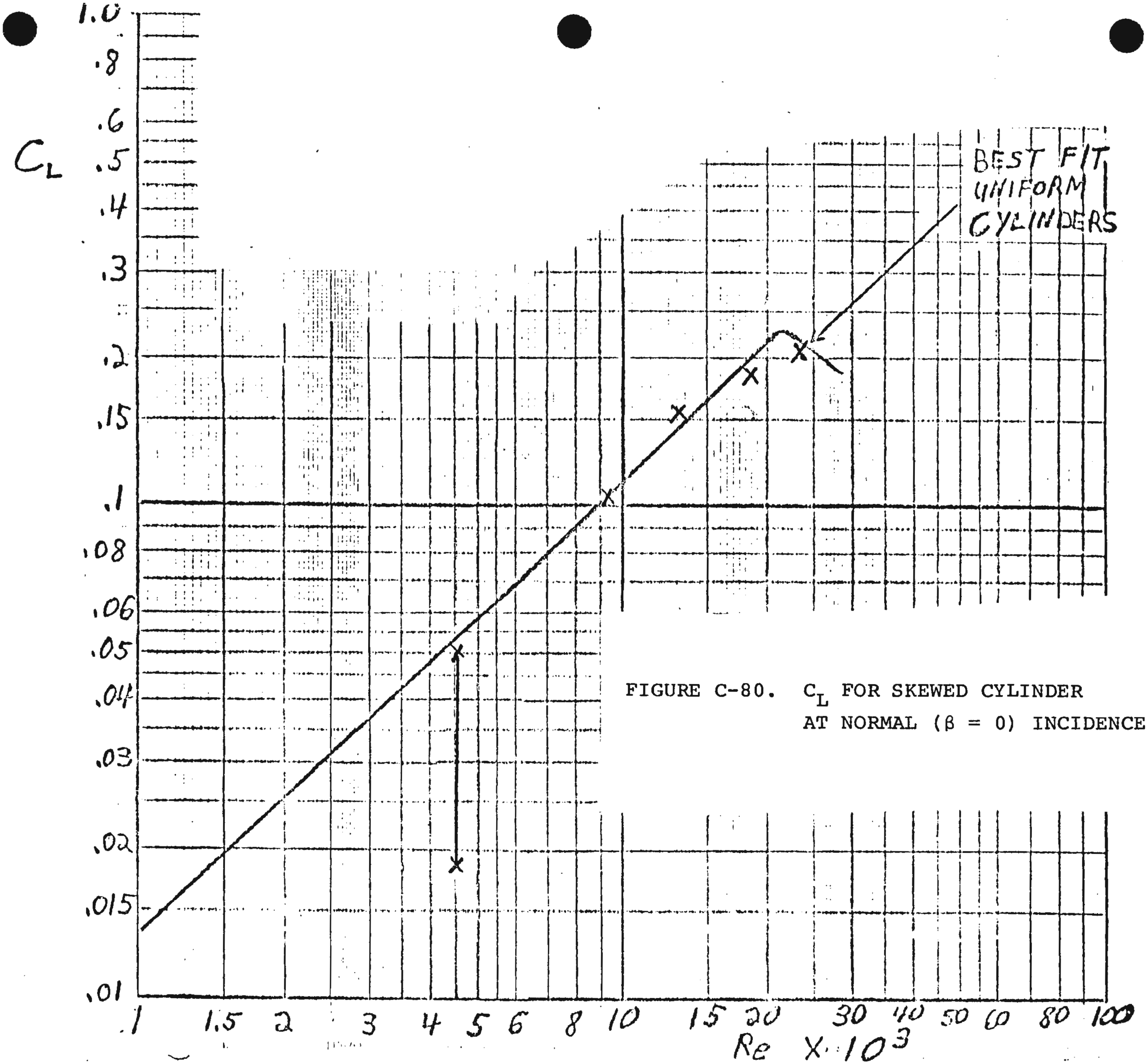

FIGURE C-80. C_L FOR SKEWED CYLINDER AT NORMAL (β = 0) INCIDENCE

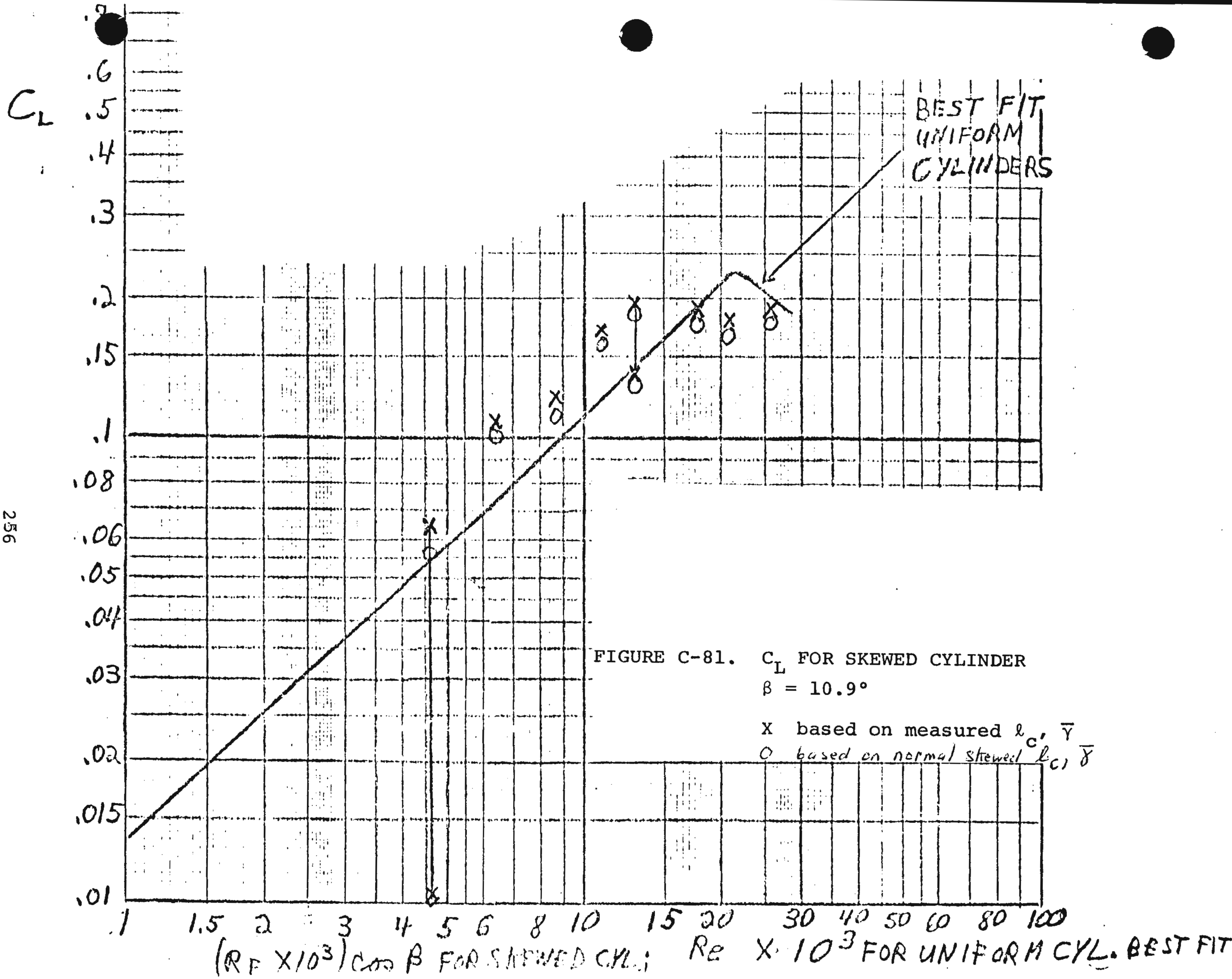

FIGURE C-81. C_L FOR SKEWED CYLINDER $\beta = 10.9°$

X based on measured ℓ_c, $\overline{\gamma}$

O based on normal skewed ℓ_c, $\overline{\gamma}$

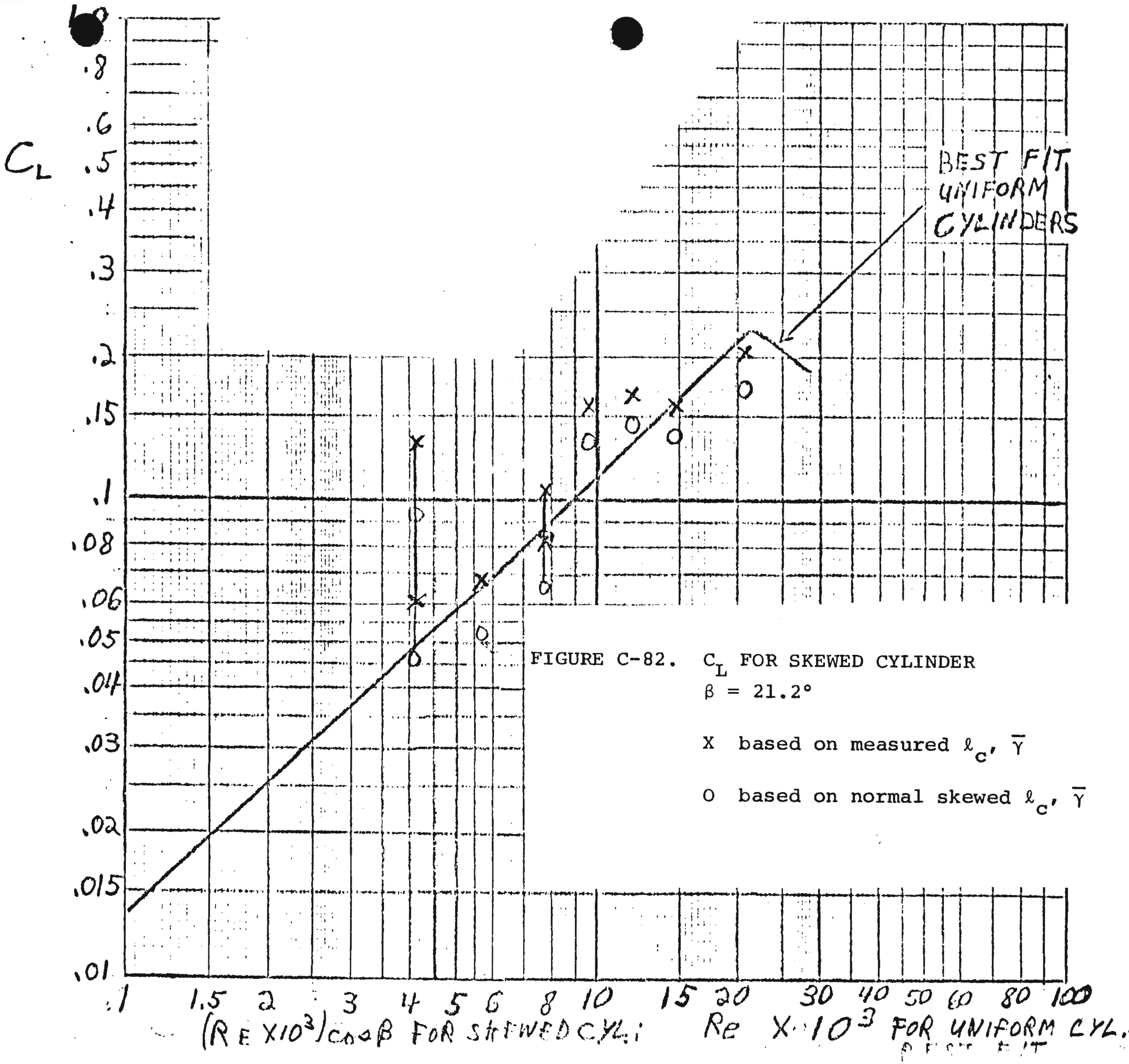

FIGURE C-82. C_L FOR SKEWED CYLINDER

$\beta = 21.2°$

X based on measured ℓ_c, $\overline{\gamma}$

O based on normal skewed ℓ_c, $\overline{\gamma}$

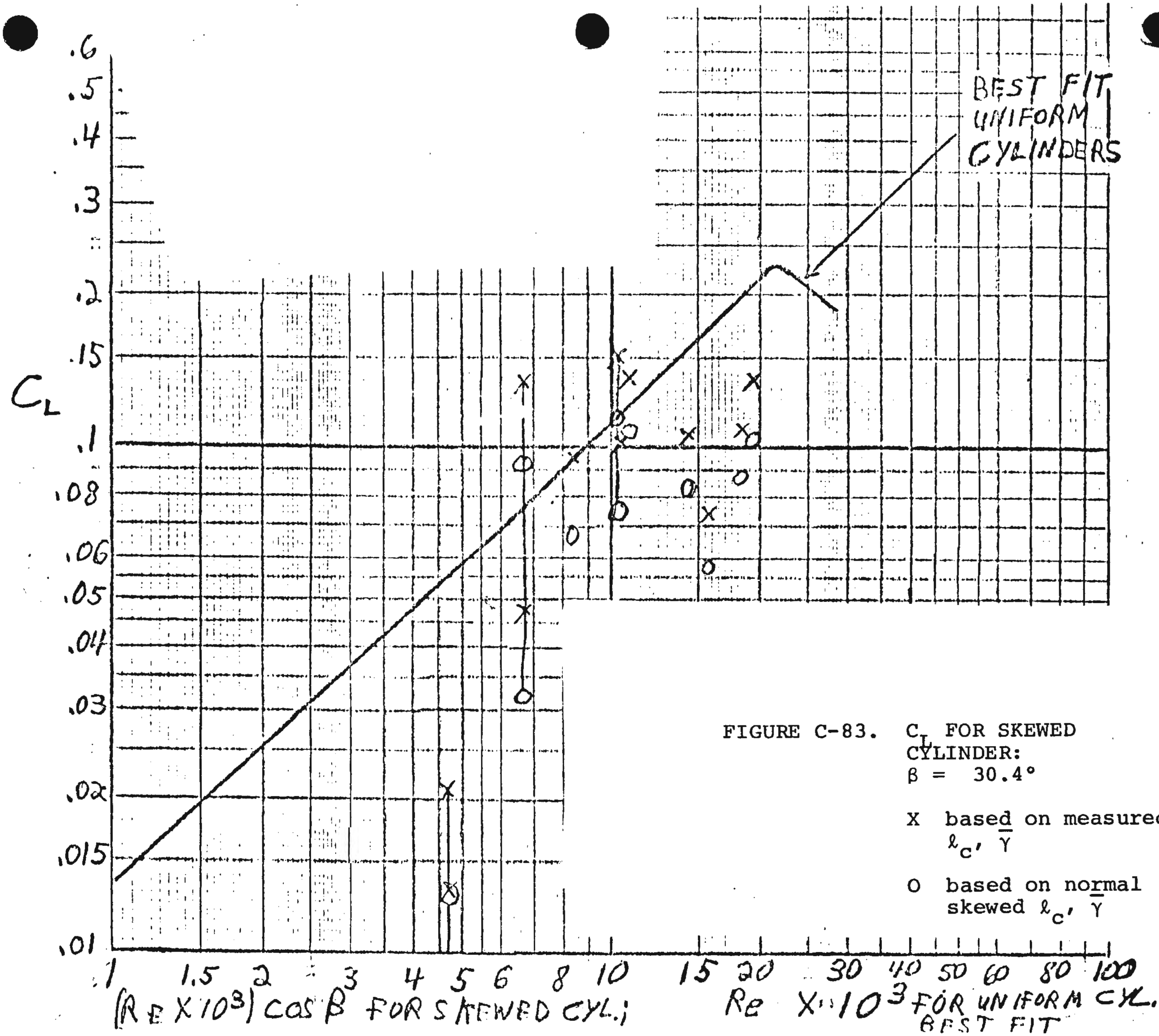

FIGURE C-83. C_L FOR SKEWED CYLINDER:
$\beta = 30.4°$

X based on measured ℓ_c, $\overline{\gamma}$

O based on normal skewed ℓ_c, $\overline{\gamma}$

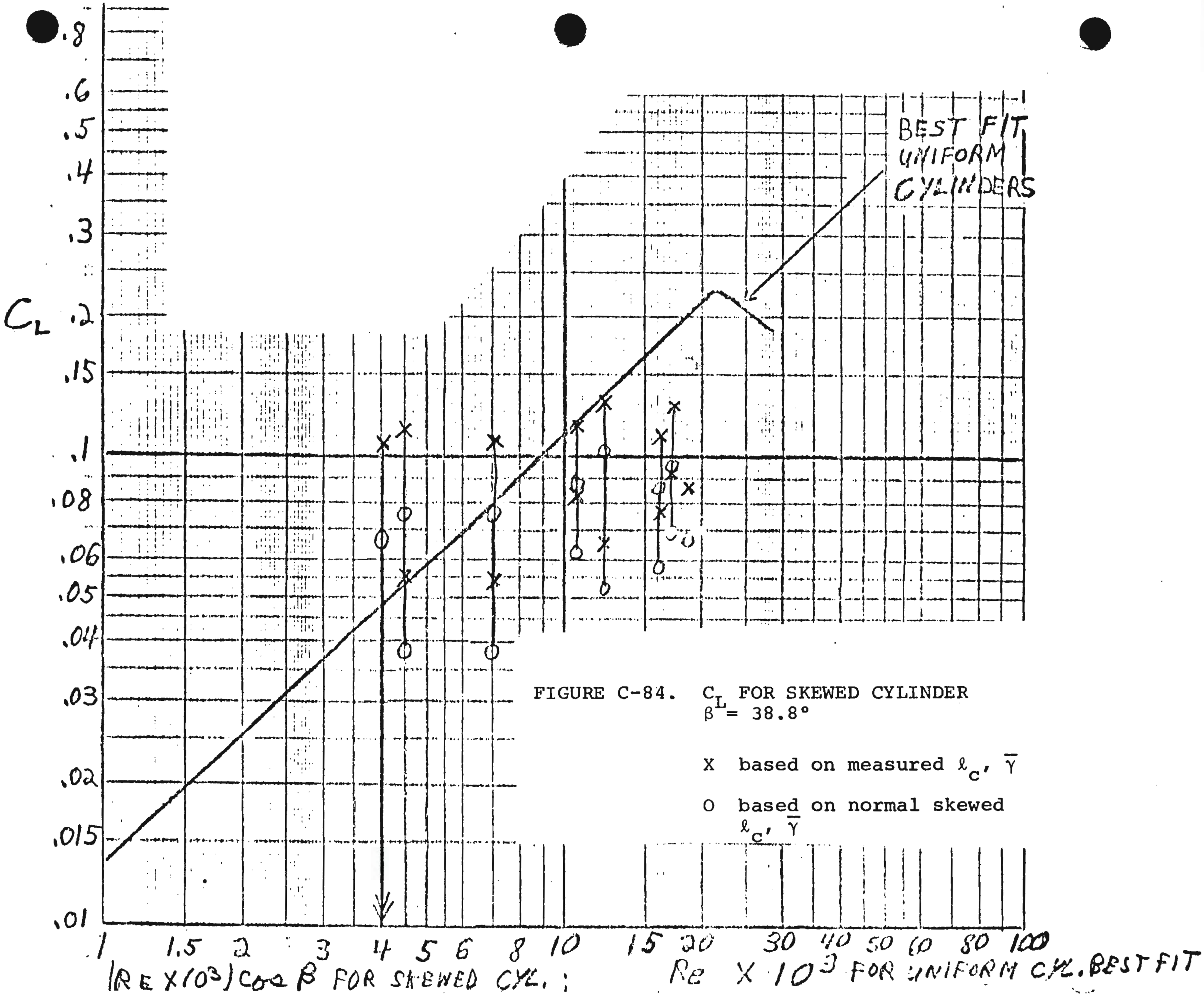

FIGURE C-84. C_L FOR SKEWED CYLINDER
$\beta = 38.8°$

X based on measured ℓ_c, $\overline{\gamma}$

O based on normal skewed ℓ_c, $\overline{\gamma}$

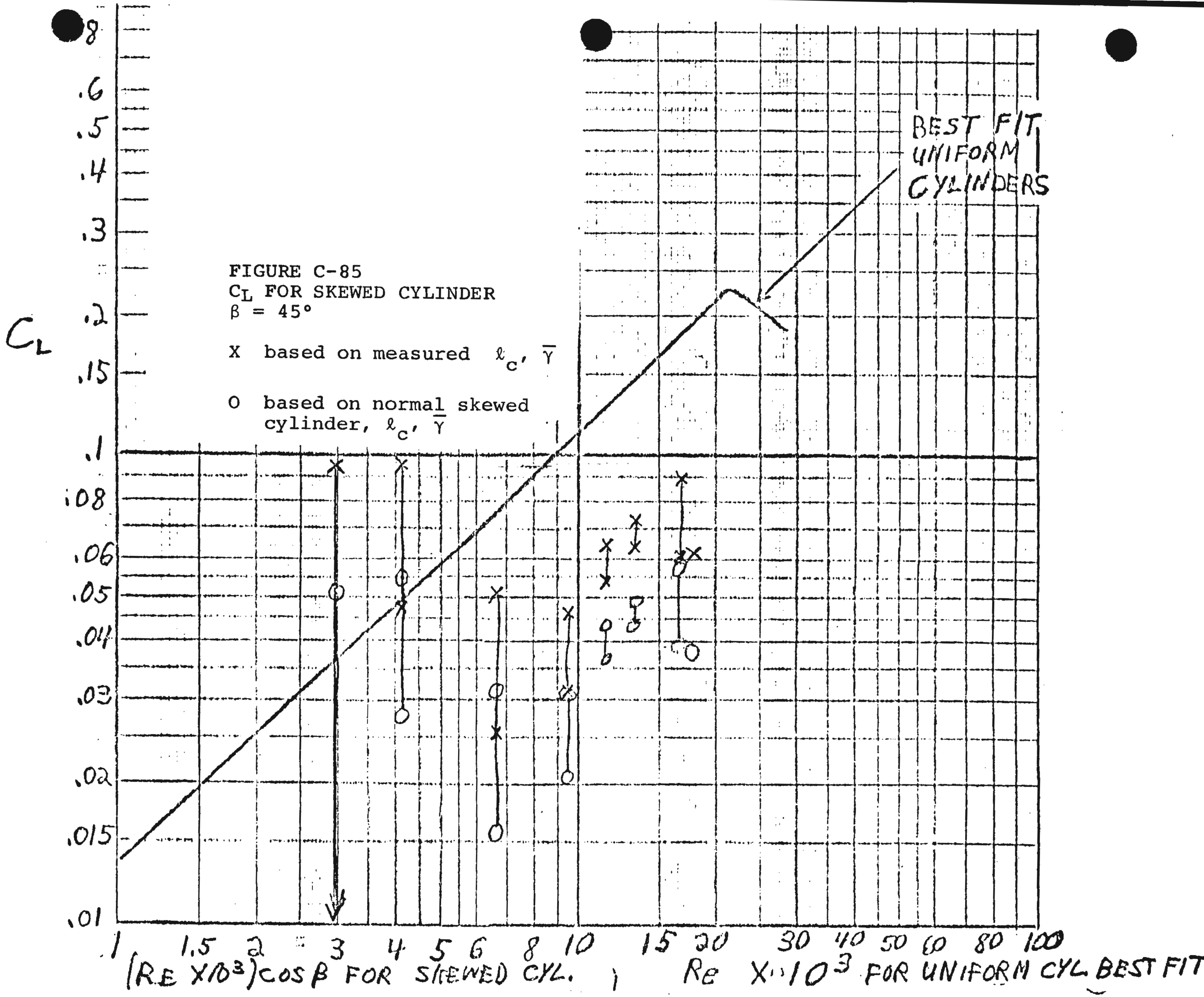

FIGURE C-85
C_L FOR SKEWED CYLINDER
$\beta = 45°$

X based on measured ℓ_c, $\overline{\gamma}$

O based on normal skewed cylinder, ℓ_c, $\overline{\gamma}$

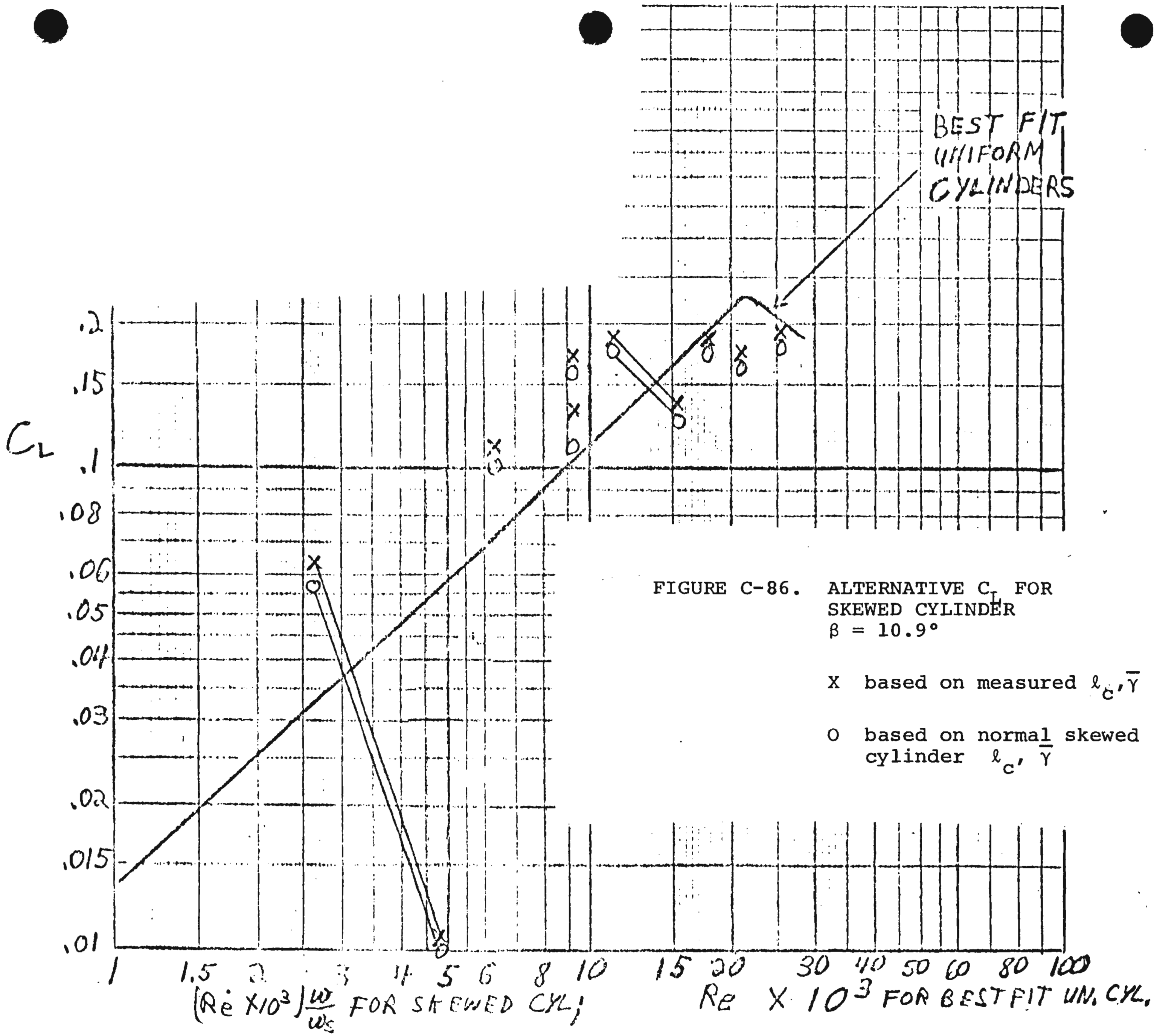

FIGURE C-86. ALTERNATIVE C_L FOR SKEWED CYLINDER
$\beta = 10.9°$

X based on measured $\ell_c, \overline{\gamma}$

O based on normal skewed cylinder $\ell_c, \overline{\gamma}$

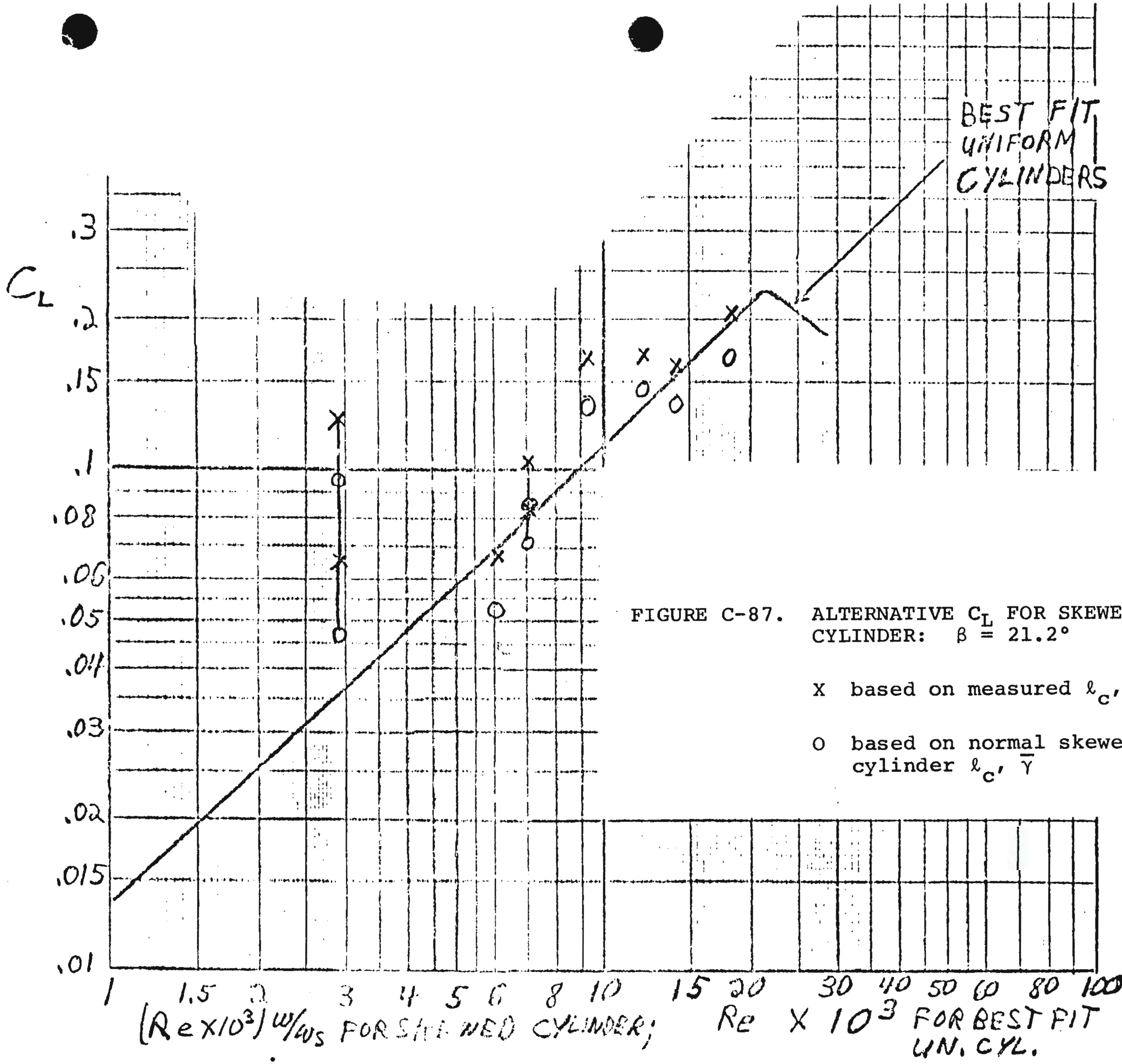

FIGURE C-87. ALTERNATIVE C_L FOR SKEWED CYLINDER: $\beta = 21.2°$

X based on measured ℓ_c, $\overline{\gamma}$

O based on normal skewed cylinder ℓ_c, $\overline{\gamma}$

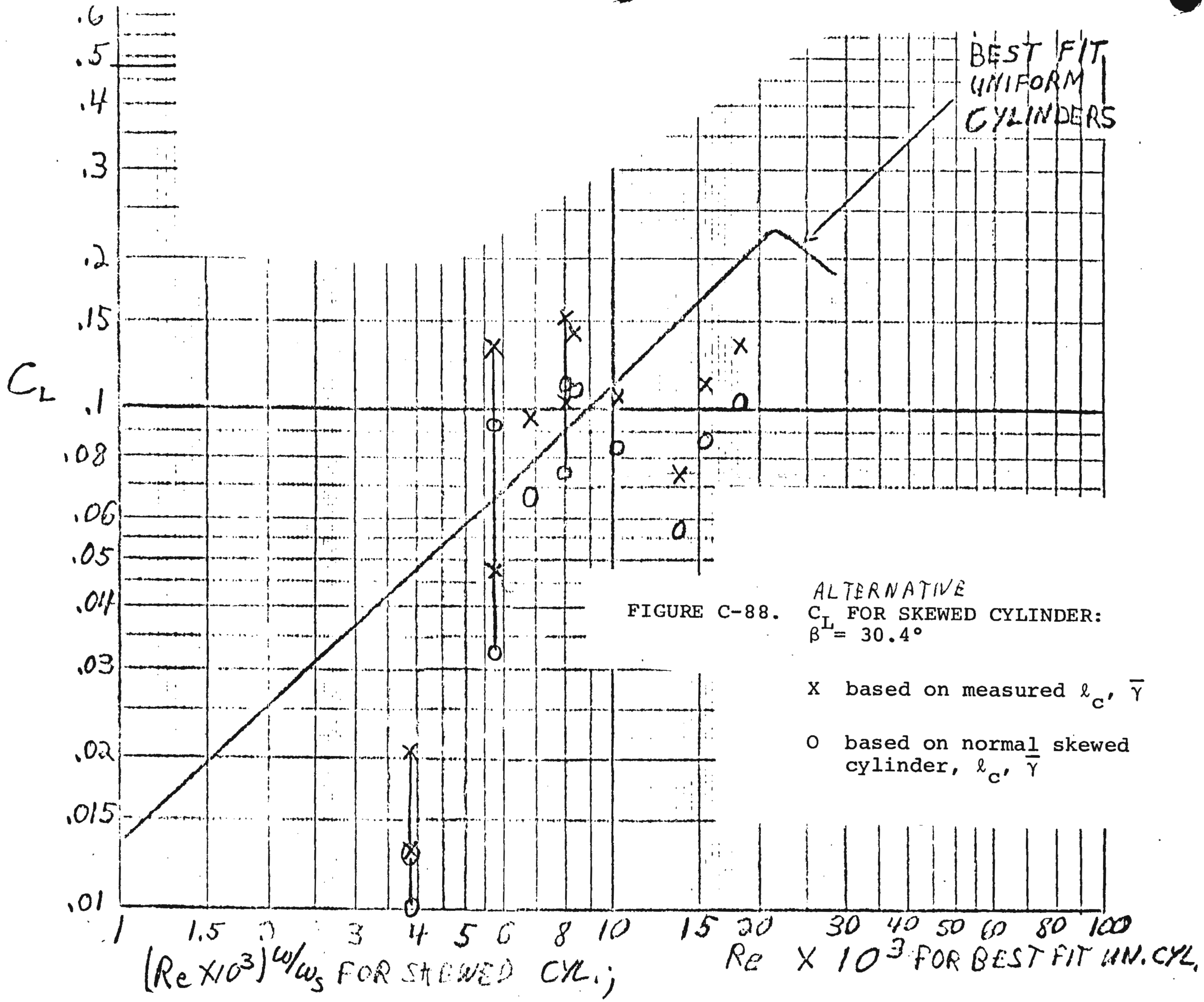

FIGURE C-88. ALTERNATIVE C_L FOR SKEWED CYLINDER: $\beta = 30.4°$

X based on measured ℓ_c, $\overline{\gamma}$

O based on normal skewed cylinder, ℓ_c, $\overline{\gamma}$

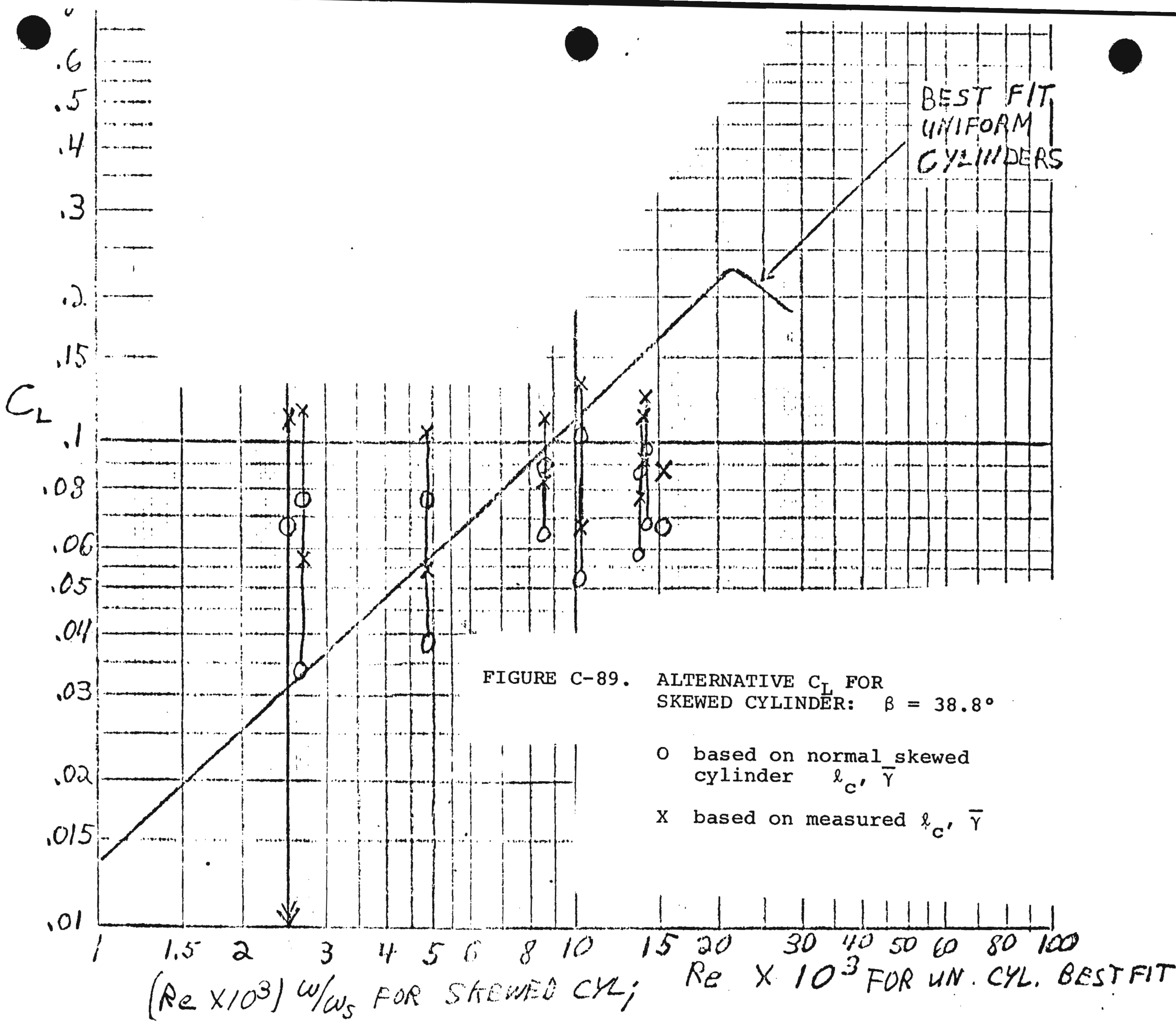

FIGURE C-89. ALTERNATIVE C_L FOR SKEWED CYLINDER: β = 38.8°

O based on normal skewed cylinder ℓ_c, $\overline{\gamma}$

X based on measured ℓ_c, $\overline{\gamma}$

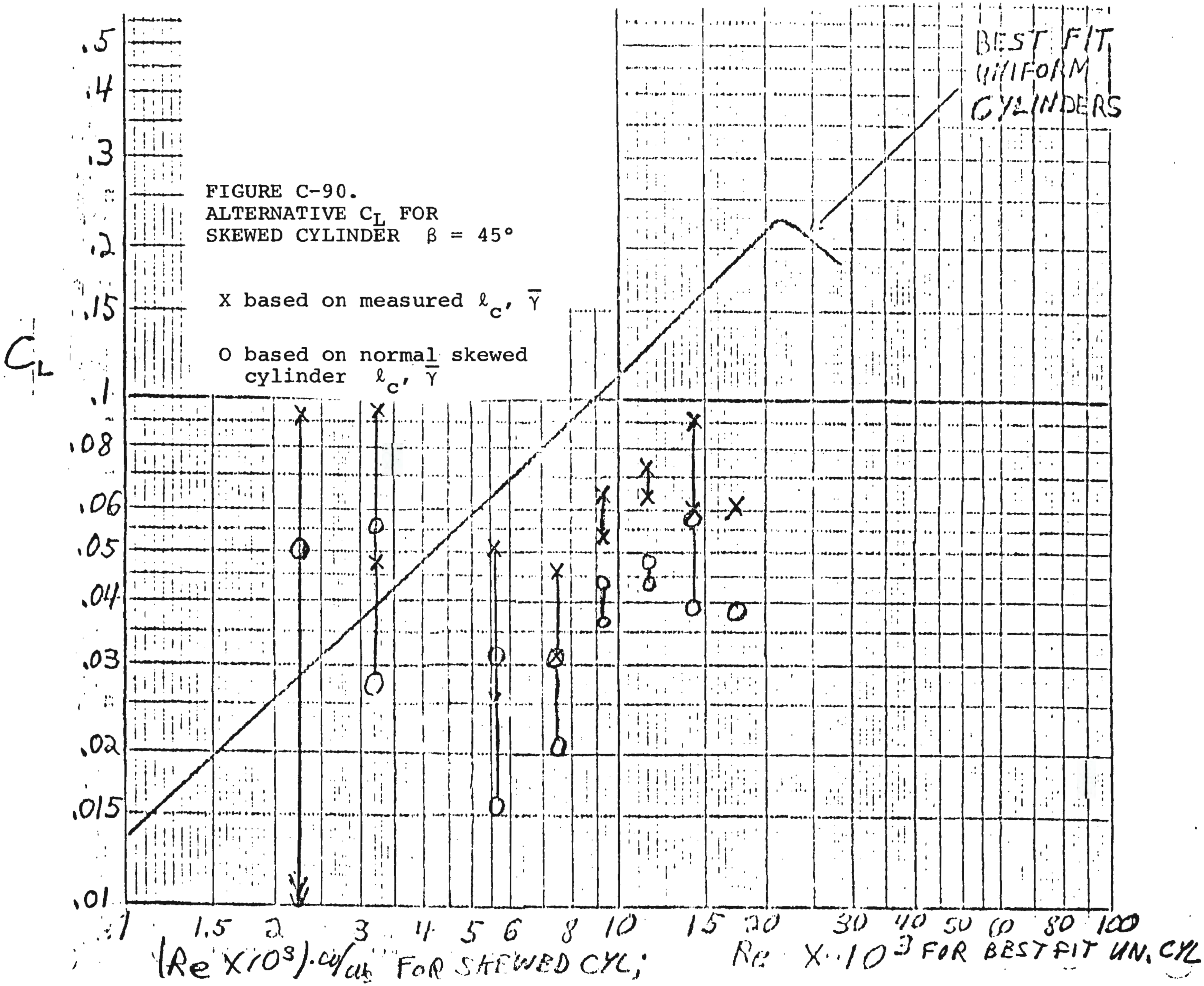

FIGURE C-90.
ALTERNATIVE C_L FOR SKEWED CYLINDER $\beta = 45°$

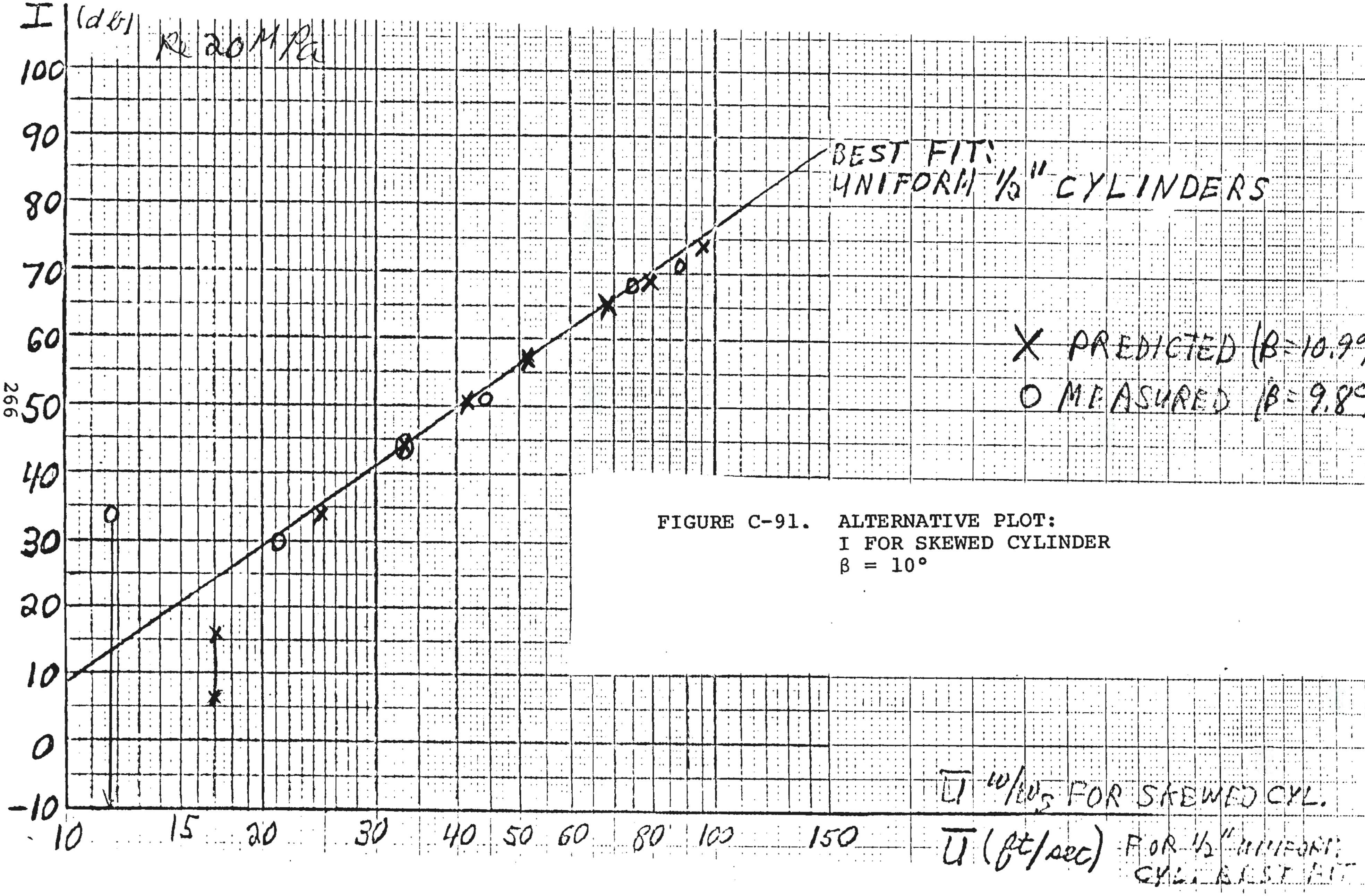

FIGURE C-91. ALTERNATIVE PLOT:
I FOR SKEWED CYLINDER
β = 10°

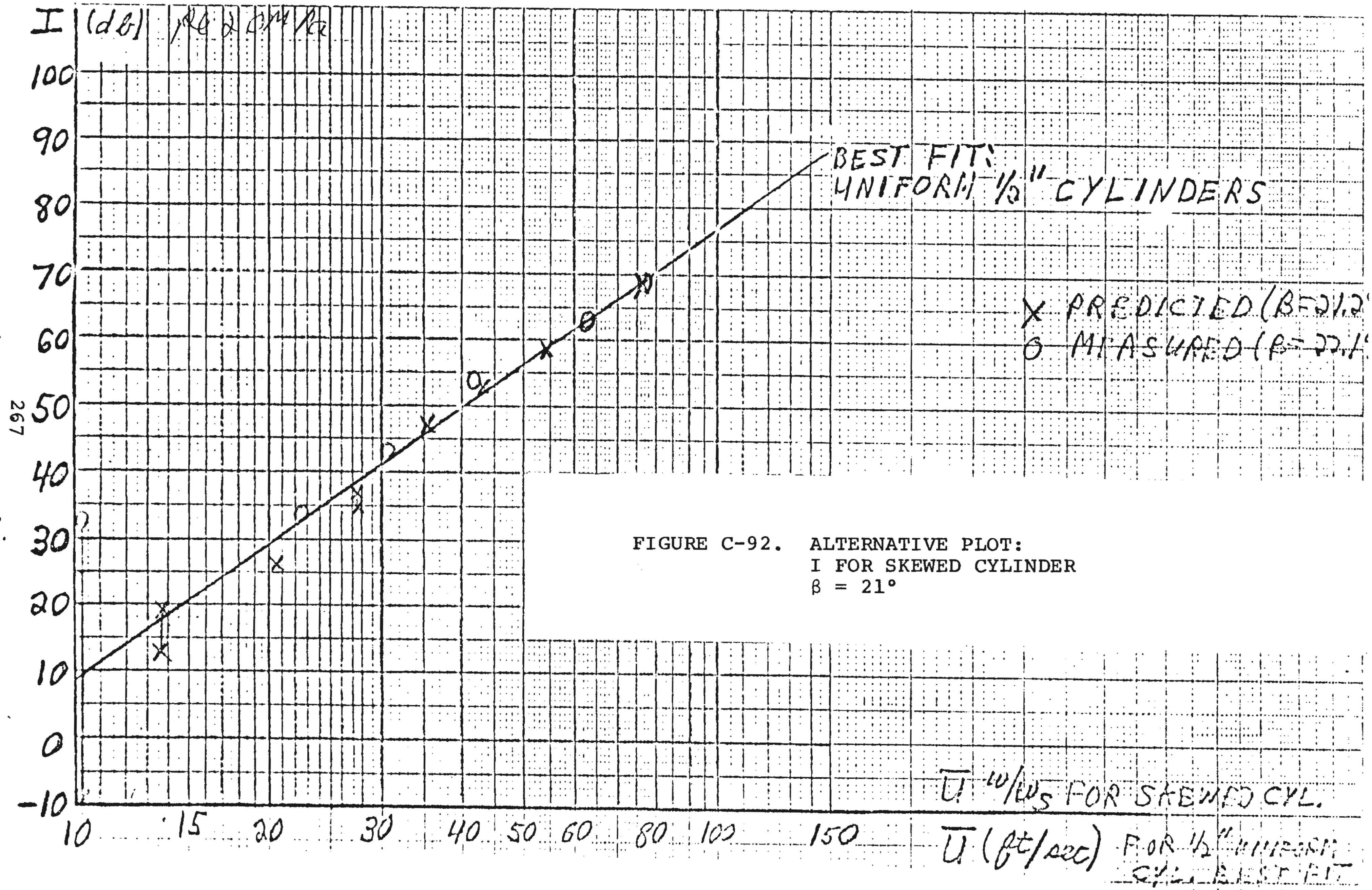

FIGURE C-92. ALTERNATIVE PLOT:
I FOR SKEWED CYLINDER
β = 21°

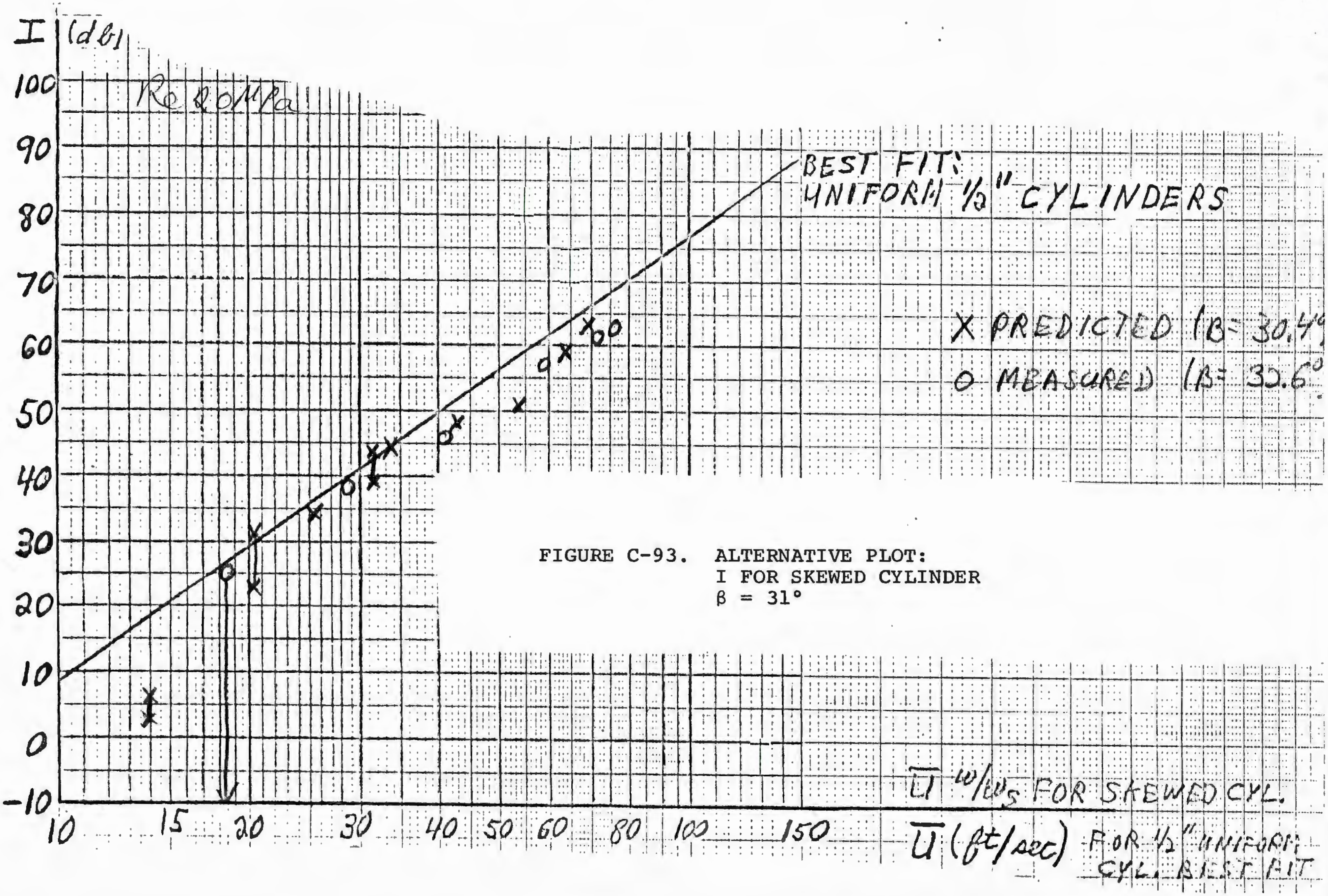

FIGURE C-93. ALTERNATIVE PLOT:
I FOR SKEWED CYLINDER
$\beta = 31°$

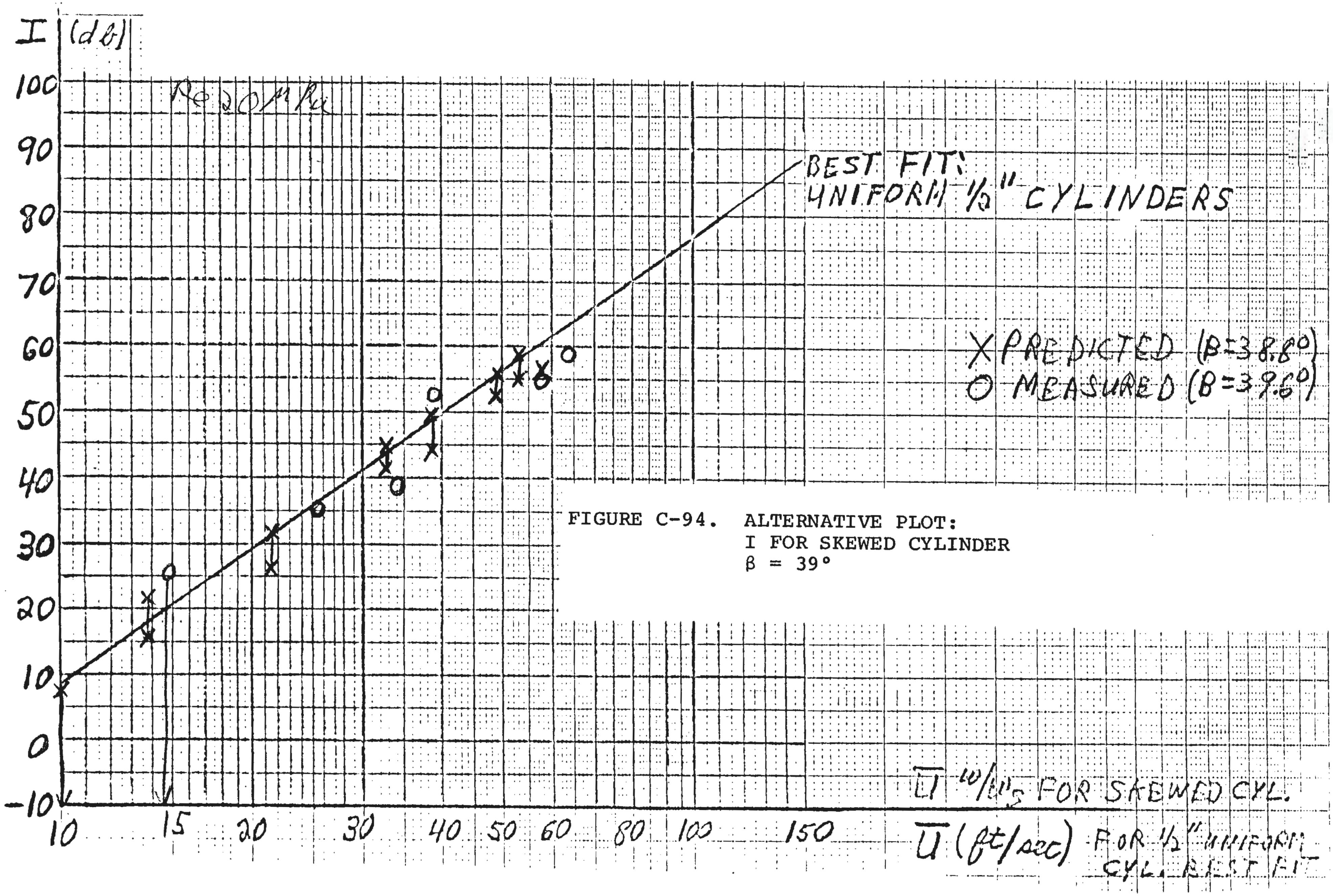

FIGURE C-94. ALTERNATIVE PLOT:
I FOR SKEWED CYLINDER
β = 39°

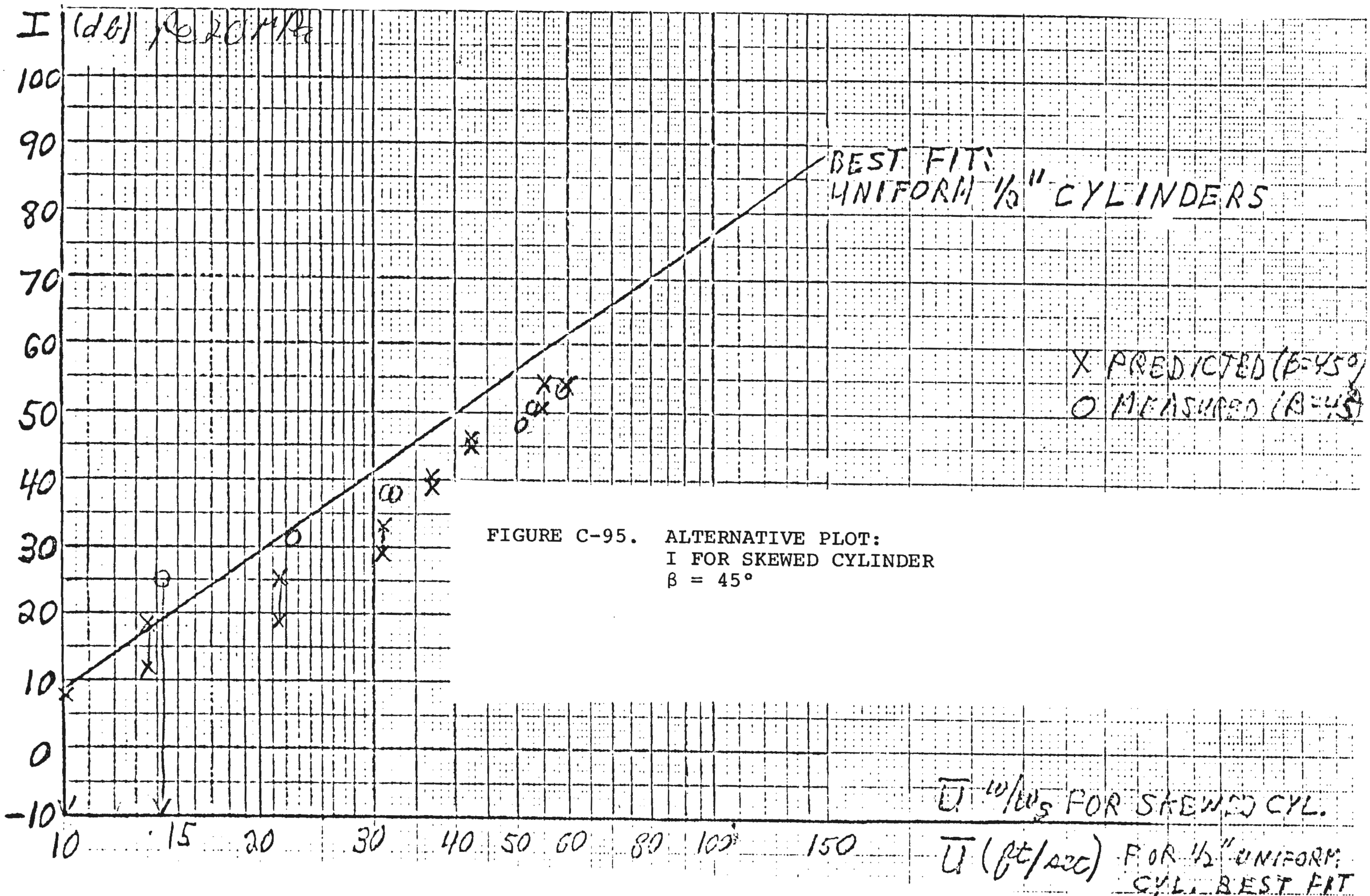

FIGURE C-95. ALTERNATIVE PLOT:
I FOR SKEWED CYLINDER
β = 45°

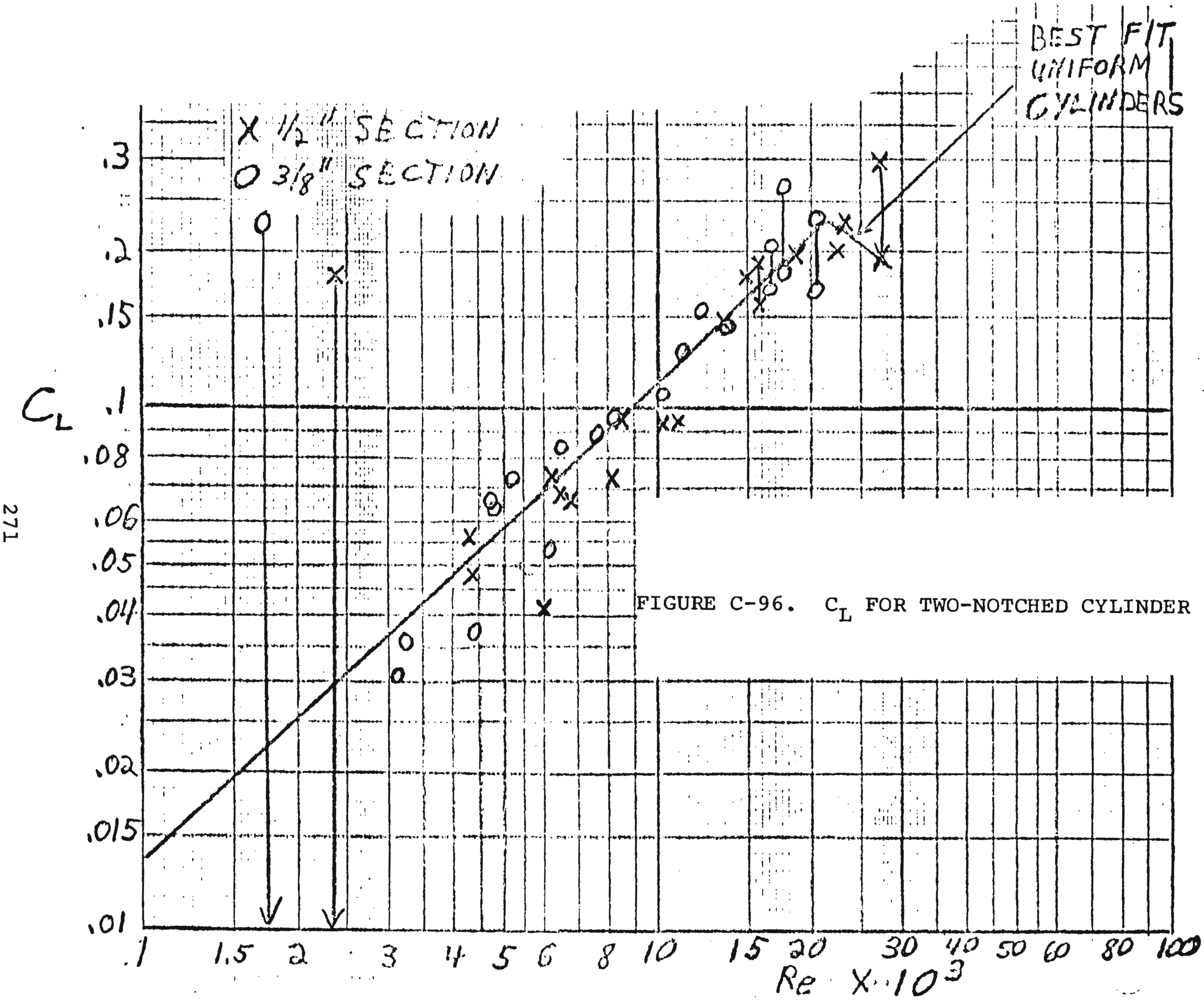

FIGURE C-96. C_L FOR TWO-NOTCHED CYLINDER

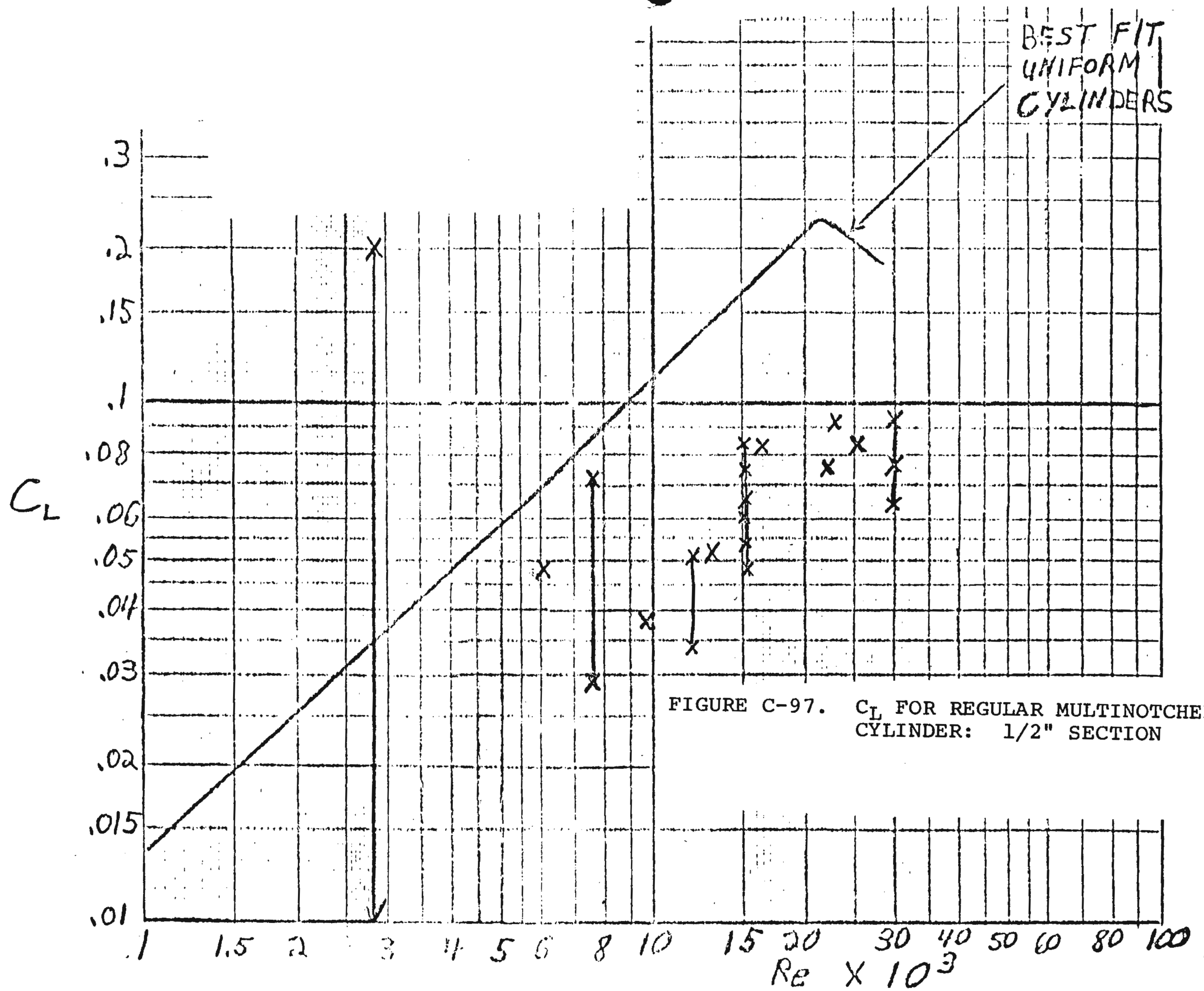

FIGURE C-97. C_L FOR REGULAR MULTINOTCHED CYLINDER: 1/2" SECTION

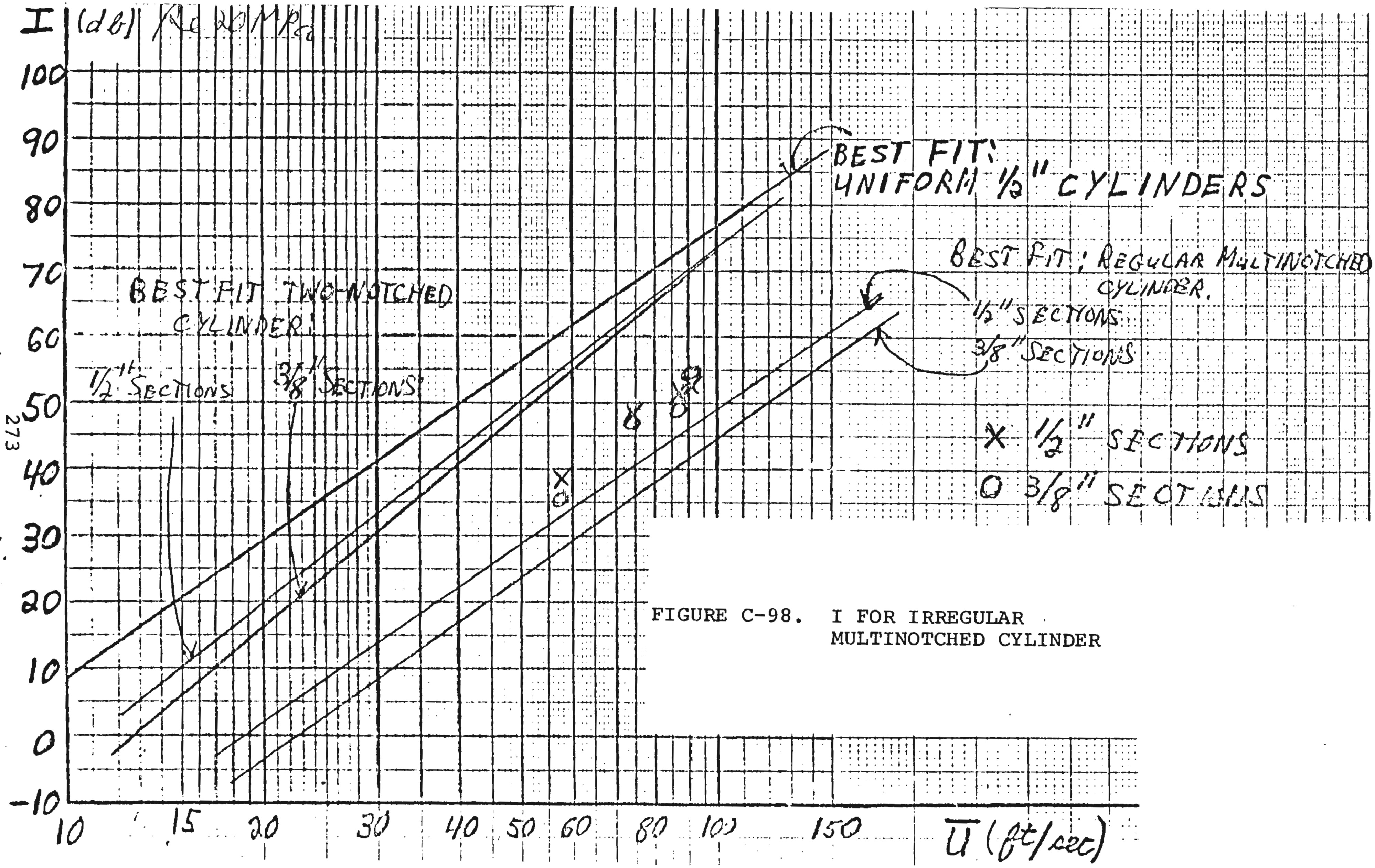

FIGURE C-98. I FOR IRREGULAR MULTINOTCHED CYLINDER

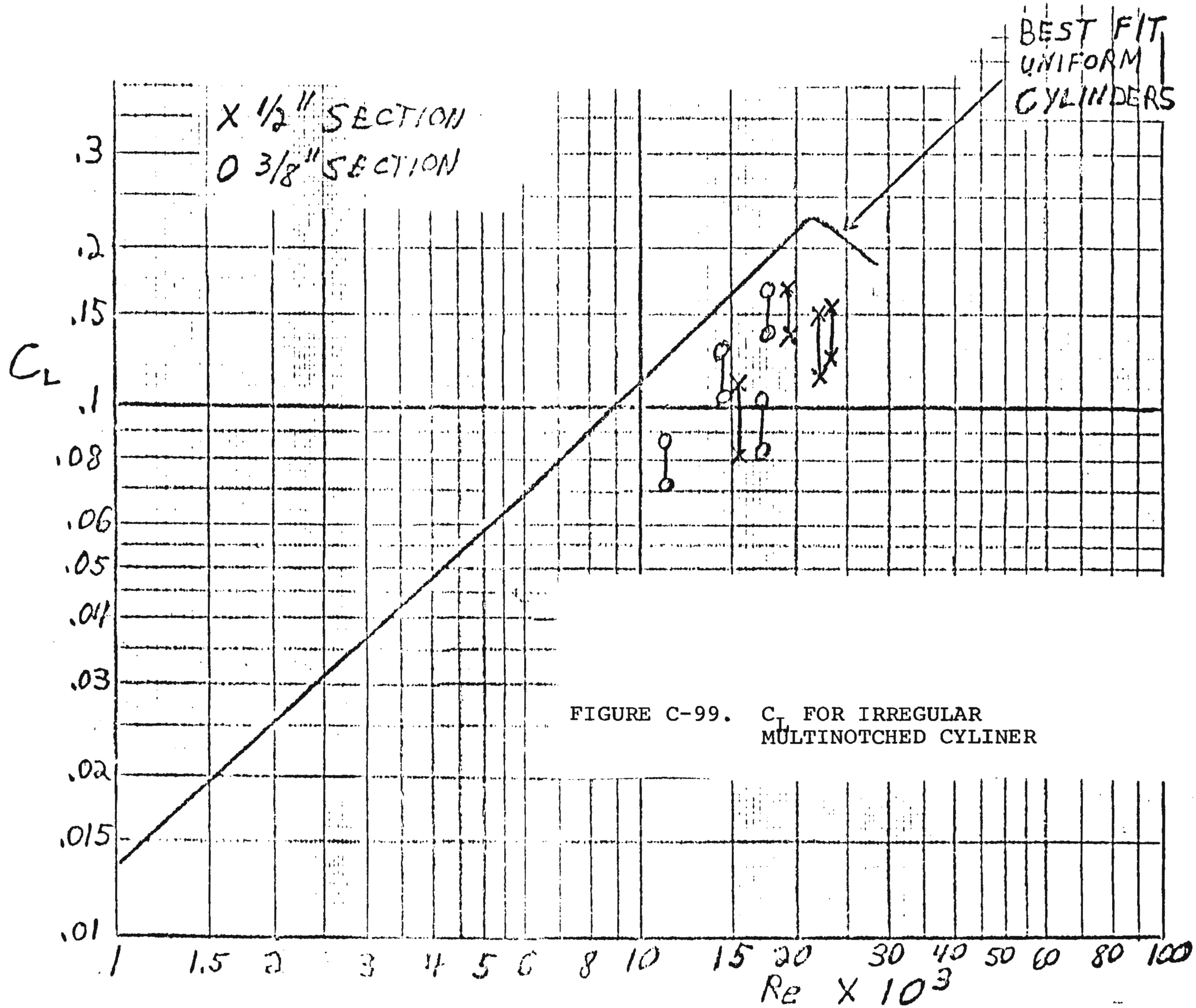

FIGURE C-99. C_L FOR IRREGULAR MULTINOTCHED CYLINER

APPENDIX D: PLATES

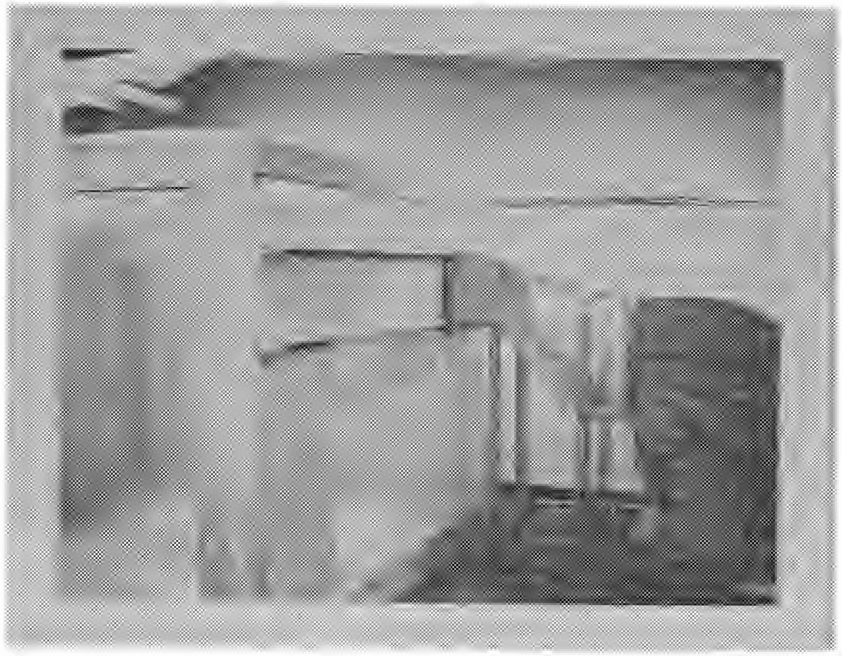

PLATE D-1. WIND TUNNEL: PLENUM CHAMBER AND BLOWER

PLATE D-2. WIND TUNNEL: PLENUM CHAMBER AND CONTRACTION (SIDE VIEW)

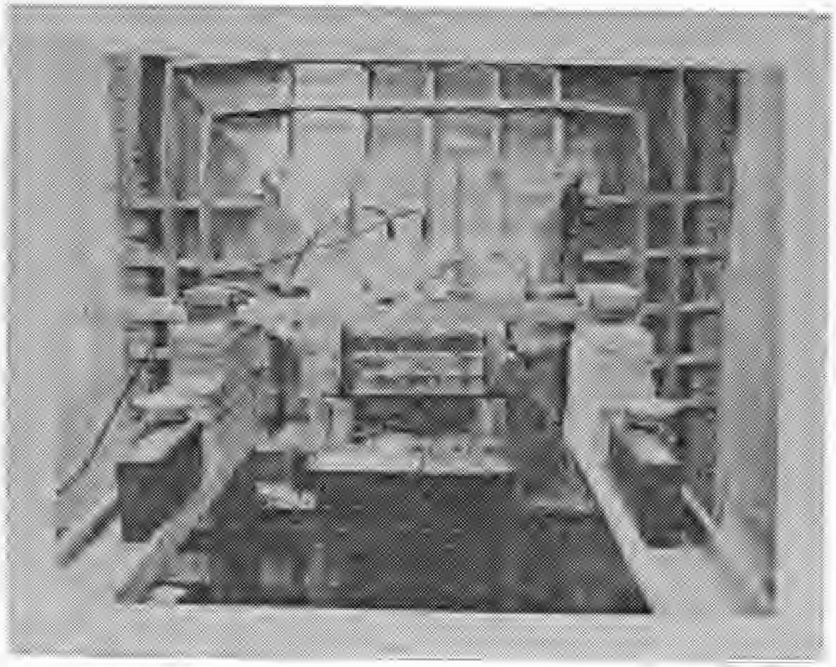

PLATE D-3. WIND TUNNEL CONTRACTION AND CYLINDER SUPPORT STAND (END VIEW)

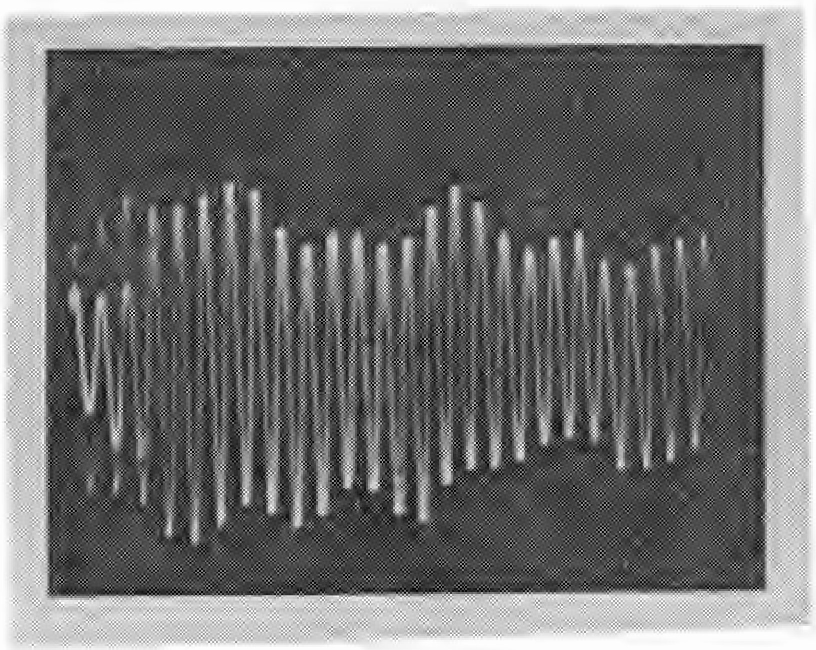

PLATE D-4. F_L: HIGH $\overline{U}$

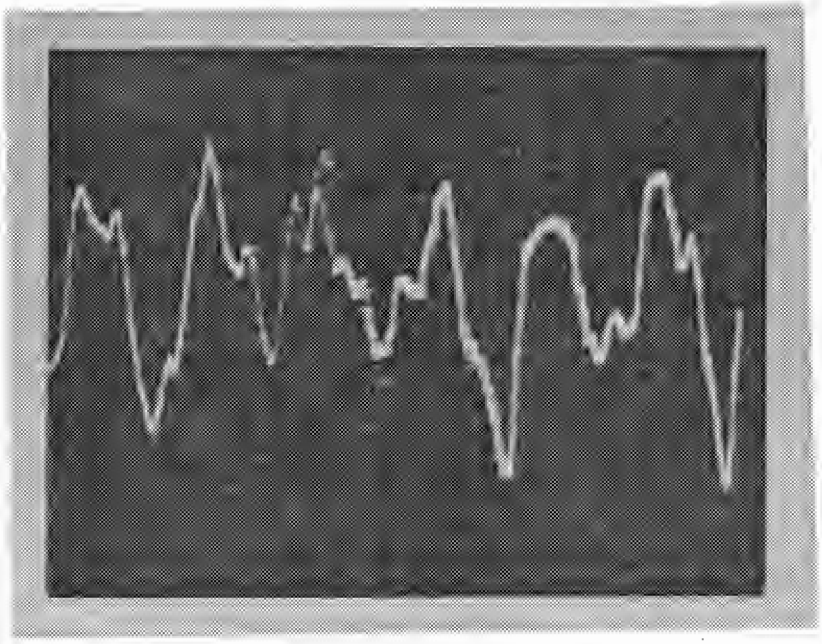

PLATE D-5. F_L: LOW $\overline{U}$

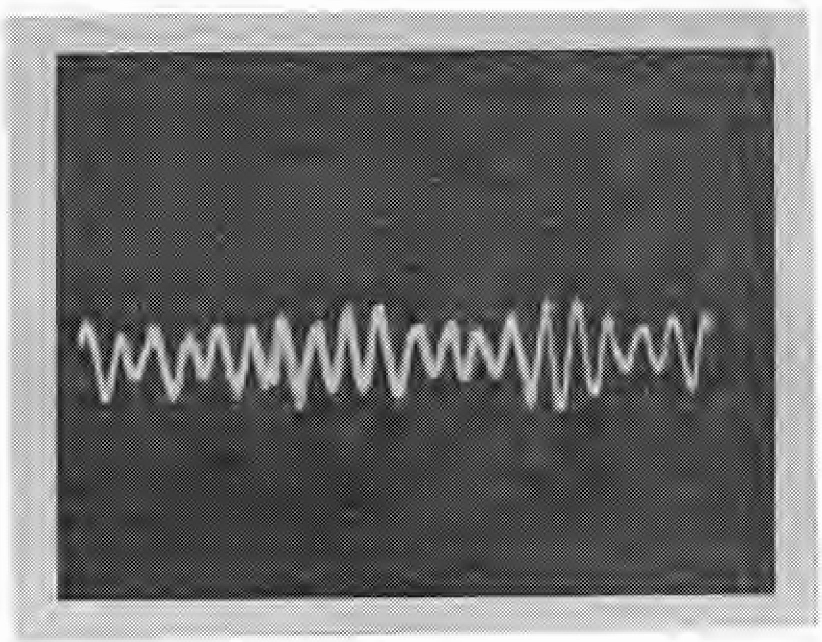

PLATE D-6. ANEMOMETER SIGNAL: GOOD LOCATION FOR $R(\gamma)$ MEASUREMENT

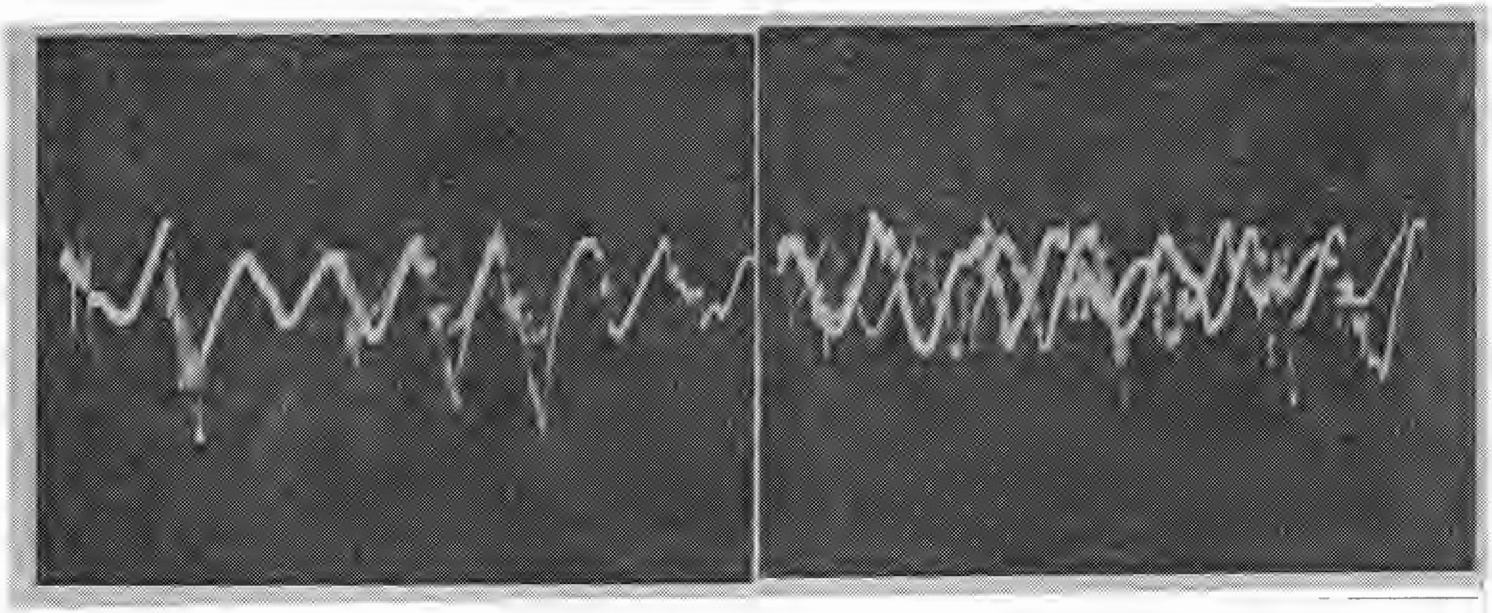

(a) (b)

PLATE D-7. ANEMOMETER SIGNAL: POOR LOCATION FOR R(γ) MEASUREMENT

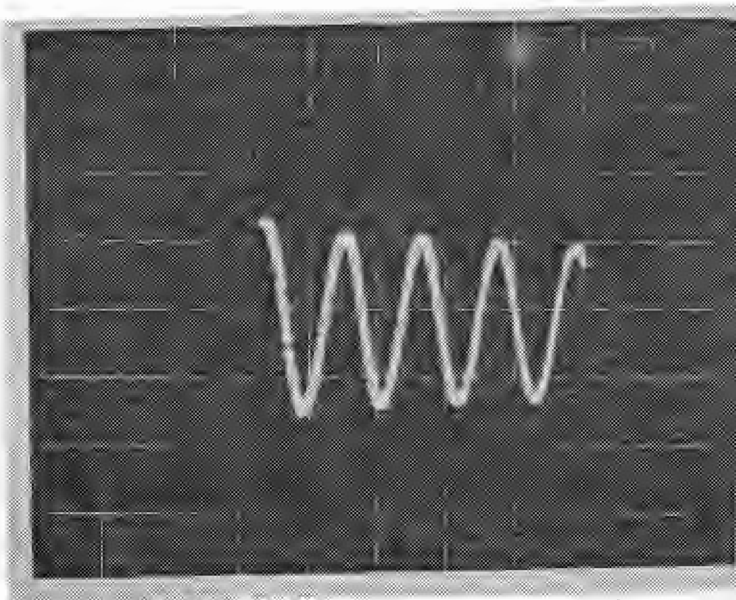

PLATE D-8. AUTOCORRELATION OF POOR S/N SIGNAL

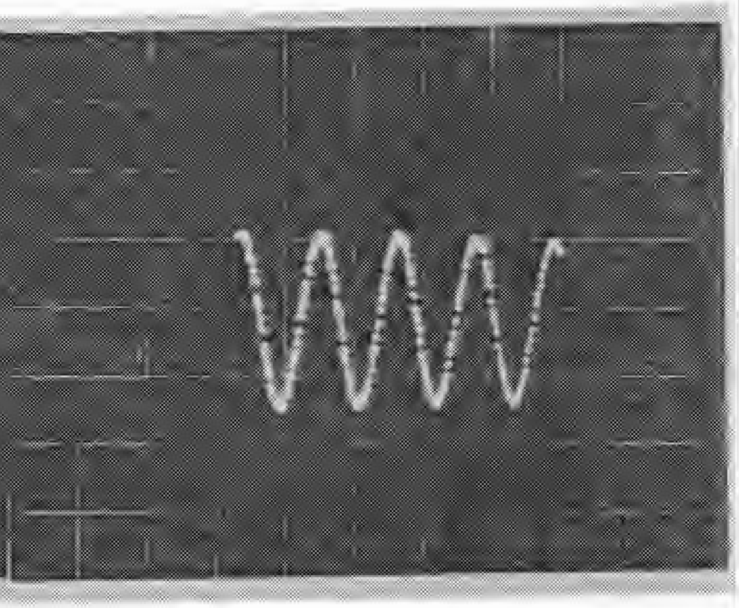

PLATE D-9. AUTOCORRELATION OF GOOD S/N SIGNAL

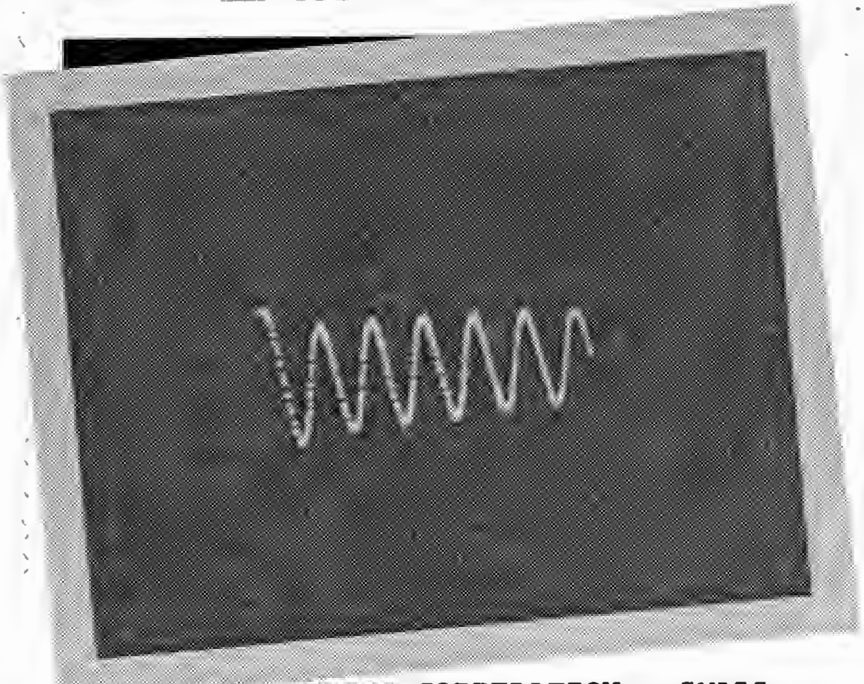

PLATE D-10. CROSS CORRELATION: SMALL γ

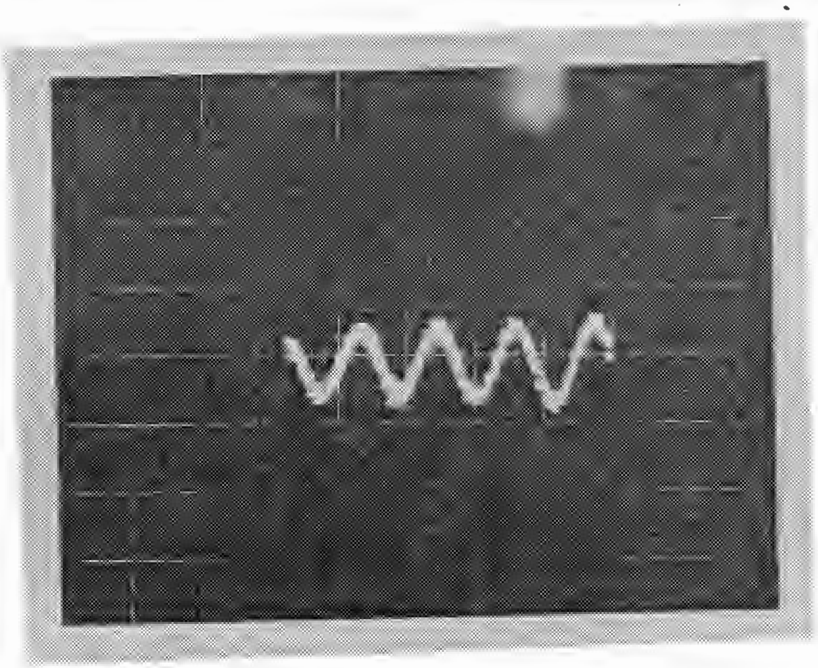

PLATE D-11. CROSS CORRELATION: LARGE γ

INITIAL DISTRIBUTION LIST

		No. Copies
1.	Defense Documentation Center Cameron Station Alexandria, Virginia 22314	2
2.	Library, Code 0212 Naval Postgraduate School Monterey, California 93940	2
3.	Prof. J. V. Sanders Department of Physics and Chemistry Naval Postgraduate School Monterey, California 93940	1
4.	Prof. O.B. Wilson, Jr. Department of Physics and Chemistry Naval Postgraduate School Monterey, California 93940	1
5.	Prof. G. S. Sackman Department of Electrical Engineering Naval Postgraduate School Monterey, California 93940	1
6.	Prof. T. M. Houlihan Department of Mechanical Engineering Naval Postgraduate School Monterey, California 93940	1
7.	Prof. K.E. Woehler Department of Physics and Chemistry Naval Postgraduate School Monterey, California 93940	2
8.	Dr. Jack Hoyt Naval Undersea Center San Diego, California 92132	1
9.	LCDR Steven R. Cohen 344 Pine Wood Lane Los Gatos, California 95030	2